NEW METHODS OF POTENTIAL FIELD DATA PROCESSING IN REGIONAL AND MINING GEOPHYSICS

YANG, WEN-CAI

(杨文采)

A thesis submitted to the Faculty of Graduate Studies and Research , McGill University, in partial fulfillment of the requirements for the degree of Doctor of Philosophy

Dept. of Mining and Metallurgical Engineering

McGill University, Montreal, Canada

February 1984

ACKNOWLEDGEMENTS

I wish to express my gratitude to Dr. D. J. Crossley for his guidance and encouragement throughout this project and to Dr. W. M. Telford and O. G. Jensen for their kindness, advice and support in many ways.

Thanks are also due to

Dr. P. P. Silvester & Dr. F. M. Reza of Department of Electrical engineering , McGill University for advice.

Dr. S. P. Huestis of The University of New Mexico and Dr G. F. West of The University of Toronto for reading parts of the Thesis and providing valuable suggestions for improving the presentation.

Fellow-students M. Pilkington & C. L. Parker for discusstions and help in English.

McGill computer center for computing fund.

Special thanks are made to my wife Guo, Ai-Ying for her selfless support during the period of my study at McGill.

Finally, I wish to thank the Quebec Education Ministry for gracious welcome.

ABSTRACT

Economic exploitation of mineral resources, especially in underdeveloped mountainous areas, requires evaluating potential base-metal deposits over a large area of mineralization. Sophisticated techniques of potential field data processing are needed for this purpose, including reliable methods for regional-residual separation, continuation of potential fields and accurate computation of magnetic field in various rock materials.

For the regional-residual separation problem, it is shown that the finite element method can be useful in conjunction with the generalized linear inverse approach, to produce improved regional and residual gravity maps compared to traditional methods. Then the generalized linear inverse method is applied to downward continuation of both regionals and residuals, giving the best trade-off in terms of noise and resolution for locating causative bodies. New techniques are also devised for efficient computation of upward continuation between general surfaces. Based on linearization of the hysteresis curves for igneous rocks, a new mathematical representation of the demagnetization phenomenon is constructed which allows a practical calculation of this effect. Again, a method using the finite element technique is developed for accurate computation of effective magnetization and magnetic field both inside and outside an arbitrary magnetized body.

Both synthetic and practical examples are given showing that these new methods are reliable and applicable in regional and mining geophysics with reasonable computational costs.

RESUME

L'exploitation des ressources minérales, et spécialement dans les régions montagneuses éloignées, demande l'évaluation du potentiel métallifère de grandes superficies minéralisées. Une telle évaluation nécessite des techniques sophistiquées traitant les données de champ potentiel, ainsi que des méthodes fiables pour la séparation régionale-résiduelle, la continuation de champs potentiels et le calcul précis de l'intensité du champ magnétique dans différents matériaux rocheux.

On démontre que la méthode des éléments finis, utilisée en conjugaison avec l'inversion linéaire généralisée, peut servir à séparer la régionale-résiduelle et produire des cartes de gravité régionale et résiduelle de qualité supérieure à celles obtenues avec les méthodes conventionnelles. L'inversion linéaire généralisée est alors appliquée pour la continuation vers le bas des régionales et résiduelles, donnant ainsi le meilleur rendement en termes de bruit et de résolution pour la localisation des corps causatifs. De nouvelles techniques sont introduites pour calculer efficacement la continuation vers le haut entre différentes surfaces. Basée sur la linéarisation des courbes d'hystérésis de roches ignées, une nouvelle réprésentation mathématique du phénomène de la démagnétisation est construite, laquelle permet un calcul pratique de cet effet. Une méthode, utilisant aussi la technique des éléments finis, est développée pour le calcul précis de l'aimantation et de l'intensite du champ magnétique interne et externe d'un quelconque corps magnétise.

Des exemples pratiques et simulés démontrent que ces nouvelles méthodes sont fiables et applicables en géophysique minière et régionale à des coûts raisonnables.

TABLE OF CONTENTS

Chapter 4. New Techniques for Continuation of Potential Fields from Arbitrary Surfaces

Chapter 5. Demagnetization and Accurate Computation of Magnetic Fields

TABLE OF FIGURES

TABLES

Chapter I. Introduction

As is indicated by the title, this thesis is devoted to a study of new methods in potential field data processing. From the viewpoint of computer sciences, potential field data processing is a form of scientific computing which requires an input of potential field data and which produces information directly related to certain geological structures. It differs from data manipulation which requires only very simple arithmetic calculations. We may also distinguish data processing from quantitative interpretation of potential data. The latter belongs to a kind of information processing which requires an input of potential field data plus some geological information, to produce a physical model with definite parameters, enabling us to explain the data by certain physical laws. Thus, potential field data analysis may be divided into three ordered steps: (1) data manipulation, such as digital data acqusition, reduction and automatic mapping, (2) data processing, such as converting different field components, continuation and regional-residual analysis, and (3) data interpretation including the quantitative interpretation (inversion) and the geological interpretation.

In the computer age, data processing plays an increasingly important role in geophysical data analysis. Regional geological studies require potential field data processing to provide useful information for recognizing deep structures. Mining and oil companies require data processing to locate causative bodies which might be related to mineralization. Moreover, the inversion methods also need data processing to produce reliable initial assessments. Unfortunately, some newly developed techniques of numerical analysis, such as those for solving functional equations, have not been fully applied to potential field data processing (see the next chapter). In addition, there have been a few intricate problems left which should be explored both physically and mathematically. Consequently the theme of this thesis is chosen as reexamining some difficult

problems and updating potential field data processing techniques in mining and regional geophysics.

A practical interest in developing new data processing methods is the evaluation of base metal minerogenetic subprovinces in underdeveloped mountainous areas. Since modern civilization is built on the development of industry, a substantial quantity of new base-metal ores must be found to meet the increasing needs of industry and to replace worked-out deposits. New deposits will be more difficult to locate because the easily found deposits have been discovered. As the probability of finding new ores in well-developed areas decreases rapidly, geologists become increasingly interested in mineral deposits on the sea floor and in desolate regions. Underdeveloped mountainous areas seem to offer the potential for locating metallic minerals, as there is an inherent association of mineralization with orogenesis.

Exploration of mineral resources in mountainous areas involves many difficulties and problems. Besides logistic and communication difficulties, topographic relief reduces the accuracy of data acquisition and causes interpratational problems. Potential field data measured on irregular terrains become functions of three spatial variables, consequently the equations involved in data processing can no longer be represented by convolution or other degenerate integrals. Another problem is the serious investment risk in exploration activities due to the lack of transportation systems and power supplies. Taking account of these arguments, the cost of exploitation of minerals can be very high in those areas. It may not be worthwhile to exploit a few ore deposits in a minerogenetic subprovince even if they are big and mineable. However, if sufficient mineral resources have been discovered in such subprovinces, the cost of exploitation can be reduced, with many mines sharing the same transpotation systems and power supplies. As a result, investors may find benefit in the exploitation, even if much capital is required. Therefore, it

is essential for investors to evaluate mineral deposits, such as iron, coal and copper, in whole subprovinces of mountainous areas.

For regional investigation in such areas, our goal is to obtain sufficient information, at a reasonable cost, to evaluate the potential mineral resources. This is an extremly hard task and its succesful achievement requires a skillful integration of all possible modern techniques as well as sound organization of exploration activites. In high mountain ranges, the cost of exploration is much increased due to difficulties of transpotation and communication. Comparison with the cost in flat or low-relief areas, in mountainous areas the cost of airborne surveys can be more than doubled and may be increased five times for ground geophysical surveys (even more for deep seismic soundings). Similarly, drilling is extremely expensive as helicopters are frequently required for logistics. There is no doubt that the advantages of geophysical and geochemical methods should be fully utilized, whereas drilling must be reduced as much as posible.

Another fact to be considered is that the exploration cost will increase steadily as more and more detailed surveys and drills are involved, with no assurance that the increasing investment is worthwhile, because the return on investment depends upon the total resources in the whole area. This problem is faced by all exploration projects and becomes more serious for projects carried out in mountainous areas. In order to save exploration investment, it is commonly accepted that an exploration programme should proceed sequentially and progressively. Based on this philosophy and experiences obtained mainly in the Canadian shield, Nicholls (1978) divided a typical base-metal exploration programme into four stages: area selection, project reconnaissance, project follow up and drilling. Considering the characteristics of mountainous areas, a similar strategy comprising three sequential stages may be suggested as follows.

The first stage may be called the preliminary reconnaissance to locate target areas for further detailed reconnaissance. As it has been found that there is a clearcut association of large orebodies with crustal structure, the recognition of major crustal fracturing is of great importance. Because in underdeveloped mountainous areas sufficient information on regional geology and geophysics is usually unavailable, interpretation of photomosaics (high-altitude satellite photographs, airphotos and side-look rader images), multiple airborne geophysical surveys and wide traverse integrated ground investigations are required to produce basic geological, structural, geophysical maps, as well as geochemical maps of trace element assemblages on a very broad scale. Compilation and comparison of these maps may enable us to locate target areas and determine their priority for further exploration.

Of all the techniques, geophysical methods are most useful to provide direct evidence of deep crustal structure. A desirable investigation might include airborne gravimeter, magnetometer and gamma-ray spectometer, plus a few seismic refraction and magnetotelluric profiles. As deep seismic sounding is particularly expensive in mountainous areas, potential field methods are more attractive for studying deep structure with a large areal coverage.

The second stage, called detailed reconnaissance within the selected areas, is aimed at progressively locolizing the target areas, possibly locating potential orebodies and maybe drilling to verifying their existence. It is also possible to reject a project in time during this stage if some target areas are not so promising. Techniques with higher cost may be employed, such as infrared scanning, multiband photography, and airborne EM in some favourable areas. Potential field methods are usually used, both for direct location of certain kinds of metallic deposits and for studying lithologic units and secondary mineralizing structures which exxert geological local control of orebodies. Because airborne surveys may miss some anomalies due to the relatively high

flighting height over rugged terrain, ground surveys are usually employed to sort airborne data as well as to track down airborne anomalies. This stage is comparable to two stages of Nicholls' divisions: the project reconnaissance which mainly employs airborne surveys and the project follow up which employs ground surveys. As airborne electromagnetic mrthods are often limited, owing to problems associated with rugged topography, a flexible combination of geological, geophysical and geochemical ground surveys may be used instead to progressively localize the areas of interest. Thus the two stages may be joined.

If the probability of discovering economic orebodies is high in several target areas and some exposed orebodies have already been found, a small amount of drilling may be worthwhile and therefore improved transportation facilities may be necessary. How to locate accurate spots for drilling is essential for reducing the exploration cost and should be an important task of data processing.

The last stage, the preliminary exploration, is to verify the existence of certain orebodies and approximately evaluate their reserves. As mentioned before, detailed exploration may be unnecessary for our evaluation purpose. With a few drill holes available, digital data processing and borehole geophysical surveys become the major tools for fulfilling the tasks. If sufficient reliable information has been obtained showing that the value of verified orebodies in a minerogenetic subprovince approaches the minimum cost of the exploitation, blueprints of mining industry development in the areas may be drawn up.

Let us now examine tha tasks of potential data processing at each stage in evaluation of base-metal minerogenetic subprovinces. During the first stage, the task of gravity and magnetic methods is recognition of deep crustal structures, especially deep mineralizing faults. It is well known today that the long aeromagnetic lineaments are very useful indications of deep crustal faults which may extend all the way down to the Curie point and to the bottom of

the upper crust. The Bouguer gravity map contains information about the lower crust and the Moho discontinuity, as the gravity field decays slower than the magnetic field. In order to locate deep crust structures, techniques for separation of regionals and residuals are first needed; then we may use field processing tenchniques to distinguish crustal patterns in some profiles and downward continuation to locate the horizontal position of deep mineralizing faults.

At the second stage, we need to locate lithologic units and secondary structures which have strong local control of ore deposition and to estimate the horizontal range of potential orebodies for drilling. Separation of regionals (due to broader structures) and residuals (due to orebodies) is again required, while downward continuation becomes significant for locating horizontal projection of orebodies and lithologic units because anomalies observed on irregular terrain often shift away from the position of their causative bodies due to the effect of topography.

High topographic relief in crystalline terrane can produce undesirable aeromagnetic anomalies which obscure anomalies caused by deeper geologic sources. Upward continuation of the anomalies may reduce the topographic anomalies but an entire removal of these anomalies may require an accurate computation of the magnetic anomalies.

At the third stage precise data analysis should be involved as we try to evaluate reserves with only a few controlling drill holes. Accurate calculation of potential fields and inverse techciques are essential while models of computation should consider all available geological, geophysical and geochemical information.

We may summarize our discussion as follows.

(1) A reliable evaluation of mineral resources within mountainous minerogenetic subprovinces is necessary because in many cases expoitation of

mineral deposits can be beneficial only if transportation and power supply systems can be shared by a certain number of mines. The evaluation may to some extent affect the long-term economy of a country or a large district.

(2) As a big research project, the evaluation itself involves certain risks of ineffectual investment. Based on commonly accepted principles of exploration and experiences, a strategy comprising three stages - the preliminary reconnaissance, detaild reconnaissance and preliminary exploration is suggested for reducing the total exploration cost and protecting investors from serious risks.

(3) Potential field methods play an important role in locating both deep crustal structures and local mineralizing faults, in locating horizontal ranges of potential orebodies for drilling and in evaluating reserves of magnetic or high-density orebodies.

(4) As field data are acquired at relatively higher cost and each step in the evaluation requires data processing results of the previous step, the technology of digital data processing is an important factor for the achievement of an evaluation project. Application of more sophisticated and expensive data processing techniques is worthwhile and can be of great value because the increasing cost for data processing is usually small in comparison with the economic benefits.

(5) At different stages, flexible integration of various data processing techniques is necessary, as each stage has different exploration aims. Techniques for accurate decomposition of regionals and residuals, continuation of potential fields from arbitrary surfaces, accurate computation of potential fields and inversions are the major data processing tools for the evaluation purpose.

In short, the task of evaluating base-metal subprovinces challenges potential field data processing to face some dificult problems. In order to meet these challenges, we shall review the current techniques of potential data

processing and explore what kinds of techniques should be further developed.

Chapter II

A Brief Review on Current Techniques of Potential Field Data Processing

Since the 1950s, the rapid development of computer sciences has provided powerful techniques for potential field data processing. The theoretical foundation for integrating data processing and interpretation has been developed and new computational methods incorporated into software program packages have become routinely available. Some of these computational methods are no longer restricted by assumptions that source models must be homogeneous in physical properties, or regular in geometry. A unified theory for geophysical data inversion has been developed which takes into account the limitations of real data and is characterized by almost complete automation. However, some intricate problems still remain and more sophisticated techniques are needed. For instance, most linear transformatiom procedures are based on the assumption of flat observation planes. They are inapplicable for our purpose as we want to evaluate mineral resources in mountainous areas. In order to show how many techniques can be integrated in our software packges for the evaluation and what kinds of techniques are still lacking and needed, a brief review of the development of potential data processing and inversions during tne last three decades is desirable. As we mentioned in the previous chapter, we shall outline the linear transformation of potential fields, regional-residual analysis, modelling and inversion, underlining some unsolved problems. The review will be also restricted to exploration and regional geophysics in order to avoid becoming involved in the much broader subject of tectonophysics.

2.1 Potential field linear transformations

The application of linear transformations was one of the important achievements in potential field data processing during the 1960s. Theoretically it reveals that the operations of derivatives, continuation, smoothing, and conversions between different field components, as well as between gravity and magnetic components due to the same sources, employ as a common tool the linear transformation, which is directly related to digital deconvolution filtering. In practice, this technique has yielded several valuable and economical approaches which are useful not only for the enhancement of specified features of the fields, but also for direct interpretation. The downward continuation for magnetization mapping (O'Brien,1970) and for determination of underlayer undulation (Gerard and Debeglia, 1975) could be taken as examples.

Although Nettleton (1954) mentioned the filtering effects of operations and Swartz (1954) made use of the Fourier integral with the spectral representation of potential data, the first definitive and complete description of linear filtering may be attributed to Dean's paper (1958). Dean compared the operations with electrical filters and pointed out that the main advantage of analysis in the frequency domain is "the equations describing these geophysical problems are often much simpler when expressed in frequency terms", because, based on tne convolution theorem, "the Fourier transform technique still reduces the differential and integral equations to algebraic frequency equations." After Dean, Danes and Oncley (1962), Byerly (1965), Mesco (1966), Darby and Davies (1967), Fuller (1967) and many others continued in a similar vein. Their efforts focused on analysis of the frequency response of existing grid operators and design of new operators in the frequency domain to improve their performance. For magnetic data, Baranov (1957,1964) proposed a new procedure called reduction to pseudo-gravimetric anomalies and to the

magnetic pole. Bhattacharyya (1965) represented these operations in terms of two-dimensional harmonic analysis. In 1969, only four years after the fast Fourier transform (FFT) algorithms appeared, Black and Scollar, as well as some others, presented practical instances to show that with the help of FFT algorithms, all linear transformations could be carried out in the frequency domain easily and economically.

There are still two procedural approaches adopted by different individuals today. One is to employ spectral analysis for filter design, then transform the filter back to the space domain and calculate the matrices which are used later in convolution calculations. Baranov's monograph (1975) offers a complete description of this procedure as well as the theoretical foundations of potential field transformations. Another approach is to carry out calculations in the frequency domain, only finally transforming the results to the space domain. The latter seems more popular these days, especially for multi-function processing of large amounts of data, because it takes the advantage of the speed of FFT algorithms. Gunn (1975) presented a unified description of the theory of many possible transformations of gravity and magnetic fields in a comprehensive summary of potential field transformations. He showed equations for potential fields both in the space and frequency domains and summarized the linear transforms as follows:

> *"The spectral representation of gravity and magnetic fields shows that the mathematical expressions describing these fields are the results of convolution of factors which depend on geometry of the causative body, the physical properties of the body and the type of field being observed. If a field is known, it is possible to remove or alter these factors to map other fields or physical property parameters which are linearly related to the observed field".*

The linear transformation techniques in potential data processing are based on the assumption that the potential fields can be treated as 2-dimensional functions; in other words, the observations are assumed to be

carried out on a horizontal plane. For surveys in mountainous areas, the theory becomes inapplicable. A procedure called the reduction to a level has therefore been proposed which is somewhat similar to the problem of continuation between general surfaces. Henderson and Cordell (1971) employed finite harmonic series for this problem. The measurements observed on an irregular surface may be expanded by using a harmonic series with an exponential modulation factor. The coefficients of the series may be determined by solving a set of simultaneous algebraic equations. Consequently the approximate fields on a horizontal plane can be obtained by the inverse process, i.e. summation of the series through multiplication with constant factors. Unfortunately the method provides satisfactory solutions only for weak topographic relief. Parker and Klitgord (1972) made use of the Schwarz-Christffel transformation for upward continuation of magnetic data taken near the bottom of the ocean. This approach can be employed only for 2-D fields. Syberg (1972) discussed the problem and deduced formulae for general continuation, based on which a procedure making use of the FFT algorithms was proposed. Unfortunately, the formulae may be neither mathematically strict nor applicable in terms of FFT algorithms.

In 1977, Bhattacharyya and Chen found another use of general continuation - that the reduction of aeromagnetic data to a surface parallel with topographic relief had the advantage of supressing the interference due to terrain-derived magnetic effects. They introduced a method named the 'equivalent source' method, which is not restricted to weak topographic relief. The equivalent source distribution on an arbitrary surface is expressed by solution of a Fredholm integral equation of the second kind, which can be solved by an iterative procedure with fast convergence. Thus the potentials above the surface may be obtained by employing numerical integration. The problem with this method is the expensive numerical intergration process

repeatedly involved. We will show , in Chapter 4, that a compact succesive approximation computational model together with an improved integration algorithm may be used for efficient continuation.

Essentially downward continuation belongs to inverse problems. Thus the Backus-Gilbert (BG) method may provide the best procedure because the non-uniqueness of inverse problems can be treated by the BG method via the concept of trade-off (Backus and Gilbert, 1967,1968,1970). The early work was done by a French group (Courtillot, Ducruix and Le Mouel, 1974-1975) who coupled the BG theory to a representation of potential functions. The approach is efficient but, as the authors acknowledged, inapplicable for continuation close to sources. Huestis and Parker (1979) provided some methods for both upward and downward continuation based on the BG theory which allow one to assess the ambiguity caused by the deficiency of data. The mathematical treatment is elegant but the criterion chosen for optimization results in a practical procedure with high computational cost. In Chapter 4 we shall use a subset of the generalized inverse method or spectral expansion method for downward continuation of potential data measured on an irregular surface, which improves the computational speed and enables us to continue potential field data to a plane close to the causative bodies.

2.2 Decomposition of regionals and residuals

A gravity or a magnetic map is seldom a simple picture of a single, isolated disturbance, but almost always is a combination of relatively sharp anomalies, which must be of shallow origin, and of very broad anomalies which may have their origin at depth or be of considerable size. Therefore decomposition of a potential field map into regionals and residuals is frequently

required before interpretation. In order to judge how many components are present in a map and what kind of features they have, procedures for analysis of field characteristics are needed. Then the decomposition can be done according to the particular featurs present. Before the 1960's, the decomposition method, regardless of whether it was graphic or numerical, served as an interpretational aid to emphasize or enhance certain components while suppressing others, but not actually removing them. Several new approaches have been since proposed; they are (1) trend surface fitting, (2) linear filtering and (3) computer modelling.

Mathematically, trend surface fitting proceeds under the assumption that the regional field can be expressed by a mathematical surface which may be ordinary polynomials (Coons et al,1964), orthogonal polynomials (Grant,1957; Van Voorfis and Davis,1964), or Fourier series (Bullard et al,1962). A least squares fit minimizing the sum of residual anomalies is often carried out to determine the potential field surface which is assumed to be the "optimal" solution for the regional field. Nevertheless, the closeness of the fit depends on the degree of the polynomial used and there is no reliable criterion to determine the best degree.

Some statistical models have been designed for field decomposition by using linear filters. Under the assumption that the fields consist of useful component plus white noise, Clarke (1969) suggested the application of Wiener filter theory to smooth potential field data. The power spectra are simply separated into signal and noise components so that the latter can be erased in the frequency domain. The procedure is combined with second derivative and continuation filtering to deppress undesirable noise. Strokhov (1964) tried to devise a linear filter which gave a best (least-squares) fit of a smoothed spectral estimate to the actual spectrum over all frequencies, while suppressing the 'noise' by a prescribed amount. Naidu (1966,1967) applied Strakhov's approach

and extended it to 2-D data processing. In most cases, the signal-plus-white-noise models may be too simple to represent actual potential fields, especially a gravity field which usually contains strong non-random components.

Experience seems to show that any approach for anomaly decomposition based purely on mathematical assumptions would not succeed without some physical interpretation. Second derivative and upward-continuation maps are commonly treated as the residual and regional anomalies respectively, since they also contain recognizable physical features. During the 1970's, power spectral analysis methods which attemped to endow decomposition procedures with some physical meanings showed significant promise. We ought to mention the contributions of some authors who revealed a causal connection between the source depths and the slopes of a logarithmic spectra (Odegard and Berg ,1965; Bhattacharyya and Spector,1966), which was later used as a basis for anomaly separation. In 1970, Spector and Grant put forward an attractive statistical model for anomaly-decomposition, based on the postulate that the expectation value of the power density function is equal to the ensemble average of the power density functions of individual anomalies. This model also assumes that the parameters of prism-like sources have a uniform distribution. Under these restrictions a reasonable criterion was proposed to recognize regional components from the power spectra. Syberg (1972) suggested a similar procedure called a 'matched filter' which emphasized the difference between pole-type regional sources and dipole-type residual sources. Cassano and Rocca (1975), Cianciara and Marcak (1976), Hahn (1976) and Pedersen (1978) advanced the discussion of these statistic models.

Although the spectral factorization techniques have been widely accepted for aeromagnetic data processing, when they were applied to regional gravity decomposition, Gupta and Ramani (1980) found that they could produce less

satisfactory maps than traditional graphical methods. Of course, this is not because the analytic methods are worse than empirical ones, but because the analytic models involve some inappropriate assumptions. In the residual maps produced by spectral approaches, the negative anomalies are unreasonably strong while the positive anomalies are ofter too small in amplidute. In fact this bias may be inherent in spectral approaches as the spectra of regional and residual anomalies usually overlap tightly. Another drawback is that the procedures are not flexible enough to allow some geological information to be considered. In order to reduce the negative residual anomalies, Rao et al (1975) suggested a successive approximation procedure in which negative anomalies were artificially erased. The procedure may improve the residual maps, but the basis of erasing was not convincing. Anyway, the analytic methods for anomalous decomposition need to be improved and will be discussed in Chapter 3, where we apply the finite element method and other techniques for better separation of the anomalies.

In an area where geology is well-known, computer modelling may provide the best decomposition of anomalies due to different types of sources. Bullard (1967) and Lange and Farguhar (1969) have given some examples to show the aspects for consideration. Proper models can be suggested if seismic data in the studied areas is available. Unfortunately, sufficient seismic data may not be available in most cases; therefore, it is often difficult to give proper models for regional field sources.

2.3 Calculation of potential fields

As we mentioned in the previous chapter, potential field calculation is an important tool for both data processing and interpretation, as well as for

evaluation of reserves of magnetic or high-density orebodies. With the aid of digital computers, the calculations of gravitational effects due to arbitrary shaped but homogeneous density bodies can be perfectly realized. A general body may be cut into many prisms (Danes,1960) or horizontal laminae which are approximately represented later by closed polygons (Talwani and Ewing, 1960). The gravity effect of the polygons can be evaluated in terms of analytic formulae. The problem of calculating the gravity field of a causative body having arbitrary variation in density was confronted in the 1970s and solutions were published by some authors. An interesting example was given by Fuller (1977) who applied Fourier transforms to compute the gravity anomaly due to a actual ore deposit. The spectrum of density distribution at different levels was evaluated first, then the spectrum of the gravity anomaly (which equals an integration of the density spectra along the depth) was transformed back to the space domain. Based on the property that potential fields due to a general body may be expressed as a convolution of Green's function with magnetization or density distribution within the body, Bhattacharyya (1978) introduced formulae for calculation of potential field anomalies due to an irregular body with inhomogeneous physical properties. This procedure is efficient because high speed FFT convolution algorithms can be employed.

Regardless of demagnetization effect, the calculation of magnetic anomalies due to finite 3-D bodies is similar to the gravity calculation. Bott (1963) and Talwani (1965) have given procedures for computation of magnetic anomalies due to irregular polygonal laminae and proposed fast algorithms. For inhomogeneous magnetized sources Bhattacharyya's algorithm (1978) may be employed as mentioned before. Difficuties arise when one considers the effect of demagnetization, which can vary everywhere inside a strongly magnetized body, depends on the geometry. Vogel (1963) suggested a lenghty iterative procedure for this problem. Sharma (1966) proposed an improved method for

estimating the demagnetization effect. Filatov (1969) proposed another method to calculate the magnetic anomalies caused by the magnetic charge density on the surface of magnetized bodies. The density can be exppresed by a Fredholm's integral equation of the second kind whose solution may be obtained again by using an iterative procedure. The assumption of homogeneous magnetization is implied in order to cancel the magnetic charges within the bodies. There are few publications on computation of magnetic field within a source region, which is an interesting topic in magnetic well-logging. Physically all current methods of magnetic field calculation are based on the theory for paramagnetic materials but most igneous rocks and ores belong to ferrimagnetic materials. Thus demagnetizing models considering the permanent magnetization should be developed for accurate megnetic field computation; which will be discussed in Chapter 5.

2.4 Inversion techniques

Before the 1950s, the inversion methods were founded on the assumption that sources were isolated and regularly shaped. Some characteristics of anomalies, such as horizontal distances between extreme or half-maximum points, projection of straight portion and slope etc, were used to estimate the top depth of the causative body while vertical and horizontal derivative maps were commonly employed for evaluation of the horizontal dimensions. Trial and error methods could be used to find the source distributions with the aid of many kinds of characteristic charts or graticules, but only for 2-D models. The computer revolution after the 1950s made a significant impact on inversion techniques for potential fields. Since then, a great number of articles on this subject have been published advocating automatic or semi-automatic methods.

As an aid to discussing the development of computer-aided inversions, we may classify them into classical methods and BG approaches. The distinction between the two involves considerations of the deficiency and inaccuracy of geophysical data and the non-uniqueness in geophysical inverse problems. The modern methods take account of these aspects and provide measures to assess the significance of a particular solution, whereas the classical methods do not. The geometry used for inversion of causative bodies may also be classified into two types: an isolated body or a single interface structure (multilayer models are mainly for studying global anomalies). We start with the classical methods in the order of Fourier approaches, then discuss matrix methods and automatic least-squares fitting.

The Fourier approach for single interface structure such as basement surface and the Moho-discontinuity was first used in terms of downward continuation and based on the principle of the equivalent stratum (Grant and West, 1965), i.e., a small undulation of the interface is approximately proportional to the anomalies at a level equal to the average depth of the interface. Spectral analysis based on statistic source models, for example, given by Spector and Grant (1970), may be used for determination of the average depth. Then downward continuation can be employed to produce the field at the average level. This approach was developed for underground interface mapping by Gerard and Debeglia (1975), Hahn et al. (1976) and others. Gerard and Debeglia provided a systematic procedure to map basement topography under the assumption that the variation of basement depth is approximately represented by a Guassian (or rectangular, triangular) probability density function. Thus the mean depth and its standard deviation can be evaluated by the least squares fit to logarithmic power spectrum. An iterative technique including downward continuation may be used for computing local depths. The premise that the variation of depth is proportional to the vertical field

component can be correct only if the maximum of the variation is much smaller than the mean depth. In many cases, this assumption may not suit actual geological structures. In fact in the frequency domain the variation of interface equals the potential anomaly at the average level plus another term which includes some high order effects of the variation (Parker,1973). Arranging Parker's forward algorithm used for the rapid calculation of gravity anomalies due to a 2-D density interface, Olderburg (1974) developed an iterative scheme which produces improved solutions without the limitation of variation depth. The convergence of the iteration was empirically assured for well-behaved surface functions. The method takes advantages of the FFT algorithms, but computational time is dependent on the speed of convergence.

Spectral inversions for single potential anomalies was first suggested by Odegard and Berg (1965), and developed by Sharma, Geldart and Gill (1970) , Eby (1972), Bhimasankakam (1977) and many others. As the spectral representations of isolated anomalies are usually much simpler than those in the space domain, the parameters of sources can be evaluated even without the help of computers. Bhattachayya and Leu (1975,1977) showed that the spectra may be expressed by a sum of exponentials multiplied by some constant factors. Each exponential contains in the exponent the location of one edge of the causative prism-like body. The exponential terms may be expanded, so the equations can be reduced into a linear system. Thus the solution for unknown exponents can be determined by employing linear numerical subroutines. Based on spectral analysis, Teskey (1978) introduced a interpretation system for 3-D magnetic anomaliy inversion. As the inversion for 3-D anomalies is much more difficult than for 2-D anomalies, a method for reducing 3-D anomalies to equivalent 2-D ones was published by Yang (1979). Yang pointed out the spectral connections between potential anomolies due to general 3-D bodies and due to corresponding 2-D bodies which may result in simplifying 3-D anomaly

inversion by proper application of the 2-D inverse techniques.

The spectral approaches enjoy the advantages of efficiency and simplicity, but they usually assume flat observation planes so that the fast Fourier transform algorithms may be used. Hence, these methods can be used for our evaluation purpose only if the observations have been continued onto flat planes. Once more we meet the problem of continuation of potential field from arbitrary surfaces.

Among the linear approaches, the matrix method proposed by Bott (1967) has been applied successfully to magnetic inversion for a particular problem of estimating the magnetization of under-ocean layers whose boundaries are known from seismic data. In this approach the linearity of potential fields with respect to magnetization or density is applied after the geometry of the sources has been specified. If the goal is to evaluate the geometric parameters of irregular sources the inverse problems will belong to the class of non-linear problems. Thus the inversion in the space domain can be carried out by at least three approaches: (1) specify the source geometry, thus making linear algorithms acceptable, (2) iterate linear procedures to get approximate solutions for non-linear problems and (3) employ least squares fitting, to get the 'optimal' solution of non-linear problems.

Representative work for iterative approximation was published by Tanner (1967) for 2-D models and Cordell and Henderson (1968) for 3-D models. The perturbing body is approximated by a set of rectangular prisms of constant density and its field is calculated. The residuals between the calculated and observed field values are used to adjust the heights of the prisms. The amounts of adjustment can be obtained by solving a set of linearized equations. These procedures are often reliable but suffer the disadvantage of slow convergence of the iteration when the number of prisms is increased.

Automatic iterative procedures for the estimation of paramters of a

selected model that yields a best-fit anomaly curve for a set of observed data have been developed by Bosum (1968), Johnson (1969), Magrath and Hood (1970) and many others. Regular geometry is usually used for the source model to limit the number of its parameters. The parameters can be determined in such a way that the so-called objective function, i.e. the sum of the squares of the deviation of the observed field from the theoretical field, is to be minimized. Since the objective function is non-linear, it may be linearized by assuming the function to be approximately linear within the vicinity of an initial guess of the model parameters. Thus a set of approximate parameters may be obtained by making use of linear algorithms and then adjusted by employing some iterative procedures, such as Newton-Raphson, Marquart, or Powell algorithms. These optimization methods may lead to a satisfactory solution; but which is one of many feasible solutions, in areas where available geological information allows us to give a close initial guess for the source parameters. The initial guess and the type of source model determine the success and the rate of convergence of the method being used, therefore, intuition and prior knowledge for selecting the initial values have important influence in all these methods. The unconstrained optimization in which the parameters vary freely can produce geologically unreasonable solutions if the initial guess is not close to the actual solution.

Disregarding the facts of finiteness and inaccuracy of experimental data as well as non-uniqueness, classical methods attempt to find a particular solution for inverse problems which could be an equivalent representation of actual sources. The equivalent sources may reflect some of the characteristics of the actual sources but they are not identical.

As an important breakthrough, the pioneering work of Backus and Gilbert (1967,1968,1970) revealed the nature of geophysical data inversion. In their first paper (1967), Backus and Gilbert showed the high degree of

non-uniqueness in geophysical inverse problems and offered a practical solution that satisfies the observed data and minimizes the departure from the initial guess for non-linear problems. The process of finding the solution, taking into account the errors in data, was later described by Gilbert (1971). In their second paper (1968), they focused their attention on the resolution in model space and introduced the "deltaness" criterion. Finally, in the third paper (1970), an extensive investigation was made of the trade-off between the ability to resolve detail of a model and the reliability of the estimate of model parameters.

As a powerful tool for inversion, the Backus-Gilbert (BG) theory has achieved increasing importance for inverting different kinds of geophysical data and has been applied to every branch of geophysics. For a mining gravity problem, Green (1975) applied a restricted form of the BG approach in order to find an acceptable model starting from some initial guess. The Lagrange multipliers method was employed for finding final solutions. Oldenburg (1976) applied the BG method to the problem of calculating the Fourier transforms of digitized data with the objective of assessing the effects of missing portions of data series and of contamination of signal by noise. The BG method has also be applied to continuation problems by Huestis and Parker (1979).

The BG form of inverse theory assumes continuous parameterisation. A discrete formulation, with a factoring of the problem into eigenvectors and eigenvalues, has been developed for the numerical solutions by many authors (Gilbert 1971; Jackson 1972; Wiggins 1972; Jupp and Vozoff 1975). The formulation is based on the Lanczos' inverse (1961), resulting in the generalized inverse approaches. For ill-posed linear problem, Franklin (1970) introduced the stochastic inverse to mitigate the undesirable effects of instability. If the unknown functions are not well-behaved, imposing some a priori information can be very helpful. Jackson (1979) suggested using a priori data while Sabatier

(1977a,b) using a priori information of positivity of the unknowns. The constraints in terms of pairs of inequalities were applied to the inversion of gravity data (Safon, Vasseur and Cuer,1977; Fisher and Howard,1980). Pedersen (1977) has applied the generalized inversion to determine a single interface of density or susceptibility. In Chapter 4, the generalized linear inverse method will be applied for solving a typical ill-posed problem - downward continuation of potential fields to top of sources.

The powerful formalism of linear inversion has been applied to non-linear inverse problems via linearization (Backus and Gilbert, 1967). Linearization can be successful at discovering an acceptable solution to a nonlinear inverse problem, but sometimes even with sufficient and accurate data a solution is not unique. The iteration of a linearized problem might diverge, or even produce incorrect solutions. The research effort may focus at the formulation of a realistic function which relates observations and physical models and not to the subsequent method of iterating to an acceptable model.

Instead of trying to find unique solutions some authors have proposed rules giving bounds on the depth and density of the causative body (Bott and Smith,1958; Smith,1959,1960). Parker (1974,1975) developed a general theory to provide rigorous limits on the density and depth. He introduced a concept of the ideal body that is a homogeneous body with minimum density which gives rise to anomalies compatible with observed data. Taking account the non-uniqueness of the inversions, the concept of the ideal body, as a particular solution, has been employed by some other investigators (Safon et al.,1977; Cuer and Bayer,1980).

Although great efforts have been made, new inversion methods are still needed as the models, such as a single body with homogeneous physical properties or a single interface , are often too simple to delineate actual geological formations. More advances are required in the complexity of the

mathematical models of causative bodies and in the efficiency and sophistication of inverse algorithms employed.

2.5 Summary

As the current techniques of potential data processing have been reviewed, we are able to suggest some methods as well as to demand some new techniques for advanced researches to meet the challenges of evaluating base-metal mineragenetic subprovinces as follows.

(1) The spectral factorization techniques (Spector and Grant, 1970; Syberg,1972) may be used for decomposition of regional aeromagnetic anomalies; but new computational techniques are needed for decomposition of gravity regionals and residuals as the current methods often fail to produce satisfactory separated anomalies.

(2) Downward continuation fron arbitrary surfaces is an very useful tool in potential data processing for the evaluation purpose in the senses of converting observations onto a flat plane, amplifying hidden anomalies due to high observation levels and localizing the spotting of drill holes for drilling. The Fourier approaches may be inapplicable due to the assumption of flat observation planes. The methods proposed by Huestis and Parker (1979) can be used, but at a high computation cost. Therefore, new techniques for downward continuation from arbitrary surfaces are required which must be able to continue potential fields to top of sources at a reasonable cost. For upward continuation the equivalent source method (Bhattacharyya and Chen, 1977) may be used for data observed on irregular surfaces, but further improvement is also needed.

(3) Many techniques for accurate calculation of gravity anomalies now

are available; but for accurate computation of magnetic anomalies, the demagnetization effect in ferrimagnetic materials should be considered. New tenchniques for calculation of both the internal and external magnetic field due to arbitrary and inhomogeneous magnetized bodies are needed.

(4) Both the classical and BG approaches of inversions can be applied to study the source geometry; the generalized inverse approach is the most favourable. Unfortunately, most inverse approaches assume flat observation planes which may yield some trouble in direct applications for our purpose. Anyhow in principle the generalized inverse and least-squares fitting are applicable for data observed on uneven surfaces.

In short, new methods are required for (1) decomposition of regionals and residuals, (2) continuation from arbitrary surfaces and (3) evaluation of demagnetization and accurate calculation of magnetic anamolies. In the next three chapters, we shall develop some new techniques to meet these demands. Each of the chapters will be devoted to one of the problems, but different chapters may employ some common techniques and share the same examples. Finally, we shall summarize the applications of the new techniques and suggestions in Chapter 6. The departure point for developing new methods includes the following aspects:

(1) Some problems in potential field data processing may be treated as inverse problems if integral equations are involved. The spectral expansion method may then be employed in the data processing stage.

(2) Potential field data processing often deals with forward problems requiring complicated boundaries. To solve them the finite element method seems desirable. The finite element method has been applied in other geophysical methods since the 1970's (e.g. Lysmer and Drake, 1972, Silvester and Haslam, 1972), but has been seldom used in gravity and magnetic methods.

(3) the physical basis of some older processing procedures might use

assumptions which inappropriately simplify physical conditions. These need to be reexamined and if possible corrected.

In this thesis we use the subscripts ~ and – to denote a matrix and a vector respectively.

CHAPTER III

THE FINITE ELEMENT METHOD FOR REGIONAL-RESIDUAL DECOMPOSITION

In this chapter, we consider a computer procedure for the regional-residual decomposition (abbreviated RRD henceforth) problem which simulates the old empirical graphical method. When certain information about the regional field can be inferred from the data, we can obtain boundary constraints for the regional field via several techniques, and then the finite element method (FEM) to estimate the regionals. Both synthetic and practical examples will be given showing that the FE procedure can improve the separation results to a considerable extent.

3.1 ANALYSIS OF THE REGIONAL-RESIDUAL DECOMPOSITION PROBLEM

3.1.1 The ambiguity of the RRD problem

In essence the regional and residual components are merely relative concepts, i.e.'regionals' represent broader and smoother anomalies having deep origins and large extensions whereas 'residuals' means sharp anomalies with shallow origins. As a matter of fact, regionals or residuals may represent different geological structures depending on the areas and targets being studied. It seems impossible to give the precise definition of a general regional or a residual component if the parameters of its source is not exactly known. In some particular cases the 'fuzzy mathematics', as a new branch of modern

mathematics, might be helpful for quantitatively defining the anomalies, but so far there are no such research results published in geophysical literature.

Let us look at the mathematical relations which can be used for the regional-residual decomposition problem. From the viewpoint of potential field theory, the equations governing the RRD problem are straightforward. Firstly, if g denotes the Bouguer gravity anomaly which contains regional g', residual g'' and observation error e, we have

$$g = g' + g'' + e \tag{3.1}$$

where g, g' and g'' are function of x and y, the spatial coordinates. Secondly, we may consider the differential equation which regionals and residuals satisfy. It can be proved that if a continuous function satisfies Laplace's equation, then its partial derivatives are also harmonic functions. Hence, we may use the term "potentials" to represent gravitational or magnetic potential and their derivatives, such as gravity anomaly and magnetic components. No matter which one we deal with, both the regional g' and the residual g'' must satisty Laplace's equation

$$\nabla^2 g' = 0 \tag{3.2}$$

and

$$\nabla^2 g'' = 0 \tag{3.3}$$

Finally, we may consider the difference between the regional and the residual. Because the regional is due to deep sources, it must be much 'smoother' than any residual. This condition can be described by comparing the horizontal derivatives as follows

$$\iint \left(\left(\frac{\partial g'}{\partial x}\right)^2 + \left(\frac{\partial g'}{\partial y}\right)^2 \right) dxdy \ll \iint \left(\left(\frac{\partial g''}{\partial x}\right)^2 + \left(\frac{\partial g''}{\partial y}\right)^2 \right) dxdy \qquad (3.4)$$

Eqs. (3.1)-(3.3) and the inequality (3.4) include all we can write for the RRD problem based on commonly accepted concepts. Obviously a unique solution for this problem does not exist unless some additional conditions are imposed.

3.1.2 The difference between gravity RRD and magnetic RRD

The upward continuation method and the spectral analysis method are commonly used for the RRD problem nowadays. They may produce similar estimates if the continuation height is appropriate. The upward continuation method presumes that residual anomalies decay vertically much faster than regionals so that they might approximately vanish above a certain height. The spectral analysis approach (Spector and Grant,1970; Syberg,1972) assumes that the residuals contain only short wavelength components which could be abstracted from power spectra of potential anomalies. These assumptions may qualitatively describe residual characteristics, but may not be precise enough for quantitative analysis of the gravity RRD problem.

The spectra of gravity and magnetic fields can be expressed by the multiplication of several factors as

$$\Delta g(u,v) = 2\pi G \rho (u,v,h)\ H(u,v,h) \qquad (3.5)$$

$$\Delta T(u,v) = 2\pi\ D_1(u,v)\ D_2(u,v)\ I(u,v)\ m_s(u,v,h)\ H(u,v,h) \qquad (3.6)$$

(Gunn, 1975), where $\Delta g(u,v)$ and $\Delta T(u,v)$ are spectra of gravity and magnetic fields respectively; G is the universal gravitational constant ; ρ is the Fourier

transform of density distribution at a level h while m_s is the spectrum of magnetization distribution at the level h. The other factors are

$$I = (u^2+v^2)^{1/2}$$

$$H = \exp(-h(u^2+v^2)^{1/2})$$

$$D_1 = jLu + jMv + N(u^2+v^2)^{1/2}$$

$$D_2 = jlu + jmv + n(u^2+v^2)^{1/2}$$

where (L,M,N) denotes the direction cosines of magnetization and (l,m,n) denotes the direction of measurement.

If both a gravity anomaly and a magnetic anomaly are due to the same causative body, dividing (3.5) by (3.6) yields

$$\Delta g(u,v) = \frac{(u^2+v^2)^{1/2}}{D_1(u,v)\,D_2(u,v)} \cdot \frac{G\,\varrho(u,v,h)}{m_s(u,v,h)}\,\Delta T(u,v) \qquad (3.7)$$

Equation (3.7) is in fact an expression of the Poisson equation in the frequency domain (Yang, 1979) and is well-known as an operator for converting magnetic fields into gravity fields and vice versa. The equation also shows that the gravity anomalies, including both regional and residual fields, contain a DC component even the magnetic anomalies do not. For a vertically magnetized body and the vertical field component ΔZ, we have, after normalizing the constant factors,

$$\Delta g(u,v) = \Delta Z(u,v)/(u^2+v^2)^{1/2} \qquad (3.8)$$

When $u=v=0$, we have $\Delta g(0,0)\neq 0$ even if $\Delta Z(0,0)=0$. Furthermore, when u and v are small, $\Delta g(u,v)$ can be large even if $\Delta Z(u,v)$ is small, implying that gravity anomalies also have strong long-wavelength components. These facts

conflict with the assumption of spectral analysis method, indicating that this method cannot be as successful for the gravity RRD as for separation of magnetic anomalies. Because the DC component never decays and the long-wavelength components decay very slowly, the assumption of the downward continuation method can be incorrect for gravity residuals.

As a gravity field decays slowly from its source, a gravity regional is often large compared to a residual. Consequently, the appearance of a residual anomaly in the frequency domain can be less clear than that in the space domain. The preceding facts can explain why the older graphical method, although it is subjective and empirical, may produce better solution of the gravity RRD problem than the newer spectral and upward continuation methods. In order to achieve a more accurate decomposition we may simulate the graphical methods by using digital computers.

3.1.3 A computer simulation of the graphical methods

The basis of the graphical methods is the assumption that one can find some Bouguer measurements in the area of interest which contain mainly regionals. These measurements may be interpreted according to the trend of gravity field and available geological information. Since a priori information about the regionals is used, the graphical method may produce more acceptable results. This a priori information could be made use of in analytic approaches as well. In mining gravity survey, we are interested in residual anomalies which are arranged to be near the centre of a survey area, so one may hope to be able to find negligible residuals in the marginal zones. In a regional gravity survey, one can find some part in a contour map with a relatively small field gradient where some boundary constraints for the regionals can be picked up.

If such constraints are distributed along a closed curve, a unique solution for the regional field within the area enclosed by the curve can be obtained. This is the solution of the Dirichlet problem

$$\nabla^2 g' = 0 \qquad (3.9)$$

and

$$g' = g' \qquad \text{on boundary} \qquad (3.10)$$

where g' denotes the regional constraints on the boundary. We may call g' the gravity boundary sequence. Thus, a possible procedure for the RRD problem can be stated as follows. Select some measurements as constraints for the regional field from a Bouguer gravity map, then evaluate the boundary sequence g' by some numerical method. The last step is to solve Laplace's equation using the given boundary sequence to produce a regional estimate. It should be note that the boundary cannot contain a maximum or minimum field value, and so these extremes must lie on the boundary. This problem can be solved if a suitably complicated boundary is selected. If many constraints of the regional field are avaliable, an arbitrary number of closed curves may be applied.

This approach could be dangerous or meaningless if calculations of the internal field amplify the inevitable errors contained in the selected constraints and a useful procedure must therefore limit the propagation of such errors. Fortunately, one technique is available with this property, it is the finite element method (FE method). The FE method is outlined in Appendix I and we will show its advantages for solving the gravity RRD problem in the coming section.

3.1.4 The advantages of the finite element procedure

The FE method for approximate solution of Laplace's equation is based on the well-known principle of minimizing the stored field energy which is given by

$$W(u) = 1/2 \iint |\nabla u|^2 ds \qquad (3.11)$$

(Silvester and Ferrari, Chapter I, 1983) where u denotes the potentials and the integration is carried out over a two-dimensional region S. This minimum energy principle is mathematically equivalent to Laplace's equation, in the sense that a potential distribution which satisfies the latter equation will also minimize the energy, and vice versa. Hence two alternative and practical approaches exist for solving potential field problems: direct approaches , such as the finite-difference method, which deals with the potential itself and the indirect FE method, which minimizes the energy. Since the field energy is generally more stable and less susceptible to influence by noise, approaches dealing with energy may take some precedence.

Suppose that $u(x,y)$ is the true solution of potential and $v(x,y)$ is some differentiable function with zero values at the boundary. If p is a small scalar parameter, the combination $(u+pv)$ represents an incorrect field with energy

$$W(u+pv) = W(u) + p\iint_S \nabla u \, \nabla v \, ds + 1/2 \, p^2 \iint_S |\nabla v|^2 ds \qquad (3.12)$$

The middle term on the right may be rewritten, using Green's theorem, as

$$W(u+pv) = W(u) + p^2 W(v) - p\iint_S v\nabla^2 u \, ds + p\oint_C v\partial u/\partial n \, dc \qquad (3.13)$$

where C is the boundary enlosing region S and n denotes its normal. The third term on the right must vanish, since the exact solution u satisfies Laplace's equation. The last term will also vanish because v becomes zero on the

boundary. Hence

$$W(u+pv) = W(u) + p^2W(v) \qquad (3.14)$$

The second term on the right in (3.14) is always positive. Consequently, W(u) is indeed the minimum value of energy, reached when p=0 for any admissible function v. As a result, if the incorrect potential does not differ very greatly from the correct one, in other words, p is small enough , the error in energy is thus much smaller than the error in potentials. This is an important advantage of the FE method.

As has been mentioned before, gravity anomalies satisfy Laplace's equation. Let the regionals g' replace u and the residuals g" replace v, Eq.(3.13) becomes

$$W(g'+pg") = W(g') + p^2W(g") + p\oint_C g"\partial g'/\partial n \, dc \qquad (3.15)$$

The last term on the right represents the error due to incorrect boundary constraints. In practice, no matter how carefully one selects the boundary constraints, some residuals and noise are inevitably included. In other words, g" can be small on the boundary, but not exactly zero. However, if the gradient of regionals should be small, which has been shown in the inequality (3.4), the last term on the right hand side of (3.15) may be neglected because of the small values in both g" and $\partial g'/\partial n$. Thus (3.15) is a good approximation of (3.14). Consequently, employing the FE method for the gravity RRD problem enables us to limit the effect of errors included in boundary constraints. As a matter of fact, the effect of errors in the boundary constraints are likely averaged within the domain enclosed by the boundary during the execution of the FE procedure. If the error has a normal distribution with zero mean, the averaging might reduce the effect. We shall later show some examples.

The application of the FEM to solve a Dirichlet problem can be found in many texts and is briefly explained in Appendix I. The cost of using the FE procedure is about 5-10 times greater than that of the upward continuation method with fast Fourier transform algorithms, depending upon the size of meshes used.

3.2 SYTHETIC EXAMPLES OF THE FE PROCEDURE FOR RRD

In a mining gravity survey, the conditions required by the FE procedure can often be satisfied without much difficulty. The regional anomalies are usually smooth and relatively strong, while the residuals, which located in the central part of the survey area, may be allowed to vanish on the boundary. We may consider a set of computational examples designed for testing the application of the finite element method.

The basic source model consists of three spheres: a large and deeply buried one is designed to represent a regional source with a contrast mass of $900*10^6$ tons and a depth of 800m and with the centre located below the lower-left corner(Fig. 3.1). The other two represent sources of residuals with masses $4*$ and $2*10^6$ tons, depths 100m and centres at (300m,300m) and (500m,500m) respectively. The study area covers $900*800$ m^2 with measurement interval equal to 100m. The gravity anomalies are shown in Fig. 3.1.a (regional), 3.1.b (residual) and Fig. 3.2 (superposition). The amplitude of the regional is about three times larger than that of the residual. Consequently, features of the residuals do not stand out clearly in Fig. 3.2.

Before using the FE method for the RRD problem, we may see some results obtained by upward continuation. Fig. 3.3 gives the regional estimate by upward continuation as 50m and 200m respectively. By comparison with Fig.

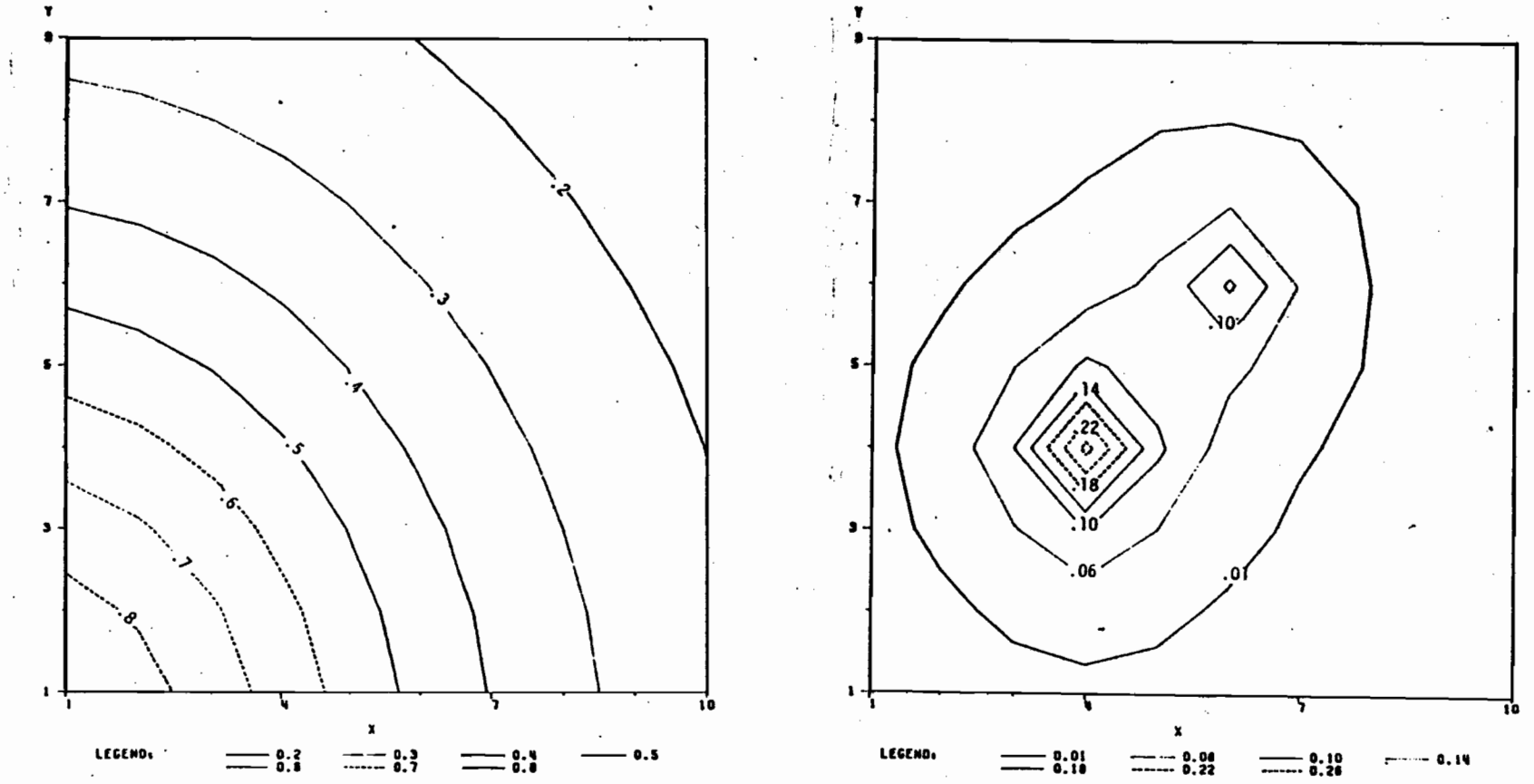

(a) (b)

Figure 3.1. Theoretical gravity regionals (a) and residuals (b). The contours are in mgals, coordinates are in intervals (Δx=100m)

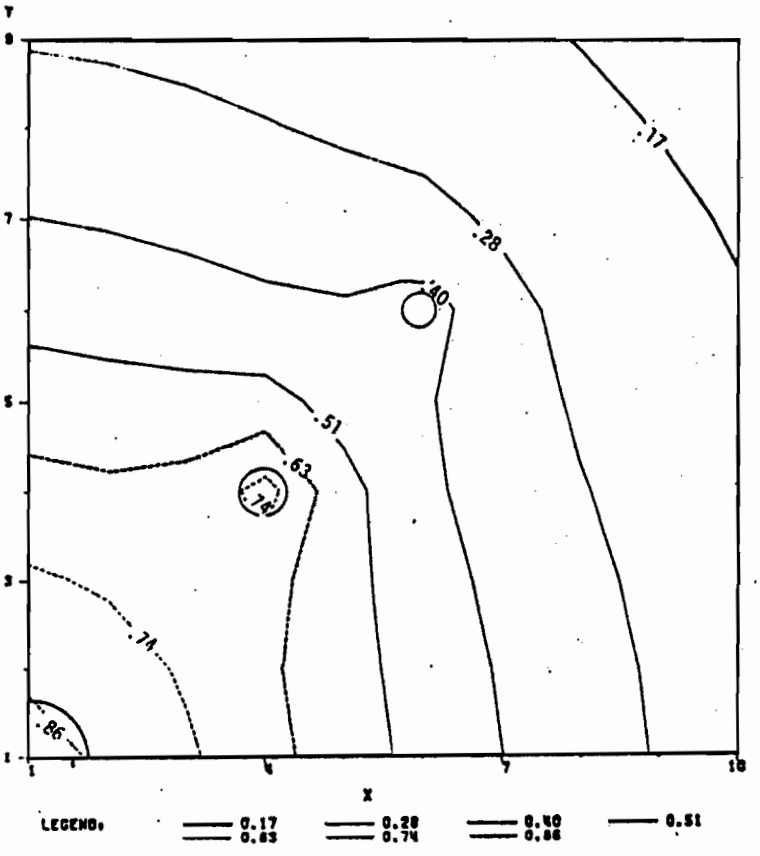

Figure 3.2. Synthetic gravity anomalies due to three spheres. The contours are in mgals and coordinates in Δx=100m.

3.1.a it is clear that these estimates are rather poor as they contain visible residual components. Equivalently, the corresponding residual estimates (Fig. 3.4) contain an obvious regional trend. Thus we see that upward continuation can be inappropriate for gravity RRD problems, especially when survey areas are small.

We may surmise that the FE method could provide better results as the three sphere model approaches the required condition, viz. the residuals are small on the boundary. The gravity data on the boundary of the studied area may be taken directly as the prescribed boundary constraints for regionals. Thus the solutions of Laplace's equation can be obtained by employing the FE method. The regional map resulting from this procedure, as shown in Fig. 3.5.a, is very close to the theoretical one (Fig. 3.1.a). The maximum error in the estimate is less than five percent. The corresponding map of residual estimate (Fig. 3.5.b) is also a good approximation of the theoretical residuals.

As we know, the smaller the observation area, the greater the effect of residuals on the boundary becomes. Thus the size of survey area may influence the FE estimates. In order to see how sensitive the FE estimates rely on the selection of boundaries, we may reduce the survey area to 600*600 m and keep the gravity values on the new boundary as the boundary constraints for regionals. Now the boundary is very close to the third sphere, the second source of residuals, implying that the prescribed constraints contain certain errors. Corresponding regional and residual estimates produced by the FE method are shown in Fig. 3.6. The regional estimate is almost as good as that obtained by using a larger mesh (Fig. 3.5.a), while the residual estimate changes slightly in the two outermost contours which decrease in size with the reduction of the survey area. Herein we see that the FE estimates of regionals and residuals are not very susceptible to the selection of boundaries.

A fact to consider is that the potential anomalies are usually imbedded

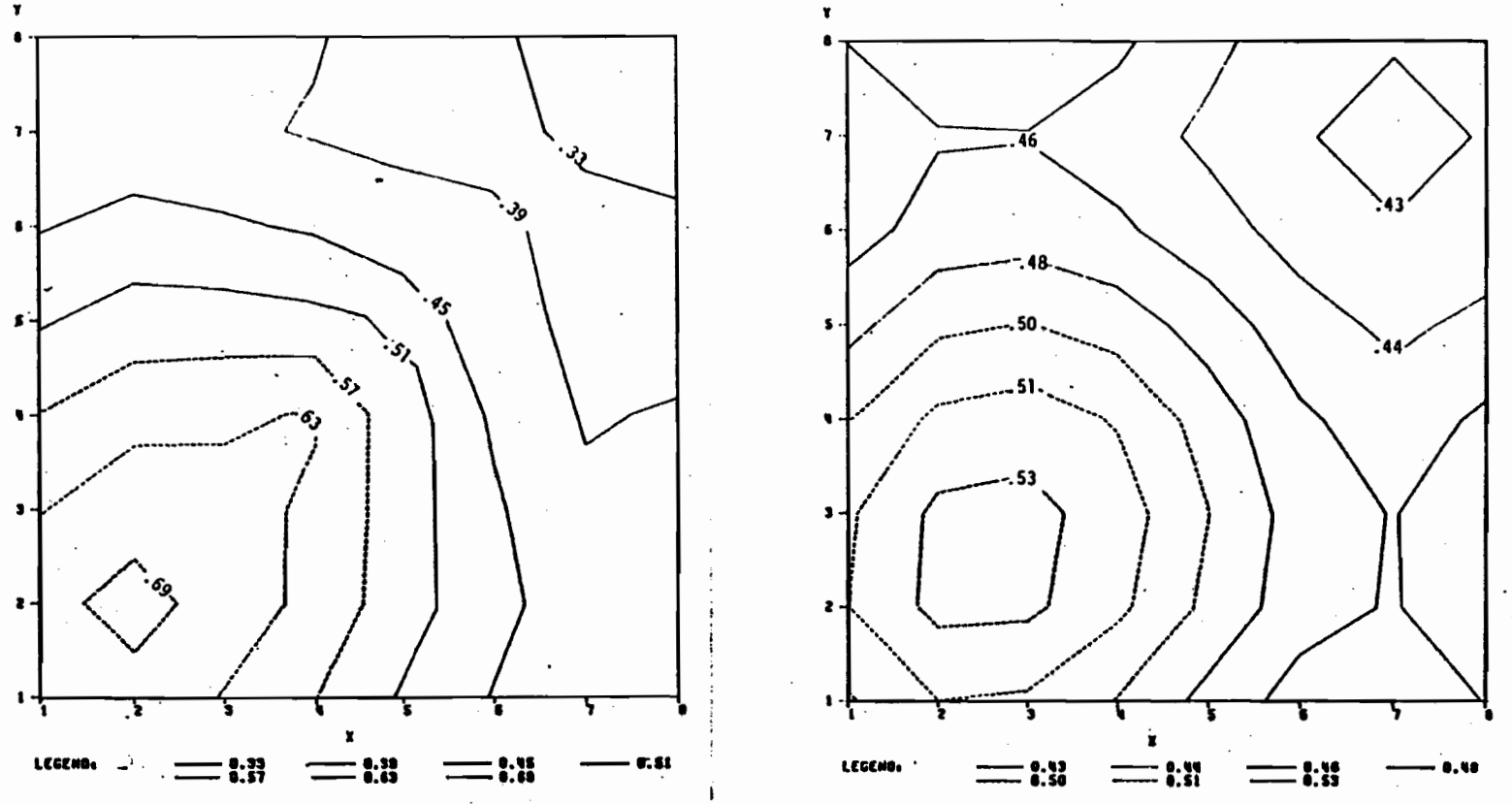

(a) (b)

Figure 3.3. Regional estimates obtained by upward continuation to 50m (a) and 200m (b) respectively.

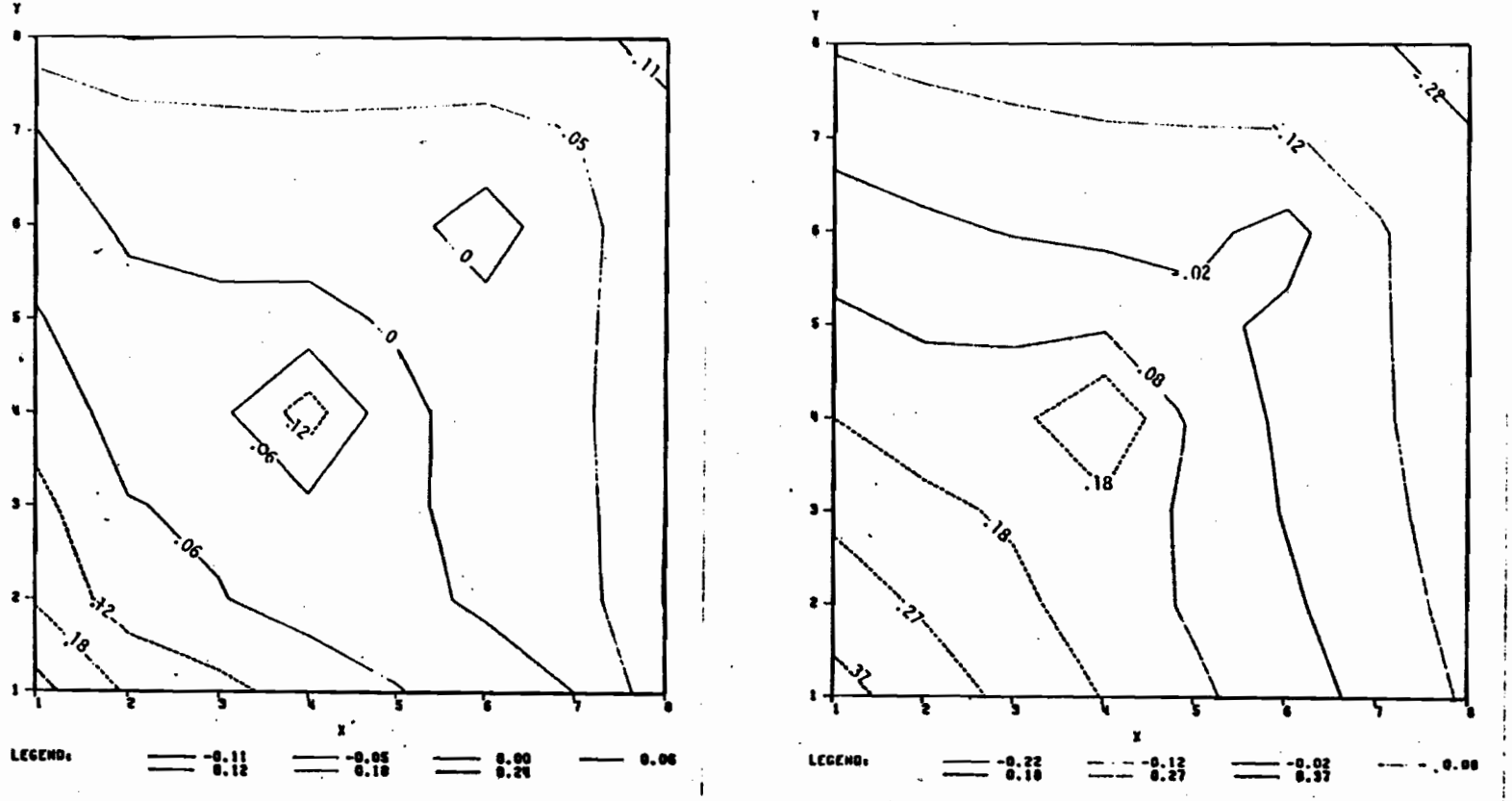

(a) (b)

Figure 3.4. Residual estimates obtained via upward continuation to 50m(a) and 200m (b) respectively.

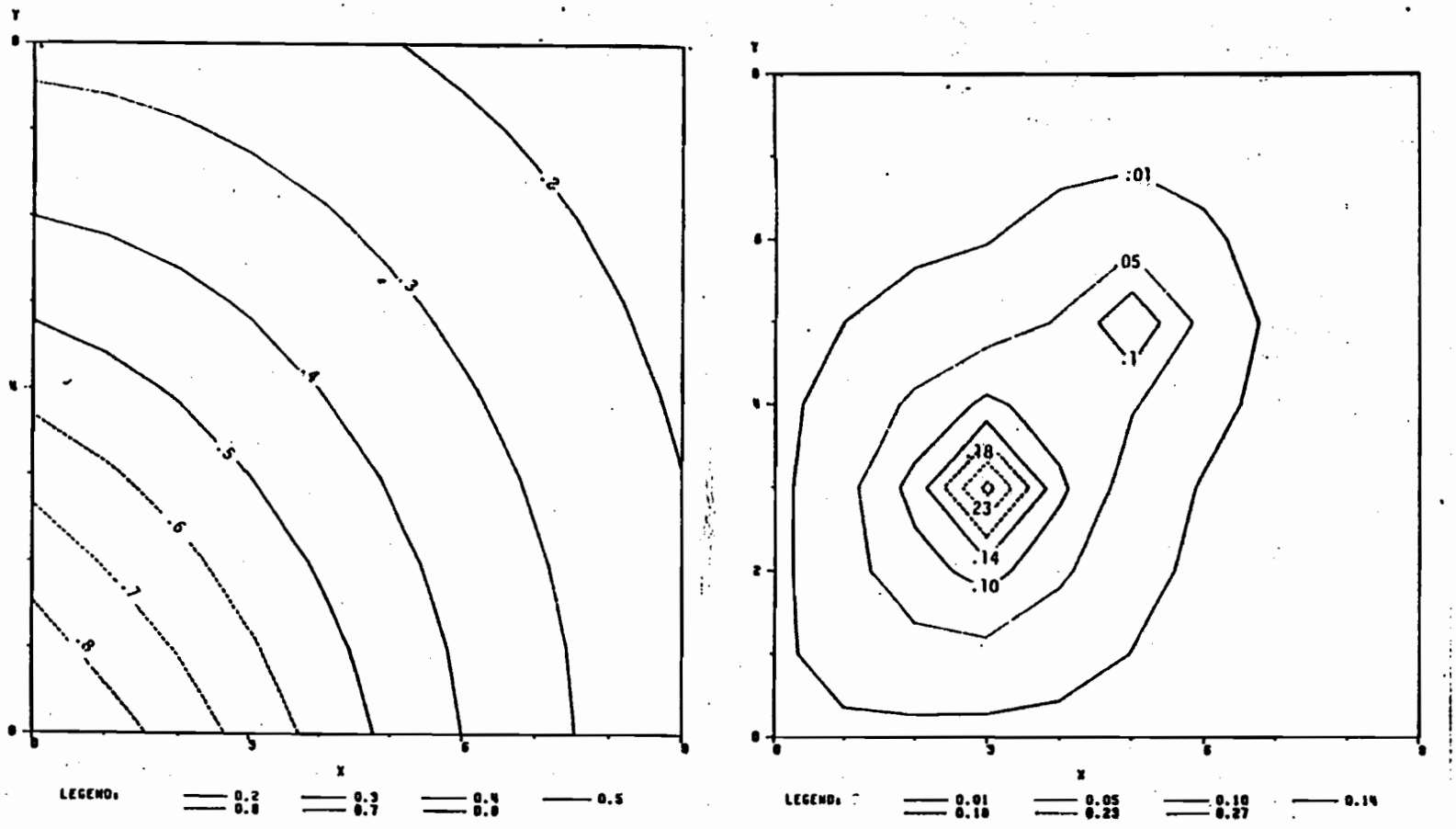

(a) (b)

Figure 3.5. Regional estimate (a) and residual (b) obtained by the finite element method (FEM).

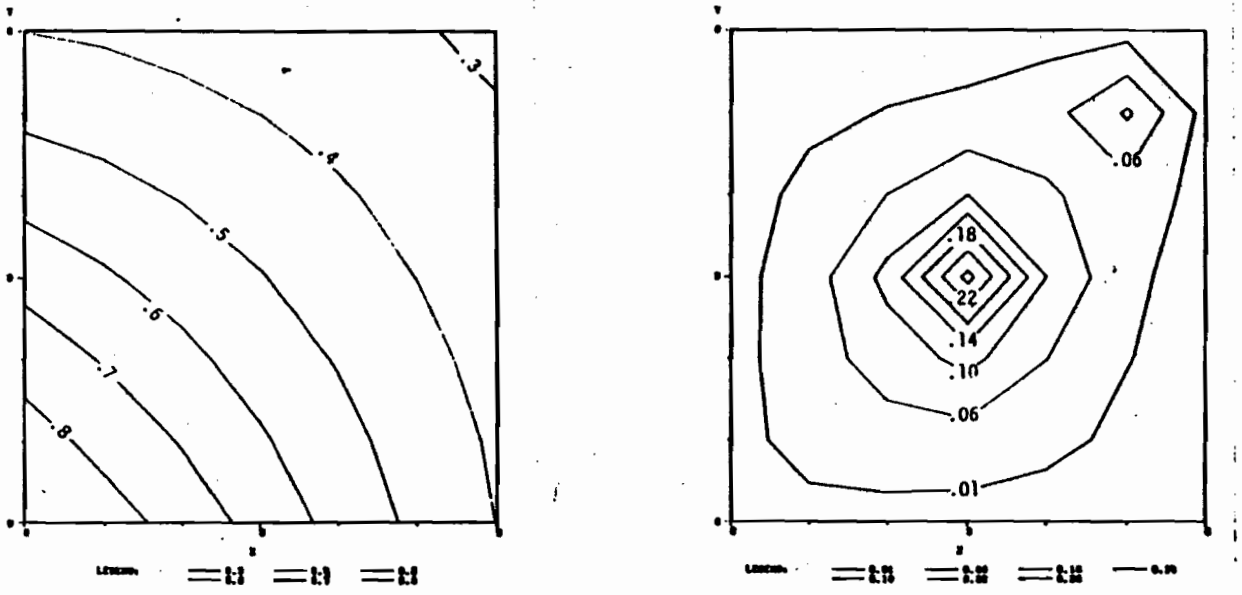

(a) (b)

Figure 3.6. Regional estimate (a) and residual (b) in a small area produced by the FEM.

in random noise. In a gravity survey, the noise comprises observation error and geological noise. Observation error may be modelled as white noise with zero mean. Geological noise is of course dependent upon local geological structures and may have various mathematical representations. For simplicity we may suppose it to be white noise as well. Thus a white noise with zero mean and standard deviation of 0.1 mgal is imposed on the three sphere model, giving a contaminated Bouguer gravity map as shown in Fig. 3.7. In this map it is almost impossible to recognize the actual residual anomalies as the amplitude of noise is comparable with residuals. The contaminated gravity values on the boundary are directly taken as the boundary constraints of regionals, the FE method then produces a regional anomaly map shown in Fig. 3.8.a. It can be seen clearly that the noise level on the boundary decreases with the advancement of the location of regional estimates to the central area. In the corresponding residual map (Fig. 3.8.b) one may easily find the two residuals located above the spherical sources. This result suggests that the residuals in selected boundary constraints could be reduced due to the average effect of the FEM performance as mentioned before. If the selected boundary gravity sequence were smoothed beforehand, additional improvement could be expected.

3.3 TECHNIQUES FOR BOUNDARY SEQUENCE PROCESSING

3.3.1 Selecting new boundaries

So far we did not consider a situation in which some residuals, or possible adjacent disturbances, exist right on the boundary. Suppose there are six causative spheres among which three spheres represent regionals and

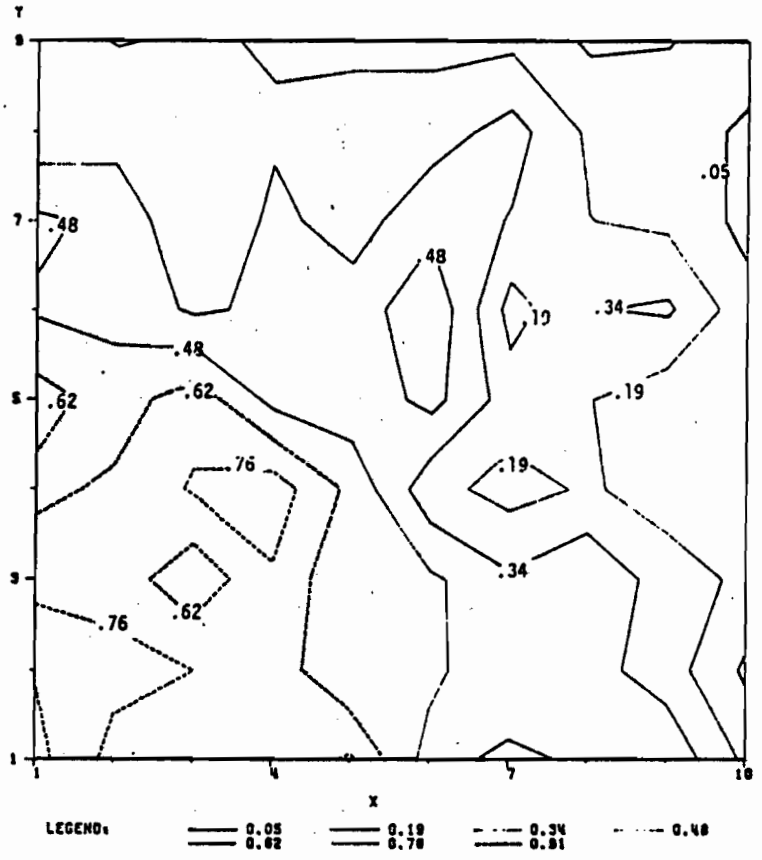

Figure 3.7. Synthetic gravity anomalies due to three spheres plus white noise.

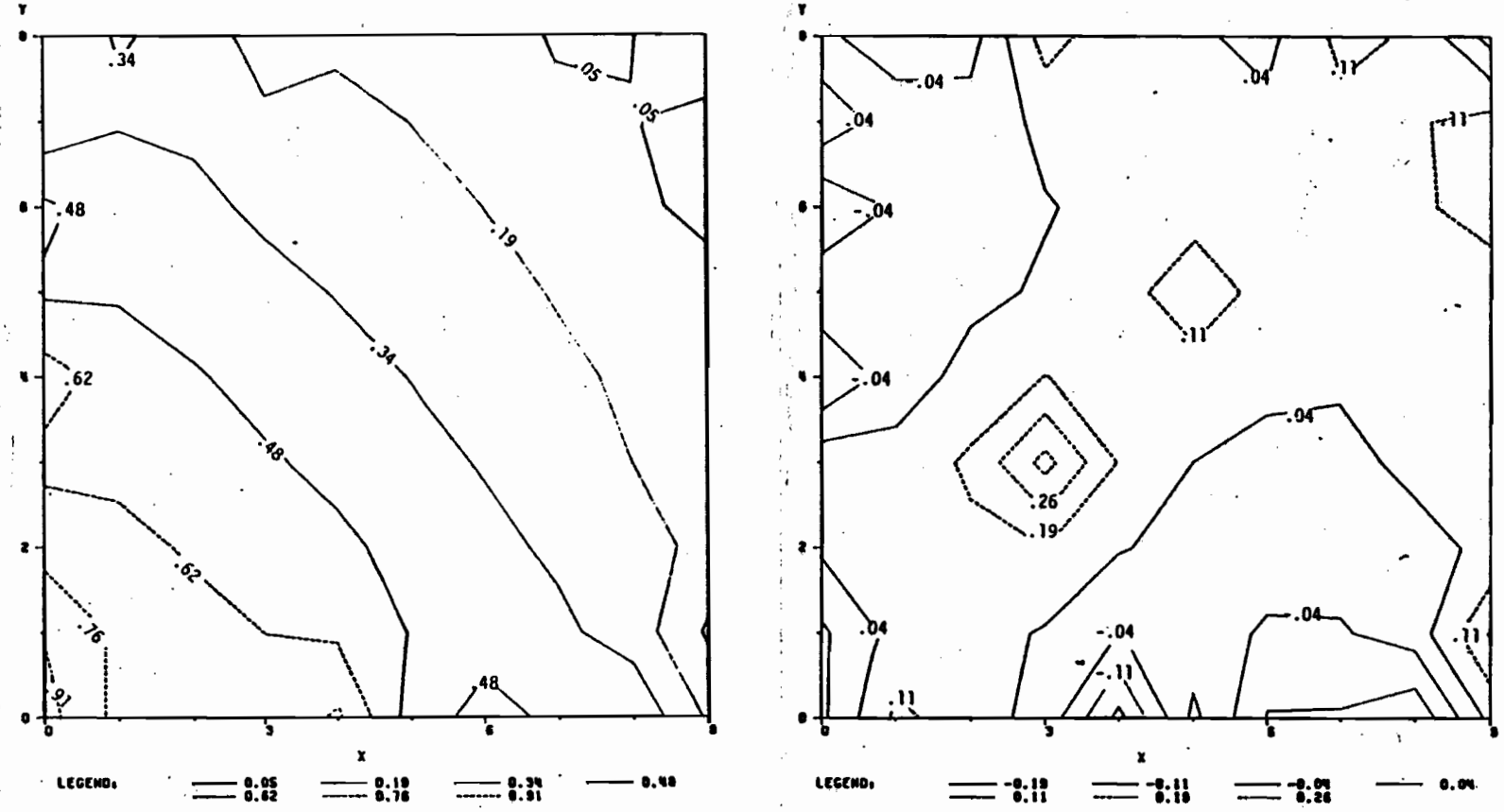

(a) (b)

Figure 3.8. Regional estimate (a) and residual (b) of the noisy anomalies produced by the FEM.

residuals as mentioned before (except the third has been shifted leftwards an interval). The other three spheres, located under the corners of the square area, generate adjacent disturbances (Fig. 3.9). The fourth sphere located under the upper-left corner and the fifth under the lower-right corner each have a mass of 10^6 tons, while the last one under the upper-right corner has a mass of $2*10^6$ tons. The depth of all three spheres is 50m. The gravitational anomalies due to the six spheres are also shown in Fig. 3.9. The residual due to the third sphere is not clear in that map because it is relatively weak.

*A convenient way to separate the regionals by employing the FE method is to select a new boundary to avoid involving disturbances directly. In Figure 3.9, we may choose a square subarea which cuts off the upper and right marginal zones, reducing the area from 800*800 to 700*700 m^2(dash lines in Fig. 3.9). On the new boundary, the effects due to the three disturbances still exist, but are considerably decreased. Taking gravity values on the new boundary as the constraints for regionals yields new regional and residual maps as shown in Fig. 3.10.a and b. Although some noise appears along the boundary, the difference between the estimates and the theoretical anomalies (see Fig. 3.1) is trivial. We note that the selected boundary can be irregular in geometry as to fully utilize available regional constraints. This flexibility is an indication of the power of the FE method, whose advantages should be made use of as much as possible, especially for regional gravity interpretation where plenty of data are available to give many different options for boundary selection. We shall further show some examples in section 3.4.*

3.3.2 The spectral expansion method for circular boundaries

In the case that prescribed regional constraints distribute rather randomly

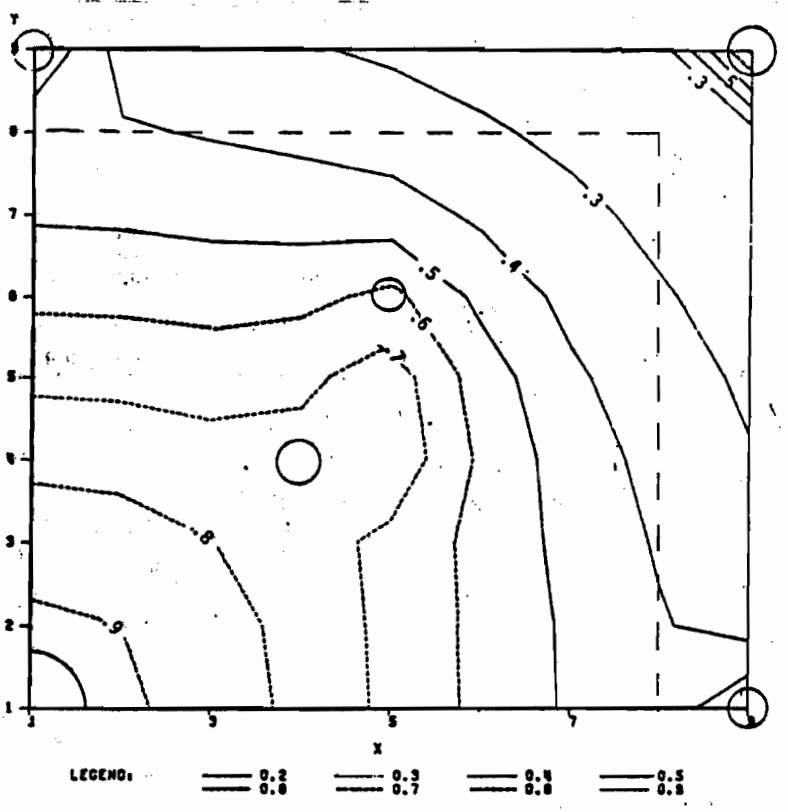

Figure 3.9. Synthetic gravity anomalies due to six spheres.

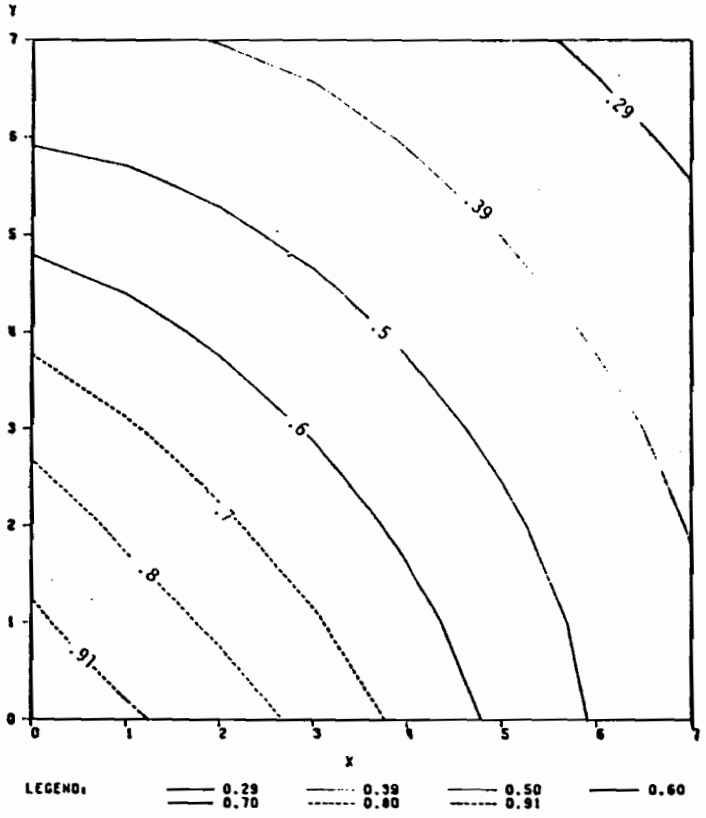

(a)

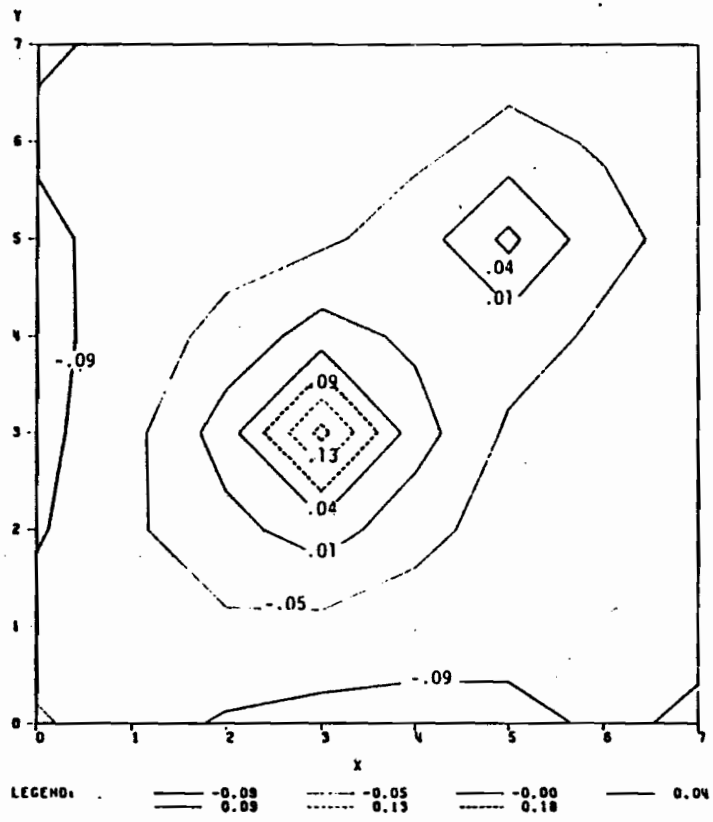

(b)

Figure 3.10. Regional estimate (a) and residual (b) of the six-sphere anomalies produced by the FEM with reselected boundary.

in a large area, it may be difficult to find a closed curve to connect all the constraints together. In order to obtain a complete boundary sequence, we may use these prescribed data to calculate regional constraints on a specified boundary. The calculation is called the boundary sequence processing and a circular boundary may be considered first because of simplicity.

We may choose a polar coordinates (r,θ) and a circle of radius a such that all the prescribed data are located outside or inside the circle (Fig. 3.11.a or 3.11.b). According to the Poisson's theorem, a harmonic function $f(r,\theta)$ either inside or outside the circle $(r=a_o)$ with $f(a_o,\theta)=g'(\theta)$ can be expressed by

$$f(r,\ ) = \frac{|a_o^2 - r^2|}{2\pi}\int_{-\pi}^{\pi} \frac{g'(\hat{\theta})\, d\hat{\theta}}{a_o^2 - 2a_o r\cos(\theta - \hat{\theta}) + r^2} \qquad (3.16)$$

(Duff and Naylor,1966,p.144-145). Equation (3.16) is a Fredholm's integral equation of the first kind when $f(r,\theta)$ is given while $g'(a_o,\theta)$ is the unknown. Provided that we have a set of independent data $f_i = f(r_i, \theta_i)$, $i=1,\ldots,n$, and want to find the boundary sequence $g'_j = g'(a_o, \theta_j)$, $j=1,\ldots,m$, we may write

$$\underline{f} = \underline{A}\,\underline{g'} \qquad (3.17)$$

where vectors

$$\underline{f} = (f_1, \ldots, f_n)^T$$

and

$$\underline{g'} = (g'_1, \ldots, g'_m)^T$$

The matrix $\underline{A}$ is of dimension n by m with elements

$$\begin{aligned} a_{ij} &= |a_o^2 - r_i^2|\,\Delta\theta_j / 2\pi d_{ij} && \text{if } r_i \neq a_o \\ &= \delta_{ij} && \text{if } r_i = a_o \end{aligned} \qquad (3.18)$$

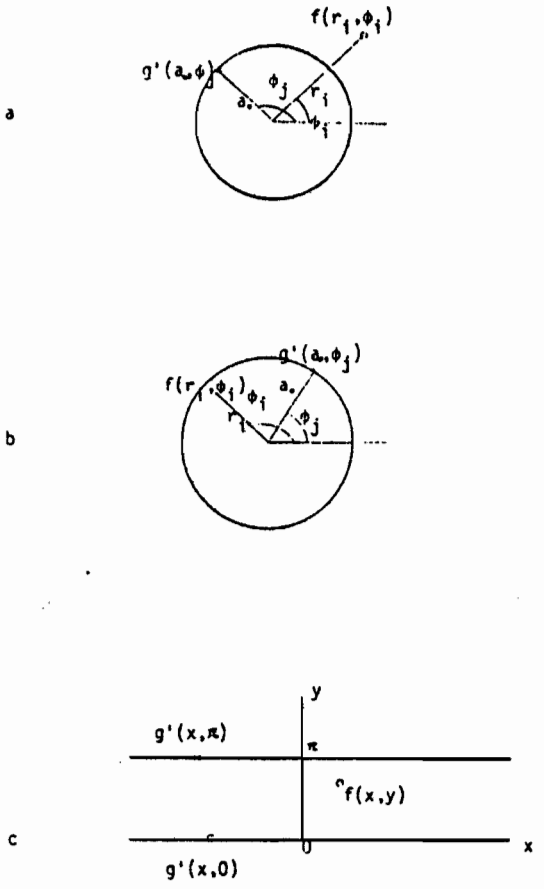

Figure 3.11. Geometry of boundary sequence preprocessing. (a) Circular boundary with external prescribed data, (b) circular boundary with internal data and (c) long-strip region with internal data.

where $\Delta\theta_j$ are the sampling intervals of θ_j, δ_{ij} denotes the Kronecker delta and

$$d_{ij} = r_i^2 - 2a_o r_i \cos(\theta_i - \theta_j) + a_o^2 \ .$$

The constraints on the circular boundary are the solution of the linear system (3.17). Because the coordinates (r_i, θ_i) of the prescribed data are rather arbitrary, matrix $\underline{A}$ can be very close to singular. In such cases the direct inverse of matrix $\underline{A}$ may produces poor solutions. Hence, we suggest to use the spectral expansion approach for a kind of optimal solutions of the boundary constraints. Because we shall use the spectral expansion method to solve such integral equations for continuation of potential fields in the next chapter, here we only outline one of the procedures of the spectral expansion method (the damped least squares). In fact, the boundary sequence processing is more or less identical to the continuation discussed in Chapter 4, in the sense of solving a Fredholm's integral equation of the first kind. Therefore the techniques presented in Chapter 4 can be employed directly for the boundary processing without any difficulty.

A solution for (3.17) can be obtained by minimizing

$$Q = (\underline{A}\,\underline{g}' - \underline{f})^T (\underline{A}\,\underline{g}' - \underline{f}) + \alpha (\underline{g}'^T \underline{g}' - c)$$

where α is a small positive number and c is a constant. Differentiating Q with respect to g' , and, setting the results equal to zero, we have

$$\underline{g}' = (\underline{A}^T \underline{A} - \alpha \underline{I})^{-1} \underline{A}^T \underline{f} \ .$$

where $\underline{I}$ denotes the identity matrix. By factoring matrix $\underline{A}$ into a product

$$\underline{A} = \underline{U}\,\underline{\Lambda}\,\underline{V}^T$$

we get the final solution

$$\underline{g}' = \underline{V}(\underline{\Lambda} + \alpha\,\underline{\Lambda}^{-1})^{-1}\underline{U}^T\underline{f} \qquad (3.19)$$

where $\underline{U}$ and $\underline{V}$ are orthogonal matrices and $\underline{\Lambda}$ is a diagonal matrix of n by n

$$\underline{\Lambda} = diag(\lambda_1, \lambda_2, \ldots, \lambda_m, 0, \ldots, 0)$$

with the eigenvalues λ_i arranged in the decreasing order. The positive number α can be treated as the trade-off parameter.

For the six-sphere model shown in Fig. 3.9, we may choose 24 gravity data (marked by black dots in Fig. 3.12) as prescribed regionals and a circle with radius 4.24264 intervals as a new boundary for processing. Letting $\Delta\theta = 15°$ and the trade-off parameter $\alpha = 0.075$, we obtain a set of boundary constraints shown in Table 3.1.

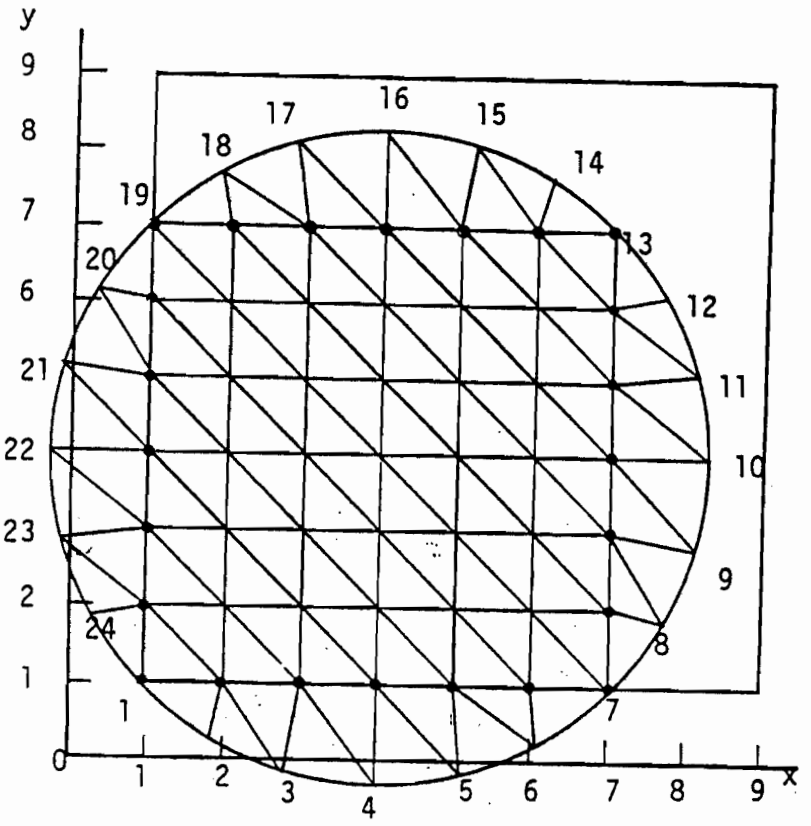

Figure 3.12. Coordinates and mesh for boundary preprocessing and the FE procedure. Black dots show the prescribed data points while the numbers on the circle show the boundary sequence. The square is the original survey area.

Table 3.1. Theoretical gravity anomalies and estimates on a circular boundary produced by the spectral expansion procedure

No. j	Theoretical values (mgals)	Estimates (mgals)
1	0.9419	0.9278
2	.9155	.9345
3	.8451	.8138
4	.7502	.7230
5	.6511	.6438
6	.5614	.5671
7	.4882	.4822
8	.4319	.4291
9	.3830	.3683
10	.3488	.3376
11	.3279	.3221
12	.3182	.3206
13	.3182	.3150
14	.3242	.3469
15	.3350	.3688
16	.3538	.3683
17	.3859	.3758
18	.4335	.4285
19	.4892	.4831
20	.5619	.5671
21	.6515	.6438
22	.7504	.7228
23	.8452	.8137
24	.9156	.9345

The maximum relative error in the estimates is less than 4%, showing that the generalized inverse can produce satisfactory constraints for further processes. The FE procedure is then applied to produce regional and residual estimates shown in Fig. 4.13. Within the circular boundary, the regional and residual estimates are very close to the theoretical values, implying the technique is reliable.

3.3.3 The spectral expansion method for long-strip regions

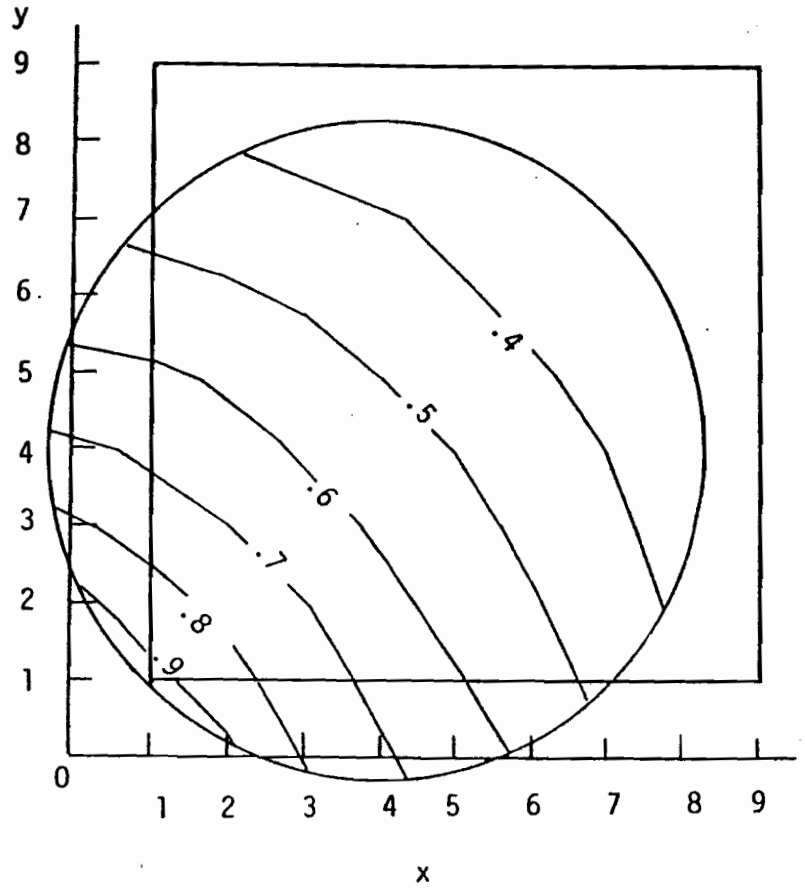

(a)

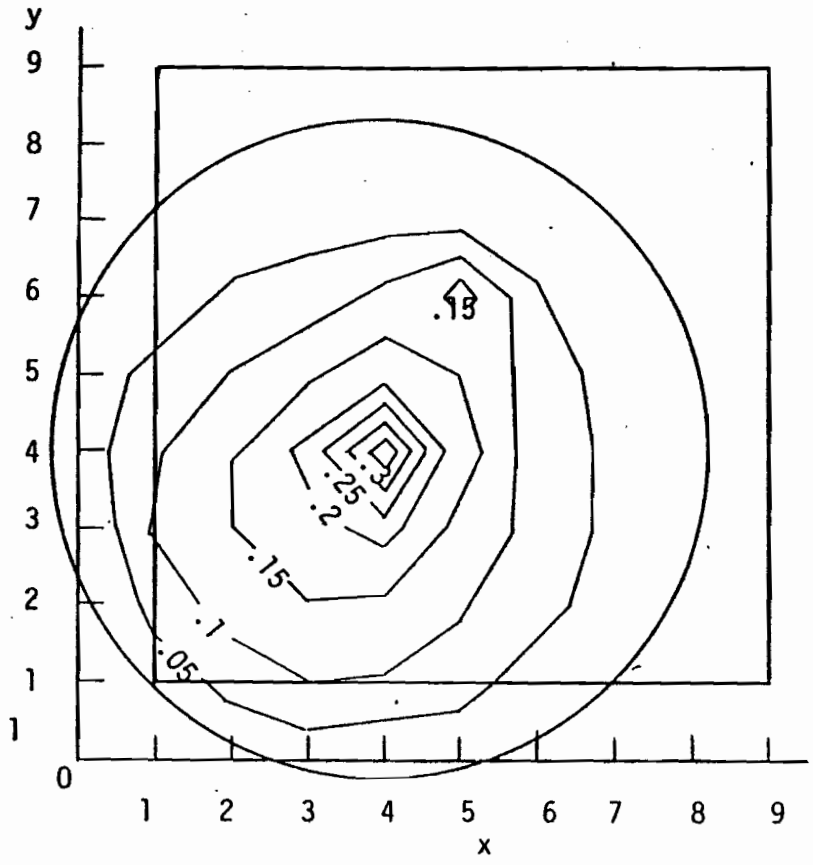

(b)

Figure 3.13. Regional estimate (a) and residual (b) produced by the finite element method with the constraints on a circular boundary estimated by the generalized linear inverse.

If a survey is carried out in a belt-like region, the method with a circular boundary becomes inapplicable. In order to use the spectral expansion method for the optimal boundary sequences, let us consider the Dirichlet boundary value problem in a long-strip region. The solution of the problem has been shown by Huestis and Parker (1979) as follows

$$f(x_i,y_i) = \frac{\sin y_i}{2\pi}\left(\int_{-\infty}^{\infty} \frac{g'(x,0)dx}{ch(x-x_i)-\cos y_i} + \int_{-\infty}^{\infty} \frac{g'(x,\pi)dx}{ch(x-x_i)+\cos y_i}\right)$$

The geometry and the parameters are shown in Fig. 3.11.c. All the distances must be scaled in this case to make the separation of the two enclosing levels equal to π.

After a set of prescribed data $\{f_i\}$ *is selected, the spectral expansion method mentioned in the previous section can be used for estimating the optimal boundary sequences* $\{g'_i\}$ *if elements of matrix* $\underline{A}$ *in (3.17) are calculated by*

$$\begin{aligned} a_{ij} &= \sin y_i/2\pi(ch(x_j-x_i)-\cos y_i)\Delta x_j \qquad \text{for } y_j = 0 \\ &= \sin y_i/2\pi(ch(x_j-x_i)+\cos y_i)\Delta x_j \qquad \text{for } y_j = \pi \end{aligned} .$$

3.4.4 Arbitrary boundaries

For arbitrary boundaries there are no analytic expressions showing the direct relationship between a harmonic function and its boundary values. However, the Dirichlet problems can be represented in terms of integral equations as well. Assume that S is a continuous surface and P is a point either inside or outside S. A harmonic function at P may be represented by the

potential of a double-layer distribution on S:

$$f(P) = \iint_S \mu(Q)\partial(1/r)/\partial n \, ds$$

(Kellog, 1953, p.286), where Q is a point on S and $r=\overline{QP}$; n is the external normal of S and μ is the intensity of the equivalent source. On the boundary S, the harmonic function $g'(Q)=f(Q)$ is related to the equivalent source by

$$g'(Q) = \pm 2\pi\mu(Q) + \iint_{S'} \mu(Q')\partial(1/r')/\partial n \, ds$$

where Q and Q' are different points on S and $r'=\overline{Q'Q}$, S' is the boundary S exterior to Q; the plus corresponds to P outside S while the minus for P inside S.

In 2-D cases we can write correspondingly

$$f(P) = \int_C \mu(Q) \cdot \cos\theta/r \, dc \qquad (3.20)$$

and

$$g'(Q) = \pm \mu(Q) + \int_C \mu(Q') \cos\theta'/r' \, dc \qquad (3.21)$$

where θ is the angle from $\overline{QP}$ to $\vec{n}$ and $\vec{\theta'}$ from $\overline{Q'Q}$ to n. For boundary processing, we have a set of values of f(P) and want to find the boundary sequency of g'(Q). We may first use the spectral expansion approach to determine the equivalent source μ by solving (3.20), which is a Fredholm's integral equation of the first kind. Then the boundary sequence can be calculated easily via the integration in (3.21). Thus in principle there is no difficulty to produce a set of constraints on arbitrary boundaries by employing the spectral expansion method.

We shall not discuss the problem any further because in most cases it

might be unnecessary to employ this relatively expensive method to obtain boundary sequences. For a large area the spectral expansion procedure may cost more then the execution of the FEM itself. Therefore we may consider other means for boundary constraints processing, such as the least squares method.

3.4.5 A least squares procedure for boundary preprocessing

The spectral expansion procedure is relatively expensive as the factorization of a matrix costs much more than ordinary inversion of matrices. In addition, sometimes one may meet a critical situation in which the boundary cannot be changed. For instance, in a mining gravity survey, where the observation areas may be critically small and adjacent disturbances may be very strong, one may not have much choice on changing boundaries. In these cases we may consider a modified least squares procedure which is fast and can provide satisfactory estimates in some cases.

Let us consider once more the six-sphere model (Fig. 3.9) and suppose that the survey area (800*800 m^2) cannot be reduced. The original gravity boundary values due to the six spheres plus a white noise - the primary boundary sequence - are shown in Fig. 3.14.a. It is evident that there are three large residuals round the points 9, 17 and 25 respectively, corresponding to the sources under the three corners. Although the sequence contains noise, the trend of the regionals can be recognized without difficulty. We notice that the residuals, as local anomalies existing at only a few segments, can be removed when we search for the trend. Least squares fitting then may be used to minimize the error. such a procedure may contain the following steps.

The first step is to remove those measurements from the primary boundary sequence which contain visible residuals or disturbances. The

remainder, mainly representing the trend , can be denoted by $f(x_i)$ with x_i, $i=1,2,...,N$, giving the locations of the remainder in nonequispaces. It is manifest that $f(x_i)$ still contains little residual components and some noise, which may be treated as error and denoted by r:

$$f(x_i) = g'(x_i) + r_i \tag{3.22}$$

Suppose that the trend sequence $g'(x_i)$ can be approximately represented by a polynomial,

$$g'(x_i) = \sum_{j=1}^{M} a_{ij}\, c_j \tag{3.23}$$

Where M is a small integer since the trend is usually smooth, and

$$a_{ij} = x_i^{j-1} \tag{3.24}$$

The equation (3.23) can be rewritten as

$$\underline{g'} = \underline{A}\,\underline{c} \tag{3.25}$$

where $\underline{A}$ is an N by M matrix with elements shown in (3.24), and $\underline{c}$ is an unkown vector of coefficients of the polynomial. Minimizing the Euclidean norm of the error $\underline{r}$, that is

$$\|\underline{r}\| = \|\underline{f} - \underline{A}\,\underline{c}\| \tag{3.26}$$

with vector $\underline{f}$ containing the prescribed regionals on the boundary, we get the so-called normal equation

$$\underline{A}^T\underline{A}\,\underline{c} = \underline{A}^T\underline{f} \tag{3.27}$$

After solving linear system (3.27) and obtaining vector $\underline{c}$, we are able to

calculate a new boundary sequence by

$$g'(x_k) = \sum_{j=1}^{M} c_j \; x_k^{j-1} \qquad (3.28)$$

where x_k denotes the location of boundary nodes in the mesh designed for the FE implementation. The new boundary sequence $g'(x_k)$ can be an approximation of the trend since the residuals have been considerably removed and the error has been minimized. However, it may be biased, as a polynomial has been assumed to represent the trend.

Computationally there are several ways to solve the normal equation (3.27). Conventional procedures, such as the Gauss elimination method, sometime cannot produce good solutions. For instance, if a general matrix $\underline{A}$ is of rank k, the computational product $\underline{A}^T\underline{A}$ might have a rank less then k. Hence, the methods which do not involve the matrix multiplication of $\underline{A}^T\underline{A}$ are more appropriate for solving the normal equation. The QR decomposition method is one of the methods which avoids executing the multiplication. A general matrix $\underline{A}$ can be uniquely decomposed into a product of an orthogonal matrix $\underline{Q}$ and an upper triangular matrix $\underline{R}$

$$\underline{A} = \underline{Q}\,\underline{R} \qquad (3.29)$$

(Stewart, 1973), where $\underline{A}$ is an N by M matrix with rank $M \leqq N$, $\underline{R}$ is also of N by M with all zero elements in its lower part except the upper triangular elements. Matrix $\underline{Q}$ is of N by N. Thus the normal equation becomes

$$\underline{Rc} = \underline{Q}^T\underline{f} \qquad (3.30)$$

After QR decomposition, (3.30) can be easily solved by back substitution since $\underline{R}$ is triangular. The QR decomposition method being used refers to Givens'

rotations (Nash,1979).

The primary boundary sequence (Fig. 3.14.a) is processed by this procedure which produces a 'trend' sequence as shown in Fig. 3.14.b. The degree of the fitting polynomial used is up to 13. Setting the trend sequence as the boundary constrains, the FE method yields a regional anomaly map shown in Fig. 3.15.a. Comparing this estimate with the theoretical one (Fig. 3.1.a) indicates that the maximum relative error of the estimate is about 12%, still much better than those produced by upward continuation. But the estimate is not as good as those yielded by the techniques mentioned in the previous sections. The corresponding residual map is shown in Fig. 3.15.b in which the residuals due to the second and the third spheres are not separated.

We note that the proposed procedure is different from the traditional trend surface fitting where all residuals join in least squares fitting without considering a priori information about the trend. In addition, we assume that the estimates are represented by polynomials only on boundaries, inside which they satisfy the Laplace's equation. Anyhow, the final estimates are produced via boundary constraints, so the estimates located near boundaries may be biased due to the biased boundary constraints. It is an disadvantage of the least squares procedure.

Another problem in the procedure is how to choose the degree of the polynomials because the polynomial fitting procedure yields the coefficients which depend upon the degree of the polynomial with which the fit is made. We suggest using different degrees for the fitting, then choosing one of the fitting consequences as the trend sequence by interpreter's experience. It would not cost much since boundary sequence usually involves a relatively small number of data. Anyway, this procedure seems not preferable when the boundaries can be reselected or the area of interest is not so large, enable to employ the spectral expansion procedure with acceptable price.

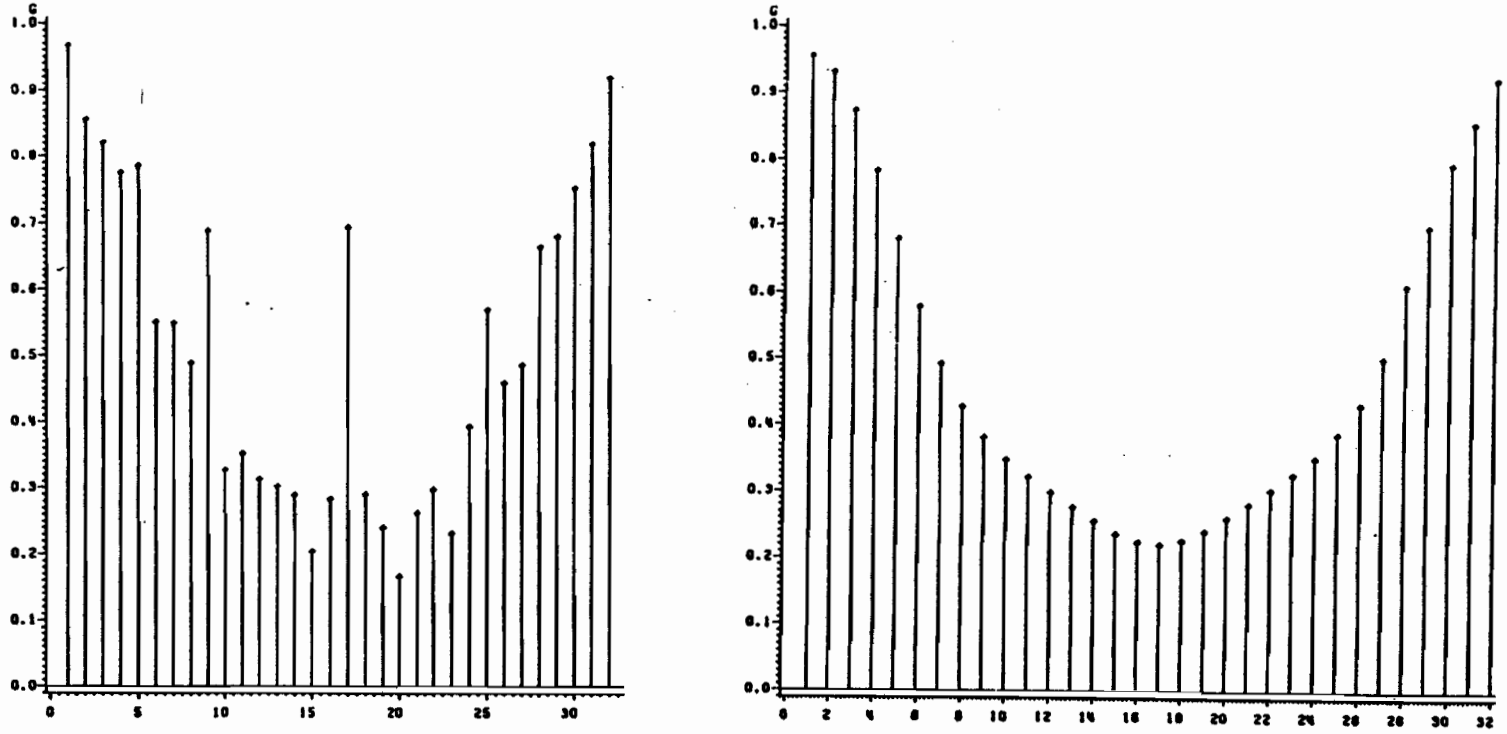

(a) (b)

Figure 3.14. Primary boundary sequence (a) and trend sequence (b) produced by the least squares procedure. The abscissa shown the sequential number of the sequences while the ordinate is in mgals.

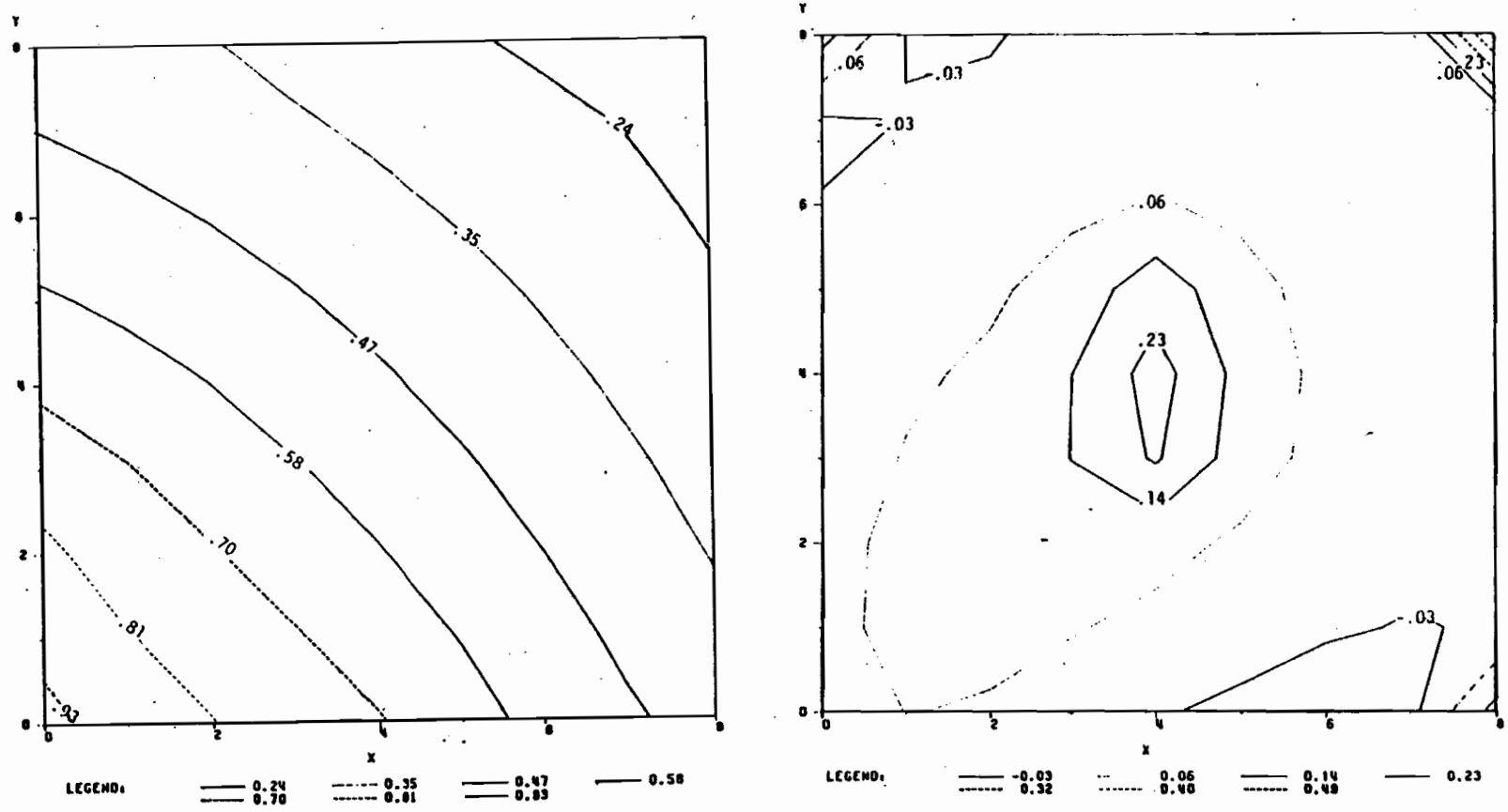

(a) (b)

Figure 3.15. Regional estimate (a) and residual (b) produced by the FEM with boundary constraints shown in Fig. 2.14.b. The contours are in mgals and coordinates in Δx=100m.

3.4 REGIONAL GRAVITY ANALYSIS OF THE ABITIBI GREENSTONE BELT

An example area chosen for illustration is the Abitibi belt, Quebec and Ontario, Canada, latitude from 47° to 50° and longitude from -83° to -73°. Geologically it belongs to the Superior Province of the Canadian Shield. The rocks in the area are mainly volcanic and sedimentary of Archean age (Fig. 3.16). As the oldest rocks in Superior Province, they were involved in the Kenoran Orogeny during which they were folded, faulted, metamorphised, and intruded by granitic rocks. In the southern portion of the area, the Archean rocks are divided into four groups (Fig. 3.17). The Malartic Group at the base consists of basic lavas and pyroclastics with acidic lavas and tuffs near the top. Numerous gabbroic and ultramafic masses occur in the basic lavas and felsic intrusions are included with acidic volcanics. The Kewagama Group comprises greywackes and argillites. The Black River Group comprises basic to intermediate flows and pyroclastics, and acidic flows and tuffs with related intrusive gabbros, diorites and felsitic rocks. These rocks are overlain by the Cadillac Group which consists of greywacke, some comglomerate, and minor amounts of tuff, iron-formation, and quartzite. All the Archean rocks are folded along easterly trending axes. These folds appear to be modified in places by cross-folds of various orientations, and cut by several easterly trending faults.

Regional gravity values have been accumulated by the Earth Physics Branch, Department of Energy, Mines & Resources, Ottawa. Bouguer gravity data are available from thousands of stations in the area, providing the gravity map shown by Fig. 3.18. By comparing the gravity and geology maps one can find that the strong local negative anomalies are roughly coincident with granitic rocks while prominent positive anomalies are probably due to exposed or concealed gabbroic and ultrabasic rocks. Outside local anomalies a regional trending field increases from east to west. However, in order to separate the

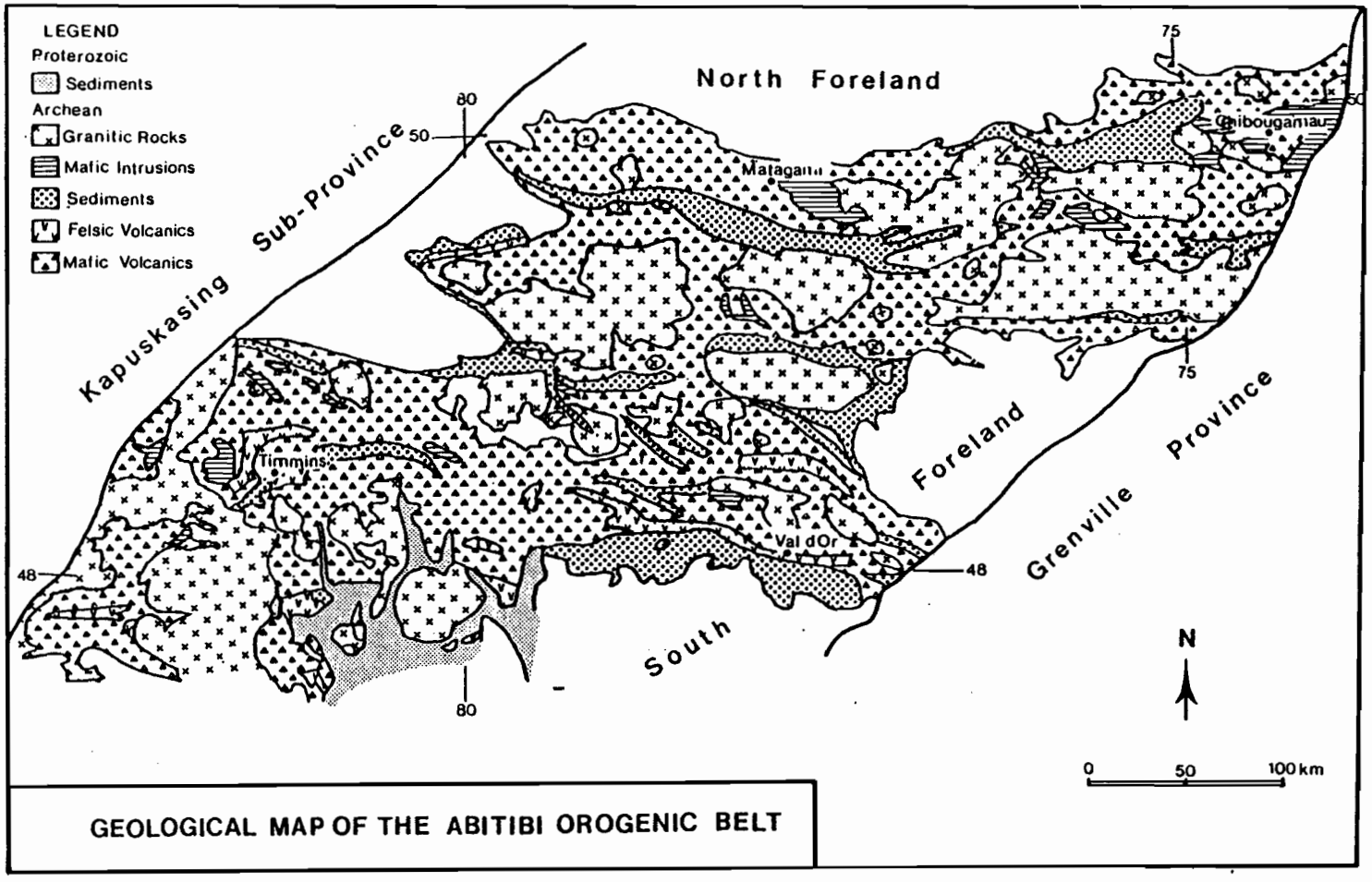

Figure 3.16. Geology of the Abitibi belt (From Parker Cr., 1984)

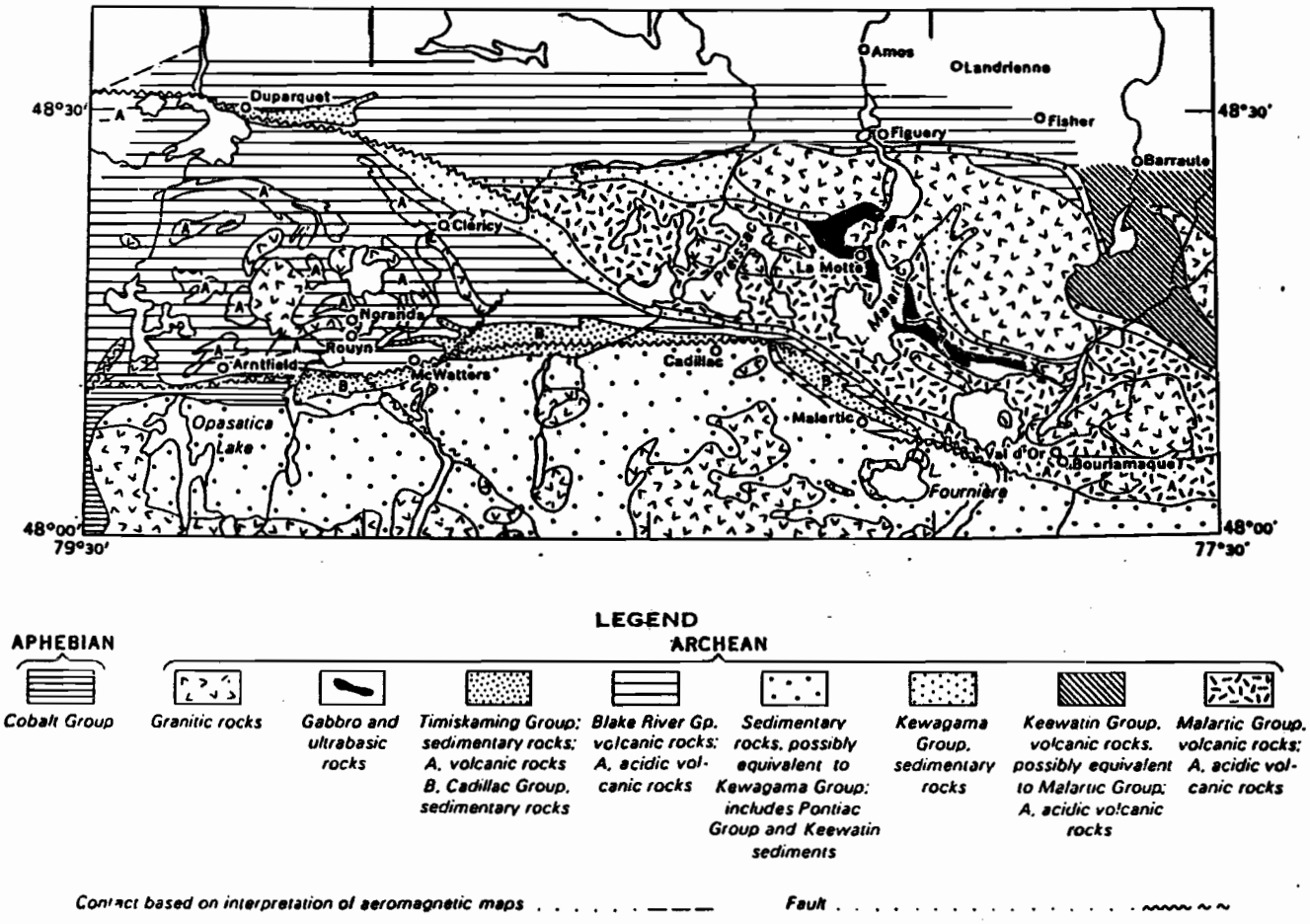

Figure 3.17. Geology of the Cadilac-Malartic area (after the Geological Survey of Canada, 1970).

regionals from the residuals, we have to consider the relationship between the global anomalies, regionals and residuals.

The global gravity anomalies have been classified as the long-wavelength anomalies (λ > few 1000 km) by Phillips and Lambeck (1980). They are supposed to originate mainly from the upper mantle. Across the Canadian shield, there is a negative gravity anomaly with amplitude from -40 to -60 mgal (see Gravity Map of Canada by Department of Energy, Mines and Resources, 1969). This anomaly is one of the outer negative anomalies adjacent to the positive gravity belt around the Circum-Pacific belt. The positive anomalies occur in the vicinity of the subducting Pacific lithosphere; they may be caused by sinking of the cool oceanic lithosphere into the mantle. The adjacent negative anomalies, including the one in the Canadian Shield, are probably caused by a complementary upflow of hot materials from the lower mantle through the transition zone into the upper mantle. It can be noticed that the underlining anomaly is blurred by a gravity high in the Hudson Bay Lowland and a gravity low on the George Plateau and the Lake Pleteau, indicating that the regianal Bouguer anomalies are partly related to isostasy in the lithosphere, especially in the lower crust. According to Phillips and Lambeck (1980, p.51), the intermediate wavelength anomalies (few 100 km < λ < few 1oookm) must be consistent to the regionals of our interests which may originate from the lateral density variations in the lithosphere.

Unfortunately, very little work has been done on separation of the intermediate wavelength anomalies. Cochran and Talwani (1977) obtained the residual gravity anomalies of ocean basins by removing the systematical gravity effect of the cooling lithosphere as a function of age or distance from the ridge axes. However, the continental lithosphere is much more complicated than the oceanic, therefore a successful separation of these on-land anomalies requires careful processing. The density variations in the lithosphere can be

caused by several factors. For example, they may be a consequence of lateral temperature variations. The regional variability of the heat flow through the Earth's surface from its interior has been recognized for many years. Besides temperature, the lateral variations of the stress state can also result in lateral density variations. Of course, the relief of the Moho and historical intrutions of mantle materials can be the major sources of the regional gravity anomalies because they represent the sharpest density contrasts in the lower crust. Thus we may speculate that the regional field in the Abitibi area is due mainly to the relief of the Moho plus the lateral density anomalies in the lower crust, caused by chemical inhomogeneity and by lateral variations of the stress or temperature. Based on this assumption, several criteria may be considered for locating the zones where the gravity field has a predominantly regional component.

The gradient of the field may be considered first. Simple calculaton of regular mass distribution models can determine that the regionals must have small spatial derivatives say less than 0.5mgal/km in the area of interest. For instance, we may use the semi-infinite slab model to evaluate the maximum derivative (the formula will be shown by (4.38) in the next chapter). If the depth of the slab is 35km, the maximum derivative will be less than 0.5mgal/km unless the thickness of the slab exceeds 10km. On contrary, the maximum derivative becomes larger than 0.5mgal/km when the top depth is 10km and the thickness is greater than 2.9km. Hence the zones where horizontal derivative of the gravity field less than 0.5mgal/km can be used for selecting the regional constraints (shown in Fig. 3.18 by slight shadows).

It can be found that the amplitude is useful for recognizing some places where prominent residuals exist. Because the trend in Abitibi varies from -45 to -75 mgals, the anomalies with amplitude smaller than -80 mgals and greater than -40 mgals (in the west) or -50 mgals (in the east) must contain

considerable residuals. As a results we should not select any regional constraints near these anomalies (see Fig. 3.18, striped shadows).

Because the first order triangles are used for elements, the average length of the triangular sides determines the smallest wavelength of the regional estimates. Suppose that the average is about 25 km, all anomalies with wavelength less than 50km are actually treated as the residuals which cannot appear in the regional estimates.

The place where the gravity field contains mainly the regional field is divided into many small cells of size 10'*20', we can evaluate the limits of the amplitude of regionals at each cell via the contour map. Picking up some represetative gravity data with each cell which falls within the limits, we obtain a set of boundary constraints of the regionals as listed in Appendix II. A mesh can be designed for the finite element performance with the nodal numbers, coordinates and the final regional estimates all listed in this appendix.

The regional anomalies thus produced are shown in Fig 4.19, from which some aspects may be noticed.

(1) As the main trend, the regional field increases from -75 mgal at the east to -45 mgal at the west. Nevertheless, a secondary trend is also visible showing that the field increases from south to north in the western part (to the west of 79°W). Recent results of the seismic refraction profile (Vald'Or-Matagami) indicate that the crustal thickness decreases from the east to the west , and might slightly decreases from the north to the south (Parker, C. L.,1984). The coincidence between the gravity and the seismic results implies that the the regional gravity trend to a certain extent reflects the relief of the Moho.

(2) Based on the features of the regional field, the Abitibi belt may be divided into three districts: the East, the North and the South. The East (to the east of 77°20'W) is characterized by a negative anomalies which may be

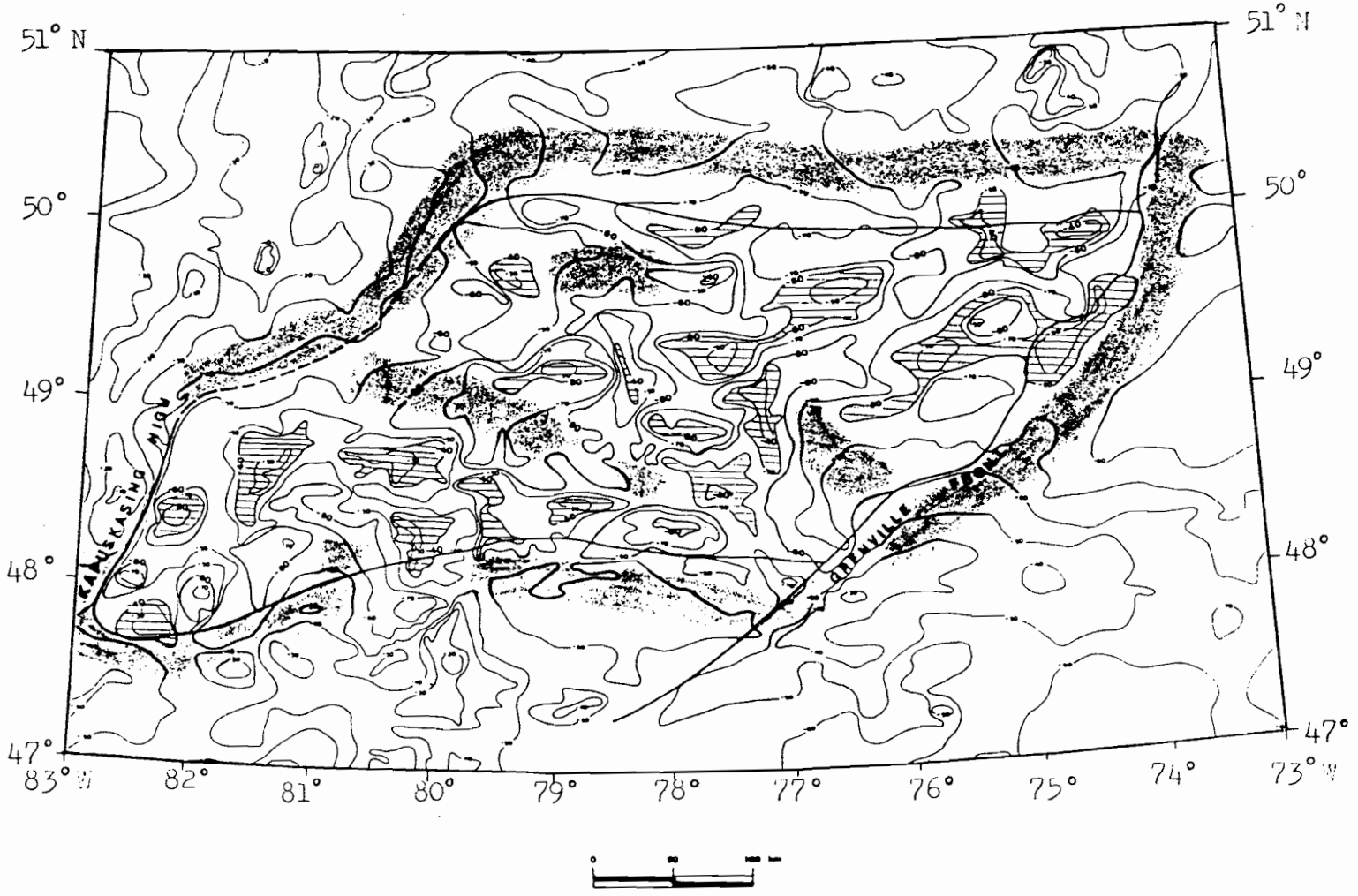

Figure 3.18. The gravity anomalies of the Abitibi belt. The striped shadows show the places where gravity field contains visible residuals while slight shadows show the zones for regional constraints (after Schwartz et al., 1982).

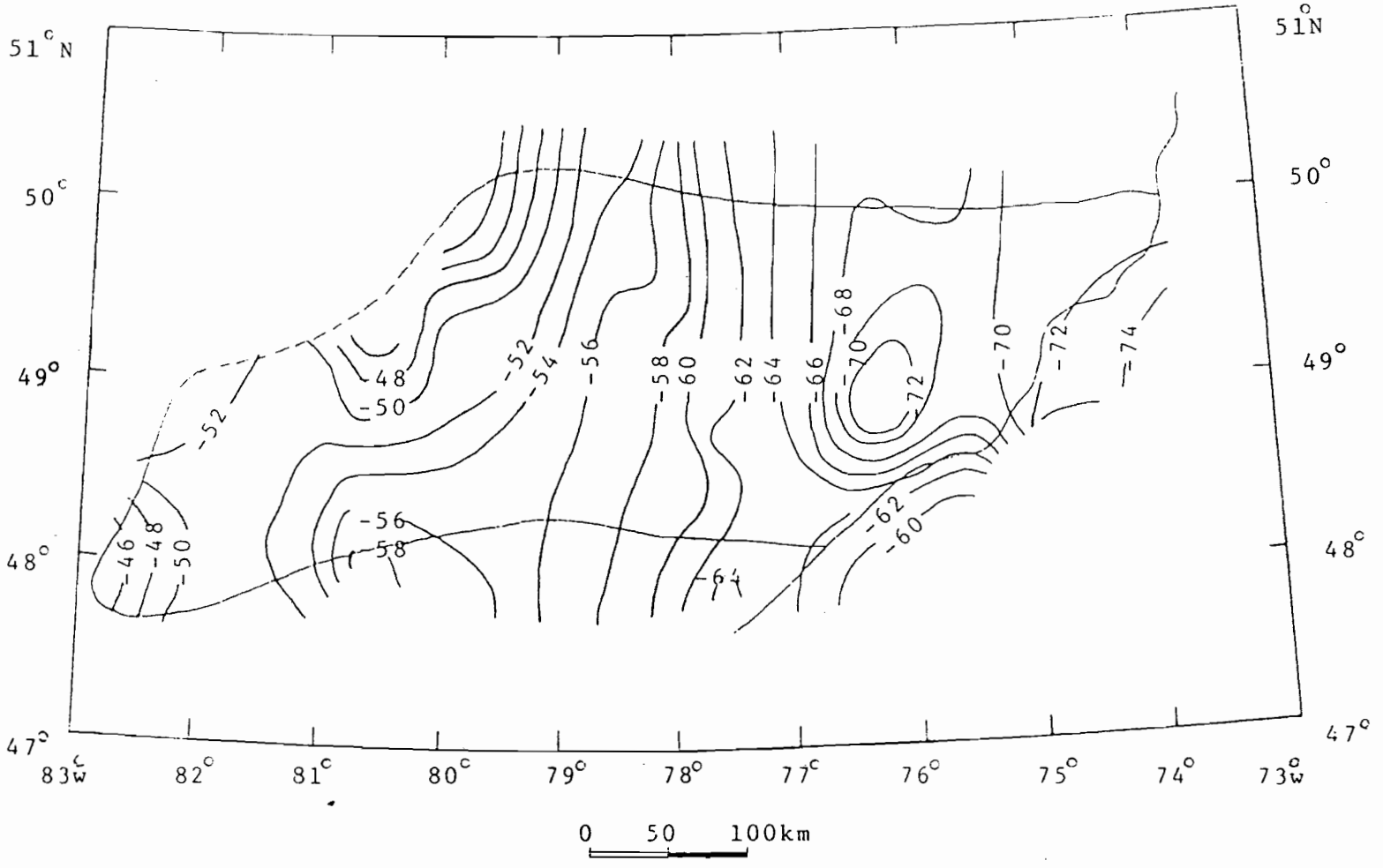

Figure 3.19. Regional gravity anomalies in the Abitibi belt.

caused by thickened crustal structure or by a large granitic batholith in the crust. Imperfect recovery from postglacial loading might also cause negative anomalies. In the North (to the north of 48°40'N) the regionals are gradually increasing from east to west with a relatively large gradient (Fig. 3.20.a).

(3) In the south Abitibi (up to 48°40'N), which is one of the most important mining areas in Canada, a step-like trend appears with small gradient within the steps and a few sudden increases between them. The sudden changes might indicate deep crustal faults. For example, a sudden increase occurs at about 77°25'W (Fig. 3.20.b), which becomes very clear after downward continued to the level of -37km (the continuation method employs the damped least squares procedure will be explained in the next chapter). Geographically it coincides with the Lake Parent and the Lake Tiblemont, together with the lakes a long diabase dike can be seen on ground. Thus we suggest the possibility of the existence of a deep fault there.

Further interpretation of the regional map is beyond the scope of the thesis as we are dealing with new data processing techniques. Now we may turn to an example of locating local anomalies. Between Val d'Or and Fisher there is both a negative anomaly and a positive one (marked by "A" in Fig. 3.21). The negative one is due to a large granitic intrusion while the positive one is due to the ultrabasic intrusion across the Lake Malartic. Upward continuation is first used for separation of these residuals with continuation height equal to 10km. The corresponding regional estimate is shown in Fig. 3.22. The remains of the local anomalies in the regional estimate indicate that the regional estimate contains undesirable residuals.

Quantitative interpretation of the residual anomalies requires separating them from the regional field. The residual estimate produced by upward continuation is not precise enough for quantitative analysis. We may try the FE procedure with the following steps. Select a boundary which goes through

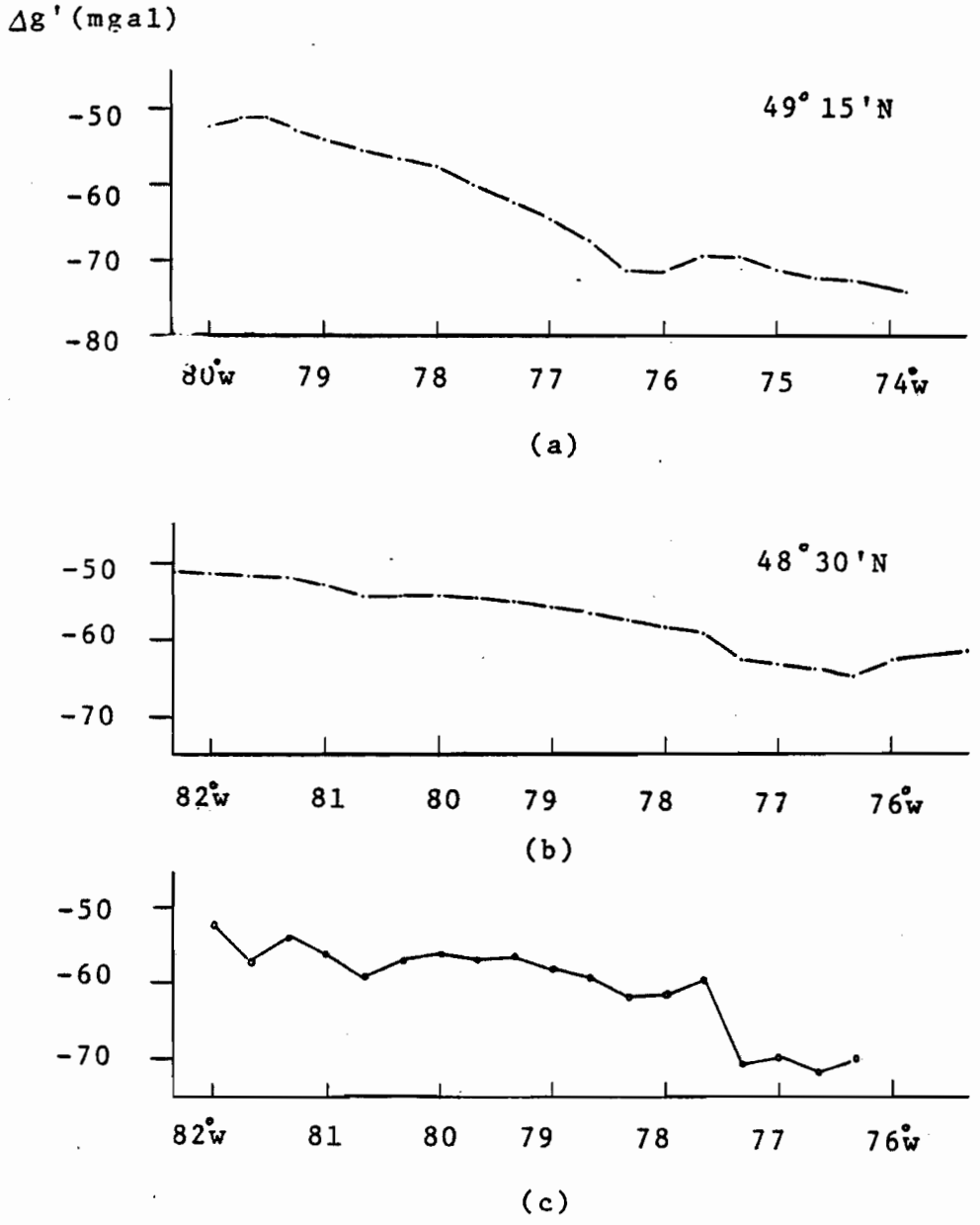

Figure 3.20. Regional gravity profiles: (a) along latitude 49° 15', (b) along 48° 30' and (c) downward continuation estimate at depth 37 km.

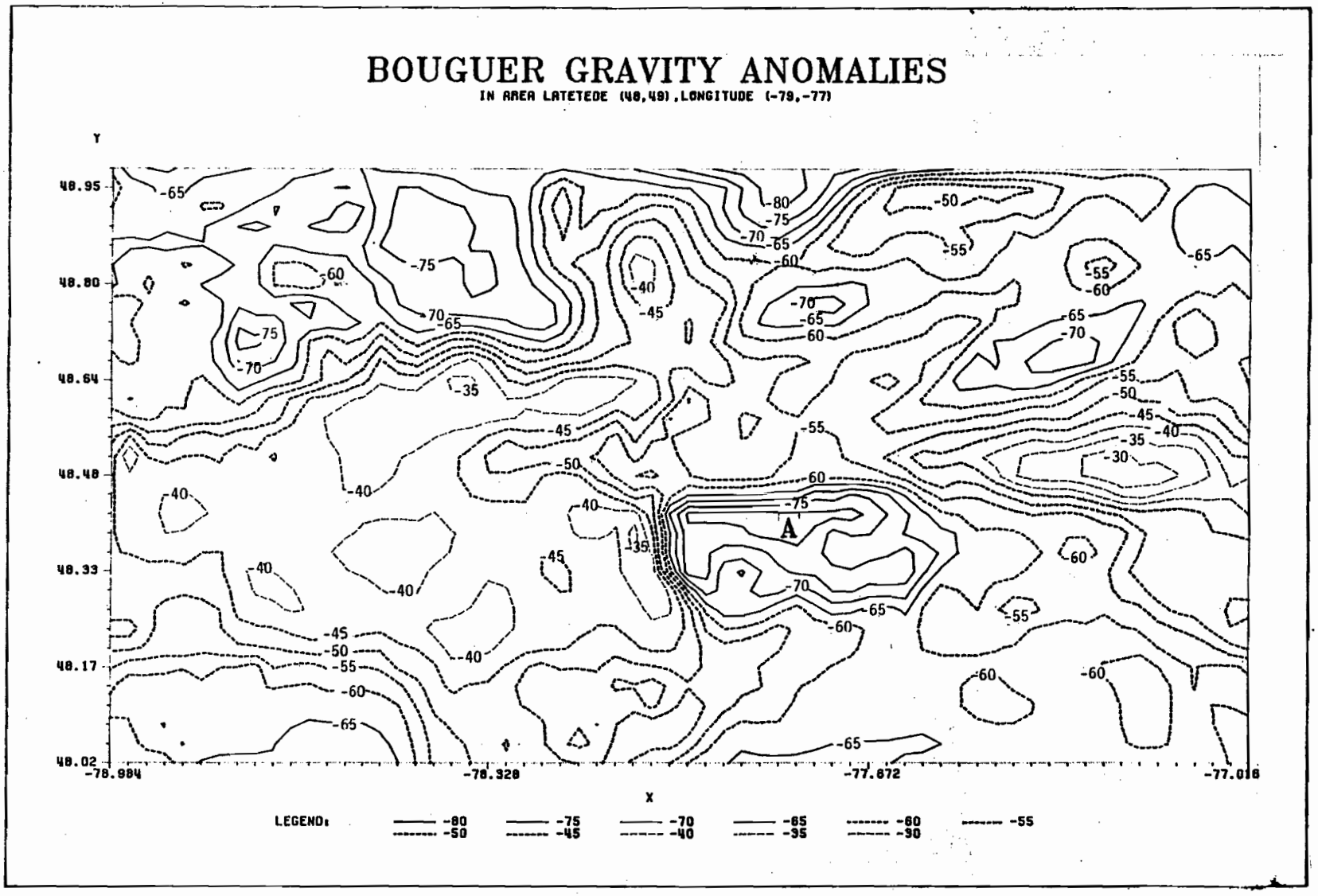

Figure 3.21. Bouguer gravity anomalies in the example area. Contours are in mgals while coordinates are longitude and latitude (in decimal system) respectively.

slowly varying zones of the gravity anomalies. The Bouguer gravity data on the boundary can be used as the boundary constraints for the Dirichlet problem. A mesh shown in Fig. 3.23 is designed for the FE procedure. The regional map thus produced (Fig. 3.24.a) shows that the regional field tends to decrease from west to east, which is consistant with the results shown in Fig. 3.19. The corresponding residual map is shown in Fig. 3.24.b. There appears to be no regional anomalies remaining in the residual map and vice versa, the anomalies seems to be well separated.

3.5 SUMMARY

As relative concepts, the regional and residual components can represent quite different structures depending upon the object of the interpretation and the area being studied. A mathematically unique solution for the regional-residual decomposition (RRD) problem does not exist due to the ambiguity of these concepts. Because the spectra of regional and residual gravity anomalies always overlap tightly in the low-frequency band, upward continuation and spectral analysis approaches for gravity RRD analysis have some inevitable problems which have been described by Gupta and Ramani (1980). A means to improve the analysis is simulating the graphical methods by using computers. If some approximate values of the regional field on a selected boundary can be specified based on the trend in gravity maps plus some available geological information, the RRD problem becomes the Dirichlet problem with perturbed boundary conditions. The finite element (FE) method, which minimizes the stored field energy, is an appropriate method for solving this kind of problem, as it can be used for very complicated boundaries and can limit the effect of errors contained in prescribed boundary constraints.

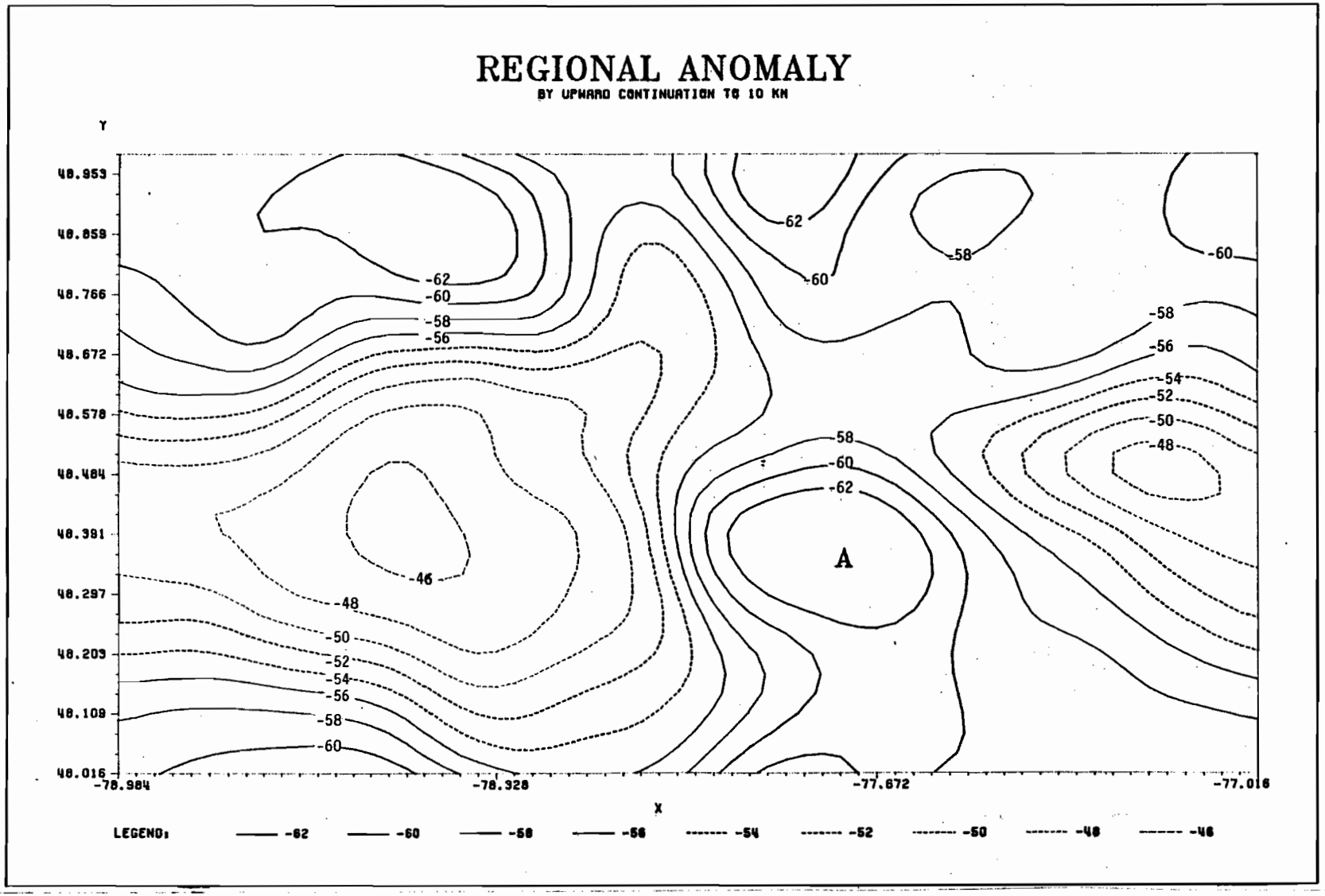

Figure 3.22. Regional estimate produced by upward continuation of 10 km. Contours in mgals and coordinates in decimal system.

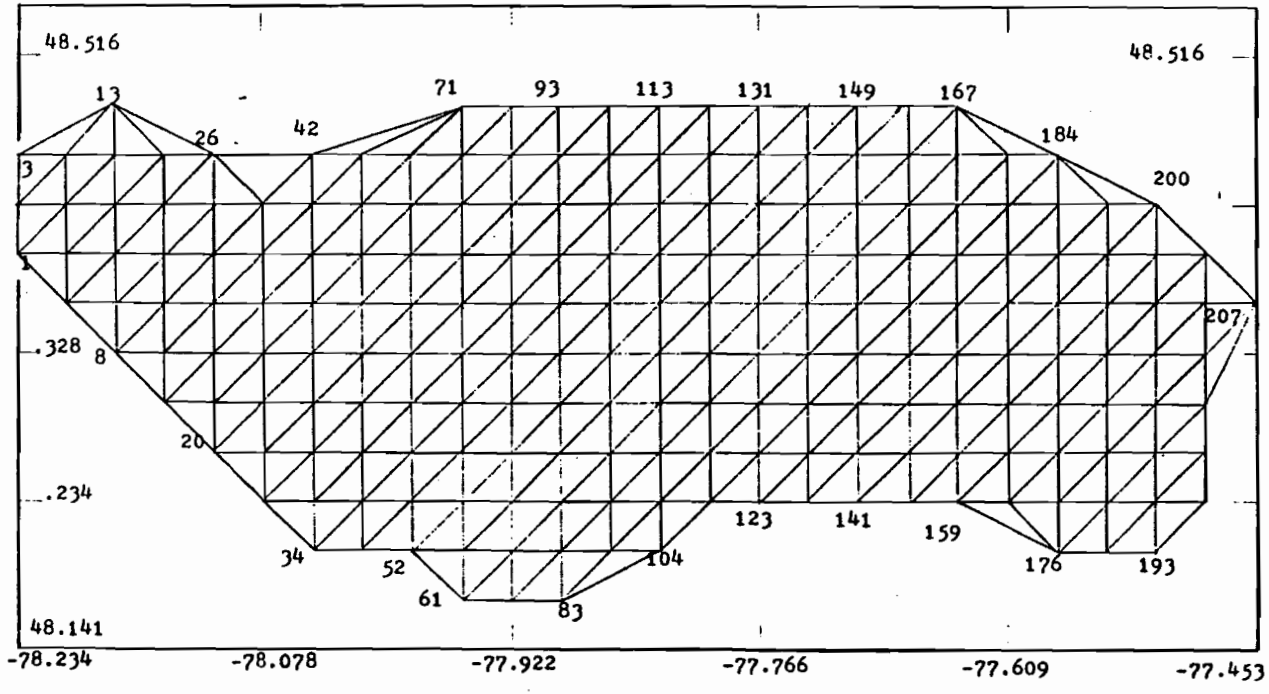

Figure 3.23. A mesh with sequential nodal numbers for analysis of anomaly A. Coordinates show the latitude and longitude.

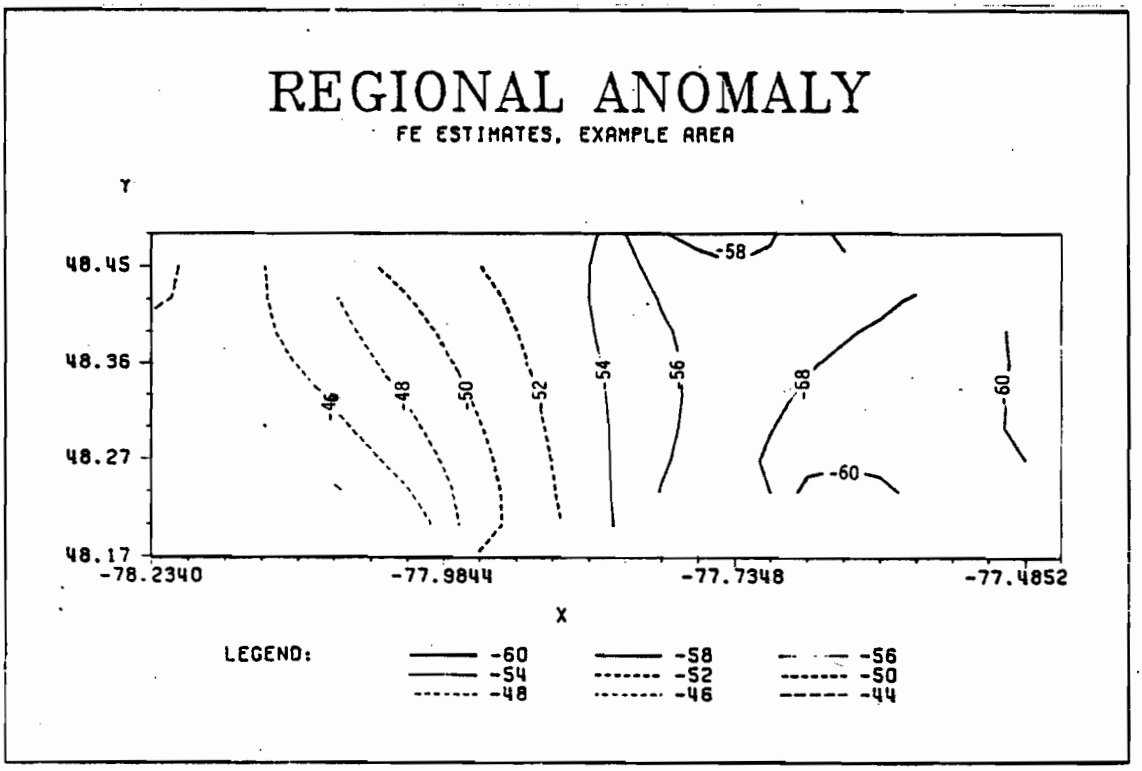

(a)

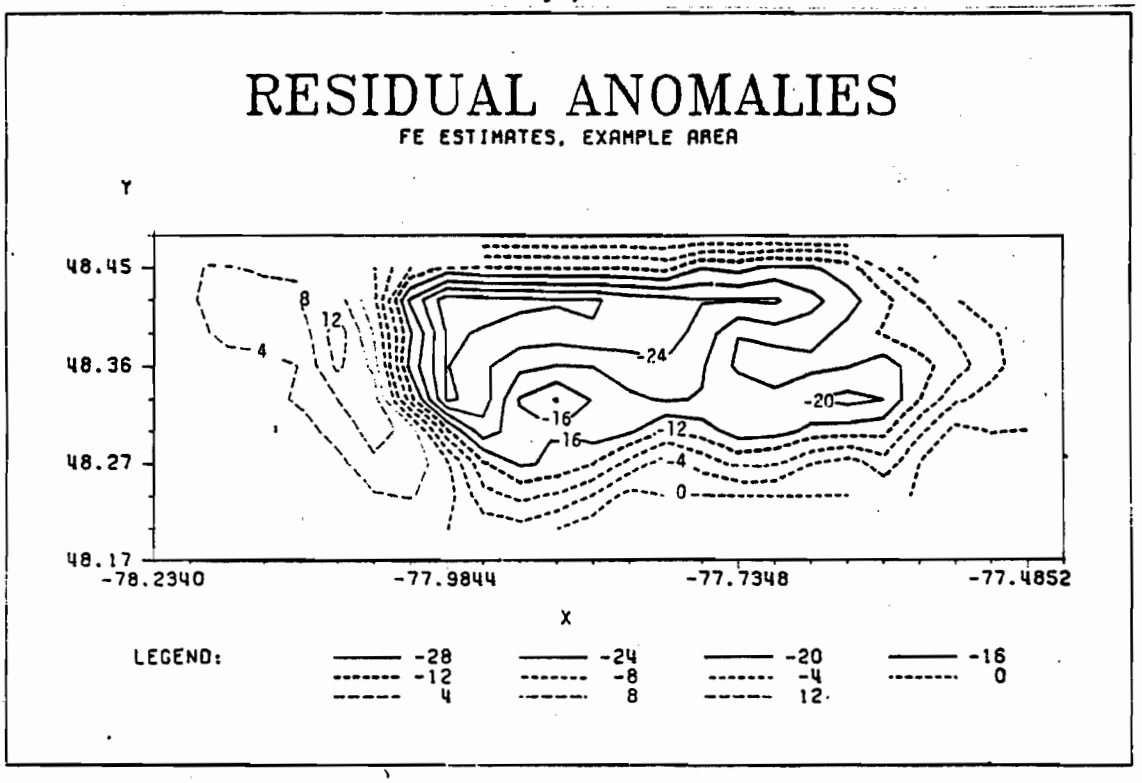

(b)

Figure 3.24. Regional estimate (a) and residual (b) of anomaly A produced by the FEM. Contours are in mgals while coordinates are in decimal system.

After boundary constraints are selected, the study area can be divided into many small elements within which regionals are approximately expressed by a linear equation. Minimizing the energy results in a system of linear algebraic equations which provides a numerical estimate for the regionals. In order to obtain good solutions, the boundary should be selected carefully so that boundary constraints may contain as few residuals as possible.

When the prescribed constraints distribute rather randomly inside or outside a specified boundary and cannot be connected by a closed curve, some techniques are needed to produce a set of constraints on the specified boundary. The spectral expansion method can be applied in such cases for boundary sequence processing and it produces satisfactory results. A least squares procedure may also be used for the process which is economical but might produce biased results.

A series of synthetic examples has been presented to illustrate the accuracy and flexibility of the FE procedure. This procedure is also used to produce a regional gravity map of the Abitibi belt within the Canadian shield. Comparing the estimates produced by upward continuation and the FE procedure shows that undesirable residuals have disappeared in the FE regional estimates whereas they evidently remain in the upward continuation estimates. Therefore we suggest applying the FE procedure for precise analysis of regionals and residuals. However, the FE procedure can produce more than one solution depending upon the selection of prescribed boundary constraints of regionals. In general, the broader the selected constraints distribute, the deeper the structures represented by the regional estimate. In order to obtain good solutions for the regional and residuals, interpreters must first determine some zones for selecting regional constraints based on the trend of potential fields plus available geological and geophysical information. The FE procedure provides a flexible way to integrate a priori information about regionals with computer

processing, therefore, improves gravity RRD results.

A disadvantage of the proposed method is the computation cost required. For a large region with several thousand of potential field data, the FE procedure can be much more expensive than upward continuation and spectral analysis methods when the spectral expansion method is needed for boundary sequence processing. In many cases the extra expense is worthwhile as the FE procedure produces much improved separation results. However the requirement of preselecting the boundary location on a map and obtaining optimum boundary constraints rules out the FE procedure as entirely automatic. This problem can be overcome if interactive graphics processing is used.

Chapter IV

New Techniques for Continuation of Potential Fields from Arbitrary Surfaces

4.1 Introduction

Because continuation provides the possibility of producing a three-dimensional image of potential fields from observations on a single surface, it has received an enormous amount of attentions. Downward continuation can be used for localizing the source areas and producing initial estimates of source parameters for further inversion. As a simplified inverse method, downward continuation enjoys the advantage of not presuming the geometry of sources. On the other hand, upward continuation is often used to suppress near-surface noise or distortion of the field due to uneven terrain and to join observations obtained at different altitudes.

Fourier transformation methods have been employed for continuation between horizontal planes since the 1950's (Dean, 1958; Baranov, 1975). For 2-D potential data observed on an arbitrary surface, a straightforward method of upward continuation is to apply the conformal mapping of complex variables (Parker and Klitgord, 1972). Also based on the theory of complex variables, Le Mouel at el (1974) suggested using simple analytical expressions to derive continuation filters. However, these methods are restricted to 2-D cases. For 3-D potential fields, Chalupka (1980) tried to develop a formulation for analytic continuation from the data observed on a spherical surface which may be considered as an analogue of the complex function methods in the 2-D cases.

Unfortunately the formulation has not been tested by any computations and the limitation that data must be taken on a spherical surface makes it difficult to apply to exploration geophysics.

For continuation of 3-D potential field data from an arbitrary surface, Henderson and Cordell (1971) proposed an approach which expands the data into a harmonic series with an exponential modulator. The procedure can be unstable for downward continuation due to the effect of the exponential modulator and the truncation of the series. Syberg (1972) tried to extend the Fourier transformation methods for potential data taken on a general surface but the formulation contained some mistakes (Granser, 1983). In 1977, Bhattacharyya and Chan proposed another procedure for upward continuation from an arbitrary surface which uses an iterative method to solve a Fredholm's integral equation of the second kind. Later on we shall show that the procedure can be developed into a compact form.

Because potential field data are usually finite and contaminated, the procedures for continuation should consider the effects of deficient and noisy data. There is no doubt that the application of the Backus-Gilbert (BG) theory can provide better procedures for continuation problems, because the nonuniqueness of model parameters can be assessed by the BG method (Backus and Gilbert, 1967, 1968, 1970). The early work was done by Ducruix et al. (1974) who treated the problem of continuation from an uneven surface as a linear inverse problem and found the smallest root mean square solution compatible with the measured data. The authors supposed that the continued potential fields are band-limited, i. e. its Fourier transform is zero outside a finite frequency domain. As pointed out by Huestis and Parker (1979), the method does not take full advantages of BG theory which provides a means of exploring the resolution power and describing the degree of non-uniqueness. Furthermore, the assumption of band-limitedness is incorrect for downward

continuation. For example, at the level of the top of the sources, the anomalies ideally have a white noise spectrum which is constant all over the wavelength domain. Ducruix et al. recognized that their methods cannot be used for continuation close to the source. For some applications, such as joining aeromagnetic maps measured at different altitudes, these methods may produce quite satisfactory results but for downward continuation from irregular topography with insufficient data, better techniques are needed. In such cases, as these authors mentioned but did not take into account (LeMouel, 1975, p.253), the spectral expansion method may be useful.

Based on the BG theory, Huestis and Parker (1979) showed some methods for both upward and downward continuation which produce a smoothed version of the true solution. The mathematical treatment is elegent but the criterion chosen for optimization causes some practical problems which we shall discuss in the next section.

In this chapter we first deal with a problem of downward continuation of potential fields on an arbitrary surface to a plane at the top of the sources. The spectral expansion approach will be employed together with some constraints. Some new procedures for modifying the eigenvalues of the mapping operator will be developed which enable us to find the best trade-off estimate for downward continuation of finite and noisy potential field data to the top of sources. Finally a compact formulation for upward continuation will be demonstrated which improves the 'equivalent source' method proposed by Bhattacharyya and Chan (1977). As the spectral expansion is well-known today, our effort will focus on the application techniques.

4.2 The BG method and Spectral Expansion Approach

4.2.1 Downward continuation of 2-D potential field data

Let us suppose $\psi(x,z)$ is a 2-D harmonic function such as the vertical component of magnetic or gravity anomalies. The total magnetic intensity ΔT can be treated as a harmonic function if, but only if $\Delta T \ll T_o$, where T_o is the magnitude of the total geomagnetic intensity and assumed to be invariant. The validity of the treatment in the case of upward continuation has been shown by Henderson (1970). However, for downward continuation to a place close to sources the condition $\Delta T \ll T_o$ can be invalid. We can examine the validity of downward continuation estimates of ΔT by their magnitudes, e. g., by some criterion such as estimates larger than $0.1T_o$ must be doubtful. However, we will not discuss this problem further as we shall not use ΔT data for our examples.

Assume that the harmonic function $\psi(x',z')$ is known on a topographic curve $z'=h(x')$ and the axis $z=0$ is placed at the lowest point of the terrain (see Fig. 4.1.c for an example). Let another horizontal line under $z=0$ be $z=-H$ and suppose there exist no sources between the two lines. If $\varphi(x,-H)$ is a harmonic function on $z=-H$ then $\psi(x',z')$ can be represented by the upward continuation integral

$$\psi(x',z') = \frac{1}{\pi}\int_{-\infty}^{\infty} \frac{(h(x')+H)\, \varphi(x,-H)}{(x'-x)^2 + (h(x')+H)^2}\, dx \ , \qquad (4.1)$$

(Dean, 1958). We may comment on equation (4.1) as follows.

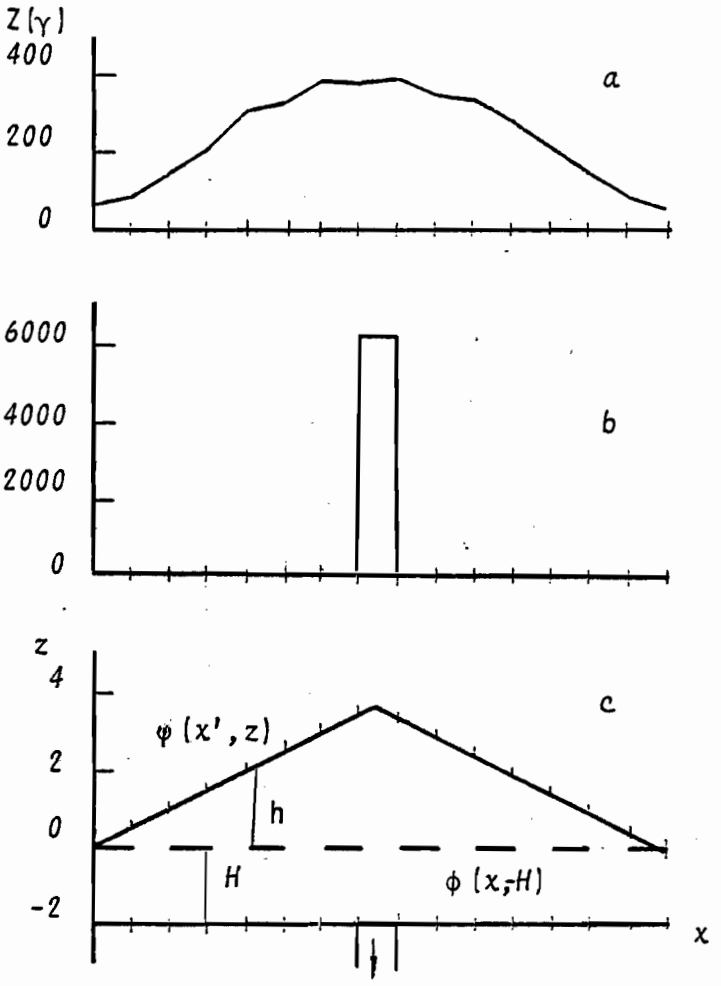

Figure 4.1. An example for downward continuation. (a) Vertical magnetic anomaly taken on triangular topography over a vertical dike model, (b) theoretical anomaly at the top of the dike and (c) geometry of the topography and the dike. All distances are in arbitrary units. One gamma is .1 nT.

(a) According to the theory of integral equations, (4.1) is a Fredholm's integral equation of the first kind whose kernel

$$\frac{(\ h(x')\ +\ H\ )/\pi}{(x'-x)^2\ +\ (\ h(x')+\ H\ )^2}$$

can be close to singular because the terrain $h(x)$ is rather arbitrary.

(b) From the viewpoint of functional analysis, (4.1) defines a Fredholm operator (equivalent to the integral kernel above) which maps a Hilbert space into itself. If, and only if, $h(x)$ is a constant, the operator is symmetric. The operator is usually bounded in a Hilbert space but the inverse operator may not be.

(c) Downward continuation represented by equation (4.1) is a typical ill-posed linear problem (Franklin, 1970) and the best known example of unstable problems (Parker, 1976), as an imperceptible change in ψ may be transformed into a large variation in φ by the inverse operator. Thus, practical approaches for mitigating the undesirable effects of instability are essential in such ill-posed problems.

(d) Finally, in engineering terminology the integral kernel represents a space-adaptive filter with an impulse response function which depends explicitly on the observation position x. The goal of downward continuation is designing a stable linear system as close to the inverse operator as possible.

4.2.2 An application of the BG method

If the potential field data are known only at points x^j, $j=1,\ldots,N$, then (4.1) becomes

$$\psi(x_j', h_j) = \int_{-\infty}^{\infty} G_j(x)\ \varphi(x,-H)\ dx \qquad (4.2)$$

where $G_j(x)$ is called the mapping kernel of the integral equation for the jth data $\psi_j = (x_j', h_j)$

$$G_j(x) = \frac{(h_j + H)/\pi}{(x - x_j') + (h_j + H)} \quad . \qquad (4.3)$$

In the absence of additional information, the data $\{\psi_j\}$ and the N equations in (4.2) comprise our total knowledge about the solution of the downward continuation problem, or the model, in terms of the BG theory. From (4.2) we see that each data ψ_j represents a moment of the model with a moment function $G_j(x)$. As Backus & Gilbert (1970) showed, the only reliable information about $\varphi(x,-H)$ obtainable from (4.2) is a moment of the model. For the value of the model at a point x_o, the only information supplied by the data are the averages

$$\tilde{\varphi}(x_o,-H) = \sum_{j=1}^{N} a_j(x_o)\ \psi(x_j', h_j) = \int_{-\infty}^{\infty} \varphi(x,-H)\ A(x,x_o)dx \qquad (4.4)$$

where

$$A(x,x_o) = \sum_{j=1}^{N} a_j(x_o) G_j(x) \quad . \qquad (4.5)$$

In equaton (4.4), $A(x,x_o)$ is called the averaging function and $a_j(x_o)$ are set of constants to be determined. The average $\tilde{\varphi}(x_o,-H)$ and its associated averaging function summarize our knowledge of $\varphi(x,-H)$ in a region around x_o. If constants $a_j(x_o)$ could be found such that $A(x,x_o) = \delta(x-x_o)$, a Dirac delta function centred on x_o, $\varphi(x,-H)$ might be recovered exactly. As this cannot happen with deficient data, the a_js are usually chosen to make the averaging

function "as close as possible" to a delta function or to a delta-like functon. The BG formalism also introduces several measures of 'deltaness' and criteria for optimal solutions. The criterion used by Huestis and Parker (1979) is the quadratic one which minimizes

$$Q(x_o) = 12\int_{-\infty}^{\infty} ((x-x_o)A(x,x_o))^2\,dx + \lambda\left(\int_{-\infty}^{\infty} A(x,x_o)dx - 1\right) . \qquad (4.6)$$

The first term on (4.6) is known as the second moment norm while the second term is subjected to the unimodular constraint

$$\int_{-\infty}^{\infty} A(x,x_o)dx = 1 \qquad (4.7)$$

with λ as the Lagrange multiplier. The minimization leads to (N+1) equations in the N+1 unkowns $\{ a_j \}$ and λ. To obtain an average $\tilde{\varphi}(x_o,-H)$ at each point of x_o requires solving an N+1 equation system because x_o is involved in the equations. It is computationally more expedient to find a method that requires solving the system only once for all values of x_o. We may consider the spectral expansion approach which has been explained in detail by Jackson (1972), Wiggins (1972), Parker (1976) and many others.

4.2.3 The spectral expansion approach

Suppose we wish to determine a set of unknown parameters φ_i (which may represent potentials or field components at the level $z=-H$), $i=1,...,M$, from a set of data ψ_j, $j=1,...,N$, the field components on a curve $z=h(x)$. Based on approximation of the continuous relationship (4.2), each ψ_j is related to all φ_i by a set of equations

$$\begin{aligned} \phi_1 &= G_1(\varphi_1, \ldots, \varphi_M) \\ &\vdots \\ \phi_N &= G_N(\varphi_1, \ldots, \varphi_M) \end{aligned} \quad . \tag{4.8}$$

We may rewrite (4.8) in the matrix form

$$\underline{\phi} = \underline{G}\,\underline{\varphi} \quad , \tag{4.9}$$

where the elements of matrix $\underline{G}$ are

$$g_{ij} = \frac{(h_j + H)/\pi}{(x_i - x_j)^2 + (h_j + H)^2} \quad . \tag{4.10}$$

The matrix $\underline{G}$ consist of N rows and M columns. Based on practical requirements in mining and regional geophysics, we may assume $N \geq M$ because in most cases we are interested in constructing a useful solution. It is possible to extend the analysis to the underdetermined problem where a large number of estimates ($M \gg N$) at the lower plane is sought, in which case the BG method (e. g. Huestis and Parker, 1979) for both construction and appraisal is appropriate. The singularlity of $\underline{G}$ depends on the continuation height H as well as the behaviour of the terrain $\{h_j\}$. In fact, matrix $\underline{G}$ can be close to singular, or computationally singular, but seldom mathematically singular. Thus we may assume that the rank of matrix $\underline{G}$ equals M but some of its eigenvalues can be very small. For flat terrain where $h(x')$=constant, the system becomes a deconvolution filter while matrix $\underline{G}$ becomes a Toeplitz matrix. In such a case the singularity of matrix $\underline{G}$ depends upon only the continuation depth. In general the deeper the continuation, the closer to singular the matrix $\underline{G}$ becomes.

We consider the general case of downward continuation from an arbitrary

surface. If N=M, the direct matrix inverse $\tilde{\underline{\varphi}}=\underline{G}^{-1}\underline{\psi}$ may produce very poor solutions with extremely large variance because $\underline{G}$ can be very close to singular. The classical least squares method can be used for both the well-posed and overconstrained cases ($N \geq M$) which minimizes the Euclidean norm of $\| \underline{G}\underline{\varphi} - \underline{\psi} \|$

$$Q = (\underline{G}\underline{\varphi} - \underline{\psi})^T(\underline{G}\underline{\varphi} - \underline{\psi})$$
$$= \underline{\varphi}^T\underline{G}^T\underline{G} - 2\underline{\psi}^T\underline{G}^T\underline{\varphi} - \underline{\psi}^T\underline{\psi}$$

where T denotes transposition. Differentiating with respect to $\underline{\varphi}^T$, and setting the result equal to zero, we have

$$\tilde{\underline{\varphi}} = (\underline{G}^T\underline{G})^{-1}\underline{G}^T\underline{\psi} \quad . \tag{4.11}$$

Equation (4.11) is the normal equation and the evaluation of the inverse $(\underline{G}^T\underline{G})$ requires that the rank of $\underline{G}$ is equal to M, or rather, $\underline{G}$ must be computationally non-singular. Thus an appropriate procedure for downward continuation should explore the singularity of $\underline{G}$ and properly treat the singular values. Hence the spectral expansion approach seems very appropriate because it has these properties.

Following the spectral expansion method (Parker, 1976), matrix $\underline{G}$ may be factored into the product

$$\underline{G} = \underline{U}\,\underline{\Lambda}\,\underline{V}^T \tag{4.12}$$

where $\underline{U}$ is an N by M orthogonal matrix with columns containing the eigenvectos u_i, i=1,...,M; $\underline{V}$ is an M by M orthogonal matrix with columns containing the eigenvectors v_i, i=1,...,M, $M \leq N$, and

$$\underline{\Lambda} = Diag(\lambda_1, \ldots, \lambda_M, 0, \ldots, 0) \qquad (4.13)$$

where λ_i, $i=1,\ldots,M$, are the eigenvalues arranged in decreasing size. Inserting (4.12) into (4.11) yields

$$\tilde{\underline{\varphi}} = \underline{V}\underline{\Lambda}^{-1}\underline{U}^T\underline{\psi} = \underline{H}_L\,\underline{\psi} \qquad (4.14)$$

where

$$\underline{H}_L = \underline{V}\underline{\Lambda}^{-1}\underline{U}^T \qquad (4.15)$$

is called the Lanczos inverse or natural inverse (Lanczos, 1961, p.124).

As pointed out by Jackson (1972), the Lanczos inverse has the following desirable properties: (a) it always exists, (b) the Lanczos inverse is a least squares inverse, as is clear from the derivation of (4.11), and (c) $\tilde{\underline{\varphi}}$ is that least squares solution which minimizes $\|\underline{\varphi}\|^2$. The resolution matrix for the Lanczos inverse

$$\underline{R} = \underline{H}_L\,\underline{G} = \underline{V}\,\underline{V}^T \qquad (4.16)$$

is the optimal resolution matrix and the Lanczos inverse also provides the best information density matrix

$$\underline{S} = \underline{G}\,\underline{H}_L = \underline{U}\,\underline{U}^T \qquad (4.17)$$

In spite of the advantages mentioned above, the Lanczos inverse approach has some problems in performance. For instance, when matrix $\underline{G}$ is close to singular, some eigenvalues in $\underline{\Lambda}$ can be pretty small, resulting in unacceptably large variances in the model parameters. In fact, equation (4.14) shows that the components of $\tilde{\underline{\varphi}}$ are proportional to the inverse eigenvalues $1/\lambda_i$. If we

assume the data to be statistically independent and have unit variance, by (4.14) we can write

$$Var\,\tilde{\varphi}_k = \sum_{j=1}^{M} \left(V_{kj} / \lambda_j \right)^2 \qquad (4.18)$$

(Jackson, 1972). Hence, when some eigenvalues become very small, the variance can be very large. Several remedies have been proposed to deal with the difficulty: (a) the stochastic inverse method and its modified versions (Franklin, 1970; Jupp and Vozoff, 1975), (b) a sharp cut-off procedure (Wiggins, 1972), (c) imposing some inequality constraints on unknown functions (Sabatier, 1977a,b) and (d) using a priori data (Jackson, 1979). For the downward continuation problem it is difficult to determine appropriate limits on the unknowns. In section 4.3, we shall further apply these techniques to the downward continuation problem and try to improve the estimates. Before we develop some techniques for downward continuation, we may show a practical method to treat 3-D potential field data.

4.2.4 Downward continuation of 3-D data

Now we consider the formula for 3-D potential fields. Let $\psi(x',y',z')$ be a harmonic function on an arbitrary surface S: $z'=h(x',y')$, and $\varphi(x,y,-H)$ be the potential on a horizontal plane $z=-H$ which is under S but above any causative bodies. The potential field data on S is given by

$$\psi(x',y',h) = \frac{1}{2\pi} \iint_{-\infty}^{\infty} \frac{(h(x',y')+H)\,\varphi(x,y,-H)}{\left((x-x')^2 + (y-y')^2 + (h+H)^2 \right)^{3/2}}\, dxdy \qquad (4.19)$$

(Grant and West, p218, 1965). Assuming that a uniform rectangular grid is

imposed on the region of interest which is large enough such that $\varphi(i,j)=0$ for any $i>I$ or $j>J$, we get after discretization

$$\psi(m,n) = \frac{1}{2\pi} \sum_{j=1}^{J} \sum_{i=1}^{I} \frac{(h(m,n) + H)\,\Delta x \Delta y}{(((m-i)\Delta x)^2+((n-j)\Delta y)^2+(h(m,n)+H)^2)^{3/2}} \varphi(i,j) \quad (4.20)$$

where Δx and Δy are intervals, J and I are the total nodal numbers of the grid in the x-axis and y-axis respectively.

In order to solve the linear system (4.20), it is convenient to write the sampled elements of matrices $\underline{\psi}(m,n)$ and $\underline{\varphi}(i,j)$ into vectors, say $\underline{\psi}$ and $\underline{\varphi}$ respectively. We achieve this by renumbering and rearranging the elements of the matrices under consideration from the first row to the last row, wherein each row we count from left to right. Specifically, we get

$$k = (n-1)I + m \quad (4.21)$$

for vector element ψ_k and

$$l = (j-1)I + i \quad (4.22)$$

for φ_l. Now equation (4.20) can be replaced by a matrix equation which is identical to (4.9) except for the sizes of the vectors and matrix, i. e. $\underline{\psi}$ is the observation vector of length $K=I*J$ and $\underline{\varphi}$ is the the solution vector, which may have a length of $L \leq K$. Matrix $\underline{G}$ is an K by L matrix whose elements are given by

$$g_{lk} = (h(m,n)+H)\Delta x \Delta y / 2\pi R^3 \quad , \quad (4.23)$$

where

$$R = ((m-i)^2\Delta x^2 + (n-j)^2\Delta y^2 + (h(m,n)+H)^2)^{1/2} \qquad (4.24)$$

Therefore the downward continuation of 3-D data from arbitrary surfaces is computationally identical to that of 2-D data and can be represented by linear algebraic operators. The discussion in section 4.2.3 can therefore be extended to the 3-D problem in a straightforward manner by rearranging the data and the following discussion will suit both the 2-D and the 3-D cases.

4.3 Thechniques for the Application of the Spectral Expansion Approach

4.3.1 The damped least squares procedure

Considering the first Dirichlet criterion which is the minimization of the Euclidean norm

$$\| \underline{G}\underline{\varphi} - \underline{\psi} \| = (\underline{G}\underline{\varphi} - \underline{\psi})^T (\underline{G}\underline{\varphi} - \underline{\psi}) \qquad (4.25)$$

provides a "optimal" solution vector $\underline{\tilde{\varphi}}$ for $\underline{\varphi}$ in the least square sense. From the viewpoint of functional analysis, the harmonic function $\varphi(x,-H)$ or $\psi(x,h)$ is an element in a Hilbert space, say space μ. As a matter of fact, they belong to two different subspaces, named $\mu_1 \subset \mu$ and $\mu_2 \subset \mu$ respectively. The elements in μ_1 consist of all possible functions $\varphi(x,-H)$ for $H \geq 0$, while μ_2 consists of all $\psi(x,h)$ for $h \geq 0$. The Fredholm's operator G, as mentioned in section 2.1, maps elements in μ_1 into those in μ_2.

In order to keep operators bounded we may consider the Hilbert space as a real-valued $L^2(a,b)$ space. By the definition, the space $L^2(a,b)$ consists of

all square (Lebesgue) integrable functions $f=f(x)$, defined in $a<x<b$, with the inner product being defined by

$$(f,g) = \int_a^b f(x)g(x)dx \qquad (4.26)$$

(Nagy, 1965, p.288), where f anf g are two square integrable functions. At first we may assume that all potential fields over a finite space domain contain finite energy, thus we have

$$\int_a^b \varphi^2(x)dx \leq c \qquad \text{and} \qquad \int_a^b \psi^2(x)dx \leq c' \qquad (4.27)$$

where c and c' are positive constants. Immediantly we see that the harmonic functions belong to the space $L^2(a,b)$ if we define the inner product by (4.26). If we consider a large space domain we have to presume that $\psi(x)$ and $\varphi(x)$ decrease sufficiently fast as $a \to \infty$ and $b \to -\infty$, and vanish at infinity. It now becomes clear that the upward continuation operator G is the Fredholm operator which maps the functions φ in a subspace $\mu_1 \subset L^2$ into the functions ψ in another subspace $\mu_2 \subset L^2$.

Introduction of the space L^2 results in a bounded inverse operator for the downward continuation problem. We say that an operator A is bounded in a Hilbert space if there exists a positive number K such that $\|Af\| < K\|f\|$. If the downward continuation operator is G^{-1} and

$$\|G^{-1}\psi\| = \|\ddot{\varphi}\| = \left\{ \int_a^b \varphi^2(x)dx \right\}^{1/2} \qquad (4.28)$$

where $\ddot{\varphi}$ square integrable, we have

$$\|G^{-1}\psi\| < c$$

where c denotes a finite positive constant. After normalizing the norm $\|\psi\|$,

it can be seen easily that G^{-1} is a bounded operator for mapping functions in the space L^2.

On the other hand, introducing the space L^2 for harmonic functions is equivalent to inserting the energy constraint (4.27). Similar to (4.27), we may express the constraint as

$$(\varphi , \varphi) = \int_a^b \varphi^2(x)dx = c'' \geq c \tag{4.29}$$

Correspondingly in the N-dimensional Euclidean space, we have

$$\underline{\varphi}^T \underline{\varphi} = c'' \tag{4.30}$$

We now seek to minimize the distance shown in (4.25) subject to the power constraint (4.30). Using the method of Lagrange multiplies, we minimize

$$Q = (\underline{\underline{G}}\underline{\varphi} - \underline{\psi})^T (\underline{\underline{G}}\underline{\varphi} - \underline{\psi}) + \alpha (\underline{\varphi}^T\underline{\varphi} - c'') \tag{4.31}$$

where α is the Lagrange multiplier. To minimize Q, we may compute $\partial Q/\partial \underline{\varphi}^T = 0$ and obtain

$$\underline{\underline{G}}^T\underline{\underline{G}}\,\underline{\varphi} - \underline{\underline{G}}^T\underline{\psi} + \alpha\,\underline{\varphi} = 0 \tag{4.32}$$

The constrained optimal solution can be then expressed as

$$\underline{\tilde{\varphi}} = (\underline{\underline{G}}^T\underline{\underline{G}} + \alpha \underline{\underline{I}})^{-1}\underline{\underline{G}}^T\underline{\psi} \tag{4.33}$$

When $\alpha = 0$, equation (4.33) becomes (4.11) which is the unconstrained optimal solution, whereas if α is large we have essentially a steepest descent solution.

Because matrix $\underline{\underline{G}}$ can be analytically calculated, we may insert (4.12) into (4.33) and obtain the solution in terms of eigenvectors:

$$\begin{aligned}\tilde{\underline{\varphi}} &= (\underline{V}\underline{\Lambda}^2\underline{V}^T + \alpha \underline{I})^{-1}\underline{G}^T\underline{\psi} \\ &= \underline{V}(\underline{\Lambda}^2 + \alpha \underline{I})^{-1}\underline{\Lambda}\ \underline{U}^T\underline{\psi} \\ &= \underline{V}\ \underline{\Lambda}_\alpha^{-1}\underline{U}^T\underline{\psi} \end{aligned} \qquad (4.34)$$

where

$$\underline{\Lambda}_\alpha = \underline{\Lambda} + \alpha\underline{\Lambda}^{-1} \qquad (4.35)$$

is a diagonal matrix containing the modified eigenvalues in its diagonal elements.

The inverse in (4.33) derived analytically is identical to the stochastic inverse introduced by Franklin (1970) where the unknown function φ was treated as a stochastic process. The spectral expansion solution in (4.34) is known as damped least squares (Wiggins, 1972; Jupp and Vozoff, 1975). If the covariance matrix of the unknown function is the simple form

$$\underline{C}_\varphi = \sigma_\varphi^2\ \underline{I}$$

and the convariance matrix of the data errors is

$$\underline{C}_n = \sigma_n^2\ \underline{I}$$

then the constant α can be written as

$$\alpha = \sigma_n^2 / \sigma_\varphi^2 \ .$$

For general covariance matrices, the stochastic inverse provides an estimate

$$\tilde{\underline{\varphi}} = (\underline{G}^T \underline{C}_n^{-1} \underline{G} + \underline{C}_\varphi^{-1})^{-1} \underline{G}^T \underline{C}_n^{-1} \underline{\phi} \qquad (4.36)$$

(Franklin,1970; Jackson,1979). Because the covariance matrices may be difficult to determine in practice, Employing (4.34) and treating α as the trade-off parpameter may be appropriate for the downward continuation problem.

Let us now use the example shown in Figure 4.1. Suppose that we have 16 data of vertical magnetic component on a 30° hill whose height equals 3.75 Δx (Δx is arbitrary). A 2-D vertical dike with depth d= 2Δx, width 2b=Δx and infinite depth extent is buried under the top of the hill. Assuming the effective magnetization has a magnitude J=100 ampere/meter (0.1 emu) and is in the vertical direction, we can calculate the data exactly by

$$\Delta Z = 2J(1+0.05e)\left(\arctan\left(\frac{i\Delta x - c + b}{h_i + d}\right) - \arctan\left(\frac{i\Delta x - c - b}{h_i + d}\right)\right)$$

where h_i is the height of the i-th point and c=8.5Δx is the central abscissa of the dike. Random additive noise e may be represented by Gaussian noise with zero mean and unit standard deviation. The data $\{\Delta Z_i\}$ is shown in Figure 4.1.a while the theoretical anomaly on top of the dike is shown by curve b in the same figure which looks like an impulse with unit width.

It may be noticed that we assume the noise to be related to the anomaly in this example. As a matter of fact, some noise is indeed associated with the signal. For instance, some geological noise is likely related to the anomaly because there often exist a disseminated 'halos' around the causative body. The geophysical records or readings observed by finite-digital devices usually contain a truncation error which is also related to the magnitude of the signal. For noise uncorrelated with signals we shall give another example in section 4.4.5.

Using the singular value decomposition algorithm (Nash, 1979, chapter

4), we factor $\underline{G}$ into the product as shown in (4.12) and obtain the ordered eigenvalues contained in the diagonal elements of matrix $\underline{\Lambda}$ as shown by curve r in Figure 4.2. Because some eigenvalues are very small, for instance, $\lambda_{16} \simeq 10^{-6}$, they must be modified in order to reduce the variance in the estimates. Employing the damped inverse procedure (4.35) to modify the eigenvalues (see curves a-e in Figure 4.2), we obtain the downward continuation estimates at the level of the top of the dike shown in Fig. 4.3. The curves a-e correspond to the trade-off parameter α=0.5, .05, .005, .0025, .001 ($*10^{-3}$), respectively.

The goodness of the estimates may be measured by the root mean square deviation between the true and the calculated anomalies. For the our simple examples, measures of the width of the main peak and the amplitude of the sidelobes, as introduced by Oldenburg (1981) may be used. The width of the main peak, i. e. the full width at one-half of anomalous maximum value. As the theoretical anomaly is an impulse of unit width, a good estimate should have the resolution width close to $2\Delta x$ (unit width plus one sampling interval). We may also use the ratio $|A_S/A_M|$ where A_S is the maximum amplitude of sidelobes while A_M is the amplitude of the main-lobe. As there is no sidelobe appearing in the theoretical anomaly, the ratio is indeed an indication of the maximum variance. Of course, it should be small.

Choosing different trade-off parameters, we obtain several estimates which enable us to draw the trade-off curves with the main peak width as abscissa and the sidelobe ratio as the ordinate (see later in Figure 4.8) The best trade-off estimate should corresponds to the lower-left corner of the curves.

From Figures 4.2 and 4.3 it can be seen clearly that as the trade-off parameter α decreases, the modified eigenvalues become closer to the true eigenvalues and the resolution width increases. The sidelobe ratio has a minimum when $\alpha = .5\times10^{-4}$. Table 4.1 shows the width and the ratio versus α.

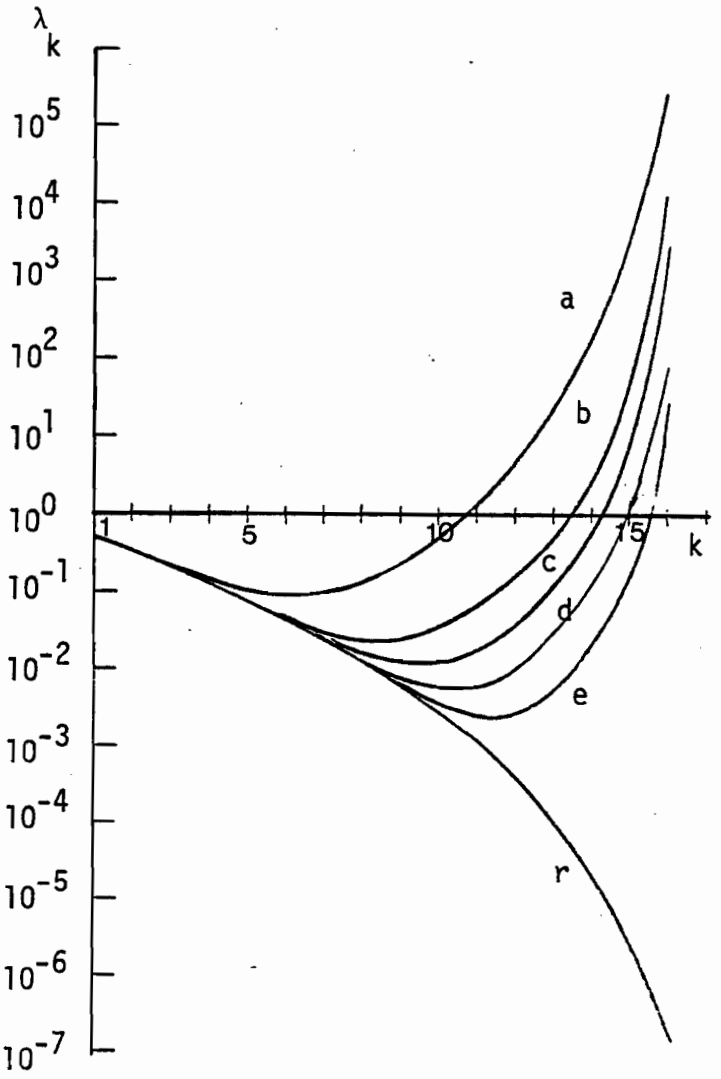

Figure 4.2. Eigenvalues and modified eigenvalues obtained from the damped least squares procedure. Curve r shows the true eigenvalues and curves a-e correspond to parameter α ($*10^{-3}$)=5, .5, .05, .025 and .01, respectively.

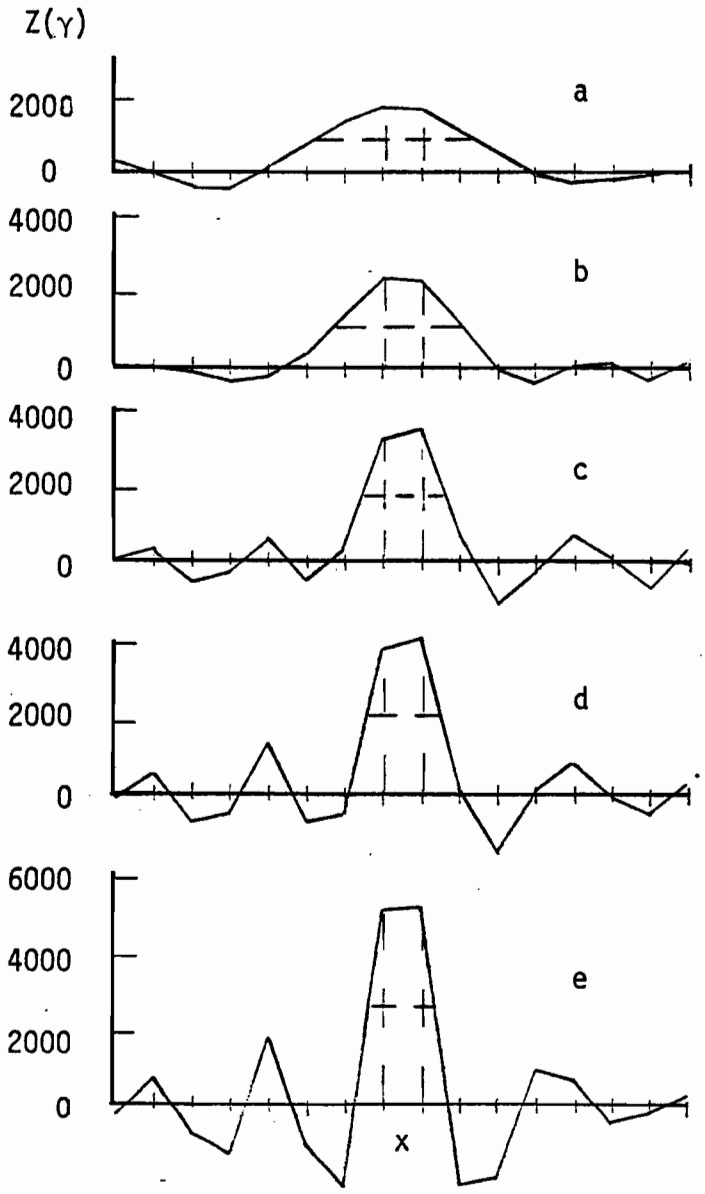

Figure 4.3. Downward continuation estimates by the damped least squares procedure. Curves a-e correspond to α *(*$*10^{-3}$*)=5, .5, .05, .025 and .01, respectively. Vertical dashed lines show the source width while horizontal dashed lines show the main-peak width.*

Table 4. 1. The main-peak width and the sidelobe ratio of the downward continuation estimates obtained by the damped least squares

α (10)	$W(\Delta X)$	$\lvert A_S/A_M \rvert$ (%)
.1	4.7	19.3
.5	4.2	18.7
.05	3.3	16.3
.01	2.4	21.1
.005	2.1	31.3
.0025	1.9	35.8
.001	1.7	54.0
.0005	1.4	68.5

The best trade-off occurs when $\alpha = 0.1*10^{-4}$ which gives a resolution width W=2.4 Δx and the maximum sidelode ratio 21.1%. The advantages of the damped least squares procedure comes from the fact that for all points x_i, i=1,...,M, and all values of the trade-off parameter α, matrix $\underline{G}$ needs only factored once. Another advantage of the procedure is the stability, which can be seen from the fact that $|A_S/A_M|$ is still less than one for very small trade-off parameters.

4.3.2 The image procedure

We have already seen that the modification of eigenvalues is usually inevitable and that the damped least squares leads to a modification formula (4.35) where the trade-off parameter α is constant for all eigenvalues. One possible question is, if the trade-off parameter α is allowed to vary for each eigenvalue, can the damped least squares approach be further improved? As the spectral expansion explicitly isolates those parts of the solution that are well determined by the data and those that are not, the answer might be positive.

Let us examine Wiggins' sharp cutoff procedure (Wiggins, 1972). Given a modest number t as the threshold for eigenvalues, the Wiggins' procedure eliminates all the eigenvalues less than t. The modified eigenvalues is thus expressed by

$$\begin{aligned} \lambda_{\alpha k}^{-1} &= \lambda_k^{-1} \qquad if \quad \lambda_k \geq t \\ &= 0 \qquad\quad if \quad \lambda_k < t \end{aligned} \tag{4.37.a}$$

Correspondingly, an integer q<M can be found such that λ_q corresponds to the smallest one among all λ_j>t. The integer q is called the effective number of

degrees of freedom in the data, depending upon the uncertainties in the data as well as on our need for certainty in the estimates (Jackson, 1972). The variance becomes, according to equation (4.18),

$$Var\tilde{\varphi}_j = \sum_{k=1}^{q} \left(V_{jk}/\lambda_k \right)^2$$

In other words, the Wiggins' procedure achieves a bounded variance by reducing the rank of matrix $\underline{G}$ and the number of eigenvectors in matrices $\underline{U}$ and $\underline{V}$, resulting in degradation of the resolution and the information density matrices.

For our example as shown in Figure 4.1, the downward continuation results obtained by the Wiggins' procedure are shown in Figure 4.4 (left curve set). The best estimate is obtained by letting t=0.005 or q=9, in which case the main-peak width equal to $2.8\Delta x$ and the ratio $|A_S/A_M|$=31.6%. It indicates , on this basis, that the Wiggins' procedure is not as good as the damped least squares procedure mentioned in the previous section.

In order to improve the procedure, we may examine various regions for the sizes of the eigenvalues (Fig. 4.5). Suppose that we have already chosen an appropriate threshold t, then any eigenvalues in the computation should be greater than t in order to keep the variance bounded. In other words the eigenvalues located under the horizontal line λ_k=t (region III in Figure 4.5) are computationally ignored because the corresponding eigenvectors represent numerically less reliable parts of the solution. In the region I all eigenvalues are greater than t, representing those parts of the solution that are well determined by the data. Therefore, these eigenvalues must remain unchanged. There exist no eigenvalues in region II, but if there were any, they could be used for computations due to their high numerical reliability. As the the eigenvalues $\lambda_k < t$ are supposed beyond the effective degrees of freedom in the data and reflect the nonuniqueness of the downward continuation problem, we

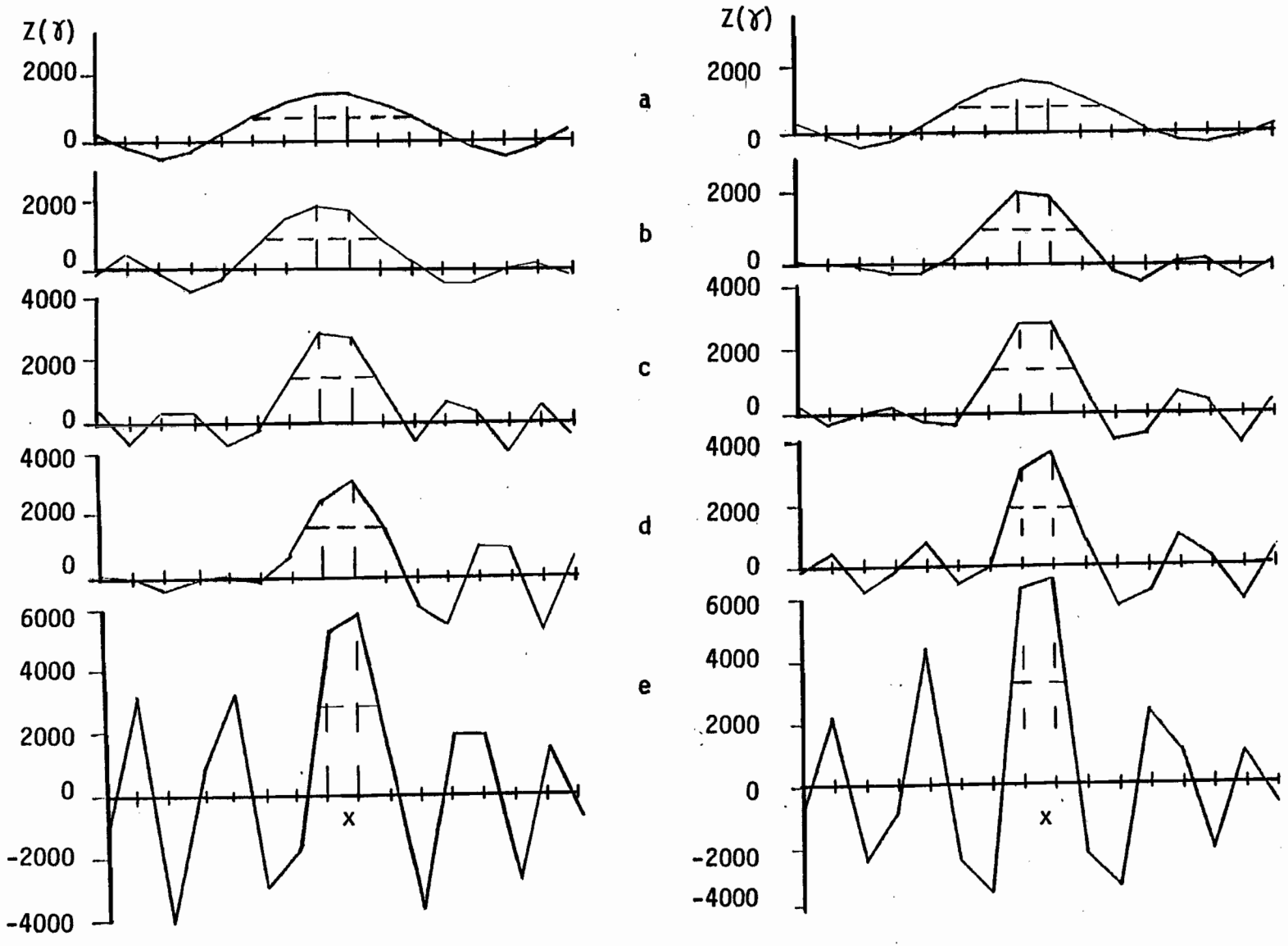

Figure 4.4. Comparison of continuation estimates obtained by using Wiggins' procedure (left) and image procedure (right). Curves a-e correspond to t=0.05, 0.01, 0.005, 0.0025 and 0.001 respectively. Vertical dash lines show the source width while horizontal dash lines show resolution width.

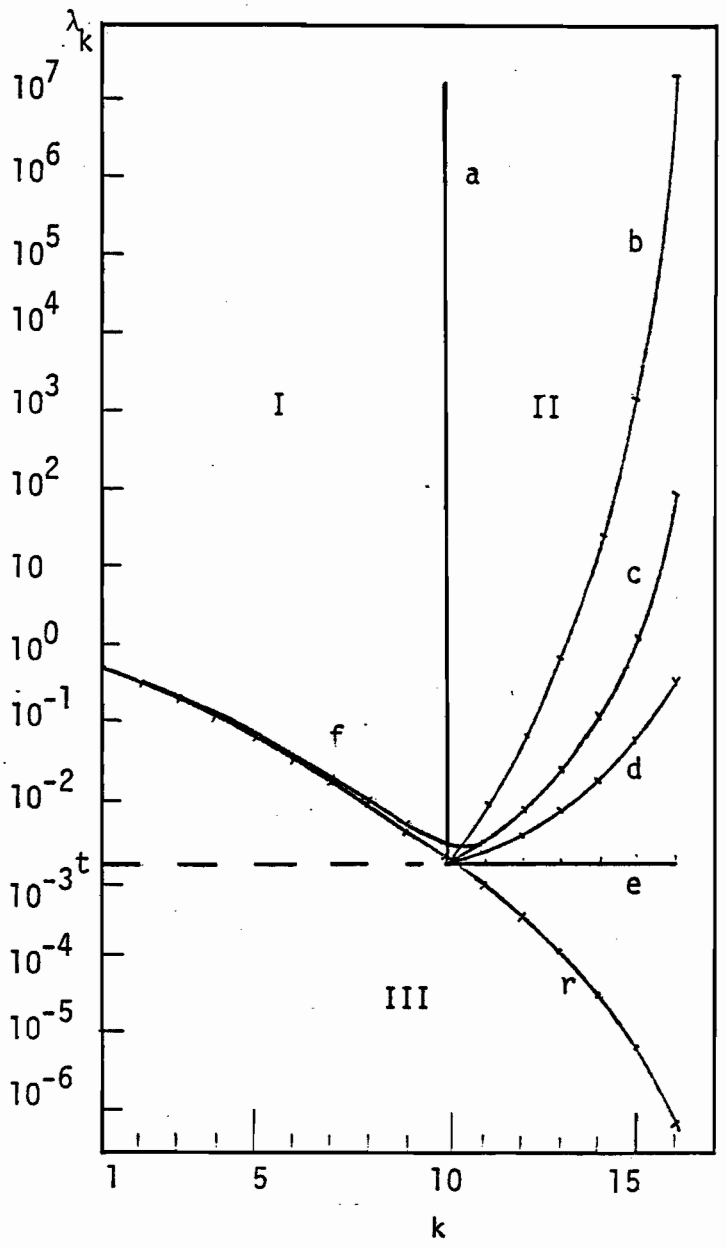

Figure 4.5. Modified eigenvalues. Curves a-f correspond to formulae (4.37.a-f) respectively. Curve r shows the true eigenvalues. Region I is the area where eigenvalues do not need to be modified, region II is a "free-choice" area for eigenvalues and in region III eigenvalues cause computational instability.

may consider a modification of the small eigenvalues to simulate their behaviour in the damped least squares method (Fig. 4.2), i.e. to convert them from region III to region II. In practice the small eigenvalues beyond k>q do not impair the ability of the new field estimates be upward continued to adequately fit the data. Thus the region II can be called the free-choice region for eigenvalues. We may now try various options to see if there exists a better one with better trade-off between the main-peak width and the sidelobe amplitude. Denoting $\lambda_{\alpha k}$ *for k>q as the modified eigenvalues, we may try the following options*

$$\lambda_{\alpha k} = t(t/\lambda_k)^2 \qquad (4.37.b)$$

$$\lambda_{\alpha k} = t^2/\lambda_k \qquad (4.37.c)$$

$$\lambda_{\alpha k} = t(t/\lambda_k)^{1/2} \qquad (4.37.d)$$

$$\lambda_{\alpha k} = t \qquad (4.37.e)$$

The corresponding modified eigenvalues are shown by curves a-e in Fig. 4.5 respectively. It is clear that the curve c is symmetric to the true eigenvalues (curve r) by the line λ_k*=t. We may then say that equation (4.37.c) presents the image procedure for modifying small eigenvalues.*

The downward continuation estimates obtained by spectral expansion method incorporated to the procedure (4.37,a-e) are shown in Fig. 4.6 (Curves a-e, respectively). From curve (a) to curve (e) the main-peak width decreases, while the smallest and uniform sidelobes appear in the curve c, corresponding to the image procedure. Comparing the estimates produced by the Wiggins' and the image procedures for different threshold values (see Fig. 4.4) ensures that the image procedure produces preferable estimates.

The main-peak width and the sidelobe ratio $|A_S/A_M|$ *in the estimstes produced by using procedures (4.37,a-e) are shown in Table 4.2.*

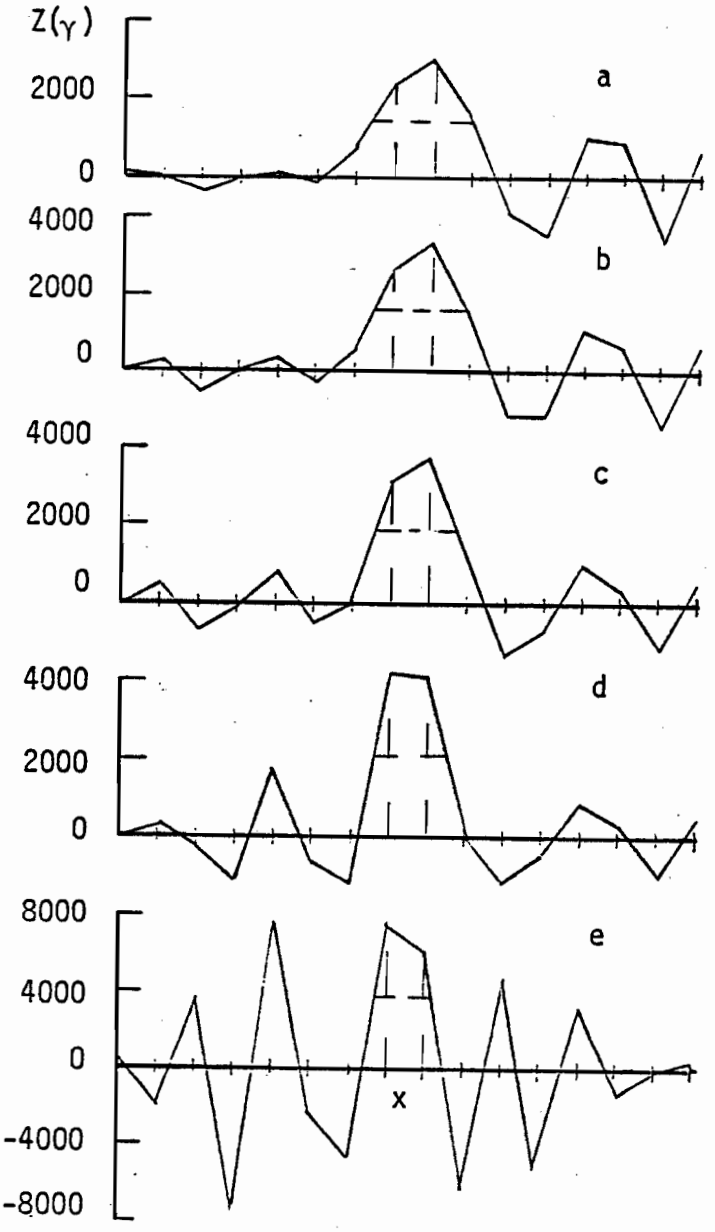

Figure 4.6. Downward continuation estimates of spectral expantion procedures (t=0.0025). Curves a-e correspond to the curves a-e of modified eigenvalues shown in Figure 4.5. Vertical dashed lines show the source width while horizontal dashed lines show the main-peak whidth.

Table 4.2. The Main-peak width and maximum sidelobe ratio for different eigenvalue modification procedures

Procedure	$W(\Delta x)$					$\lvert A_S/A_M \rvert$ (%)				
$t=$	.001	.0025	.005	.01	.05	.001	.0025	.005	.01	.05
(4.37.a)	1.80	2.60	2.80	3.70	5.20	66.4	45.6	36.6	33.7	34.0
(4.37.b)	1.72	2.40	2.72	3.50	5.20	61.9	42.1	34.3	25.1	33.4
(4.37.c)	1.70	2.10	2.60	3.20	4.60	67.7	36.1	33.1	16.3	29.9
(4.37.d)	1.48	1.90	2.20	2.80	4.60	77.3	45.5	28.3	19.0	25.7
(4.37.e)	1.30	1.50	1.64	1.80	3.00	124.	101.	66.2	60.0	33.9
(4.37.f)	1.70	2.10	2.80	3.10	4.90	51.7	25.8	18.4	13.2	28.5

From the table it can be seen that sharp main-peak cannot be achieved with a large threshold t, whereas it is impossible to obtain small variances if t is too small. The best main-peak width (W=1.3) is produced by (4.37.e) with t=0.001 but the corresponding sidelobe is extremely large ($|A_S/A_M|$=1.24). The best trade-off estimates seem to be produced by the image procedure with t=0.0025 (q=10), correspondingly W=2.1 and $|A_S/A_M|$=0.36, or the procedure (4.37.d) with t=0.005. In general, changing the threshold and using the image procedure can be a fast way to find the best trade-off estimate of downward continuation.

4.3.3 An improved procedure

Although we have found that the image procedure can be better than the Wiggins', the estimates are still not as good as that produced by the damped least squares method. A problem to be considered is the discontinuity of the modified eigenvalues around k=q. Because the true eigenvalue sequence is continuous, one might require the modified eigenvalues to show similar behaviour. In order to eliminate the discontinuity the eigenvalues λ_k in region I may also be modified slightly. A continuous version of the image procedure can be obtained by adding a linearly weighted difference $(\lambda_{\alpha q+1}-\lambda_q)$ to $\lambda_k(k\leq q)$. This empirical modification can be expressed as

$$\lambda_{\alpha k} = t^2/\lambda_k \qquad \text{if } k>q$$

$$\lambda_{\alpha k} = \lambda_k + k(t^2/\lambda_{q+1} - \lambda_q)/q \qquad \text{if } k\leq q \qquad (4.37.f)$$

Employing this new modification procedure, which will be called the improved procedure, we obtain a better estimates as shown in Table 4.2 (last

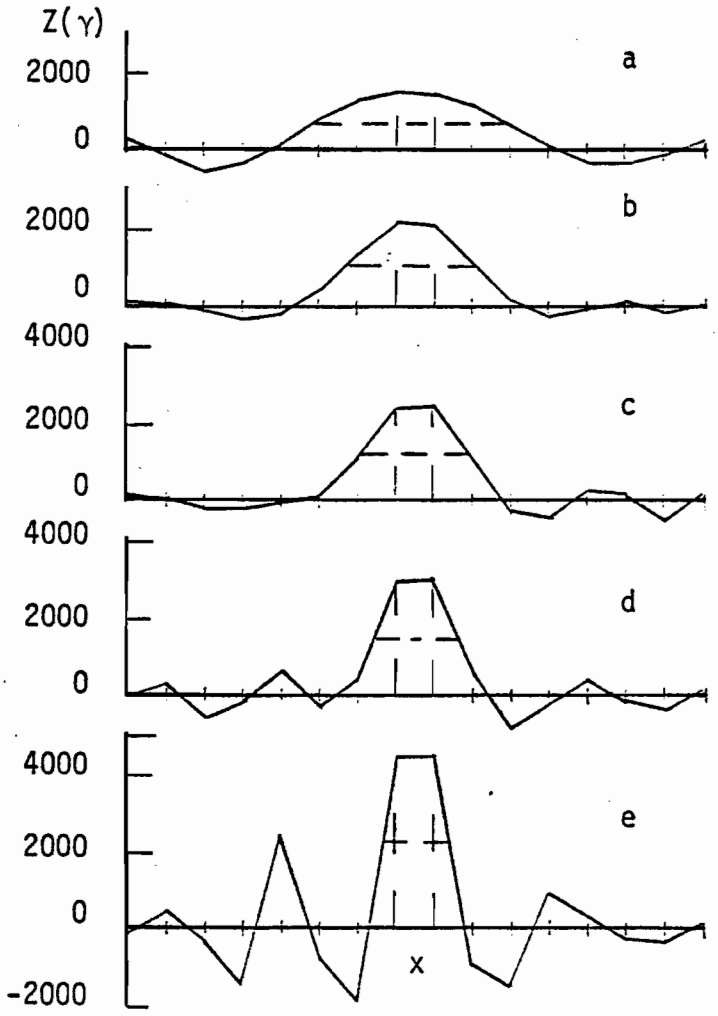

Figure 4.7. Downward continuation estimates from the improved procedure. Curves a-e correspond to t=.05, .01, .005, .0025 and .001 respectively. Curve d shows the best trade-off between the main-peak width (2.1Δx) and the maximum sidelobe (25%).

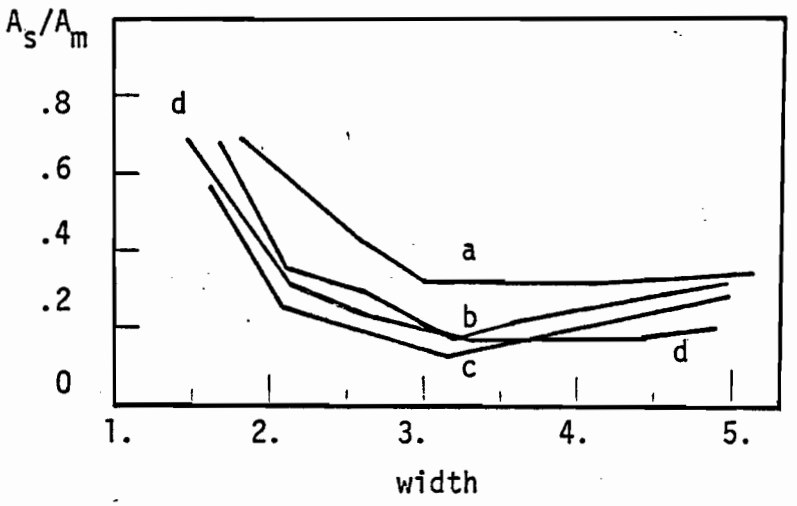

Figure 4.8. The trade-off Curves from different spectral expansion procedures: (a) the Wiggins', (b) the image , (c) the improved procedure and (d) the damped least squares.

row) and Fig. 4.7. Comparing the improved procedure with the image procedure, we find that the maximum sidelobe is reduced from 36% to 25.8% for t=0.0025 while the main-peak width remains the same. We may compare different procedures via the trade-off curves (Fig. 4.8). The four different procedures, including the Wiggins', the image, the damped least squares and the improved procedure, have distinct but almost parallel trade-off curves, showing that the image is better than the Wiggins'; the damped least squares precedes the image and the improved procedure is the best, in the sense of producing an estimate with both sharp main-peak width and small sidelobes.

We are able to explain why the procedure improves the estimate by examining the covariance matrices in (4.36). If $\underline{C}_{\varphi}^{-1} = \alpha \underline{I}$, (4.36) becomes the solution of the damped least squares as shown in (4.33). We may consider a more complicated case where both $\underline{\varphi}$ and $\underline{\psi}$ are stochastic processes with containing noise. Then the general expression (4.36) becomes

$$\underline{\tilde{\varphi}} = (\underline{G}^T\underline{G} + \underline{C}_{\varphi}^{-1})^{-1} \underline{G}^T\underline{\psi} \qquad (4.36.a)$$

With E denoting the expectation value, the covariance matrix is given by

$$\underline{C}_{\varphi} = E \left[(\underline{\varphi} - \underline{\bar{\varphi}})(\underline{\varphi} - \underline{\bar{\varphi}})^T \right]$$

where $\underline{\bar{\varphi}}$ is the mean vector of $\underline{\varphi}$. Denote $\underline{\bar{\psi}}$ as the mean vector of $\underline{\psi}$, $\underline{C}_{\varphi}$ can be further expressed by

$$\underline{C}_{\varphi} = \underline{G}^{-1}\underline{C}_{\psi} (\underline{G}^{-1})^T$$

where $\underline{C}_{\psi}$ is the covariance matrix of the data. Inserting (4.12) we get

$$\underline{C}_{\varphi} = \underline{V}\,\underline{D}\,\underline{V}^{T}$$

where

$$\underline{D} = \underline{\Lambda}^{-1}\underline{U}^{T}\,\underline{C}_{\psi}\,\underline{U}\,\underline{\Lambda}^{-1}$$

Thus, (4.36.a) becomes

$$\tilde{\underline{\varphi}} = \underline{V}(\underline{\Lambda} + \underline{D}^{-1})^{-1}\underline{U}^{T}\underline{\psi} \qquad (4.36.b)$$

When $D^{-1}=diag(\lambda_{\alpha 1},\ldots,\lambda_{\alpha M})$, *(4.36.b) yields estimates from the improved procedure which corresponds to the covariance matrix having the spectral expansion of* $\underline{V}\underline{D}\underline{V}^{T}$. *An more complicated covariance matrix might be assumed, but the resulting procedure will no longer take advantage of the orthogonal diagonalization.*

So far we have shown the results for downward continuation to a level of the top of sources. We may expect that better results can be obtained if the continuation depth is smaller. Fig. 4.9 shows the best trade-off estimates of continuation to $H=0$ *and* $H=-\Delta x$ *for our example in Fig. 4.1. As the continuation depth decreases, the sidelobe amplitude in the estimates decreases. In order to achieve the best trade-off the threshold t for modifying the eigenvalues must increase, because matrix* $\underline{G}$ *becomes better conditioned and the eigenvalues become larger for a smaller continuation depth. As the integer q is the the effective number of degrees of freedom in the data, it is not affected by the continuaton depth being large or small. When* $\underline{G}$ *becomes better conditioned as* H *becomes smaller, we must increase the threshold t to keep the integer q unchanged. For the case shown in Fig. 4.9, the effective number q equals ten for all three estimates.*

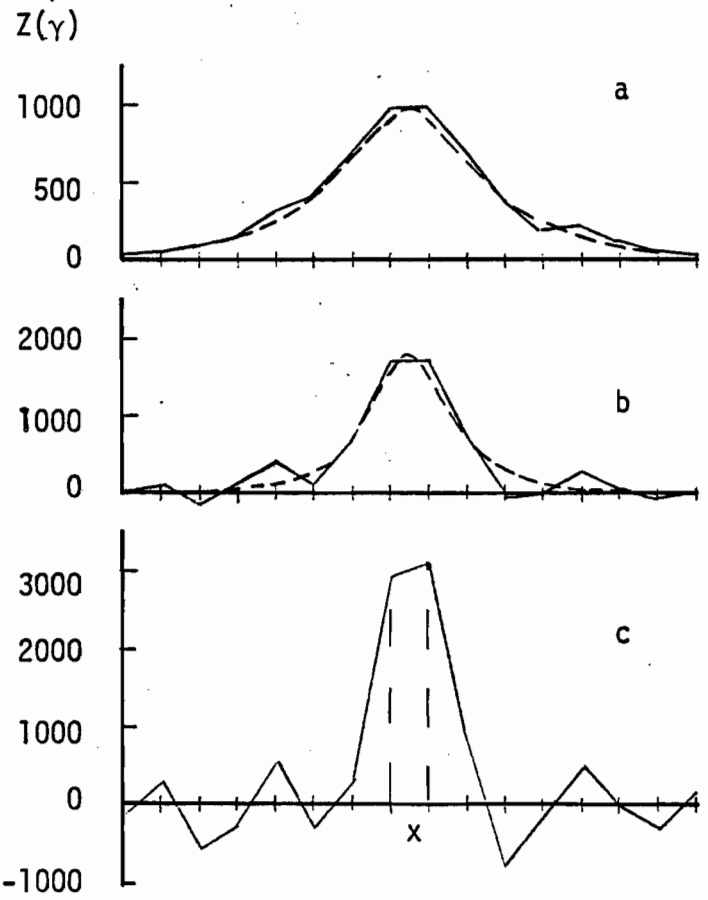

Figure 4.9. Downward continuation estimates (solid lines) on different levels. Curves a-c correspond to H=0, Δx and $2\Delta x$ and t=0.05,0.01 and 0.0025, respectively. Dash lines show the theoretical anomaly on the levels.

4.3.4 The overconstrained case

Because the energy of potential fields is concentrated close to the sources when downward continuation is performed, the field sufficiently far away from the sources may be considered negligible. In Figuer 4.1, the vertical magnetic component becomes zero at the level of $H=-2\Delta x$ except on top of the dike. Hence we may impose some more constraints on the solution, such as $\varphi_i=0$ for $i=1,2,3$ and $14,15,16$ in this example. As a result, the equation (4.9) becomes an overconstrained system. In section 4.2.3 we have shown the Lanczos inverse for an overconstrained linear system and application of the previously discussed procedures for eigenvalue modification is straightforward. We first consider the uncontaminated data (Fig. 4.10.a) generated by the same source shown in Fig. 4.1.c. Because now the unknown vector has only ten elements, φ_i, $i=4,5,\ldots,13$, correspondingly the matrix $\underline{G}$ is dimensioned 16 by 10 and has only ten non-zero eigenvalues. The best trade-off estimate is achieved by setting $t=0.0001$, or $q=9$, as shown in curves b and c in Figure 4.10. The main-peak width is $2\Delta x$ for all the curves (that is the best we can do) while the maximum sidelobe is 11.9% for the improved procedure (curve c) and 16% for the image procedure (curve b). Comparing curve b with curve d, which corresponds to the well-posed case and has a maximum sidelobe 20.6%, we see that as expected the overconstrained system produces better solutions than the well-posed for uncontaminated observations.

A surprising fact is that imposing more constraints on the solution does not improve the downward continuation estimates for noisy data (curve e in Fig. 4.10). The maximum sidelobe becomes 38.3%, larger than that in the well-posed case, probably due to concentration of the power of the noise in the shorter profile. For our example, on the hill the noise is originally distributed in all 16 observations, but after downward continuation via the

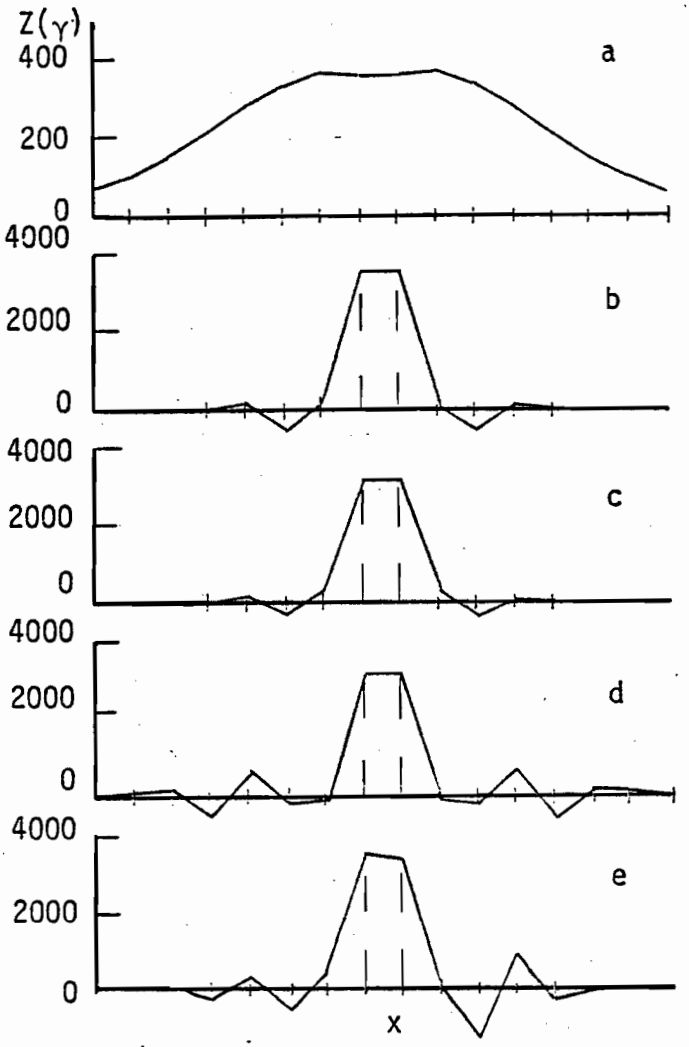

Figure 4.10. Downward continuation estimates. (a) Uncontaminated anomaly on the hill. (b) Overconstrained case and the image procedure. (c) Overconstrained case and the improved procedure. (d) Well-posed case and the image procedure. (e) As the same as (b) but continued from the noisy data shown in Figure 4.1.a.

overconstrained system the power of the noise is concentrated into only ten estimates. As a result, we would not suggest using the overconstrained inverse when the data are seriously contaminated.

4.4.5. Examples of downward continuation

So far we have seen a typical example of magnetic data contaminated by a signal-associated noise. We may see what will happen for purely independent noise. Assume that a white noise with zero mean and standard deviation $\sigma = 15$ nT (about 4% of magnitude of the anomaly) is added to the anomaly due to the dike (Fig. 4.1.c). Employing the damped least squares and the improved procedure, we obtain two sets of estimates whose main-peak width and sidelobe ratio are shown in Table 4.3.

Table 4.3. Main-peak width and sidelobe ratio for the data contaminated by independent noise

Improved procedure				Damped least squares		
t	q	$W(\Delta x)$	$\lvert A_S/A_M \rvert$(%)	$\alpha(\cdot 10^{-3})$	$W(\Delta x)$	$\lvert A_S/A_M \rvert$(%)
.02	7	4.3	21.8	.1	3.8	19.0
.01	8	3.5	22.5	.05	3.3	26.9
.005	9	2.7	39.8	.025	2.8	36.6
.0025	10	2.2	36.1	.01	2.4	44.9
.001	11	1.8	49.5	.005	2.1	45.6

By choosing $\alpha = .025 \cdot 10^{-3}$ for the damped least squares or $t=0.0025$ for the improved procedure we get the best trade-off estimate. The improved procedure once more produces better results for downward continuation.

It might be desirable to compare the downward continuation results obtained by the spectral expansion and by Huestis and Parker's procedure (1979), who gave an example of a gravity anomaly due to a uniform, semi-infinite slab of density ρ in the region $0 \leq x$, $-h \leq z \leq 0$ with $h > 0$. The gravity field at (x,z) with $z \geq 0$ is

$$g(x,z) = G\rho\left(\pi h + x \, Ln\frac{x^2+(z+h)^2}{x^2+z^2} + \frac{z+h}{2}\tan^{-1}\left(\frac{x}{z+h}\right) - \frac{z}{2}\tan^{-1}\left(\frac{x}{z}\right)\right) \qquad (4.38)$$

This field was sampled on a constant level at eight points $((n+1/2)h, 3h)$, $n=-4,-3,\ldots,2,3$ (see Fig.4.11.a). These data were then used to compute estimates of field at several different levels below $z=3h$. For $x \geq 0$, the true field values (solid lines in Fig. 4.11.b) and the downward continuation estimates obtained by Huestis and Parker (dashed lines) are compared with the damped least squares estimates (dot lines).

Comparing the results indicates that the spectral expansion techniques can produce a downward continuation estimate as good as those by the method minimizing a functional form of the model subject to some constraints; while the former takes the advantage of computation convenience. This example also shows that the field estimates from the spectral expansion might be in serious error at the edges of the model because the anomaly has infinite energy and in such a case the trade-off parameter must be chosen very carefully. For instance, we show on purpose the large variance in the estimate at $x=3.5h$ and $z=0.5h$ (Fig. 4.11.b, first diagram), which corresponds to the standard least squares estimate in which the trade-off parameter equals zero. Appropriate

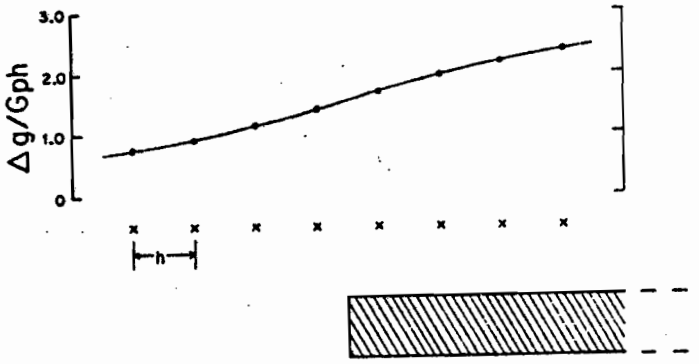

a

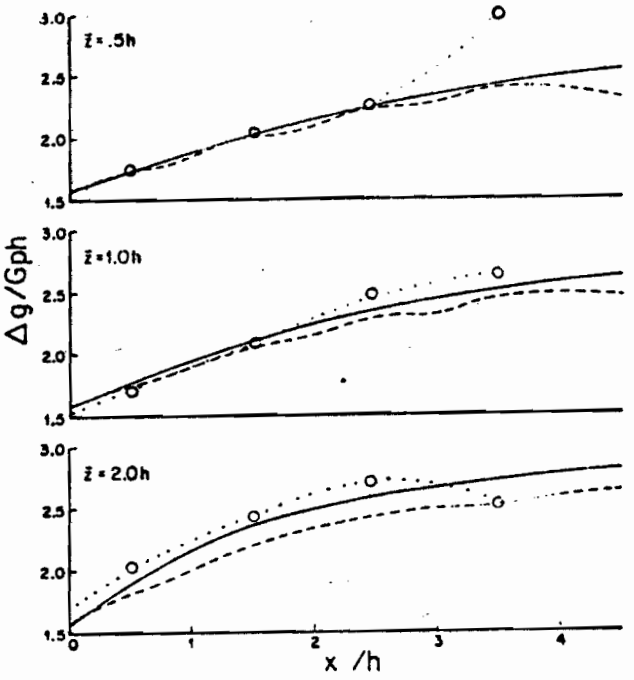

b

Figure 4.11. An example given by Huestis & Parker (1979). (a) Geometry of the model and gravity anomaly. The crosses mark the observation points above the slab (shown shaded). (b) True field values and downward continuation estimates at levels $\bar{z}$ below the observation level. Solid curves show the true field values, dash lines are estimates by Huestis and Parker and the circles joined by dot lines show the estimates by the stochastic inverse procedure with the tradeoff parameter 0.15 for $\bar{z}$=1.0h and 2.0h, zero for $\bar{z}$=0.5h.

choice of the parameter may reduce the edge-effect as shown by the estimate of $\tilde{z}$=1.0 (second diagram in that figure). In this example, possibly also for other anomalies with infinite energy, the damped least squares procedure produces better results than the improved procedure which is more sensitive to the edge-effect.

Let us now see examples of 2-D potential field data. Suppose that a gravity survey is carried out in a small uniform (8 by 8 with inteval 200m) grid on a two-dimensional 30° slope mountain range (striking in the y-direction), with maximum of height 350 meters. The source of the gravity anomaly, shown by a circle in Figure 4.12.a, is a vertical mass line with a mass of 0.2 tons/meter, depth of 200m and length of 200m. Due to the topography, it can be seen that the maximum point os the anomaly is located 200 meters away from the projection of the source. It implies that drilling at the maximum point of the anomaly would miss the target. The damped least squares is employed to continue the anomaly to a level on top of the mass with gravity estimates on the plane as shown in Fig. 4.12.b. This anomaly is now well concentrated at the top of the mass without any shift. The overconstrained case is used in the example and the trade-off parameter of $0.25*10^{-5}$ gives the results.

Another example is a gravity anomaly due to a square prism on a 2-D mountain similar to that in the previous example (Fig. 4.13.a). The prism has a density of 0.5 g/cm^3, horizontal sides of 400m, depth of 200m and depth extent of 200m. The ground anomaly is elongated perpendicular to the strike of the hill, which tends to produce a false impression that the source is a non-equiaxial body. After downward continuation to the level at bottom of the hill, the anomaly appears equiaxial and coincides well with the square prism (Fig. 4.13.b). The well-posed case is used in this example.

In chapter 3 we have already shown a practical example of downward continuation of a gravity profile in the Abitibi belt (p.3.32). The results shown

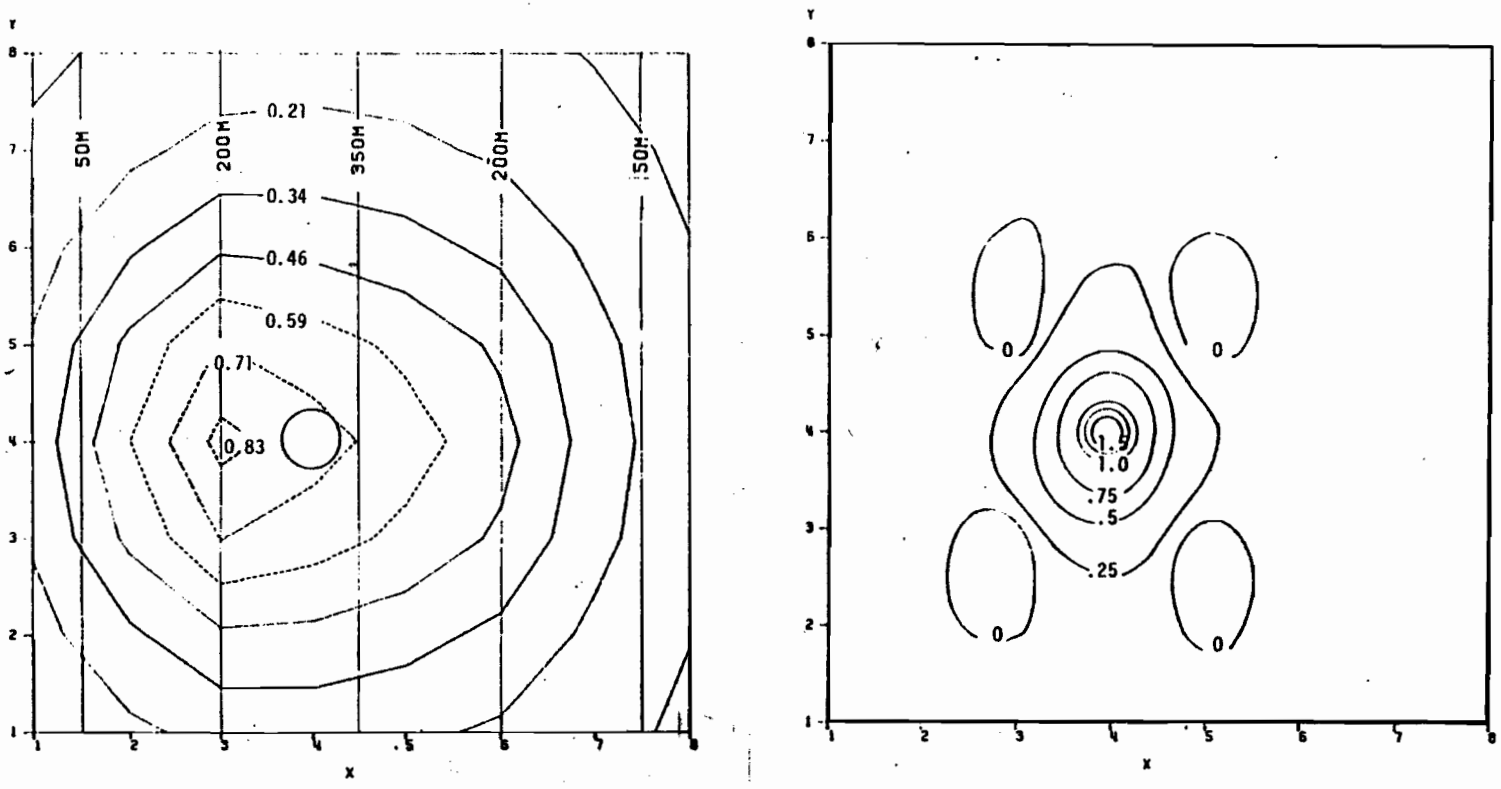

a b

Figure 4.12. The gravity anomaly with topografpy (a) and its downward continuation estimate on top of the source (b). The values in contours are in mgals and coordinates are in $\Delta x = \Delta y = 200m$.

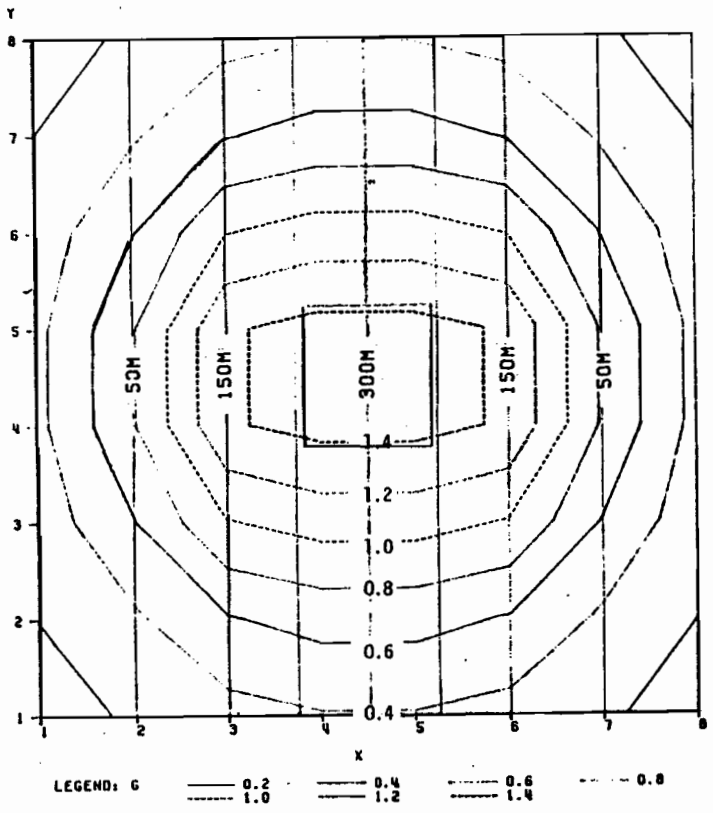

a

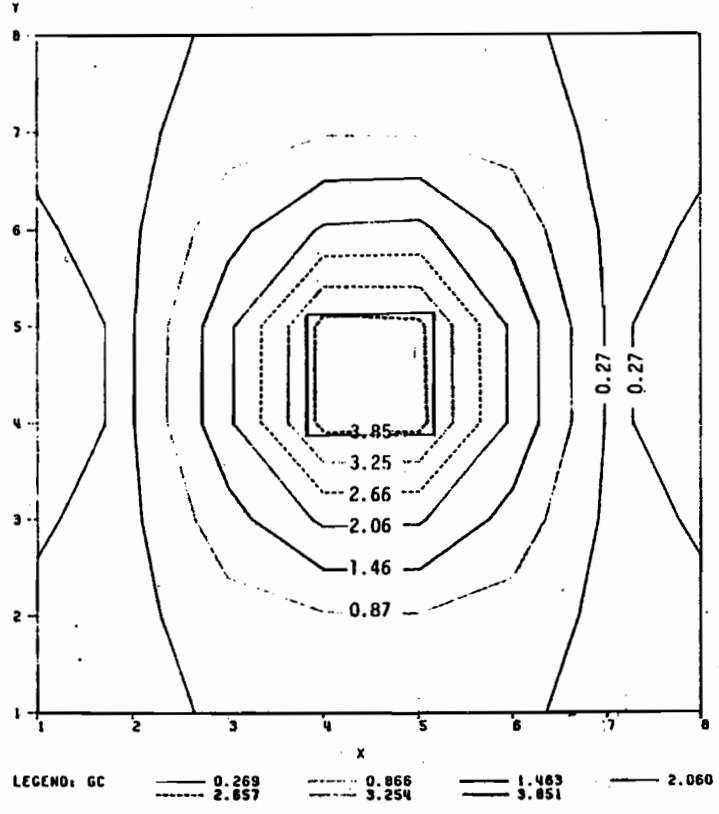

b

Figure 4.13. The gravity anomaly with topography (a) and its downward continuation estimste to the bottom of the hill. The values in contours are in mgals and coordinates are in $\Delta x=\Delta y=200m$.

in Figure 3.20.c were obtained by employing the damped least squares procedure with the trade-off parameter equal to 0.003.

To end this discussion on downward continuation, we invert a magnetic profile with topography (Fig. 4.14.b). A ground magnetic anomaly (C5) appears in a steep mountain area within the Sichuan province of China (Fig. 4.14.a). Although the anomaly is a weak one with a maximum of 470 nT(gamma), it could be due to magnetite deposits because the only outcrops that can be seen in the area are marble layers. Five drilling wells, numbered zk8, zk9, zk10, zk18 and zk19, were completed, but only well zk18 touched upon ore deposits, at a depth of 277 meters. The high topographic relief causes great difficulty in interpretation. In order to locate the ore bodies, a profile across the center of the anomaly is shown in Fig. 4.14.b. Using 14 observations along the profile, the improved procedure (t=0.01) produces anomalies on the levels at H=50m and H=100m (see Fig. 4.15), the latter is close to the top of the ore bodies discovered in well zk18. On the observation surface, the peak of the anomaly appears around point 9, but it disappears at the level H=100m, implying that the peak is probably affected by topographic relief. From the continuation results, it is clear that the ore body is probably located under points 4 to 9, but not under 7 to 11 as shown by the ground anomaly. That explains why no ore body was found in well zk19. In general, potential anomaly peaks in mountainous areas are likely to appear shifted horizontally from their sources. Application of the downward continuation procedure may successfully eliminate the shift and provide a more reliable estimate of the source location, so that the probability of finding ore deposits by drilling can be considerably enhanced.

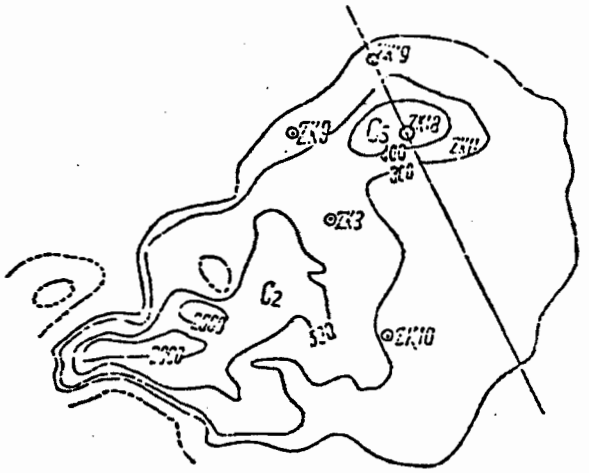

(a)

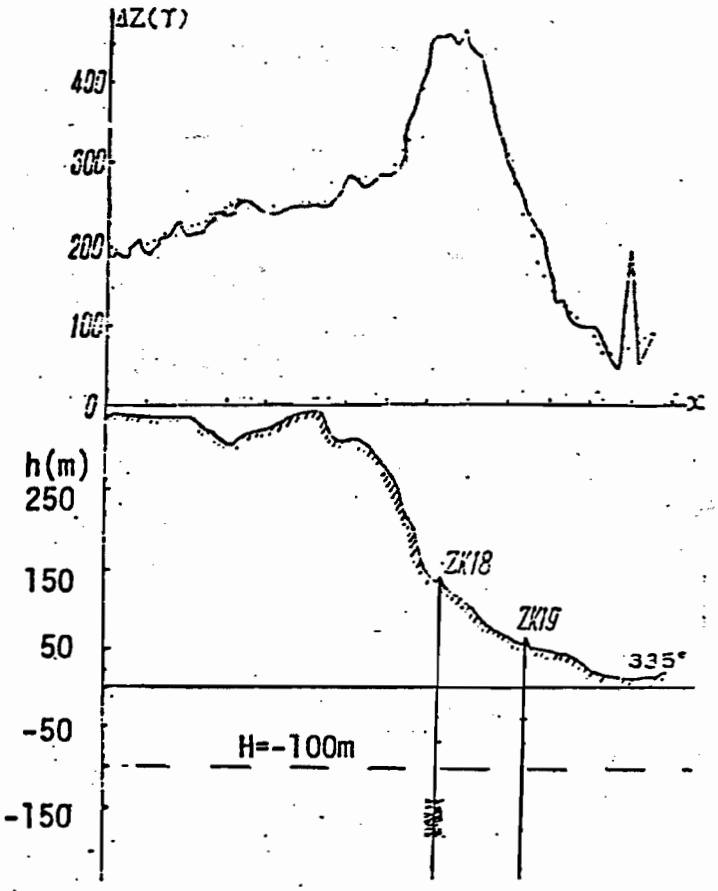

(b)

Figure 4.14 . A vertical magnetic anomaly in Sichuan province of China. (a) contuour map and (b) a profile with topography.

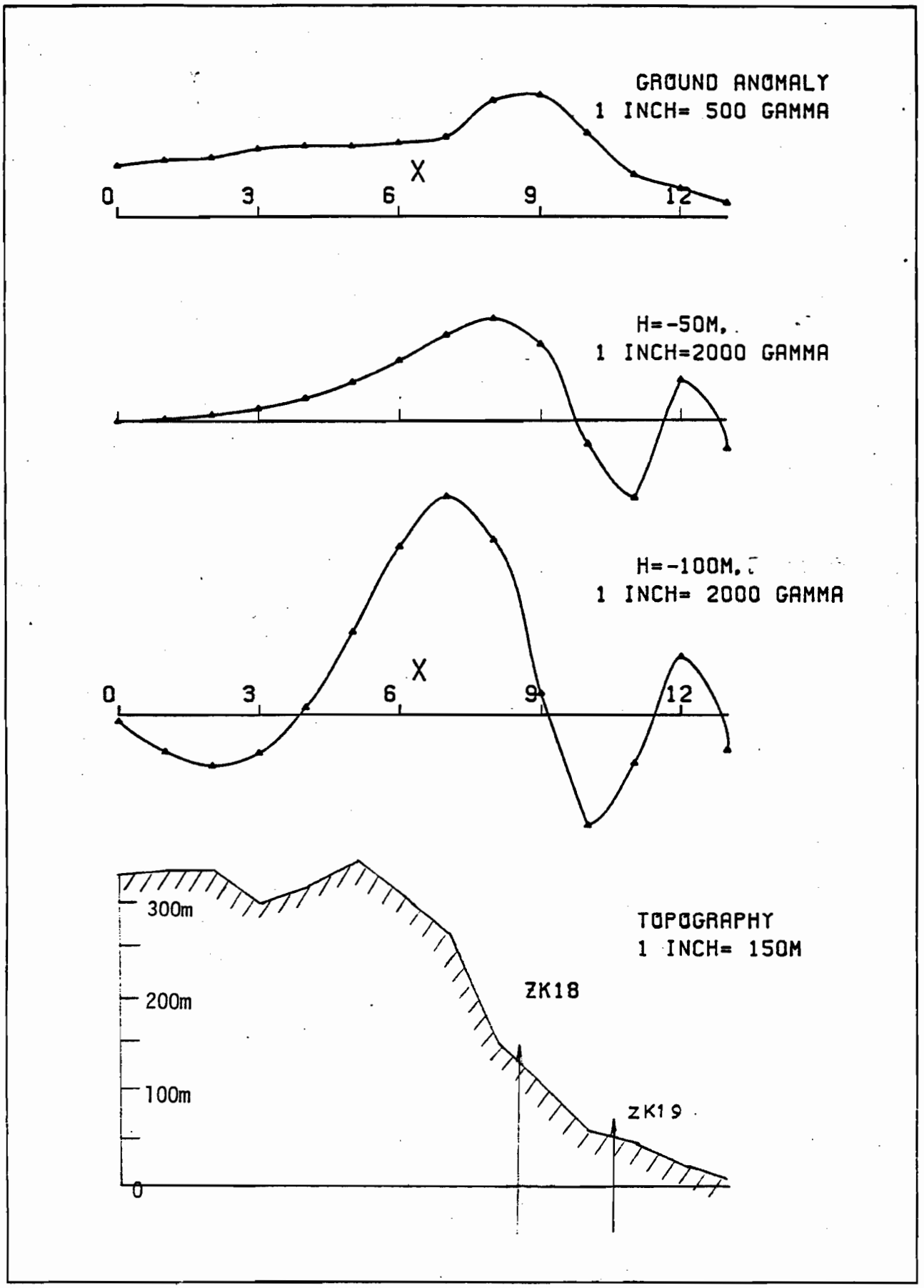

Figure 4.15. The downward continuation estimates of the profile shown in Fig. 4.14.b.

4.4 Upward Continuation between Arbitrary Surfaces

4.4.1 The equivalent source method

From the viewpoint of potential theory, upward continuation is a Dirichlet problem. Let $\Phi(x,y,z)$ be a harmonic function at a point $P(x,y,z)$ in a volume V which is enclosed by an arbitrary surface S. If there is no source in V, Φ must satisfy Laplace's equation. With given boundary values on S, the solution for this problem is unique, and therefore can in principle be obtained via any numerical methods for solving partial differential equations, such as the finite difference method. The Dirichlet problem can also be expressed by the variational principle, that is, the solution Φ of the Dirichlet problem is that which minimizes the functional

$$F(\Phi(x,y,z)) = \iiint_V \left(\left(\frac{\partial \Phi}{\partial x}\right)^2 + \left(\frac{\partial \Phi}{\partial y}\right)^2 + \left(\frac{\partial \Phi}{\partial z}\right)^2 \right) dxdydz$$

subject to given boundary values on S. As a matter of fact, the functional represents stored energy of the potential fields. Thus the finite element method, which we have disccussed in Chapter 3, is also applicable to upward continuation. Difficulty in this application arises when the volume V becomes very large, because an enormous number of nodes, which in turn means the same number of equations, will be involved. Hence these methods are suggested for two-dimensional field continuation, but may be too expensive for 3-D data processing.

In general the specification of the boundary values is equivalent to sources which are distributed outside the boundary. Solution of Dirichlet

problems can be represented by the so-called " double layer potential" as follows:

$$\Phi(p) = \iint_S \mu(q) \frac{\partial}{\partial n} \left(\frac{1}{r(p,q)} \right) ds \qquad (4.39)$$

(Kellog, 1953, p.286), where n denotes the external normal of S and μ is the intensity of the equivalent source. If Φ also satisfies the given boundary condition, it should be the solution of the Dirichlet problem because of the uniqueness of the solution of the boundary-value problem. Let us denote the boundary value of $\Phi(p)$ by $\Psi(q)$. Restriction of Φ to the observation surface S yields

$$\Psi(q) = 2\mu(q) + \iint_{S'} \mu(q') \frac{\partial}{\partial n} \left(\frac{1}{r(p,q)} \right) ds' \qquad (4.40)$$

where S' is the surface S excluding a small area around point q (Fig.4.16). Equation (4.40) is a Fredholm integral equation of the second kind and could be solved by an iterative scheme. This procedure was suggested by Bhattacharyya and Chan (1977) and called the equivalent source method. Following this procedure, the first step for upward continuation from an arbitrary surface is to determine the equivalent sources by employing an iterative technique to solve the integral equation (4.40). In the second step, equivalent sources are substituted into (4.39) for computing the field at any point above the observation surface S. It will be shown that the two steps can be joined together to make the method more compact.

There is no doubt that the BG method is applicable for the upward continuation problem and can take precedence over other methods if the data is deficient and contaminated (Huestis and Parker, 1979), albeit some

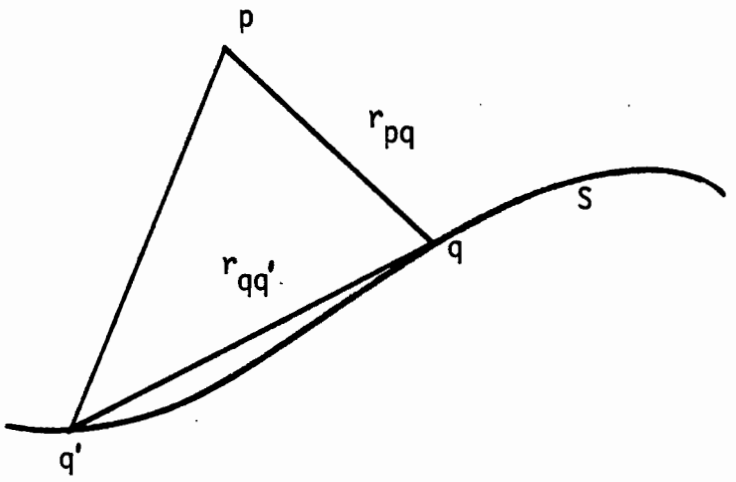

Figure 4.16. The geometry for upward continuation from an arbitrary surface.

computational cost. We notice that the application of upward continuation is mainly in regional data processing but is not ofter used for local anomalies. When it is employed for regional data processing, plenty of data is usually available. In such cases the equivalent source method is applicable and practically useful.

4.5.2 A compact implementation of the equivalent source method

Let us rewrite (4.40) as

$$\mu(q) = \frac{1}{2\pi}\left(\Psi(q) - \iint_{S'} \mu(q') \frac{\partial}{\partial n}\left(\frac{1}{r(q,q')}\right) ds'\right) \qquad (4.41)$$

Inserting this into (4.39) yields

$$\Phi(p) = \iint_{S} \frac{\Psi(q)}{2\pi} \frac{\partial}{\partial n}\left(\frac{1}{r(p,q)}\right) +$$

$$\iint_{S} \frac{\partial}{\partial n}\left(\frac{1}{r(p,q)}\right)\left\{\iint_{S'} \frac{(-1)\mu(q')}{2\pi} \frac{\partial}{\partial n}\left(\frac{1}{r(q,q')}\right) ds'\right\} ds \qquad (4.42)$$

Repeated application of (4.41) to replace $\mu(q')$ in (4.42) yields successive approximation to the solution expressed by

$$\Phi(p) = \iint_{S} \left(\sum_{k=0}^{\infty} I^k(q)\right) \frac{\partial}{\partial n}\left(\frac{1}{r(p,q)}\right) ds \qquad (4.43)$$

where I^k is an integral, with k denotes the number of the iteration, given by

a recursion formula as follows:

$$I^{\circ}(q) = \frac{1}{2\pi}\,\Psi(q) \qquad (4.44)$$

$$I^{k}(q) = \iint_{S'} \left(\frac{-1}{2\pi}\, I^{k-1}(q')\right)\frac{\partial}{\partial n}\left(\frac{1}{r(q,q')}\right) ds' \qquad (4.45)$$

Thus the continuation process becomes a forward approximation. After initializing the integral I° by substituting the boundary values Ψ into (4.44), we may calculate the integer I^{k} via (4.45) until its maximum becomes less than a given tolerance. The sum of I^{k} may be accumulated simultaneously and used to obtain a solution via (4.43). The similarity of the integrals in (4.43) and (4.45) can be utilized to unify the integration programs and rapid convergence of successive approximations has been proved (Bhattacharyya and Chan, 1977).

Denoting N_x,N_y and N_z as the components of the normal n, we have

$$\partial(1/r)/\partial n = (N_x|x-x'| + N_y|y-y'| + N_z|z-z'|)/r^3 \qquad (4.46)$$

Assuming that S is a large hemispherical surface closed by the observation surface. Since potential fields vanish at infinity, for a large radius, the integral in (4.43) vanishes everywhere except on the observation surface. We may further assume that the observation surface is continuous, differentiable, and can be expressed by a function $z'=h(x',y')$. If the z-axis is directed downwards, the angle between the z-axis and the normal n on S is acute. Then the components of the normal are given by

$$N_x = - H_x/(1+ H_x^2 + H_y^2)^{1/2}$$
$$N_y = - H_y/(1+ H_x^2 + H_y^2)^{1/2} \qquad (4.47)$$
$$N_z = 1/(1+ H_x^2 + H_y^2)^{1/2}$$

where H_x, H_y are the first horizontal derivatives of $h(x,y)$. The surface element in (4.43) may be expressed by

$$ds = (1+ H_x^2 + H_y^2)\, dx'dy' = dx'dy'/N_z \qquad (4.48)$$

Substituting (4.46)-(4.48) into (4.45), we get

$$I^k(x',y') = - \frac{1}{2\pi} \iint_{-\infty}^{\infty} I^{k-1}(x'',y'') \frac{|z'-z''| - H_x|x'-x''| - H_y|y'-y''|}{((x'-x'')^2+(y'-y'')^2+(z'-z'')^2)^{3/2}} dx''dy'' \qquad (4.49)$$

where the primed variables ($z'=h(x',y'),x',y'$) and double primed ones ($z''=h(x'',y''),x'',y''$) denote the coordinates of points on the surface, the latter being the integrated variable. The integration in (4.49) should exclude the singular point $(x',y')=(x'',y'')$. The potential at an arbitrary point $P(x,y,z)$ above S is given by

$$\Phi(x,y,z) = \iint_{-\infty}^{\infty} \left(\sum_{k=0}^{K} I^k(x',y')\right) \frac{|z-h| - H_x|x-x'| - H_y|y-y'|}{((x-x')^2+(y-y')^2+(z-h)^2)^{3/2}} dx'dy' \qquad (4.50)$$

where h, H_x and H_y are the elevation and its partial derivatives, respectively.

4.4.3 Computation techniques and examples

There are several methods for speeding the computation. We first notice

that the integral kernel $1/r^3$ has to be repeatedly calculated for each step when equation (4.50) is employed directly. Using a table of possible values of $1/r^3$ may eliminate the repetition, and therefore, speed up the computation.

To deal with the infinity in the integral limits, a window of dimensions (2s+1, 2t+1) is usually employed. Thus after discretization we actually calculate

$$\Phi(m,n) = \sum_{j=-s}^{s} \sum_{i=-t}^{t} \sum_{k=1}^{K} I^k(i,j) * \frac{|h(m,n)-h(i,j)| - H_x(i,j)|m-i|\Delta x - H_y(i,j)|n-j|\Delta y}{\left((m-i)^2x^2 + (n-j)^2 y^2 + (h(m,n)-h(i,j))^2 \right)^{3/2}} \Delta x \Delta y$$

The larger the window, the smaller the truncation error but the less efficient the computation becomes. Thus we now have to introduce a trade-off between the accuracy and the efficiency. The proper size of the window depends upon the continuation height and the anomalous characteristics, and may be determined by trials. However, the truncation error can be somewhat reduced. A rough correction formula for reducing the truncation error may be derived from a consideration similar to continuation between horizontal planes (Xie Qin-Feng, 1966), that is adding a residual

$$res = \hat{\Psi}\,\hat{H}/1.81\,d$$

where d is the side length of a square window, $\hat{\Psi}$ is the average value of potential data on the sides of the window, and $\hat{H}$ is the average height of the upward continuation.

In general, procedures for continuation from an arbitrary surface cost ten times more than a similar procedure for continuation between horizontal planes by employing the FFT algorithms. For the compact procedure with the

aid of the measures stated above, the cost can be reduced to about five times as that of employing the FFT algorithms for corresponding plane continuation, which is shown by the following example. Suppose that a sphere is concealed under a hill which can be described by a 2-D normal-distribution function (Fig. 4.17)

$$h(x,y) = 636.6 \exp (-(x^2/4 + y^2)/12.5) \qquad (4.43)$$

with a height of 636.6 meters. The sphere has a mass of 100 million tons, depth of 300m from the bottom of the hill (z=0). A uniform grid is used for sampling, with an interval equal to 100m. The gravity anomaly due to the sphere is shown in Fig. 4.18. It is clear from the figure that the center of the anomaly shifts away from the sphere due to the effect of topography. Using a 2km*2km window, the procedure produces a gravity anomaly at the level of z=1km as shown in Fig. 4.19. The number of iterations for the estimate is only two. The center of the continued anomaly now moves back to the sphere. Unfortunately, a visible distortion can be found near the boundaries. Increasing the iterations would not improve the results, because it is due to the effct of truncation. In fact, in order to produce the results on a 30*30 grid, a data set on a 50*50 grid has been chosen. It still seems insufficient if high accuracy is required.

4.5 Summary

(1) Because the energy (or power) of potential field anomalies is always in practice finite, we can introduce the space L^2 to represent all harmonic functions for the downward continuation problem. Applying the standard least squares inversion to minimize the L^2 norm results in a bounded inverse operator

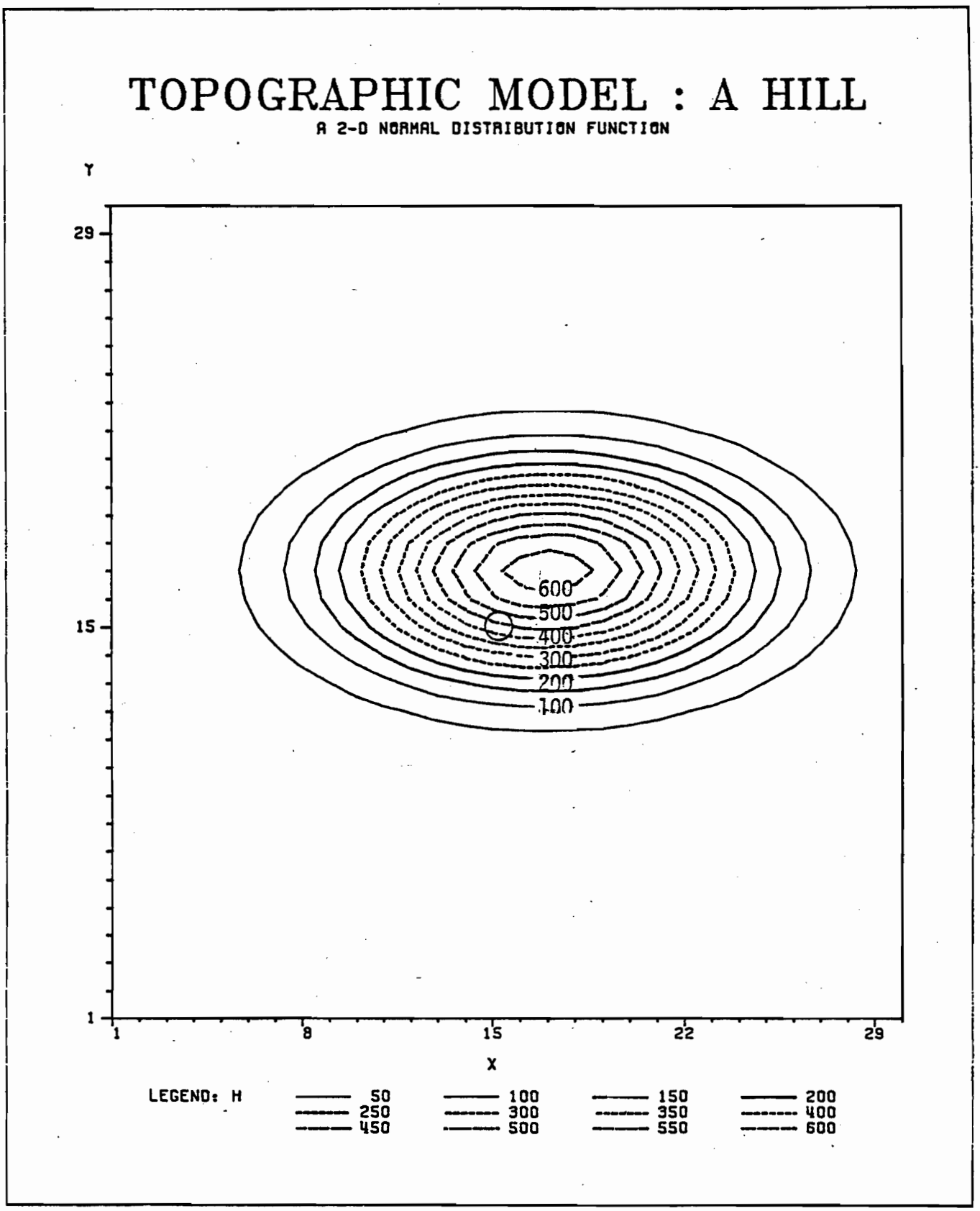

Figure 4.17. A topographic model for upward continuation. The values on contours are in meters and coordinates are in Δx(100m).

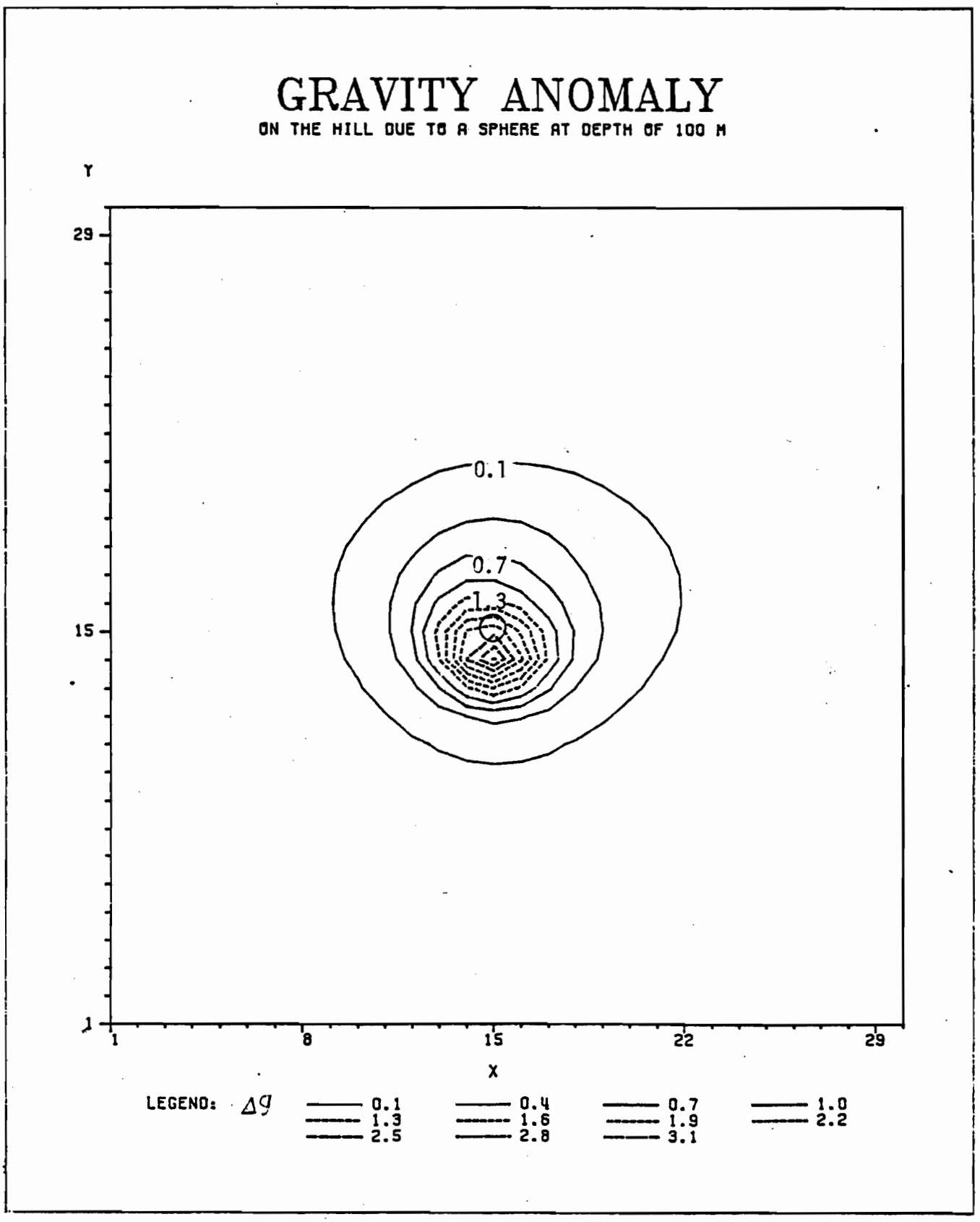

Figure 4.18. The gravity anomaly on the hill due to a sphere. The values on contours are in mgals.

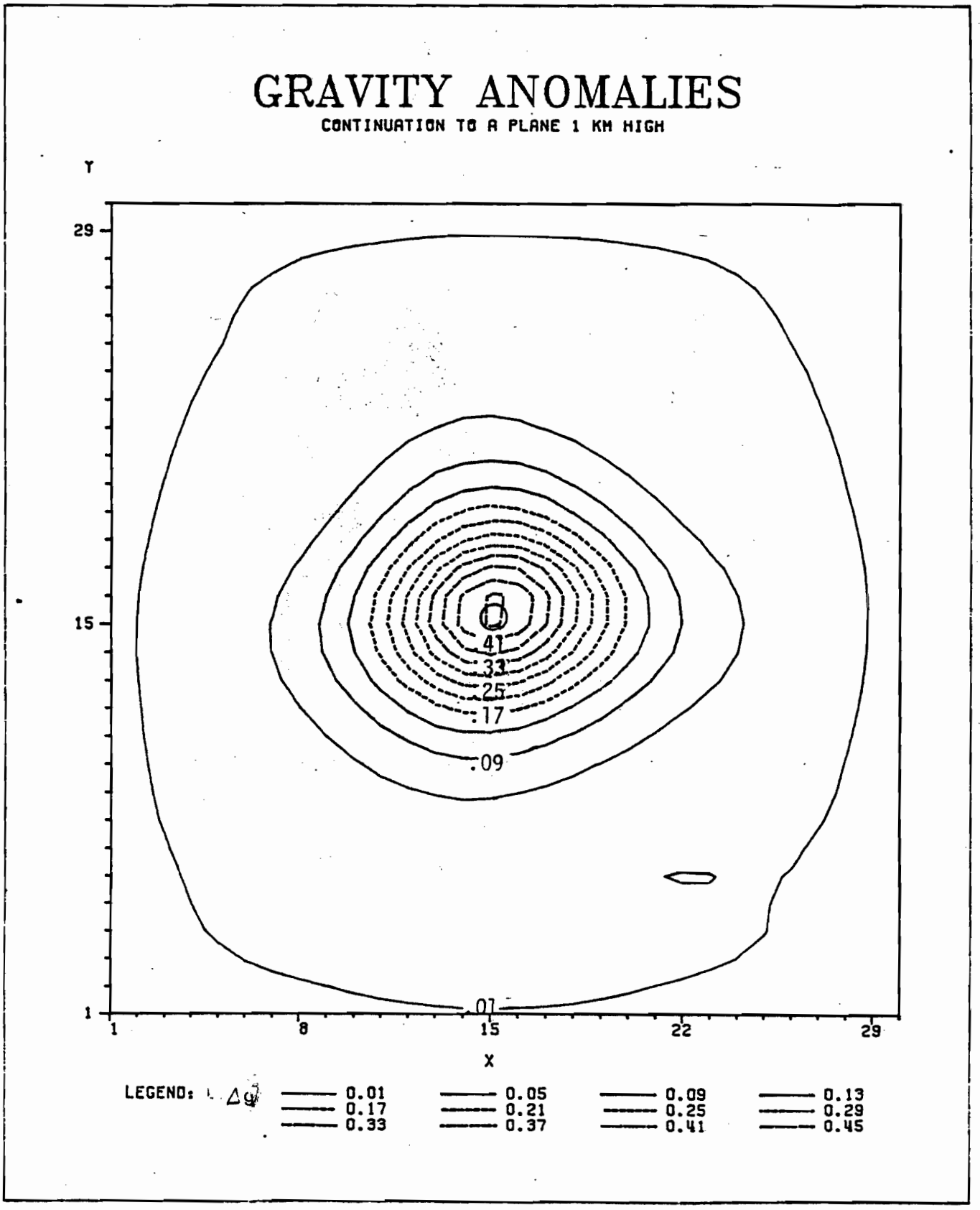

Figure 4.19. The upward continuation estimate of the anomaly in Fig. 4.18. The values on contours are in mgals.

for an optimal solution of downward continuation, which is identical to the stochastic inverse. The procedure is relatively efficient because it requires factoring the mapping matrix only once.

(2) The estimate of the damped least squares approach can be improve by assuming that the covariance matrix of the unkown function is diagonal but more complicated than $\sigma^2 \underline{I}$. *The resulting improved procedure also takes the advantages of the spectral expansion and can produce better estimates for downward continuation of finite-energy anomalies.*

(3) The examples show that these generalized inverse procedures enable us to produce a satisfactory estimate of potential fields on top of sources. In mountain ranges, local anomalies observed are likely to shift away horizontally from their sources. Applying the downward continuation procedures can successfully eliminate the shift and produce a more reliable estimate for locating sources, such as deep faults, lithologic strata of interest and orebodies in mountainous areas.

(4) The equivalent source method (Bhattacharyya and Chan, 1977) has been improved by using a compact formulation which, together with some technical improvements, speeds the computation of upward continuation. The procedure can be useful for compilation of aeromagnetic maps as well as for determining the correct position of orebodies.

Chapter V

Demagnetization and Accurate Computation of Magnetic field

5.1 Introduction

The objective of this chapter is to develop a computational method for calculation of the effective magnetization and the magnetic field both inside and outside any rock materials (including ferro- and ferrimagnetic minerals) with an arbitrary distribution of magnetic parameters. The results are applicable in the following aspects.

(1) Study of the demagnetization phenomena. Some troublesome questions about demagnetization have not been answered which to some extent cause uncertainty both in the specimen measurements of magnetic parameters and in interpretation of anomalies. For instance, does the natural remanent magnetization (NRM) have an effect on demagnetization? If it does, how should one evaluate the effect? Without considering the effect, how large an error would occur for various igneous rocks? An answer to these questions would be useful in both magnetic exploration and in studies of rock magnetism.

(2) Accurate calculation of magnetic anomalies for evaluation of the reserves of magnetic ore-deposits or for elimination of aeromagnetic anomalies due to high topographic relief in crystalline terranes.

(3) Interpretation of ground magnetic anomalies. After discovery of an ore-deposit or even after its exploitation, it is worthwhile to search for blind ore bodies which may be nearby or probably deeper. If a magnetic survey has

been carried out and the magnetic parameters at each location in the bady or bodies are available via specimen measurements or well-logging, a precise calculation of the anomaly due to the known ore-body can determine whether or not a 'residual' anomaly exists. If so, this is usually a reliable indication of another hidden deposit. A precise method is needed which should consider the effect of demagnetization and the inhomogeneity of magnetic parameters.

(4) Interpretation of magnetic well-logging anomalies. Because the magnetic field near and in the sources can become very complicated, a precise procedure for the calculation of both the internal and the external field can help to produce reliable models of magnetic bodies with the aid of magnetic parameters measured on core specimens.

When the demagnetization effect can be ignored, the computational methods for the calculation of magnetic anomalies have been thoroughly documented (Bott,1963; Sharma,1966; Bhattacharyya,1978). However, in some cases the effect of demagnetization should be considered because the magnetization in permeable bodies generates a secondary field which partly counteracts the external magnetizing field. Thus, mathematically it is inexact to equate the induced magnetization $\vec{M}_i$ to the product of volume susceptibility K and external magnetizing field intensity $\vec{H}_o$.

According to the theory of boundary-value problems, the magnetic field inside a susceptible body can be uniform only if the body is bounded by a quadric surface and has constant susceptibility. Under the assumption that the medium is uniformly magnetized, the traditional formula often used for evaluation of induced magnetization is

$$\vec{M}_i = K\vec{H}_o/(1+NK) \qquad (5.1)$$

(Grant and West, p.318, 1965) where N is a constant called the

demagnetization factor, which varies from zero to 4π depending upon only the geometry of magnetized body. For instance, N equals $4\pi/3$ for spheres, 2π for infinite cylinders magnetized transversely, and 4π for flat plates magnetized transversely. Since susceptibilities of rock-forming minerals seldom exceed 0.01 emu (to convert demagnetizaton values in the emu to the SI system multiply by 4π;the CGS emu system has been traditionally used in magnetic exploration, see Telford et al., 1976, p.109), the demagnetization effect computed from (5.1) is usually not noticeble except in magnetite bodies, where K may be as large as 0.5 emu, might demagnetization become significant. However, (5.1) is valid only for bodies of dia- and paramagnetic materials which are bounded by quadric surfaces and have constant susceptibility. More general models and more precise formulae may be needed for evaluating the demagnetization effect.

On account of the demagnetization effect, the effective magnetization usually varies from point to point within an arbitrary body. Because of the difficulty of rigorous computation, most of the computational methods for magnetic calculations have first disregarded the demagnetization effect and calculated a first approximation to the field ; then (5.1) may be used to judge whether or not demagnetization is important. There are only a few articles which consider specificaly the demagnetization effect in magnetic calculations. Vogel (1963) suggested a lengthy iterative procedure for this problem which is based on the assumption that the effective magnetization for a volume element of a magnetized body can be expressed by a series expansion. Each term of the series, except the first one, is the result of integration of the preceeding terms for all the volume elements. If K is large, the series may diverge. Sharma (1966) presented a method for computation of the demagnetization caused by a body of arbitrary shape. A magnetized body can be divided into N prismatic cells and the effective magnetization in each cell can then be represented by the solution of a linear system consisting of 3N

equations. Uniform susceptibility is involed in the equations and the permanent magnetization is ignored. Filatov (1969) proposed another method for 2-D magnetic evaluation. The essence of this method is to calculate the magnetic anomalies caused externally by the magnetic charge density on surfaces of magnetized bodies which is defined by a Fredholm's integral equation of the second kind. The solution of the integral equation is obtained by using an iterative procedure which converges slowly when the susceptibility is greater than 0.1 emu. The assumption of homogeneous magnetization is implied in order to cancel the magnetic charges within the bodies. The method can be used for calculating the field only outside the bodies.

In this chapter we suggest a physical model for a general magnetic material and develop a computational method for the calculation of the effective magnetization and magnetic field both inside and outside an arbitrary body. This method considers fully the effect of demagnetization and inhomogeneity of both the susceptibility and permanent magnetization. Examples are presented for 2-D bodies and theoretical formulae are also developed for 3-D bodies. The theoretical problems of demagnetization will be discussed in section 5.5 while some practical problems will be illustrated in section 5.6.

The notations used are listed below. In order to unify notation for both mathematical formulae and computational formulae (where a subscript often denotes the number of vector or matrix elements) we use $\vec{P}$, instead of $\vec{M}_o$ or $\vec{M}_r$, to denote the permanent magnetization.

K - the volume magnetic susceptibility.

$\vec{M}_i$ - the induced magnetization.

$\vec{P}$ - the permanent magnetization.

$\vec{M}$ - the effective magnetization.

$\vec{H}_o$ - the external magnetizing field.

$\vec{H}_s$ - the secondary external field due to

magnetized bodies.

$\vec{H}_1$ - the total external field, $\vec{H}_1 = \vec{H}_o + \vec{H}_s$.

$\vec{H}_d$ - the secondary internal field due to magnetization in the bodies.

$\vec{H}_2$ - the total internal field, $\vec{H}_2 = \vec{H}_o + \vec{H}_d$.

A_d - the scalar magnetic potential of $\vec{H}_d$.

Because a rough formula $\vec{M} = K\vec{H}_o + \vec{P}$ is often used for evaluating the total magnetization, we may call $\vec{M}$ the effective magnetization to emphasize that $\vec{M}$ includes the demagnetization effect.

5.2 The mathematical model for the magnetic calculations

5.2.1 Linearization of the M(H) characteristics

We may consider a mathematical model for describing the magnetic field inside a ferromagnetic (or ferrimagnetic) material existing in the Earth's crust. This model should also suit other materials (e.g. para- and diamagnetic materials). In ferromagnetic materials the relationship between the magnetization M and H is nonlinear and usually shown graphically as hysteresis. Figure 5.1 (a,b) shows examples of the magnetic hysteresis of igneous rocks as measured by Nagata (1961). It can be seen clearly that the igneous rocks usually have considerable permanent magnetization which should not be ignored. Problems involving materials with such nonlinear M(H) characteristics are very difficult to solve. These problems become more tractable when the characteristic can be linearized over a small interval. Thus in the vicinity of P in Fig. 5.1 (a,b), we can write that

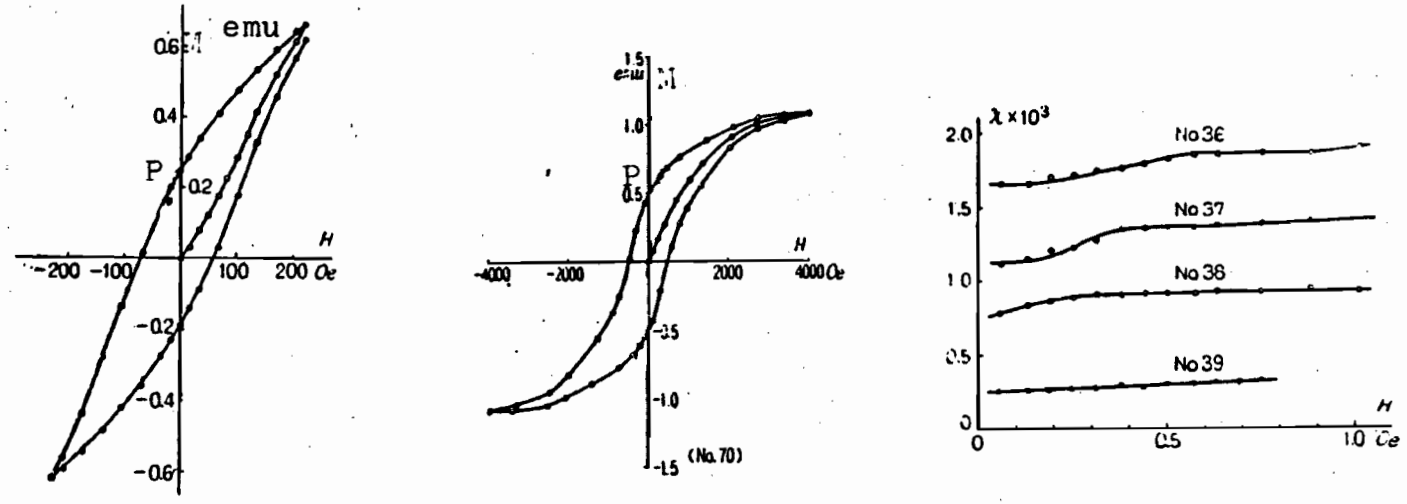

(a) (b) (c)

Figure 5.1. Magnetization characteristics of rock specimens: (a) a magnetic hysteresis curve of igneous rock, (b) a hysteresis curve of volcanic rock and (c) magnetic susceptibility of volcanic rock in weak alternating magnetic fields. (after Nagata, 1961)

$$\vec{M} = K\vec{H}_2 + \vec{P} \qquad (5.2)$$

(Van Bladel, 1964, p.162). Eq. (5.2) is valid for ferromagnetic materials only if the field is very small. It implies that (a) both the susceptibility and the permanent magnetization are independent of the magnetic field and (b) the induced magnetization is proportional to the internal field. According to Nagata (1961) and Strangway (1967), the susceptibility of rock materials does depend on the applied field strength (Fig.5.1,c). For field strengths in the range from 0.4 to 1.0 oersted (which includes the Earth's field), the change of K due to variation of the applied field is very small so that K can be actually treated as a constant. Thus the magnetization inside most crustal materials in practice satisfies (5.2) (here crustal materials refer to both minerals and rocks magnetized by the Earth's field).

Let us now consider the magnetic field produced by magnetized bodies. The magnetic induction $\vec{B}$ due to magnetized distribution of a matter can be expressed as the sum of two terms (e.g. Reitz, p.189, 1967): the gradient of a scalar field plus a term proportional to the local magnetization

$$\vec{B}_2 = \vec{H}_2 + 4\pi\vec{M}$$

(in the SI system, omit the 4π). By inserting (5.2) we get

$$\vec{B}_2 = \mu\vec{H}_2 + 4\pi\vec{P} \qquad (5.3)$$

where μ is the magnetic permeability. When P=0, (5.3) becomes $\vec{B}_2 = \mu\vec{H}_2$ which represents the relationship between $\vec{B}$ and $\vec{H}$ in paramagnetic and diamagnetic materials. Thus, (5.3) is a general formula for any crustal materials.

Inside the magnetized bodies, the magnetic field consists of the external magnetizing field $\vec{H}_o$ and a secondary field $\vec{H}_d$, so that (5.2) becomes

$$\vec{M} = K(\vec{H}_o + \vec{H}_d) + \vec{P} \qquad (5.4)$$

The external magnetizing field $\vec{H}_o$ *is usually treated as a constant in magnetic exploration. The secondary field* $\vec{H}_d$ *is due to both the induced magnetization and the permanent magnetization of the bodies. As mentioned previously, if a permeable body is bounded by a quadric surface and has constant magnetic parameters,* $\vec{H}_d$ *is constant and negative. Comparing (5.1) and (5.4) we obtain*

$$NK = (1-(H_d/H_o))^{-1} - 1$$

The apparent susceptibility K_a *which is defined by* $K_a = K/(1+NK)$ *can then be expressed by*

$$K_a = K(1-(H_d/H_o)) \qquad (5.5)$$

It is clear that the secondary field $\vec{H}_d$ *causes a reduction in the apparent susceptibility, and therefore a reduction in the internal magnetic field* $\vec{H}_2$. *Thus, the secondary field* $\vec{H}_d$ *represents the effect of demagnetization. For spheres, the internal field is* $\vec{H}_2 = \vec{H}_o - 4\pi\vec{M}_i/3$ *(Grant and West, 1965, p318), and it can be easily seen that*

$$\vec{H}_d = -\frac{4\pi K}{3 + 4\pi K}\vec{H}_o$$

For an arbitrarily magnetized body, $\vec{H}_d$ *is variable and will be further discussed in section 5.5.*

5.2.2 The integral equations for the effective magnetization

The scalar magnetic potential A_d *may be used to represent the secondary magnetic field* H_d *inside a magnetized body, which is defined by*

$$\vec{H}_d = -\nabla A_d \qquad (5.6)$$

The scalar potential of the secondary internal field can be expressed by the integral

$$A_d(\vec{r}) = \int_v \frac{\vec{M}(\vec{r}')\cdot\vec{R}}{R^3}\, dv \qquad (5.7)$$

where $\vec{R}=\vec{r}-\vec{r}'$; $R=|\vec{R}|$, $\vec{r}$ *represents the point* (x,y,z) *at which* A_d *is evaluated, and* $\vec{r}'=(x',y',z')$ *denotes a position vector variable of an element of the body with volume* dv *and magnetization* $\vec{M}$ *(Fig. 5.2). Substituting equation (5.7) into (5.6) yields*

$$\vec{H}_d(\vec{r}) = -\nabla\cdot \int_v \frac{\vec{M}(\vec{r}')\cdot\vec{R}}{R^3}\, dv \qquad (5.8)$$

where the gradient operator ∇ *is evaluated with respect to the unprimed coordinates r. With the aid of (5.8) , (5.4) can be written as*

$$\vec{M}(\vec{r}) = \bar{K}(\vec{r})\vec{H}_o + \vec{P}(\vec{r}) - K(\vec{r})\nabla\bullet \int_v \frac{\vec{M}(\vec{r}')\cdot\vec{R}}{R^3}\, dv \qquad (5.9)$$

This is the integral equation for calculation of the effective magnetization $\vec{M}$ *by given parameters* $\vec{H}_o$, K *and* $\vec{P}$. *In the case of a 2-D source region, the equation becomes*

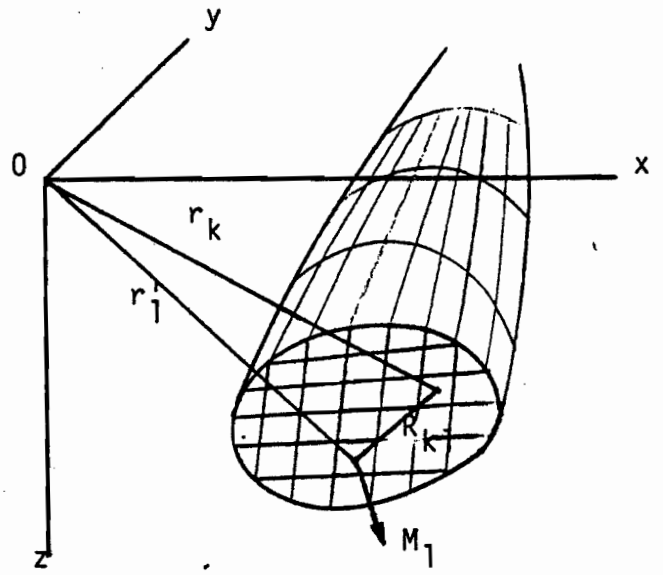

Figure 5.2. Geometry of the magnetic body and the division of finite elements.

$$\vec{M}(\vec{r}) = K(\vec{r})\vec{H}_o + \vec{P}(\vec{r}) - 2K(\vec{r})\ \nabla\cdot\int_s \frac{\vec{M}(\vec{r}')\cdot\vec{R}}{R^2}\,ds \qquad (5.10)$$

where $\vec{r}=(x,z)$ and $\vec{r}'=(x',z')$, taking the field to be invariant in the y-direction. Equations (5.9) and (5.10) are Fredholm's integral equations of the second kind with vector unknowns. The third term on the right of (5.9) or (5.10) represents the effect of demagnetization. If this term is omitted, we will have a formula which ignores the demagnetization effect.

We note that the integrals in the right hand side of (5.9) and (5.10) have a singular point at $r=r'$. To deal with the singularity, we may divide the volume v into two parts which may be denoted by v_o and v'. The region of v_o is a small sphere of radius d with its center at point o (Fig. 5.3) while v' denotes v exterior to v_o. Thus the integral in (5.9) becomes

$$\int_v \frac{\vec{M}(\vec{r}')\cdot\vec{R}}{R^3}\,dv = \int_{v'} \frac{\vec{M}(\vec{r}')\cdot\vec{R}}{R^3}\,dv + \int_{v_o} \frac{\vec{M}(\vec{r}')\cdot\vec{R}}{R^3}\,dv \qquad (5.11)$$

The first term on the right of (5.11) is non-singular. If the sphere v_o is small enough, the second term of (5.11) becomes

$$\int_{v_o} \frac{\vec{M}(\vec{r}')\cdot\vec{R}}{R^3}\,dv \leq 8\pi dM \qquad (2.12)$$

(Grant and West, 1965, p.214). If ϵ is a small quantity and the radius of the sphere satisfies the following inequality

$$d \leq \epsilon/8\pi M \qquad (5.13)$$

then the second term on the right of (5.11) will be negligible. In fact, the inequality (5.12) and (5.13) shows that the singular point $\vec{r}=\vec{r}'$ is removable.

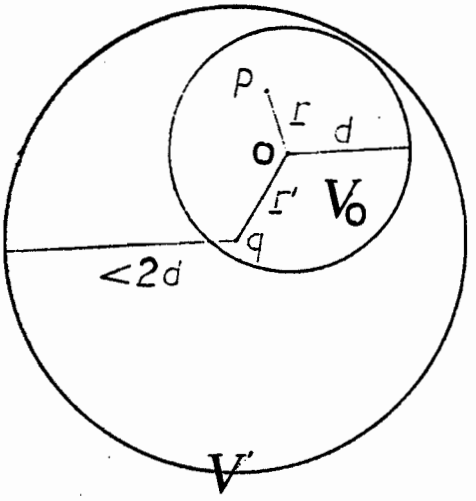

Figure 5.3. Diagram of singular point.

Hence, we are assured that there is no difficulty caused by the singularity whenever the integral equation (5.9) or (5.10) is performed.

A common method for solving a Fredholm integral equation of the second kind employs successive approximations. If one assumes the uniformity of magnetization, (5.10) can be reduced to a scalar equation which has be used by Filatov (1969) for the case when P=0. As we are not going to make this assumption, alternative methods are needed to deal with the vector equations. A new method can be developed which is based on the division of magnetized bodies into finite elements. This method was originally proposed for designing and calculating the field of magnets (Newman el al., 1972; Silvester and Ferrari, 1983). Because it is a direct method, the resulting procedure possesses the advantages of high speed, high accuracy and flexibility.

5.3 The computational method for magnetic calculation

5.5.1 The finite element technique

In the case of a 2-D magnetic field, performing the gradient operation in (5.10) gives

$$\vec{M}(\vec{r}) = K(\vec{r})\vec{H}_0 + \vec{P}(\vec{r}) - 2K(\vec{r}) \iint \left(\frac{\vec{M}(\vec{r}')}{R^2} - \frac{2\vec{M}(\vec{r}')\cdot\vec{R}}{R^4}\vec{R} \right) dx'dy' \quad (5.14)$$

Suppose that a cross-section of a magnetized body can be divided into N elements (Fig. 5.2). Let an arbitrary point within the l-th element be $\vec{r}_l'$, *l=1,...,N, and suppose as an approximation the magnetization is constant within*

each element. Then also as an approximation, which becomes increasingly more accurate as the number of elements increases, the magnetization at a point $\vec{r}_k$, k=1,2,...,N, can be written as the sum of contributions from each of the elements l=1,2,...,N, (including one from the k-th element, in which it is assumed that the field point $\vec{r}_k$ lies). Using Eq.(5.14), this sum is

$$\vec{M}_k = K_k \vec{H}_o + \vec{P}_k - 2K_k \sum_{l=1}^{N} \iint \left(\frac{\vec{M}_l}{R^2} - \frac{2\vec{M}_l \cdot \vec{R}}{R^4} \right) \vec{R} \, dx' dz' \qquad (5.15)$$

Because the magnetization vector $\vec{M}_l$ is assumed to be constant within each element, the integrations in Eq.(5.15) can readily be performed and the results will be dependent purely upon the element geometry. The integration over each individual element must be performed relative to some reference point $\vec{r}_l$. If these points for integration $\vec{r}_k$ are chosen to be the same as the field points $\vec{r}_l$, we can write

$$\vec{M}_k = K_k \left(\vec{H}_o + \vec{P}_k/K_k - \sum_{l=1}^{N} \vec{C}_{kl} \vec{M}_l \right) , \qquad (5.16)$$

where $\vec{C}_{kl}$ represents a second order tensor

$$\vec{C}_{kl} = \begin{bmatrix} C_{kl}^{xx} & C_{kl}^{xz} \\ C_{kl}^{zx} & C_{kl}^{zz} \end{bmatrix} , \qquad (5.17)$$

so that

$$\vec{C}_{kl} \vec{M}_l = \left(C_{kl}^{xx} M_l^x + C_{kl}^{xz} M_l^z \, , \, C_{kl}^{zx} M_l^x + C_{kl}^{zz} M_l^z \right) \qquad (5.18)$$

where superscripts x and z denote components which corresponds to the x and z directions respectively.

Thus the problem of determining the effective magnetization has been

discretized. After rearranging terms, (5.16) becomes

$$\sum_{l=1}^{N} (\vec{C}_{kl} + \delta_{kl} /K_k) \vec{M}_l = \vec{H}_o + \vec{P}_k/K_k \qquad (5.19)$$

where the Kronecker delta, δ_{kl}=1 for k=l or δ_{kl} =0 for k≠l, is introduced. The solution of (5.19) provides the effective magnetization components for each element so that the magnetic field $\vec{H}_2$ inside the body can be calculated , according to Eq. (5.4), as

$$\vec{H}_{2l} = (\vec{M}_l - \vec{P}_l)/K_l \qquad (5.20)$$

5.5.2 The representation of the tensor elements

In order to find analytic expressions for the tensor $\vec{C}_{kl}$, let us use components to replace the vectors in (5.19). In two-dimensional Cartesian coordinates, we substitute

$$\vec{M}(r')\cdot\vec{R} = M^x(x-x') + M^z(z-z') \qquad (5.21)$$

into (5.15), where M^x and M^z represent x and z components of $\vec{M}$ respectively, the magnetization components can be expressed by

$$M_k^x = K_k H_o^x + P_k^x - 2K_k \sum_l \iint \left\{ M_l^x \left(\frac{1}{R^2} - \frac{2(x-x')^2}{R^4} \right) - M_l^z \frac{2(x-x')(z-z')}{R^4} \right\} dx'dz' \qquad (5.22)$$

and

$$M_\kappa^z = K_\kappa H_o^z + P_\kappa^z - 2K_\kappa \sum_l \iint \left\{ -M_l^x \frac{2(x-x')(z-z')}{R^4} + M_l^z \left(\frac{1}{R^2} - \frac{2(z-z')^2}{R^4} \right) \right\} dx'dz' \qquad (5.23)$$

Comparison of (5.22) and (5.23) with (5.16) shows that the tensor elements can be expressed as follows:

$$C_{\kappa l}^{xx} = 2 \iint \left(\frac{1}{R^2} - \frac{2(x-x')^2}{R^4} \right) dx'dz'$$

$$C_{\kappa l}^{xz} = C_{\kappa l}^{zx} = -4 \iint \frac{(x-x')(z-z')}{R^4} dx'dz' \qquad (5.24)$$

$$C_{\kappa l}^{zz} = 2 \iint \left(\frac{1}{R^2} - \frac{2(z-z')^2}{R^4} \right) dx'dz'$$

The integrations in (5.24) can be further reduced after specifying the geometry of elements. For instance, if elements are small rectangulars with sides dx and dz, in Cartesian coordinates the tensor elements can be represented as follows:

$$C_{\kappa l}^{xx} = -2(\arctan(X1/Z1) - \arctan(X1/Z2) - \arctan(X2/Z1) + \arctan(X2/Z2))$$

$$C_{\kappa l}^{xz} = C_{\kappa l}^{zx} = Ln((Z1+X1)(Z2+X2)/((Z1+X2)(Z2+X1))) \qquad (5.25)$$

$$C_{\kappa l}^{zz} = -2(\arctan(Z1/X1) - \arctan(Z1/X2) - \arctan(Z2/X1) + \arctan(Z2/X2))$$

for k≠l ,where

$$X1 = x - x' - dx/2$$

$$X2 = x - x' + dx/2$$

and

$$Z1 = z - z' - dz/2$$

$$Z2 = z - z' + dz/2$$

with unprimed coordinates describing the center of k-th element and the primed for l-th element. When k=l, (5.24) becomes singular. As stated in the previous section, we can prove that the singular point is removable if the element is small enough. However, an approximate evaluation of the singular value may be necessary for an accurate calculation. In the 2-D case it can be shown that

$$C_{ll}^{xx} \doteq C_{ll}^{zz} \doteq 4\pi d \quad ,$$

where d is the radius of a small circular element. Converting the circular element into the rectangular element, we have

$$C_{ll}^{xx} = C_{ll}^{zz} \doteq 2.2568\pi(dx \cdot dz)^{1/2}$$

For an approximate evaluation of the singular value, we let

$$C_{ll}^{xx} = C_{ll}^{zz} = 2\pi(dx \cdot dz)^{1/2}$$

$$C_{ll}^{xz} = C_{ll}^{zx} = 0 \quad .$$

5.5.3 The 3-D magnetized bodies

There is no difficulty in extending the previous discussion to the 3-D magnetic problem. According to (5.9), the gradient operator yields

$$\nabla \frac{\vec{M}(\vec{r}')\cdot\vec{R}}{R^3} = \frac{\vec{M}(\vec{r}')}{R^3} - 3\frac{\vec{M}(\vec{r}')\cdot\vec{R}}{R^5}\vec{R} \quad .$$

Thus (5.9) becomes

$$\vec{M}(\vec{r}) = K(\vec{r})\vec{H}_o + \vec{P}(\vec{r}) - K(\vec{r})\iiint\left\{\frac{\vec{M}(\vec{r}')}{R^3} - 3\frac{\vec{M}(\vec{r}')\cdot\vec{R}}{R^5}\vec{R}\right\}dx'dy'dz' \qquad (5.26)$$

Comparing (5.26) with (5.14) indicates that Eqs. (5.16), (5.19) and (5.20) are also correct for the 3-D magnetic problem if the second tensor in Eq. (5.17) is replaced by the tensor

$$\vec{C} = \begin{bmatrix} C^{xx} & C^{xy} & C^{xz} \\ C^{yx} & C^{yy} & C^{yz} \\ C^{zx} & C^{zy} & C^{zz} \end{bmatrix} \qquad (5.27)$$

with

$$\vec{C}\cdot\vec{M} = (C^{xx}M^x + C^{xy}M^y + C^{xz}M^z,\ C^{yx}M^x + C^{yy}M^y + C^{yz}M^z,$$
$$C^{zx}M^x + C^{zy}M^y + C^{zz}M^z) \qquad (5.28)$$

where we omit the subscripts for simplicity. The elements of $\vec{C}$ *can be expressed by*

$$C^{xx} = \iiint \left(\frac{1}{R^3} - \frac{3(x-x')^2}{R^5}\right) dx'dy'dz'$$

$$C^{xy} = C^{yx} = -3\iiint \frac{(x-x')(y-y')}{R^5}\, dx'dy'dz'$$

$$C^{xz} = C^{zx} = -\,3 \iiint \frac{(x-x')(z-z')}{R^5}\, dx'dy'dz'$$

$$C^{yy} = \iiint \left(\frac{1}{R^3} - \frac{3(y-y')^2}{R^5} \right) dx'dy'dz' \qquad (5.29)$$

$$C^{yz} = C^{zy} = -\,3 \iiint \frac{(y-y')(z-z')}{R^5}\, dx'dy'dz'$$

$$C^{zz} = \iiint \left(\frac{1}{R^3} - \frac{3(z-z')^2}{R^5} \right) dx'dy'dz'$$

5.5.4 The algorithm

We now go back to the 2-D problem where the solution for the effective magnetization is represented by (5.22) and (5.23). After rearranging terms, these equations become

$$\sum_{i=1}^{N} \left(\left(C_{ki}^{xx} + \delta_{ki} / K_k \right) M_i^x + C_{ki}^{xz} M_i^z \right) = H_o^x + P_k^x / K_k \qquad (5.30)$$

and

$$\sum_{i=1}^{N} \left(C_{ki}^{zx} M_i^x + \left(C_{ki}^{zz} + \delta_{ki} / K_k \right) M_i^z \right) = H_o^z + P_k^z / K_k \qquad (5.31)$$

This is a bilinear system and can be further expressed in matrix form by using the following notations

$$\underline{A} = C_{ki}^{xx} + \delta_{ki} / K_k$$

$$\underline{B} = C_{ki}^{xz}$$

$$\underline{D} = H_o^x + P_\kappa^x / K_\kappa$$

$$\underline{E} = C_{\kappa\iota}^{zz} + \delta_{\kappa\iota} / K_\kappa$$

$$\underline{F} = H_o^z + P_\kappa^z / K_\kappa$$

$$\underline{X} = M^x$$

$$\underline{Z} = M^z$$

where $\underline{A}$, $\underline{B}$ *and* $\underline{E}$ *are N by N matrices,* $\underline{D}$ *and* $\underline{F}$ *are right-hand-side vectors of length N. Under these simplifications (5.30) becomes*

and

$$\underline{AX} + \underline{BZ} = \underline{D}$$

$$\underline{BX} + \underline{EZ} = \underline{F} \qquad (5.32)$$

Equation (5.32) provides a linear system of 2N equations, a direct solution of which is inappropriate in the sense of achieving high accuracy and high speed. We can further decompose them into two independent linear systems each containing only N equations. After substitution, the bilinear system can be represented by

and

$$(\underline{A} - \underline{BE^{-1}B})\underline{X} = \underline{D} - \underline{BE^{-1}F} \qquad (5.33)$$

$$(\underline{E} - \underline{BA^{-1}B})\underline{Z} = \underline{F} - \underline{BA^{-1}D} \qquad (5.34)$$

Either (5.33) or (5.34) is an independent linear system of N algebraic equations, therefore any linear algorithm can be used for solution. We here use the QR decomposition algorithm (Nash, chapter 4, 1979) for the effective magnetization components because it guarantees high accuracy. After the magnetization components at each element are obtained, the magnetic field $\vec{H}_2$ *inside a magnetized body can be calculated directly by (5.20). The exetrnal secondary field* $\vec{H}_s$ *is the sum of the contributions from each and every element. If we also use* $\vec{r}_\kappa$ *to denote a point outside magnetized bodies, the*

anomalous field can be estimated by

$$\overline{H_{S\kappa}} = -\sum_{\iota=1}^{N} \overline{C_{\kappa\iota}}\,\overline{M_\iota}$$

with the tensor $\overline{C_{\kappa\iota}}$ given by (5.24) or (5.29).

5.4 Accuracy of the Method

The accuracy of the method can be tested via some models for which the effect of demagnetization is known. We may use flat-plates as a test model since they have the most intensive demagnetizing effect. As mentioned previously, the magnetization factor N is 4π for an infinite plate magnetized transversely. In such a case the internal field is uniform and can be expressed, according to (5.1), by

$$M = KH/(1+4\pi K)$$

If the plate (K=0.2 emu,P=0) is magnetized by a vertical external field of 0.5 oersted, then M = 0.002846 emu. A horizontal flat-plate model with finite width is used for the test. The thickness of the plate equals an interval and the width is 10, 20, and 30 intervals respectively. All the rectangular elements used to divide the plate have equal size of 1*1 intervals, correspondingly the total element number n=10, 20, and 30 respectively. Let $H_0^x=0$, $H_0^z=0.5$ oersted , and K=0.2 emu, the effective magnetization can be calculated via (5.33) and (5.34). The estimate of M^x at each and every element are zero. The estimates of the vertical component M^z are shown in Table 5.1. The elements are numbered from the left to the right.

Table 5.1. Estimates of the effective magnetization in a flat-plate magnetized transversely (dx/dz=1)

Element No.	n=10	n=20	n=30
1	0.03641 emu	0.03621 emu	0.03615 emu
2	0.03059	0.03039	0.03033
3	0.03006	0.02983	0.02976
4	0.02980	0.02951	0.02944
5	0.02970	0.02934	0.02926
6		0.02924	0.02915
7		0.02917	0.02907
8		0.02913	0.02902
9		0.02910	0.02898
10		0.02909	0.02895
11			0.02892
12			0.02891
13			0.02890
14			0.02889
15			0.02888
error	0.00124	0.00063	0.00042

Table 5.1 gives only half of the estimates, with the others being found by symmetry. The error is the difference between the theoretical value (0.02846 emu) and the estimate at the central element. The estimates on edges should be different from the theoretical value due to the finite width of the plate. The results show that the accuracy of the method depends upon the total number n of the elements. For this example, using 20 elements is enough to produce an good solution for the effective magnetization with a relative error about 2%. Using 30 elements produces a more accurate estimate with the relative error only 1.4%, but at the price of about triple the computer time.

The appropriate selection of the element shape plays an important role in speeding the computation as well as in enhancing the accuracy. For this flat-plate model, we may choose the element with sizes dz=1 and dx=1, 2, and 3 intervals respectively. Let the total element number n=10 or 20, then the estimates of the effective magnetization at the centeral element are shown in Table 5.2.

Table 5.2. The estimates of effective magnetization at the centre of the plate magnetized transversely (dz=1)

	n=10		n=20	
	M (emu)	error	M (emu)	error
dx=1	0.02970	4.3 %	0.02909	2.2 %
dx=2	0.02905	2.0 %	0.02874	< 1 %
dx=3	0.02748	-3.4 %	0.02728	-4.1 %

* error=(M -0.02846)/0.02846

From this table it can be seen clearly that using n=20 and dx=2 produces the best results, which is even better than the results of using n=30 and dx=1 (in column 4 of Table 5.1). The estimates with dx=3 intervals is worse then those of dx=2, maybe due to the very large size of the elements.

We should note that the errors in the estimates are not the roundoff error in solving the bilinear system (5.31) and (5.32). We have substituted the estimates back into the equations and found that the roundoff errors for all these computations are less than 10^{-6} emu. Thus the error is mainly due to the use of a finite plate as an approximation to an infinite plate.

Another test model is an infinite horizontal cylinder magnetized by a transverse field with amplitude of 0.5 oersted and inclination of 45° . As mentioned in section 5.1, the demagnetization factor is 2π in this case. Let k=0.2 emu and P=0, the effective magnetization is uniform and equal to 0.04471 emu. In order to test the method we use a square mesh with 52 elements to approximately replace the cylinder as shown in Fig. 5.4. The estimates of the effective magnetization are also shown in that figure. Except for a few estimates at corners of the mesh, the estimates produced by this procedure vary slightly from 0,0447 to 0.0451 emu, indicating the relative error in the estimates is less than 2 percent. The visible errors at corner elements are due to the approximation of using the square mesh and can be reduced by increasing the element number.

We have comfirm the accuracy and reliability of this procedure. In the next sections we may use the method to analyze some problems of the demagnetization effect. The theoretical problems may be dealt with first.

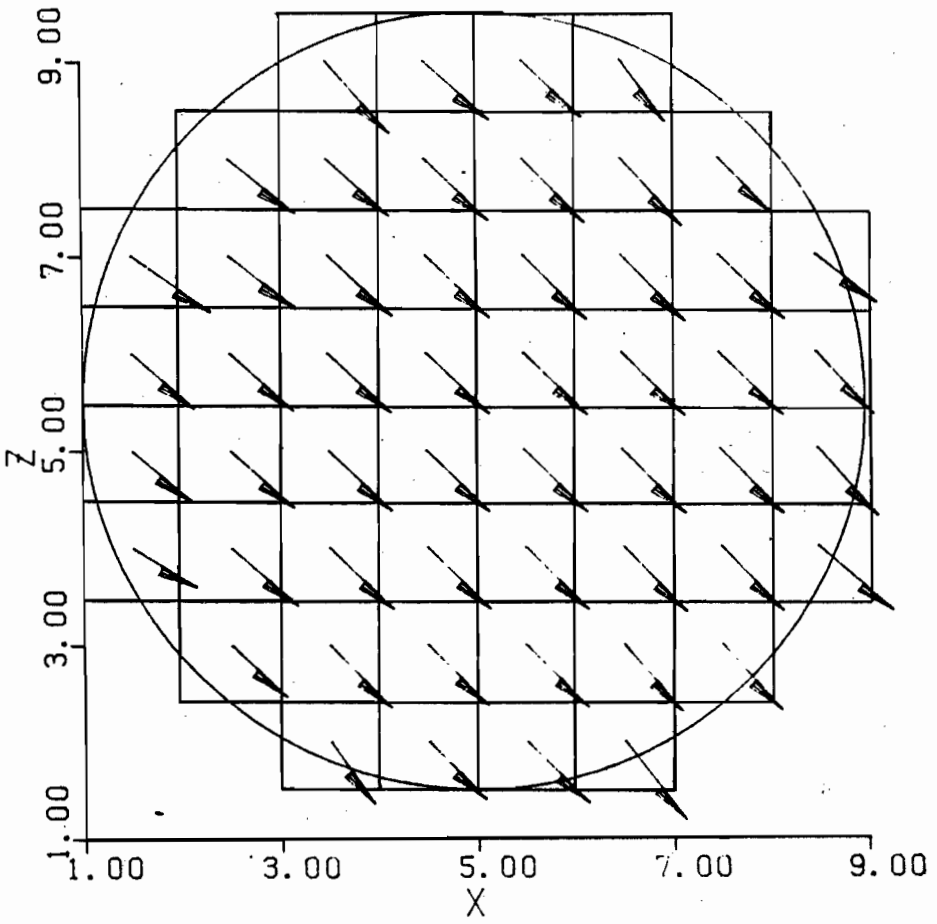

Figure 5.4. Square mesh and magnetization estimates within a horizontal cylinder (susceptibility K=0.2 emu) magnetized by an external field of magnetude 0.5 oersted and inclination 45°. The arrows denote the intensity and direction of magnetization at the elements with scale 1 inch= 0.5 emu.

5.5 Demagnetization in general crustal materials

5.5.1 Demagnetization due to natural remanent magnetization (NRM)

As discussed previously, the demagnetization effect has been applied only in the case of induced magnetization and the problem of demagnetization due to the NRM has been seldom touched. It is well-known today that for many rocks the magnitude of the NRM exceeds that of induced magnetization. Hence studying the demagnetization due to the NRM is significant for both magnetic exploration and rock magnetism.

This problem somewhat resembles the determination of the magnetic field inside a magnet when no other magnetic field are present. According to the boundary-value problems, the magnetic fields inside a spherical magnet with a uniform magnetization $\overline{M}$ can be expressed by

$$\overline{H_2} = -N\,\overline{M} \qquad (5.35)$$

(Reitz, p.213, 1967), where $N=4\pi/3$ is the demagnetization factor of spheres. The magnetic intensity $\overline{H_2}$ is called the demagnetizing field, and the magnetized sphere is subjected to its own demagnetizing field. The demagnetization factors for some simple geometric shapes have been calculated in design of magnets (Stoner, 1945; Bozorth, 1942).

For general crustal materials, letting $H_o=0$ in (5.9) results in

$$\vec{M}(\vec{r}) = \vec{P}(\vec{r}) - K(\vec{r})\nabla\int_V \left(\vec{M}(\vec{r}')\cdot\vec{R}/R^3\right)\,dv \qquad (5.36)$$

The demagnetizing field caused by the permanent magnetization is

$$\vec{H}_2(\vec{r}) = \vec{H}_d(\vec{r}) = -\nabla \int_V (\vec{M}(\vec{r}') \cdot \vec{R}/R^3) \, dv \qquad (5.37)$$

Thus (5.36) can be written in the form

$$\vec{M}(\vec{r}) = \vec{P}(\vec{r}) + K(\vec{r}) \, \vec{H}_d(\vec{r}) \qquad (5.38)$$

It is clear that when the external magnetizing field is absent, the effective magnetization in an NRM substance is less than the permanent magnetization; the difference between the two is proportional to the susceptibility because the demagnetizing field is the secondary field induced by the permanent magnetization. Hence, the smaller the susceptibility, the weaker the demagnetizing field becomes; consequently the closer the effective magnetization is to the true permanent magnetization. This concept is useful in paleomagnetism where one usually deals with the rocks having very small susceptibility and relatively large permanent magnetization. It can be inferred that the demagnetization correction may be unnecessary in such a case. Later on we will show an example in section 5.6.1.

5.5.2 The magnetic field equations in general crustal materials

According to the discussion above, we summarize the demagnetization model for general crustal materials as follows. The demagnetizing field $\overline{H_d}$ *due to both the induced and permanent magnetization is expressed by the integral shown in (5.8) while the internal magnetic field* $\overline{H_2} = \overline{H_o} + \overline{H_d}$. *The effective magnetization is the solution of equation (5.26)*

$$\vec{M}(\vec{r}) = K(\vec{r})\vec{H}_o + \vec{P}(\vec{r}) + K(\vec{r})\vec{H}_d(\vec{r})$$

In general, there is no analytic expression for the effective magnetization.

The demagnetization model is based on the linearization of the M(H) characteristic for ferro- and ferrimagnetic materials as mentioned in section 2.1.1. This model is correct for diamagnetic and paramagnetic materials and well approximates for ferromagnetic materials magnetized by the Earth's magnetic field. The magnetic induction $\overline{B}$ in general crustal materials can be represented by (5.3)

$$\overline{B} = \mu \overline{H} + 4\pi \overline{P} \quad ,$$

which yields

$$div(\mu \overline{H}) = -4\pi div \overline{P} \quad .$$

From the continuity of the normal component B_n, it is derivable that the magnetic field must satisfies the boundary condition

$$\mu_e H_{en} - \mu_i H_{in} = 4\pi(P_{in} - P_{en}) \qquad (5.39)$$

(Van Bladel, 1964, p.163) where the subscript e denotes 'external' while i denotes 'internal', and n denotes normal. In order to compare the field equations with those for non-ferromagnetic substances, let us define

$$\overline{B'} = \overline{B} - 4\pi \overline{P} = \mu \overline{H} \qquad (5.40)$$

as the apparent induction in general crustal materials. The field equations can then be expressed by

$$\begin{aligned} div\overline{B'} &= -4\pi div\overline{P} \quad , \quad B'_{en} - B'_{in} = 4\pi(P_{in} - P_{en}), \\ \overline{B'} &= \mu \overline{H} \quad , \quad \overline{H} = -grad\ A \ . \end{aligned} \tag{5.41}$$

Equations (5.41) are the general equations applicable to any magnetic media existing in the Earth's crust. In regions where no ferromagnetic materials exist, i.e. P=0, we have $\overline{B'}=\overline{B}$ *and* $div\overline{P}=0$, *thus (5.41) becomes the familiar equations for non-ferromagnetic materials:*

$$\begin{aligned} div\overline{B} &= 0 \quad , \quad B_{en} = B_{in} \quad , \\ \overline{B} &= \mu \overline{H} \quad , \quad \overline{H} = -grad\ A \ . \end{aligned} \tag{5.42}$$

5.5.3 Demagnetization of a uniformly magnetized body.

The assumption of uniform magnetization is correct for the bodies bounded by quadric surfaces and having constant magnetic parameters. Practically, the assumption of uniformity is often assumed for specimen measurements because we are interested only in the average values of the parameters in such cases. Under this assumption, the effective magnetization can be written, according to (5.26), as

$$\overline{M} = M\overline{m} = K\overline{H}_o + \overline{P} - K\overline{MN} \tag{5.43}$$

where $\overline{m}$ *is the unit vector of* $\overline{M}$ *and*

$$\overline{N} = \nabla \int (\overline{m}\cdot\overline{R}/R^3)\ dv \tag{5.44}$$

is the demagnetizing factor for any uniformly magnetized bodies and is valid only for such bodies. Rearranging the terms in (4.43) yields

$$M(\vec{m} + K\vec{N}) = K\vec{H}_o + \vec{P} \qquad (5.45)$$

Inserting (5.43) into (5.20) gives the internal field

$$\vec{H}_2 = \vec{H}_o - M\vec{N} \qquad (5.46)$$

In the Cartesian coordinates, (5.45) can be further decomposed into the components

$$M^x = (KH_o^x + P^x)/(1 + KN^x)$$

$$M^y = (KH_o^y + P^y)/(1 + KN^y) \qquad (5.47)$$

$$M^z = (KH_o^z + P^z)/(1 + KN^z)$$

Equations in (5.47) are the formulae for evaluating the effective magnitization in a uniformly magnitized body. We suggest using (5.47) to replace the traditional formula (5.1) for rough evaluation of magnetization because in the latter the demagnetization effect of the NRM is ignored. For spheres $\vec{N}=4\pi\vec{m}/3$, *we can use a scalar demagnetization factor* $N=4\pi/3$ *so that*

$$\vec{M} = (K\vec{H}_o + \vec{P})/(1 + NK) \qquad (5.48)$$

and

$$\vec{H}_2 = \vec{H}_o - N(K\vec{H}_o + \vec{P})/(1 + NK) \qquad (5.49)$$

When P=0, (5.48) becomes (5.1); while for $\vec{H}_o = 0$ *(5.35) can be derived from (5.48) and (5.49).*

In order to show how serious the error would be if the effect of the NRM is ignored, we may look at a dike-like magnetite ore body with uniform k=0.1 and p=0.1 emu, magnetized by a field of $H_o = 0.5$ *oersted transversely. If*

the induced and permanent magnetization intensities are in the same direction, then the effective magnetization is 0.06647 emu as calculated by (5.47). But if the demagnetization effect of $\overline{P}$ is ignored, using (5.1) gives an erroneous estimate of magnetization of 0.1222 emu that is about twice of the actual effective magnetization. This example shows if the demagnetization effect of the NRM is ignored, the estimated reserve of a magnetite body can be only a half of the actual reserve.

Thus we have described the physical basis of a general model for crustal materials which contains all the previous models as particular cases. Next we are going to apply these theoretical expressions to answer some practical questions.

5.6 Some practical demagnetization problems

5.6.1 Demagnetization in typical igneous rocks

Regardless of the demagnetization effect of permanent magnetization, (5.1) implies that since the susceptibilities of rock-forming minerals seldom exceed 0.01 emu, the demagnetization effect is usually not noticeble in igneous rocks. Hence, the effect is usually ignored except for magnetite bodies. However, studies have shown that in most igneous rocks the permanent intensity may completely dominate the intensity induced by the earth's field (Strangway, 1967; Parasnis, p.8-9, 1972). As demagnetization is also affected by the permanent magnetization, reevaluation of this effect is worth considering. We may pose the question: how large is the error in ignoring the demagnetization effect in various igneous rocks?

For practical purpose, basalt, diabase, gabbro and peridotite are included in the study. The typical parameters of basalt lava flows are chosen from a study by Cox and Doell (1962) with samples collected from hole EM 7 of the Mohole Project off the coast of Baja California. For the other rocks the average susceptibility and the ratio Q are abstracted from textbooks by Telford et al. (1974, p.121), Parasnis (1972, p.9), and an article by Strangway (1967). These typical parameters are listed in Table 5.3 As the extreme case for demagnetization, we use the flat-plate model for computation of the effective magnetization. The model has been described in section 5.4 for Table 5.2 with n=20 and dx/dz=2 which produces the most accurate results.

Table 5.3. The effective magnetization estimates for typical igneous rocks (flat-plate model with elements n=20, dx/dz=2, magnetized transversely)

	Basalt	Diabase	Gabbro	Peridotite
K (10^{-3}emu)	0.25	4.5	6.0	13.0
P (10^{-3}emu)	5.0	6.5	10.0	20.0
M_e (10^{-3}emu)	5.125	8.750	13.00	26.50
M (10^{-3}emu)	5.110	8.290	12.10	22.82
Error e (%)	0.3	5.5	7.4	16.1
M_c (10^{-3}emu)	5.1089	8.282	12.09	22.78

* $M_e = KH_o + P$, $H_o = 0.5$ oersted.

Regardless of demagnetization, the erroneous magnetization is the sum $M_e = KH_o + P$. *The computational estimates of the effective magnetization* M *for these typical rocks are close to constants throughout all elements. For instance, the deviation for basalt is in the order of* 10^{-7} *emu. Both* M *estimates and the erroneous* M_e *are shown in Table 5.3 with the reletive errors* $e = (M_e - M)/M$. *Because an infinite plate is magnetized uniformly with the demagnetization factor* $N = 4\pi$ *in such a case, we can use (5.47) to estimate the magnetization as well. The results calculated via (5.47) are also shown in Table 5.3 (see the row marked by* M_c *). Both the finite element estimates* M *and the calculated* M_c *are consistent with each other, showing the reliability of (5.47).*

In Table 5.3 e *is the maximum value of the error in evaluation of the effective magnetization when the demagnetizing effect is being ignored. As* M *is calculated in the extreme case of demagnetization, the computational result for the basalt confirmes that the effect is negligible for rocks having small susceptibility.*

Following the consequences shown in table 5.3, it can be inferred that

(1) For volcanic rocks with small susceptibility but relatively large NRM, the demagnetizatation effect is negligible.

(2) For a typical diabase intrusive with both K *and* P *about* $5*10^{-3}$*emu, the demagnetization effect might be considered in the case where intrusive body is magnetized transversely because an error greater than 5% could occur in this case.*

(3) For an accurate calculation, the demagnetization effect probably should be taken into account for typical gabbro intrusives which have a relatively large NRM intensity.

(4) For most ultrabasic rocks in which K *is greater than 0.01 emu, the demagnetization effect should not be ignored, otherwise a maximum error about 16% could be involved.*

5.6.2 The inhomogeneous magnetization in 2-D ferromagnetic bodies

Although in principle the demagnetization effect should be included in the interpretation of the anomalies due to magnetite ore bodies, a uniform magnetization is commonly presumed in such cases. A question then arises: how serious would the error be if the assumption is incorrect? We may use a set of models with different geometry and physical parameters for the study. In order to demonstrate the effect of inhomogeneous magnetization, we assume that all the models have a uniform susceptibility equal to 0.2 emu and the geomagnetic field has an amplitude of 0.5 oersted.

We may begin with a simple model, an infinite prism with square section. When the geomagnetic field is vertical and the permanent magnetization equals zero, the estimates of effective magnetization are shown in Figure 5.5. Although the susceptibility is uniform, the effective magnetization varies from 0.03955 emu to 0.05207 emu, implying that the demagnetization factor N for a square prism is far from constant. The inclination varies from -79.4 to -108.6 degrees, coinciding with the magnetizing field only at the center. If we take $N=2\pi$ for the constant in Eq. (5.1) as a rough estimate of the effective magnetization, then the maximum error can be as large as 17.5% in magnitude and 21% in inclination. Nearer the edges of the prism, the effective magnetization becomes less uniform. It tends to increase on the sides parallel to the magnetizing field, while it decreases on sides normal to the field.

When the geomagnetic field is imposed at an angle of 45 degrees to the sides (Fig. 5.6), the inhomogeneity of magnetization becomes more manifest. Its magnitude varies from 0.03198 to 0.06235 emu while the inclination varies from 35° to 55°. If one assume that the magnetization is uniform, the relative error can be as large as 41% in magnitude and 22% in inclination. The largest variation occures along the boundary, especially at corners. The smallest

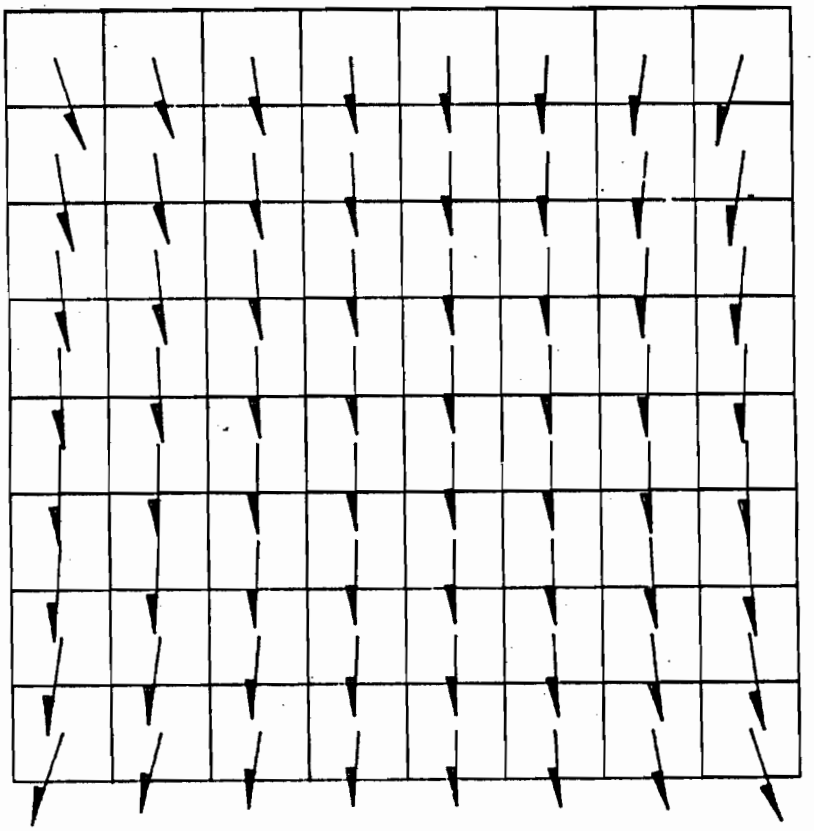

Figure 5.5. Magnetization within a horizontal prism of K=0.2 emu magnetized by an external field of magnetude 0.5 oersted and inclination 90°. The arrows denote the intensity and direction of effective magnetization at the elements with scale 1 inch= 0.5 emu.

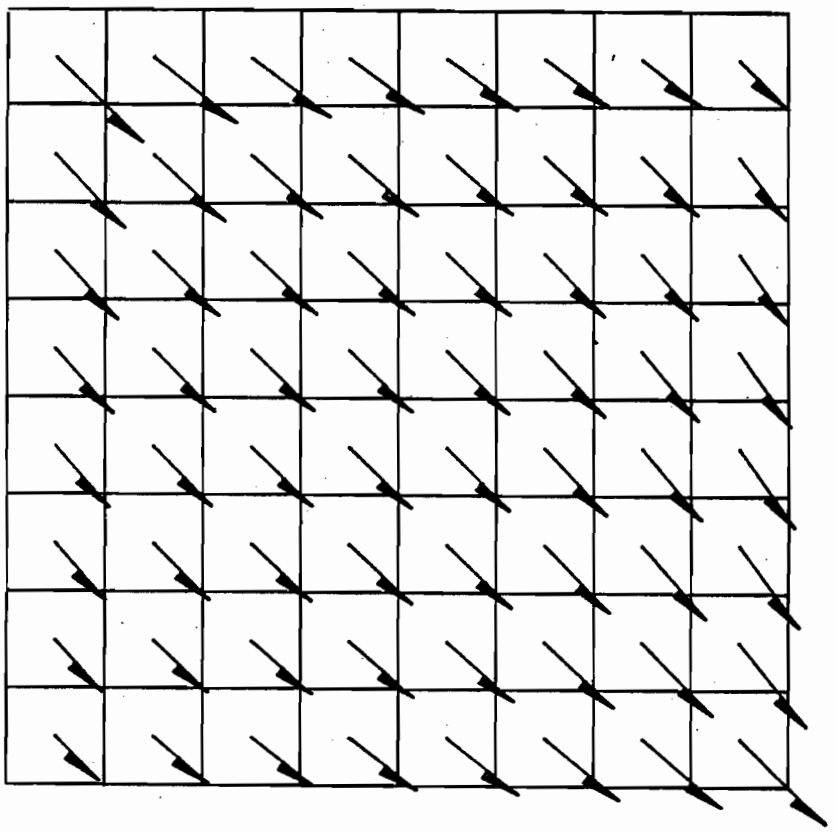

Figure 5.6. As Figure 5.5 but inclination 45°.

effective magnetization appears at the corners on the diagonal line normal to the magnetizing field.

The effect of a permanent magnetization on the effective magnetization is shown in Figures. 5.7 to 5.9. Comparing Figure 5.7 with Figure 5.6 it is clear that the inhomogeneity of the effective magnetization is substantially increased by the permanent magnetization. When $\vec{H}_o$ and $\vec{P}$ have the same direction (Fig. 5.7), the magnitude of $\vec{M}$ at the centre is about twice as large as those at the two corners transverse to the external field. Because $\vec{M}$ is decreased considerably near these corners, a uniformly magnetized elliptic cylinder, rather than a uniformly magnetized prism, can better represent a non-uniformly magnetized prism in the sense of producing a secondary field outside the source. Thus the inhomogeniety of $\vec{M}$ due to demagnetization should be taken into account, otherwise an interpretation may not be able to infer the correct source geometry. The non-uniformity in direction of the effective magnetization is also manifest (see Figs. 5.8 and 5.9.).

For a sheet-like body magnetized along its long axis (Fig. 5.10), the effective magnetization, also far from homogeneous, has a maximum value at its center (0.08046 emu) and values graduately decreasing towards both the top and the bottom (0.05948 emu), with a relative variation of the magnetization of about 36%. The maximum deviation in inclination is about 11° at the top, where the direction of magnetization tends to point towards the center, while at the bottom it is directed away from the center. This example shows once more that the assumption of uniform magnetization is too simple to represent the effective magnetization within an idealized ore deposit which has a simple and regular geometry. Within actual ore bodies, these effects are combined with problems of inhomogeneous composition and irregular geometry.

When the magnetizing field crosses the sheet at an angle of 45 degrees, the magnetization vector is, as expected, rotated towards the direction of the

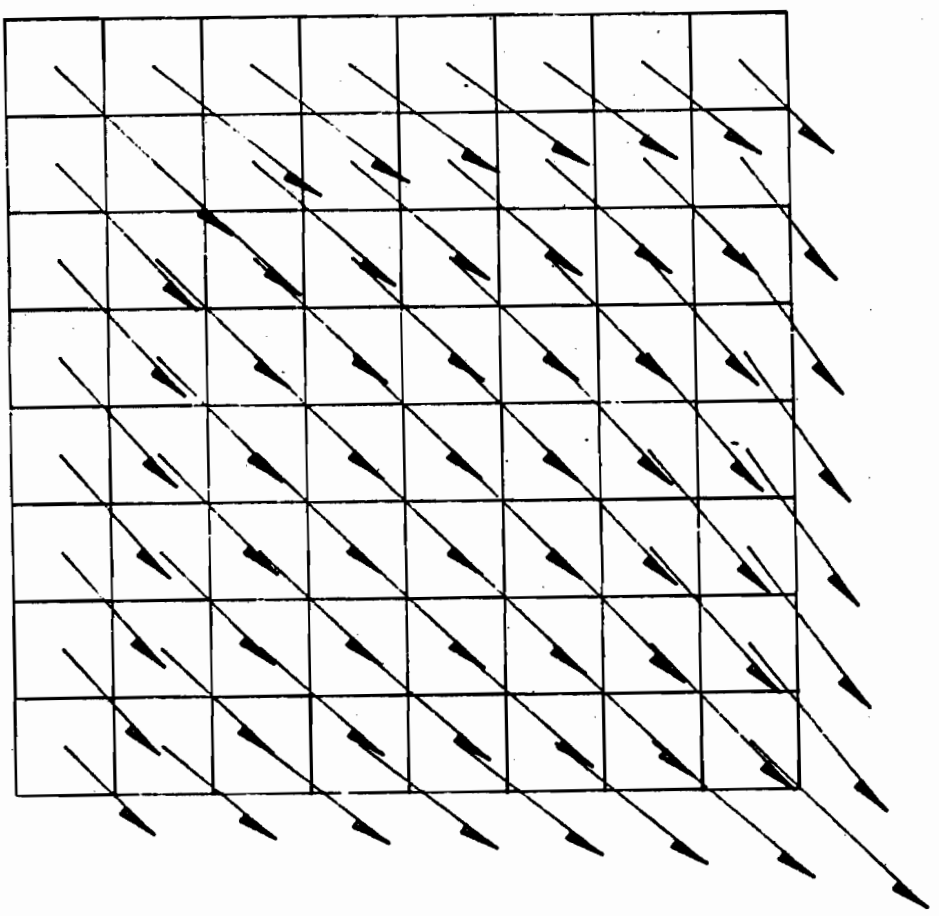

Figure 5.7. As Figure 5.6 but with permanent magnetization of magnetude 0.1 emu and inclination 45°.

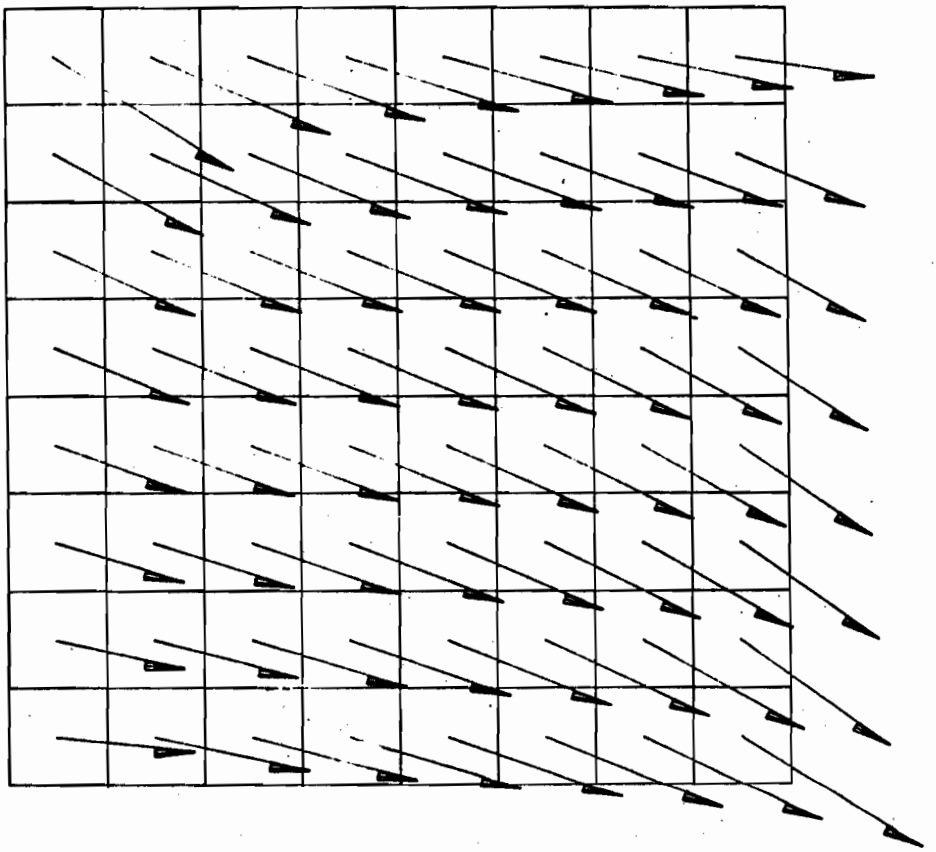

Figure 5.8. As Figure 5.6 but with horizontal permanent magnetization of 0.1 emu.

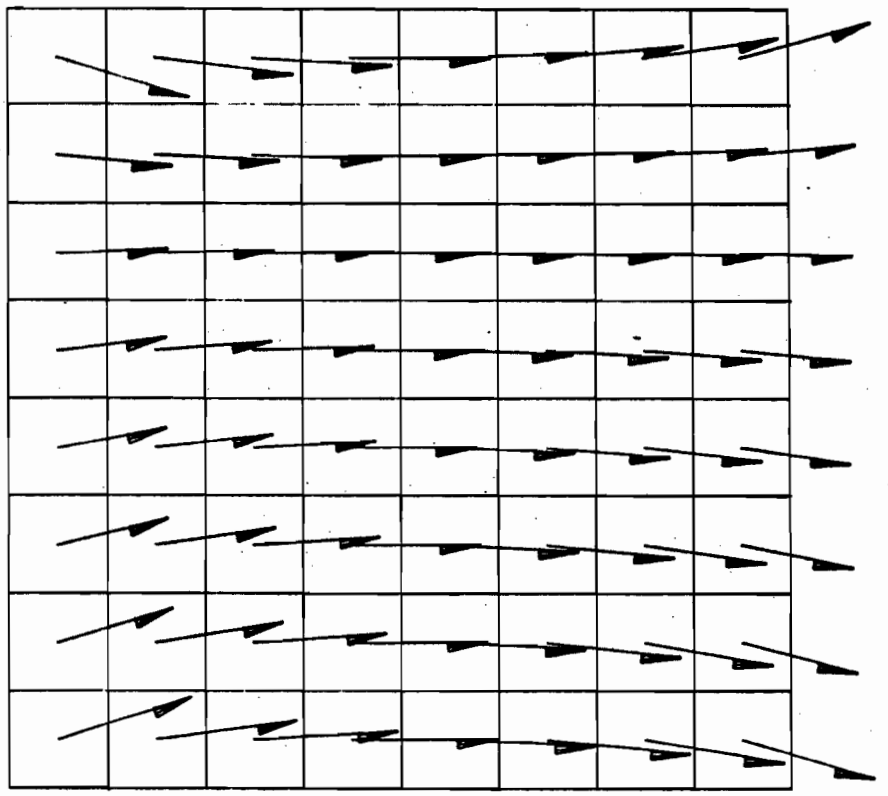

Figure 5.9. As Figure 5.7 but inclination -45°.

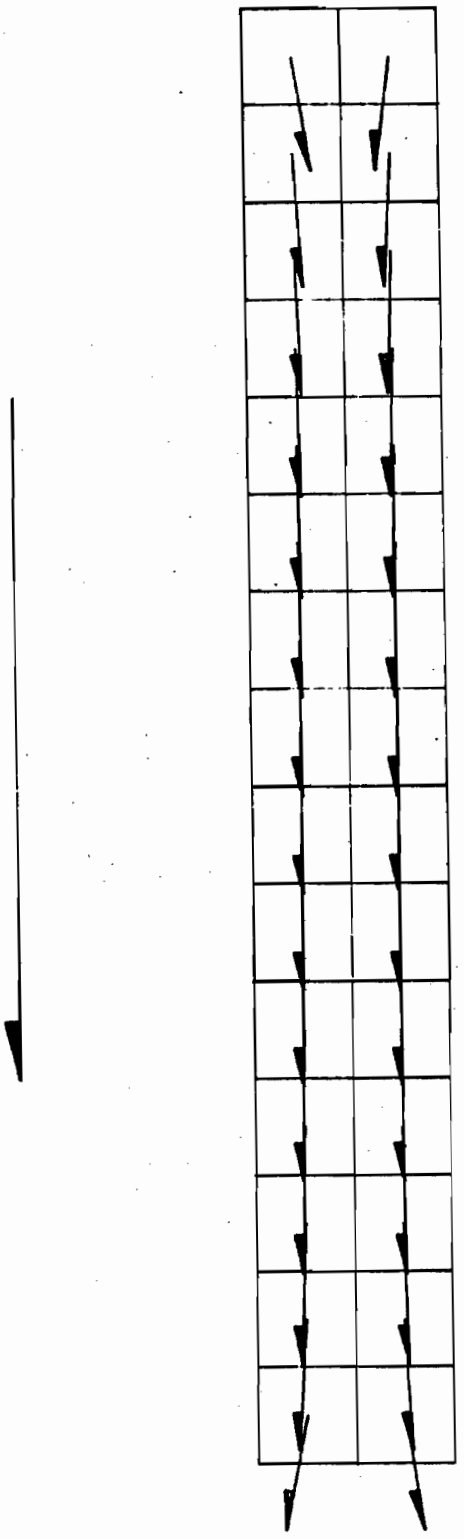

Figure 5.10. Magnetization within a vertical sheet of K=0.2 emu magnetized by an external field of magnetude 0.5 oersted and inclination 90°. The arrows denote intensity and direction of the magnetization at the elements with scale 1 inch= 0.5 emu.

long axis of the sheet (see Fig. 5.11). The rotation angles are about 7 degrees at the top and bottom ,and about 25 degrees at the middle. The magnetization decreases as the angle between the geomagnetic field and the long axis increases. If this angle becomes normal, the magnetization magnitude becomes a minimum as shown in Figure 5.12.

In summary, we suggest that the inhomogeneity of effective magnetization may in certain circumstances be relevant to the interpretation of magnetic well-logging anomalies and the ground anomalies due to near-surface magnetite bodies. For anomalies due to deeply buried sources, the assumption of uniform magnetization is more tolerable, but the effect of demagnetization on the NRM should be considered.

5.6.3 The effect of multiple bodies

When more than two magnetized bodies lie close together, each of them must also be magnetized by the fields generated by other bodies. Their mutual interaction can enhance or weaken their effective magnetizations, depending upon the geometrical arrangement of these bodies. In the case of two parallel sheets (Fig. 5.13), the direction of the effective magnetization is also changed, the arrows in the thinner sheet point slightly toward the thicker sheet. When two sheets are placed normal to each other, such as in the case of two wings of a fold, the demagnetizing effect plays a more important role. Figure 5.14 shows the effective magnetization in two sheets which have the same susceptibility and are magnetized by a field parallel to one of them. The effective magnetization in the parallel sheet is about three times larger as that in the sheet normal to the field due to the demagnetizing effect. Thus the existence of the latter could be mistakenly overlooked if the demagnetizing

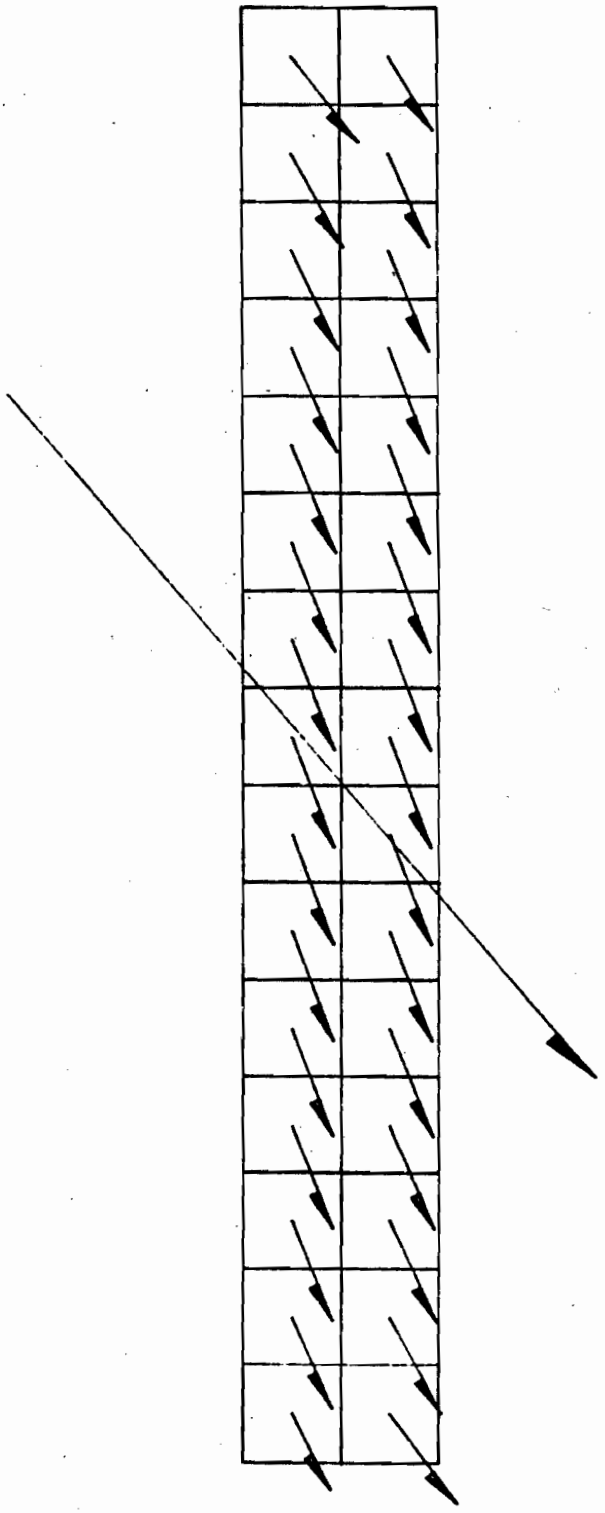

Figure 5.11. As Figure 5.10 but with inclination 45°.

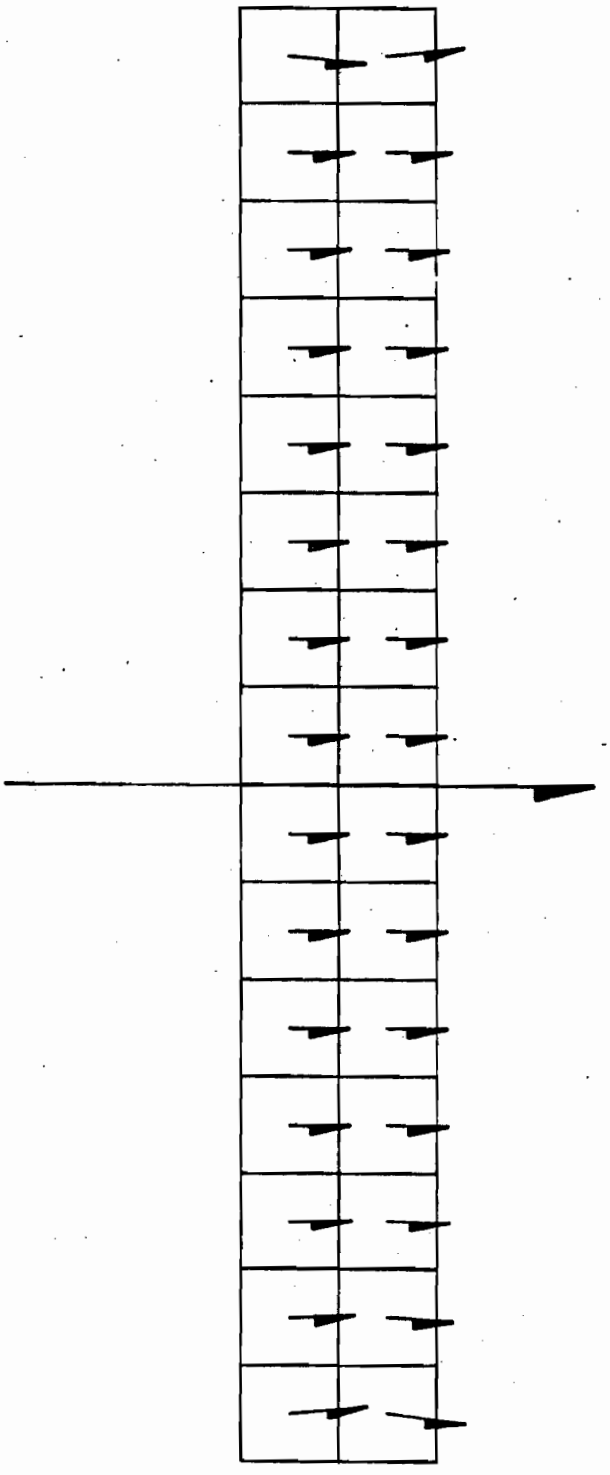

Figure 5.12. As Figure 5.10. but with inclination 0°.

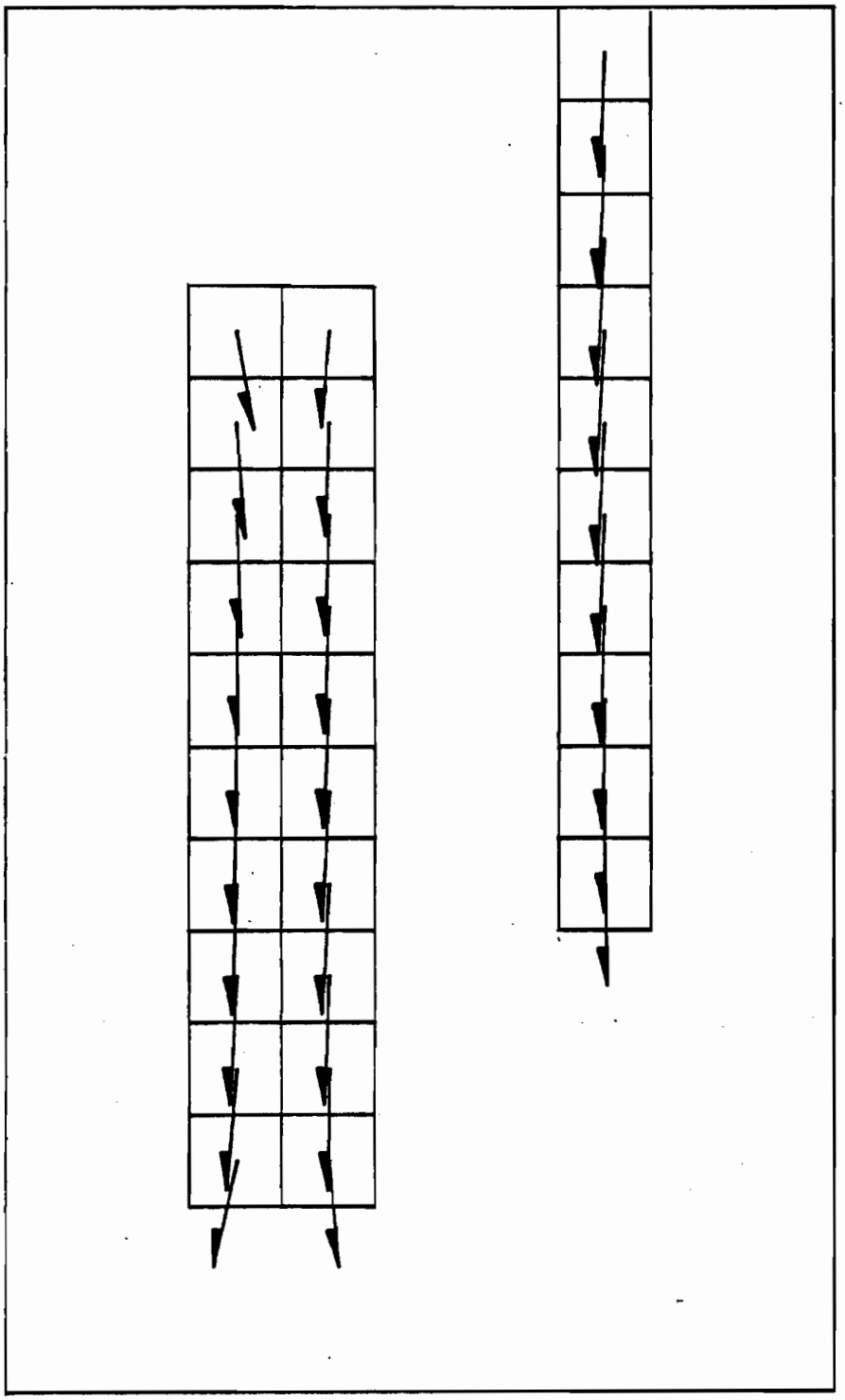

Figure 5.13. Magnetization within two parallel sheets (K=0.2 emu) magnetized by a vertical external field of 0.5 oersted. The arrows denote intensity and direction at square elements with scale 1 inch= 0.5 emu.

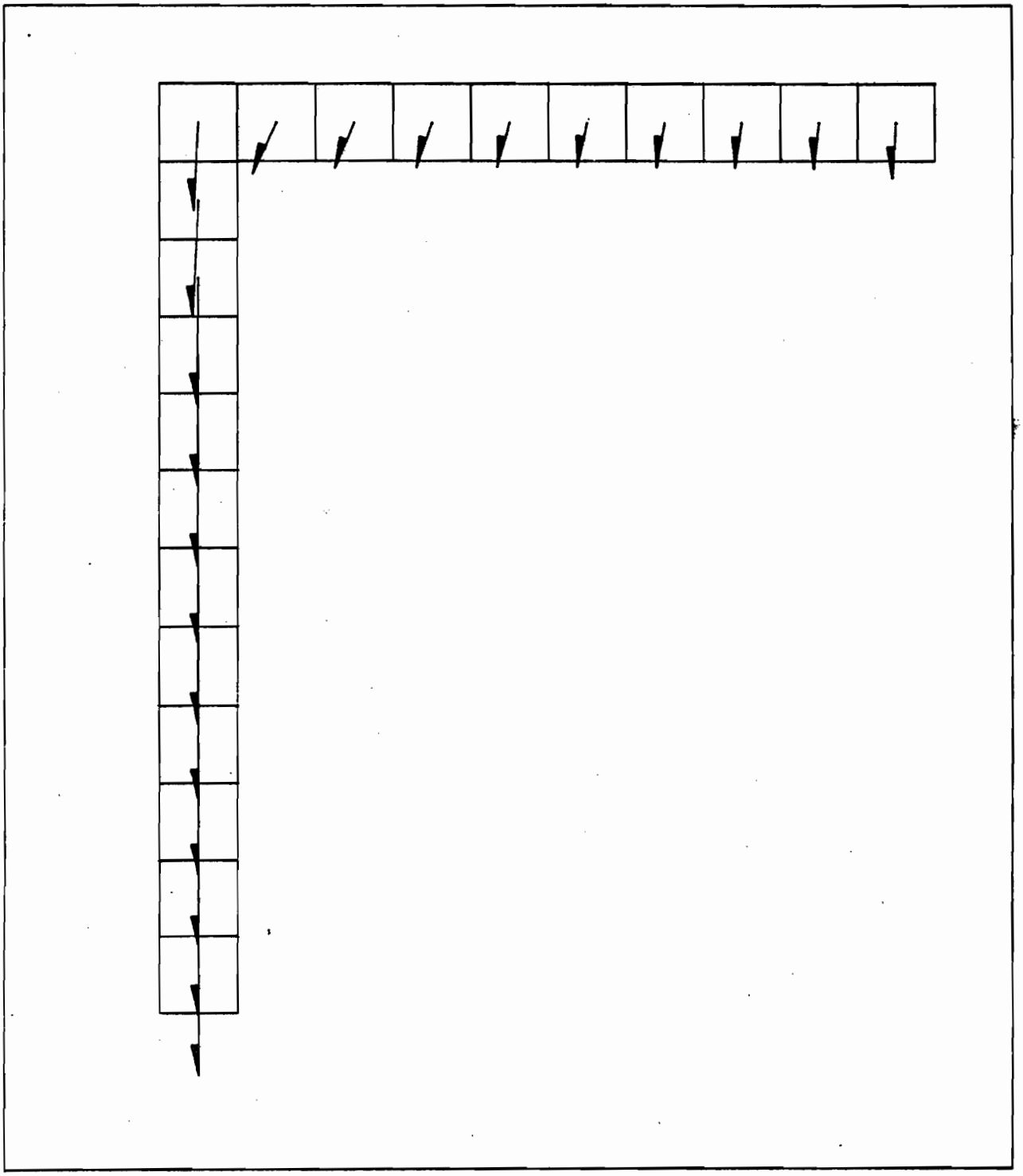

Figure 5.14. Magnetization within two perpendicular sheets(K=0.5 emu) magnetized by a vertical external field of 0.5 oersted. The arrows denote intensity and direction at square elements with scale 1 inch= 0.5 emu.

effect had not been included. As a matter of fact, from the ground anomaly (Fig. 5.15), these is no clear indication of the existence of the normal sheet because the anomaly resembles that due to a single sheet magnetized along the magnetizing field. In such a case only precise calculation can help us to distinguish the fold-generating anomaly from those due to a single sheet.

The mutual interaction becomes very complicated if many sources exist nearby. Figure 5.16 shows an example of five sheets to simulate a problem in magnetic well-logging. Because the field around such magnetized bodies varies considerably, the interpretation can be extremely difficult if one has not considered how the field is distributed in such a complicated situations. As the inhomogeneous magnetization and internal field must be taken into account in well-logging interpretation, the method presented in section 5.3 can be used for the magnetic calculation. The procedure can be incorporated into a method of trial and error as follows: (a) design a model of ore bodies based on geological information obtained by drilling, then (b) use the procedure to calculate the magnetic field both inside and outside the bodies. Comparing the computational results with observations we can produce some informatiom for adjustment of the original models. Then (c) calculate the magnetic field of the new models until the computational results fit the observations. This procedure gains advantage over other methods as it deals with all the effects of demagnetization, inhomogeneity, and intermagnetizing betweem different bodies, therefore can produce the most reliable source models.

5.7 Conclusion

Previous work on demagnetization has been based on a physical model for dia- and paramagnetic materials and considered the effect only for induced

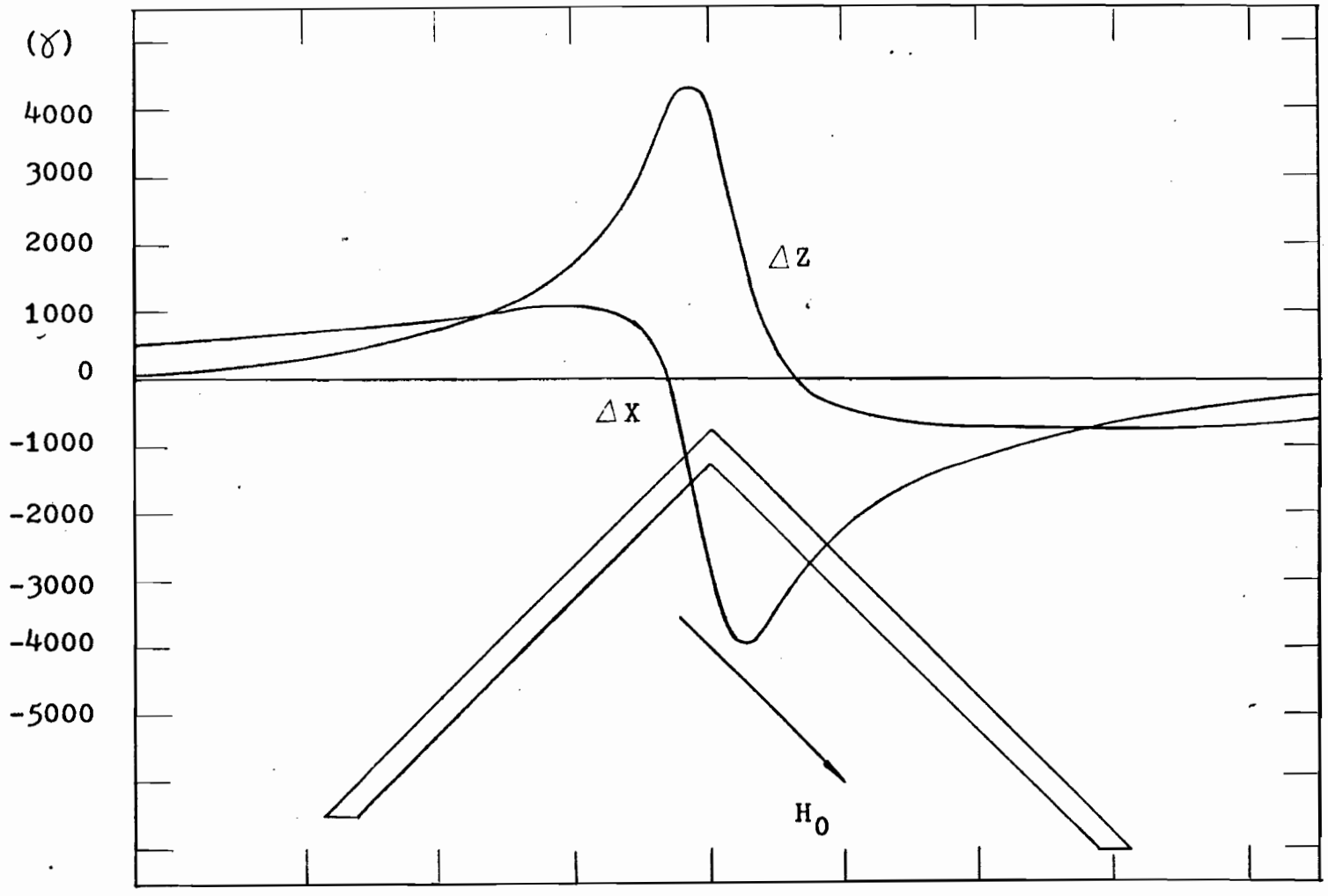

Figure 5.15. Ground magnetic anomaly due to the two sheets as shown in Figure 5.14. The spacial coordinates are in arbitrary unit.

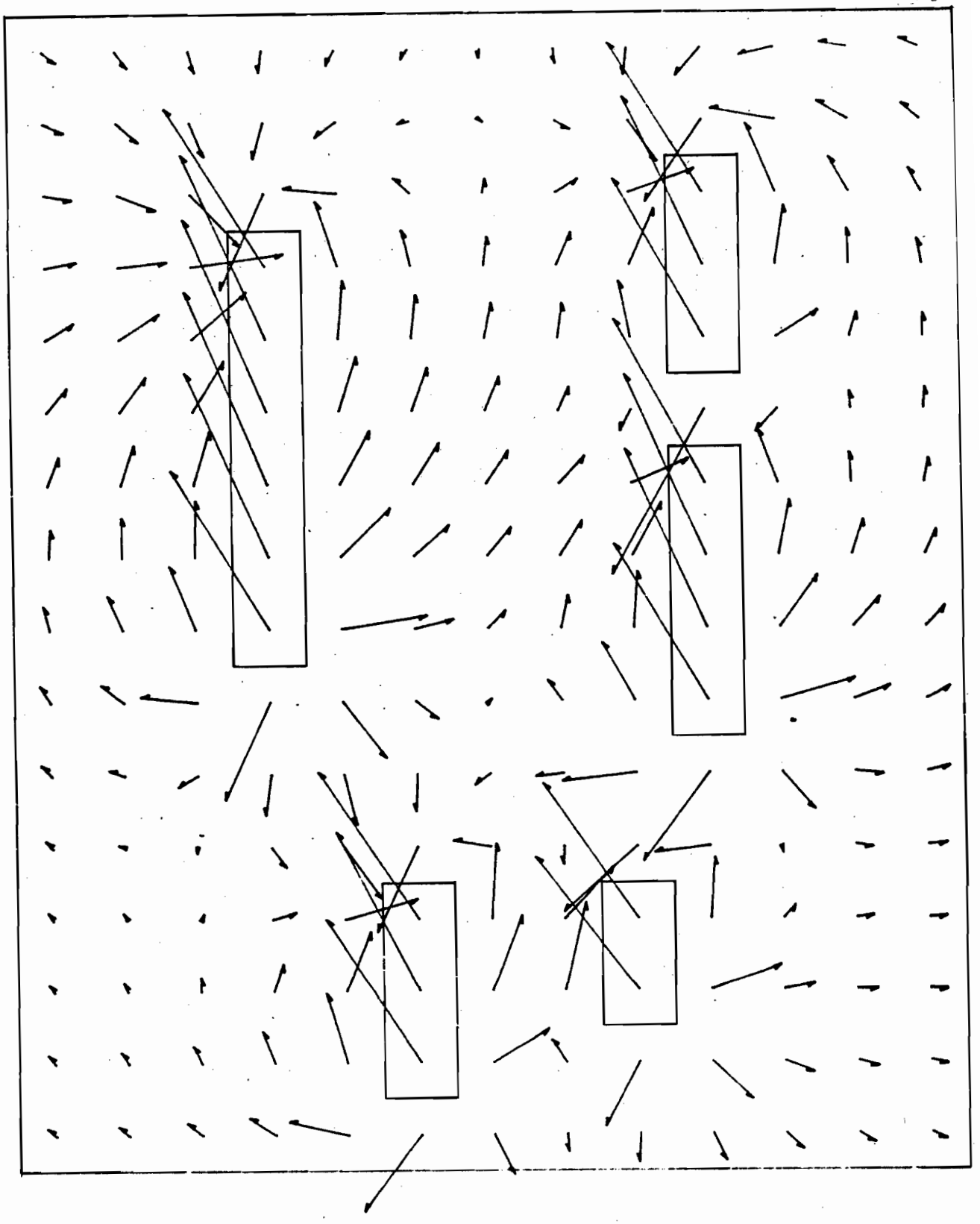

Figure 5.16. Secondary magnetic field due to five sheets magnetized in an external field of 0.5 oersted and 45°. All the sheets have uniform susceptibility of 0.2 emu and zero permanent magnetization. The arrows denote the intensity and direction of the field (scale 1 inch= 0.2 oersted)

magnetization. Because in many igneous rocks the NRM completely dominates that induced by the Earth's field, ignoring the demagnetization due to the NRM may yield erroneous estimates of effective magnetization. Based on linearization of the M(H) characteristics for ferro- and ferrimagnetic materials, a physical model for describing magnetic field in general crustal materials was presented in sections 5.2.1 and 5.5.2, which contains all the previous models as particular cases.

A precise method for magnetic field computation should take account of the inhomogeneity of the magnetic parameters and the demagnetization due to both the induced and permanent magnetizations within magnetized bodies. Based on the physical model mentioned above, such a method was developed in sections 5.2 and 5.3 for calculation of the effective magnetization and the magnetic field both inside and outside magnetized bodies. The numerical method employed divides the magnetized bodies into finite elements and results in linear systems of algebraic equations. The examples showed that this method can be accurate and fast if the size of the elements are chosen properly.

The physical model and the computational method can be useful in (a) calculation of magnetic anomalies in order to evaluate reserves of magnetic ore bodies and to find blind ore-bodies in explored mines; (b) interpretation of magnetic well-logging anomalies and (c) studies of theoretical and practical problems in demagnetization which are related to applied geophysics, rock magnetism and paleomagnetism. The studies presented in sections 5.5 and 5.6 have lead to the following conclussionss.

1. The NRM also causes a demagnetization field which is the secondary field induced by the permanent magnetization in ferromagnetic materials. The decrease in the effective magnetization due to this cause is proportional to the magnetic susceptibility. When the susceptibility of volcanic rocks is less than a few 10^{-3} emu, the demagnetization effect can be negligible (i.e. the

maximum error in effective magnetization is less than 5%) even if the NRM is relatively large.

2. For typical basic and ultrabasic igneous rocks in which the NRM intensity exceeds that induced by the Earth's field, ignoring the demagnetization effect can result in a maximum error greater than 16% (see Table 5.3). Thus, it may be necessary to consider the demagnetization effect in ultrabasic intrusives and the basic intrusives if which are magnetized transversely.

3. In many cases the assumption of uniform magnetization can be incorrect for magnetite deposits even though their magnetic parameters are uniform. For anomalies due to deeply buried sources this assumption may be tolerable, but the demagnetization effect of the permanent magnetization needs to be considered. Nevertheless, in many practical situations the effect of inhomogeneous structure in a magnetite deposit may dominate the demagnetization and both of them should be considered. In the case of multiple magnetized bodies, the mutual interaction is present between different bodies and results in a change of the effective magnetization in both magnitude and direction. The inhomogeneity in the magnetization and the complexity in the field near sources become serious in such cases.

The demagnetization model and the computational method are able to provide a basis for reevaluating some of the current methods of estimating in-situ susceptibility and sample measurements. In addition, if we treat equations (5.19) and (5.20) as an inverse problem, it might be possible to estimate NRM of a formation from its magnetic anomalies. Anyhow, these applications require further researches.

Chapter VI. Summary

In the three previous chapters, we have presented several new techniques for analysis of potential data to meet the challenge of evaluating base-metal subprovinces in mountainous areas. The finite element method has been incorporated with the spectral expansion method to form a complete procedure which provides much improved regional and residual gravity maps when some regional constraints are appropriately selected. This procedure has been applied to the regional-residual analysis of gravity data in the Abitibi greenstone belt in Quebec and Ontario. After the separation, downward continuation can be used for the regional field, to study the deep geologic structure or for the residual field, to localize the horizontal range of potential orebodies. We have demonstrated that the spectral expansion method is an appropriate method for downward continuation from an arbitrary surface to the top of sources and have recommended the damped least squares procedure for continuation of infinite-energy anomalies together with an improved procedure for finite-energy anomalies. In order to suppress undesirable aeromagnetic anomalies due to high topographic relief in crystalline terranes and topographic distortion of gravity anomalies, the equivalent source method has been improved for upward continuation of potential fields between arbitrary surfaces. The entire removal of the topographic anomalies may require accurate computation of the magnetic field which as shown in Chapter 5, should consider the demagnetization effect if igneous rocks have intermediate susceptibility and dominant remanent magnetization. The study of demagnetization is also essential for evaluation of reserves of magnetic orebodies and the interpretation of magnetic well-logging data. Based on linearization of the hysteresis curves of ferro- and ferri-magnetic materials, we have constructed both a physical and a mathematical model resulting in a new technique for calculating the effective

magnetization and magnetic field both inside and outside an arbitrary magnetized body. This procedure applies the finite element technique to solve a Fredholm's integral equation. These new techniques are useful for potential data processing whenever sophisticated techniques are needed for advanced data analysis, particularly for our evaluation purpose which requires processing potential field data measured on high topographic relief.

The major computational methods adopted in the thesis are the finite element method for forward geophysical problems and the spectral expansion approach for the inverse problems. As the FEM is mathematically involved in unconstrained minimization while the generalized inverse method applies constrained minimization, both of the methods are related to the optimization of functional equations. As a powerful tool in applied mathematics, optimization methods will continue to be applied in geophysical data analysis in the future. A successful application of optimization principles requires a careful exploration of the contact between the applied sciences and developments in computational methods. That is the reason why the FEM and the generalized inverse, although they have become well-known today, have seldom been used in the potential data processing (excluding the inversion which employs the generalized inverse as mentioned in Chapter 2). A sophisticated application often requires systematically integrated techniques, such as our regional-residual decomposition procedure which integrates the methods for solving both forward and inverse problems. As we showed in Chapter 3 and 4, the application of the generalized inverse method is not restricted to solving the inverse problem; it can also be used in the data processing stage via careful mathematical treatments.

As a basis of gravity and magnetic methods, the classical potential theory was mature even in Gauss's age. Stimulated by the exploration of outer space and deep underground structures and armed by modern computer sciences, the

potential data processing techniques have already had a solid framework since the 1970s. Further development in this area depends upon society's demand for new mineral deposits and upon new developments in the fundamental sciences. A brief perspective on some possible advances and future developments in potential data processing might be constructive before we end our discussion.

As a result of highlighting regional geophysics since the 1970s, compilations of gravity and magnetic anomaly maps in major countries are underway and will be completed in this decade. The interpretation of these maps will meet a serious problem of separating the contributions from the crust, lithosphere, asthenosphere, and even the lower mantle. This is more complicated than merely separating the two kinds of sources: regionals and residuals. The high degree of non-uniqueness in potential data inversion implies the impossibility of the separation by using the potential field data alone. Integrated modelling and joint inversion with other geophysical data might be helpful in dealing with this problem.

Because lineations in aeromagnetic maps are reliable indicators of crustal structures, the use of digital computers to automatically produce a lineament map would be very attractive to geologists. There is no doubt that this is a challenge to geophycisists in their attempts to simulate a complicated interpretation process. Pattern recognition and digital filtering might be the techniques useful for this problem.

It has been realized for a long time that the single interface model is too simple to represent actual crustal structures while the multi-interface model for inversion is more desirable for both the regional geophysics and oil geophysics. Unfortunately, it is a most difficult problem at present time since this is an extremly underdetermined non-linear inverse problem. More advanced methods must be needed for tackling this problem.

The coincidence of very weak potential field anomalies and the "bright

spots" of seismic exploration has been revealed in some oil fields (Roma and Bradley,1982), so the automatic recognition and location of these anomalies would be valuable in oil exploration. For a fruitful result sophisticated data processig techniques are required.

So far, stochastic modelling has not achieved full applications in potential data processing compared with seismic data processing. This is probably due to the requirement of strong assumptions on potential data for making progress. For instance, in order to develop some efficient procedures one may have to assume the potential data to be a realization of a stationary random process. This assumption in nature is incorrect for potential field signals which are usually space-variant. Theoretically employing the Hilbert probability space (Loeve, 1963, p.91-92) to describe actual potential fields seems promising for developing new data processing methods.

A.0

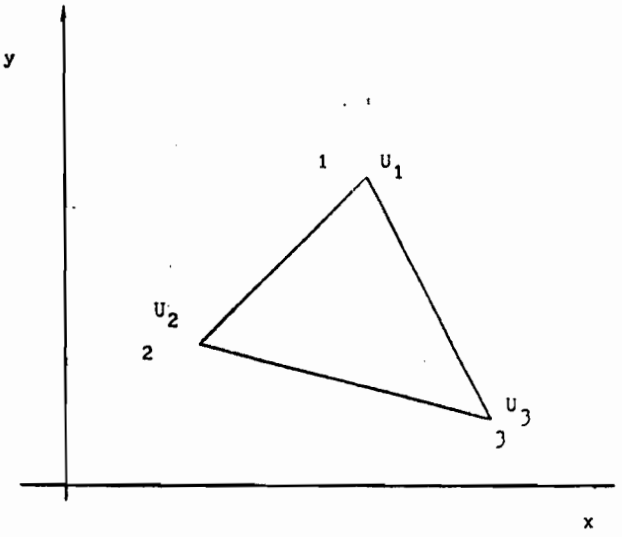

Fig. A-1. Typical triangular finite element in x-y plane.

Appendix I

The Finite Element Method for Plane Dirichlet Problems

The finite element method with its applications has been described in many texts (e.g. Silvester and Ferrari, 1983). For our application it is sufficient to outline only some practical aspects about the first order triangular elements for solving plane Dirichlet problems. A systematic and penetrating discussion can be found in Silvester and Ferrari's book which also contain some Fortran programs.

To obtain an approximate solution by the FE method, we may devide the studied region into many triangular elements. The potential (or other harmonic function) within a triangle may be adequately represented by the expression

$$u(x,y) = a + bx + cy \qquad (A.1)$$

Inserting particular coordinates x_i and y_i and corresponding potentials u_i at the three vertices of the triangle (Fig. A.1), we obtain three equations for coefficients a, b and c. Substituting a, b and c back to (A.1) yields

$$u = \sum_{i=1}^{3} u_i r_i (x,y) \qquad (A.2)$$

where r_i is a linear function of position only. If A denotes the surface area of the triangle, we have

$$r_1 = ((x_2y_3 - x_3y_2) + (y_2 - y_3)x + (x_3 - x_2)y)/2A \qquad (A.3)$$

$$r_2 = ((x_3y_1 - x_1y_3) + (y_3 - y_1)x + (x_1 - x_3)y)/2A \qquad (A.4)$$

$$r_3 = ((x_1y_2 - x_2y_1) + (y_1 - y_2)x + (x_2 - x_1)y)/2A \qquad (A.5)$$

The potential gradient within the element can be expressed from (A.2) as

$$\nabla u = \sum_{i\ 1}^{3} u_i \nabla r_i \qquad (A.6)$$

According to (A.6), the element energy of the potential will be

$$W^{(e)} = 0.5 \int_{triangle} |\nabla u|^2 \, ds = .5 \underset{-}{U}^T \underline{\underline{S}}^{(e)} \underset{-}{U} \qquad (A.7)$$

where $\underline{U}$ *is the column vector of* u_i *and the superscript* T *denotes transposition. The matrix* $\underline{\underline{S}}$ *has elements as*

$$S_{ij}^{(e)} = \int_{triangle} \nabla r_i \, \nabla r_j \, ds \qquad (A.8)$$

which depend on location and geometry of the element. For any given triangular mesh, the matrix is readily evaluated on substitution of the general expression (A.3) - (A.5) into (A.8).

In the assemblage of elements, potential values at all nodes may be described by a column vector of length N, where N is the total number of the nodes. Following the requirement that potential fields are continuous across interelement boundaries, a matrix $\underline{\underline{S}}$ *of N by N, named the Dirichlet matrix, can be defined from disjoint matrix* $\underline{\underline{S}}_{dis}$ *which can be expressed by (A.8). Suppose That an existing triangle (vertices 1,2 and 3) is to be jointed by another triangle (vertices 4,5,*

and 6) to form a quatrilateral region. In the connected assembly the potentials at corresponding vertices (say 1 and 3 to 4 and 6 respectively) must be identical. If we rewrite the potential vector

$$U_{dis} = (u_1, u_2, \ldots, u_6)^T$$

where the subscript dis indicates the disjoint elements. The total energy associated with the assemblage of the elements is the sum

$$W = \sum_{all\ e} W^{(e)} = 0.5\, U_{-dis}^{T}\, \underline{S}_{dis}\, U_{-dis} \qquad (A.9)$$

where

$$\underline{S}_{dis} = \begin{pmatrix} S^{(1)} & 0 \\ 0 & S^{(2)} \end{pmatrix}$$

The equality constraints at vertices may be expressed in matrix form, as a rectangular matrix $\underline{C}$ relating potentials of disjoint elements to the potentials of the conjoint set of elements:

$$U_{-dis} = \underline{C}\, U_{-con}$$

where $\underline{U}_{con} = col(u_1, u_2, u_3, u_4)$ for our two-triangle mesh, and

$$\underline{C} = \begin{pmatrix} 1 & 0 & 0 & 0 \\ 0 & 1 & 0 & 0 \\ 0 & 0 & 1 & 0 \\ 0 & 1 & 0 & 0 \\ 0 & 0 & 0 & 1 \\ 1 & 0 & 0 & 0 \end{pmatrix}$$

Thus, the energy in (A.9) for the connected system becomes

$$W = 0.5\, U^T_{-con} \; S \; U_{-con} \qquad (A.10)$$

where the Dirichlet matrix

$$S = C^T S_{dis} \; C$$

After the connected assembly of elements, the total energy (A.10) has a quadratic form like (A.7) with the Dirichlet matrix $\underline{S}$ *replacing the disjoint matrix. In practice, the disjoint coefficients may be calculated continuously while their contributions to the essembly can be embedded to the conjoint matrix* $\underline{S}$ *at the same time.*

To obtain an approximate solution of Laplace's equation, we need to minimize the stored energy in the connected finite element model, i.e., to set

$$\partial W/\partial u_k = 0$$

where the index k refers to nodal numbers while u_k *denotes nodal potentials. Since the energy expression (A.10) is quadratic, a unique minimum of the energy is guaranteed. The differentiation with respect to each and every k thus corresponds to an unconstrained minimization, with the potential allowed to vary at every node except for those prescribed on the boundary. The minimization leads to a matrix equation (see Silvester and Ferrari, section 1.5, 1983)*

$$\underline{\underline{S}}_{ff}\,\underline{U}_{f} = \underline{\underline{S}}_{fp}\,\underline{U}_{p} \qquad (A.11)$$

where the subscripts f and p refer to nodes with free and prescribed potentials respectively; $\underline{U}_p$ denotes the boundary constrains, while $\underline{U}_f$ is the solution for potentials at internal nodes. Matrix $\underline{\underline{S}}_{ff}$ denotes coefficients corresponding to internal elements at which potential can vary freely, while $\underline{\underline{S}}_{fp}$ corresponds to elements which have potentials at one or more vertices on the boundary. In general, the matrix $\underline{\underline{S}}_{ff}$ is square, symmetric and non-singular, so the solution $\underline{U}_f$ can be obtained by employing some efficient linear algorithms, such as Cholesky decomposition.

If the number of elements is large, considerable storage can be needed because the coefficient matrix involves the square of the total nodal number. Fortunately, discretization of differential equations by means of finite elements tends to produce sparse matrices, because any one nodal variable will be directly connected only to nodal variables which appear in the same finite element. Therefore, it is customary to arrange for storage of the matrix in one of several compact forms, such as band-matrix storage or profile storage. These problems are discussed in detail in Silvester and Ferrari (1983, chapter 6).

Appendix II. The mesh and the regional gravity estimate in the Abitibi belt

NODAL NUMBER OF TRIANGLES		
1	2	5
2	5	6
2	3	3
3	6	7
3	7	8
4	4	8
4	8	9
1	5	10
5	10	11
5	11	12
5	6	12
6	12	13
6	7	13
7	13	14
7	8	14
8	9	14
9	14	20
10	11	15
11	15	16
11	16	17
11	12	17
12	17	18
12	13	18
13	13	19
13	14	19
14	19	20
19	20	26
15	16	21
16	21	22
21	22	27
16	22	23
16	17	23
17	23	24
17	18	24
18	24	25
18	19	25
19	25	26
22	27	28
22	28	29
22	23	29
23	29	30
23	24	30
24	30	31
24	25	31
25	31	32
25	26	32
28	29	33
29	33	34
29	34	35
29	30	35
30	35	36
30	31	36
31	36	37

31	32	37	65	66	76	98	109	110
32	37	38	66	76	77	98	99	110
33	39	40	66	77	78	99	100	111
33	34	40	67	79	80	100	111	112
34	40	41	67	68	80	100	112	113
34	35	41	68	80	81	100	101	113
35	41	42	68	69	81	101	113	114
35	36	42	69	81	82	101	102	114
36	42	43	69	70	82	103	115	116
36	37	43	70	82	83	103	104	116
37	38	43	70	71	83	104	116	117
38	43	44	71	83	85	104	105	117
39	45	46	71	84	85	105	117	118
39	46	47	71	72	84	105	106	118
39	40	47	73	84	87	106	118	119
40	47	48	84	86	87	106	107	119
40	41	48	84	85	86	107	119	120
41	48	49	86	87	88	107	108	120
41	42	49	74	87	88	108	120	121
42	49	50	73	74	87	108	109	121
42	43	50	74	88	89	109	121	122
43	44	50	74	75	89	109	110	122
44	50	51	75	89	90	99	111	122
45	57	58	75	76	90	111	122	123
45	46	58	76	90	91	111	123	124
46	58	59	76	77	91	111	112	124
46	47	59	77	91	92	112	124	125
47	59	60	77	78	92	112	113	125
47	48	60	79	103	93	113	125	126
48	60	61	79	80	93	113	114	126
48	49	61	80	93	94	115	116	127
49	61	62	80	81	94	116	127	129
49	50	62	81	94	95	127	128	129
50	62	63	81	82	95	116	117	129
50	51	63	82	95	96	117	129	130
51	52	63	82	83	96	117	118	130
52	63	64	83	96	97	129	130	132
53	64	65	83	85	97	118	130	131
53	54	65	85	97	98	118	119	131
54	65	66	85	86	98	119	131	133
54	55	66	86	98	99	119	133	134
55	56	66	86	88	99	119	120	134
56	66	78	88	89	99	120	134	135
57	67	68	89	99	100	120	121	135
57	58	68	89	90	100	121	135	136
58	68	69	90	100	101	121	122	136
58	59	69	90	91	101	122	136	137
59	69	70	91	92	101	122	123	137
59	60	70	92	101	102	123	137	138
60	70	71	93	103	104	123	124	138
60	61	71	93	104	105	124	138	139
61	71	72	93	94	105	124	125	139
61	62	72	94	105	106	125	126	139
62	72	63	94	95	106	126	139	150
63	72	73	95	106	107	127	128	129
63	73	74	95	96	107	128	129	140
63	64	74	96	107	108	129	140	141
64	74	75	96	97	108	129	141	142
64	65	75	97	108	109	129	132	142
65	75	76	97	98	109	132	142	143

132	133	143
133	143	144
133	134	144
134	144	145
134	135	145
135	145	146
135	136	146
136	146	147
136	137	147
137	147	148
137	138	148
138	148	149
138	139	149
139	149	150
149	150	162
128	140	151
140	151	152
140	152	153
140	141	153
141	153	154
141	142	154
142	154	155
142	143	155
143	155	156
143	144	156
144	156	157
144	145	157
145	157	158
145	146	158
146	158	159
146	147	159
147	159	160
147	148	160
148	160	161
148	149	161
149	161	162
161	162	173
151	152	163
152	163	164
152	164	165
152	153	165
153	165	166
153	154	166
154	166	167
154	155	167
155	167	168
155	156	168
156	168	169
156	157	169
157	169	170
157	158	170
158	170	171
158	159	171
159	171	172
159	160	172
160	161	172
161	172	173
172	173	174
163	164	175
164	175	177

164	165	177
165	177	178
165	166	178
166	167	179
166	178	179
167	179	168
168	181	180
168	169	181
169	181	182
169	170	182
170	182	183
170	171	183
171	183	184
171	172	184
172	174	184
174	184	185
175	176	177
176	186	187
176	177	187
177	178	187
178	179	187
179	187	188
179	188	189
188	189	191
189	190	191
190	191	192
190	192	193
190	181	193
181	182	193
182	193	194
182	183	194
183	184	195
183	194	195
184	185	195
185	195	196
186	187	198
186	197	198
187	188	198
188	198	199
188	191	199
191	199	200
191	192	200
192	200	201
192	193	201
193	201	202
193	194	202
194	202	203
194	195	203
195	196	203
196	203	204
197	198	205
198	205	206
198	199	206
199	206	207
199	200	207
200	207	208
200	201	208
201	208	209
201	202	209
202	203	210

202	209	210
203	204	211
203	210	211
205	206	212
206	212	213
206	207	214
212	213	219
206	213	214
207	214	215
207	208	215
208	215	216
208	209	216
209	216	217
209	210	217
210	217	218
210	211	218
213	219	221
219	220	221
213	221	222
213	214	222
214	222	223
214	215	223
215	223	224
215	216	224
216	217	224
217	224	225
217	218	225
220	221	226
220	226	231
221	226	227
221	222	227
222	223	228
222	227	228
223	228	229
223	224	229
224	225	230
224	229	230
226	231	232
226	227	232
227	232	233
227	233	234
227	228	234
233	234	237
234	235	237
228	234	235
228	229	235
229	230	236
229	235	236
235	236	237

ECUNDARY CONSTRAINTS

NODE	Y	X	VALUE
1	47.71	-82.59	-47.30
2	48.18	-82.68	-44.40
3	48.50	-82.56	-50.30
4	48.67	-82.44	-52.50
9	48.98	-82.08	-55.60

10	47.74	-82.10	-50.80
15	47.78	-81.80	-51.30
20	49.06	-81.83	-44.20
21	47.63	-81.59	-50.50
27	47.66	-81.08	-52.00
28	47.91	-80.91	-54.50
32	49.19	-80.99	-52.50
33	48.14	-80.62	-60.30
38	49.20	-80.61	-44.10
39	47.94	-80.32	-58.10
44	49.12	-80.20	-47.90
45	47.81	-79.92	-56.30
51	49.31	-79.94	-52.60
52	49.52	-79.89	-49.20
53	49.85	-79.90	-43.00
54	50.01	-79.82	-40.30
55	50.22	-79.98	-43.40
56	50.43	-79.81	-41.20
57	47.75	-79.64	-58.80
64	49.63	-79.68	-47.90
67	47.77	-79.27	-53.10
72	49.01	-79.40	-53.20
73	49.25	-79.42	-51.00
78	50.52	-79.42	-42.10
79	47.67	-78.97	-59.10
84	49.01	-79.16	-54.70
99	49.62	-78.79	-54.80
102	50.44	-78.65	-55.30
103	47.70	-78.45	-56.90
110	49.57	-78.44	-56.30
114	50.42	-78.35	-52.00
115	47.86	-78.02	-61.60
122	49.54	-78.03	-56.00
126	50.40	-77.89	-59.20
127	47.85	-77.83	-63.60
128	47.88	-77.53	-65.40
130	48.52	-77.76	-57.40
131	48.62	-77.82	-58.60
132	48.60	-77.51	-61.70
133	48.78	-77.62	-62.60
150	50.47	-77.41	-62.80
151	47.82	-77.13	-63.20
162	50.47	-77.10	-63.90
163	47.81	-76.65	-59.70
168	48.99	-76.88	-65.10
174	50.30	-76.52	-67.20
175	47.93	-76.42	-57.90
176	48.06	-76.17	-56.30
179	48.78	-76.24	-72.30
180	48.92	-76.53	-74.50
185	50.21	-76.17	-69.60
186	48.36	-75.81	-54.80
189	48.86	-76.06	-72.80
190	49.22	-76.17	-73.30
196	50.12	-75.86	-66.20
197	48.43	-75.50	-60.50
204	50.24	-75.69	-65.00
205	48.66	-75.44	-65.60
211	50.21	-75.22	-69.10
212	48.79	-75.11	-70.20

218	50.16	-75.03	-72.30
219	48.80	-74.90	-74.10
220	48.86	-74.58	-74.10
230	50.07	-74.39	-68.40
231	48.82	-74.19	-73.50
232	49.18	-73.88	-74.30
233	49.42	-73.85	-74.30
236	50.02	-74.05	-70.80
237	49.83	-73.78	-71.60

NODAL COORDINATES
AND REGIONAL ESTIMATE

NODE	Y	X	SOLUTION
1	47.71001	-82.59000	-47.30000
2	48.17999	-82.67999	-44.39999
3	48.50000	-82.56000	-50.30000
4	48.67000	-82.44000	-52.50000
5	48.00000	-82.33000	-48.76688
6	48.25000	-82.33000	-49.30519
7	48.50000	-82.33000	-50.99237
8	48.75000	-82.25000	-53.20204
9	48.98000	-82.08000	-55.60001
10	47.74001	-82.10001	-50.80000
11	48.00000	-82.00000	-50.53859
12	48.25000	-82.00000	-50.62056
13	48.50000	-82.00000	-51.14676
14	48.75000	-82.00000	-51.95361
15	47.78000	-81.80000	-51.30000
16	48.00000	-81.67000	-51.25995
17	48.25000	-81.67000	-51.16188
18	48.50000	-81.67000	-50.81209
19	48.75000	-81.67000	-49.75536
20	49.06000	-81.83000	-44.20000
21	47.63000	-81.59000	-50.50000
22	48.00000	-81.33000	-52.11612
23	48.25000	-81.33000	-52.17848
24	48.50000	-81.33000	-51.75551
25	48.75000	-81.33000	-51.16545
26	49.00000	-81.33000	-51.10789
27	47.66000	-81.08000	-52.00000
28	47.91000	-80.91000	-54.50000
29	48.25000	-81.00000	-54.02361
30	48.50000	-81.00000	-52.96672
31	48.75000	-81.00000	-51.86632
32	49.19000	-80.99001	-52.50000
33	48.14000	-80.62000	-60.30000
34	48.25000	-80.67000	-57.68883
35	48.50000	-80.67000	-54.25394
36	48.75000	-80.67000	-51.60030
37	49.00000	-80.67000	-48.72911
38	49.20000	-80.61000	-44.10001
39	47.94000	-80.32001	-58.10001
40	48.25000	-80.33000	-56.52431
41	48.50000	-80.33000	-54.15646
42	48.75000	-80.33000	-51.72278
43	49.00000	-80.33000	-48.85301

44	49.12000	-80.20000	-47.89999
45	47.81000	-79.92000	-56.30000
46	48.00000	-80.00000	-56.46249
47	48.25000	-80.00000	-55.56326
48	48.50000	-80.00000	-54.17821
49	48.75000	-80.00000	-52.61313
50	49.00000	-80.00000	-51.07736
51	49.31000	-79.94000	-52.60001
52	49.52000	-79.89000	-49.20000
53	49.85001	-79.89999	-43.00000
54	50.00999	-79.82001	-40.30000
55	50.22000	-79.98000	-43.39999
56	50.42999	-79.81000	-41.20000
57	47.75000	-79.64000	-58.80000
58	48.00000	-79.67000	-56.51886
59	48.25000	-79.67000	-55.49907
60	48.50000	-79.67000	-54.51375
61	48.75000	-79.67000	-53.45258
62	49.00000	-79.67000	-52.33217
63	49.25000	-79.67000	-51.30122
64	49.63000	-79.67999	-47.89999
65	49.89999	-79.60001	-45.27028
66	50.25000	-79.67000	-42.66386
67	47.77000	-79.27000	-53.10001
68	48.00000	-79.33000	-55.17355
69	48.25000	-79.33000	-55.37013
70	48.50000	-79.33000	-54.99770
71	48.75000	-79.33000	-54.40027
72	49.00999	-79.39999	-53.20000
73	49.25000	-79.42000	-51.00000
74	49.50000	-79.33000	-50.58702
75	49.75000	-79.33000	-49.10565
76	50.00000	-79.33000	-47.50089
77	50.25000	-79.33000	-45.90619
78	50.52000	-79.42000	-42.10001
79	47.67000	-78.97000	-59.10001
80	48.00000	-79.00000	-56.60608
81	48.25000	-79.00000	-56.25156
82	48.50000	-79.00000	-55.86536
83	48.75000	-79.00000	-55.42279
84	49.00999	-79.16000	-54.70000
85	49.00000	-79.00000	-54.97978
86	49.25000	-79.00000	-53.97758
87	49.25000	-79.25000	-52.39290
88	49.50000	-79.00000	-53.23941
89	49.75000	-79.00000	-52.13831
90	50.00000	-79.00000	-50.95370
91	50.25000	-79.00000	-50.17606
92	50.50000	-79.00000	-49.78513
93	48.00000	-78.67000	-57.43520
94	48.25000	-78.67000	-57.18855
95	48.50000	-78.67000	-56.83159
96	48.75000	-78.67000	-56.44611
97	49.00000	-78.67000	-56.04091
98	49.25000	-78.67000	-55.58678
99	49.62000	-78.78999	-54.80000
100	50.00000	-78.67000	-53.69768
101	50.25000	-78.67000	-53.77251
102	50.44000	-78.64999	-55.30000
103	47.70000	-78.45000	-56.89999

104	48.00000	-78.33000	-58.59778
105	48.25000	-78.33000	-58.35512
106	48.50000	-78.33000	-57.87929
107	48.75000	-78.33000	-57.53658
108	49.00000	-78.33000	-57.22363
109	49.25000	-78.33000	-56.78983
110	49.57001	-78.44000	-56.30000
111	49.75000	-78.33000	-55.41922
112	50.00000	-78.33000	-55.01605
113	50.25000	-78.33000	-53.88150
114	50.42000	-78.35001	-52.00000
115	47.86000	-78.02000	-61.60001
116	48.00000	-78.00000	-61.32011
117	48.25000	-78.00000	-59.89999
118	48.50000	-78.00000	-58.66084
119	48.75000	-78.00000	-58.54257
120	49.00000	-78.00000	-58.58543
121	49.25000	-78.00000	-57.94656
122	49.53999	-78.03000	-56.00000
123	49.75000	-78.00000	-57.00525
124	50.00000	-78.00000	-57.28160
125	50.25000	-78.25000	-54.89711
126	50.39999	-77.89000	-59.20000
127	47.85001	-77.83000	-63.60001
128	47.88000	-77.53000	-65.39999
129	48.25000	-77.67000	-61.51521
130	48.52000	-77.75999	-57.39999
131	48.62000	-77.82001	-58.60001
132	48.60001	-77.50999	-61.70000
133	48.78000	-77.62000	-62.60001
134	49.00000	-77.67000	-61.13525
135	49.25000	-77.67000	-60.41580
136	49.50000	-77.67000	-59.89272
137	49.75000	-77.67000	-59.86668
138	50.00000	-77.67000	-60.07808
139	50.25000	-77.67000	-60.56854
140	48.00000	-77.33000	-63.72699
141	48.25000	-77.33000	-62.77206
142	48.50000	-77.33000	-62.53893
143	48.75000	-77.33000	-62.78375
144	49.00000	-77.33000	-62.77713
145	49.25000	-77.33000	-62.60196
146	49.50000	-77.33000	-62.42447
147	49.75000	-77.33000	-62.36571
148	50.00000	-77.33000	-62.45096
149	50.25000	-77.33000	-62.70825
150	50.47000	-77.41000	-62.80000
151	47.82001	-77.13000	-63.20000
152	48.00000	-77.00000	-62.41576
153	48.25000	-77.00000	-62.71547
154	48.50000	-77.00000	-63.36002
155	48.75000	-77.00000	-64.12296
156	49.00000	-77.00000	-64.40329
157	49.25000	-77.00000	-64.72821
158	49.50000	-77.00000	-64.67177
159	49.75000	-77.00000	-64.53659
160	50.00000	-77.00000	-64.45004
161	50.25000	-77.00000	-64.39948
162	50.47000	-77.10001	-63.89999
163	47.81000	-76.64999	-59.70000

164	48.00000	-76.67000	-60.52979
165	48.25000	-76.67000	-62.05806
166	48.50000	-76.67000	-63.97510
167	48.75000	-76.67000	-66.37277
168	48.99001	-76.88000	-65.10001
169	49.25000	-76.67000	-67.51906
170	49.50000	-76.67000	-67.05618
171	49.75000	-76.67000	-66.62285
172	50.00000	-76.67000	-66.38680
173	50.35001	-76.80000	-65.35158
174	50.30000	-76.52000	-67.20000
175	47.92999	-76.42000	-57.89999
176	48.06000	-76.17000	-56.30000
177	48.25000	-76.33000	-60.67245
178	48.50000	-76.33000	-64.91653
179	48.78000	-76.24001	-72.30000
180	48.92000	-76.53000	-74.50000
181	49.25000	-76.33000	-71.49780
182	49.50000	-76.33000	-69.45917
183	49.75000	-76.33000	-68.41313
184	50.00000	-76.33000	-68.13530
185	50.21001	-76.17000	-69.60001
186	48.36000	-75.81000	-54.80000
187	48.50000	-76.00000	-61.67888
188	48.75000	-76.00000	-68.79996
189	48.86000	-76.06000	-72.80000
190	49.22000	-76.17000	-73.30000
191	49.00000	-76.00000	-71.78894
192	49.25000	-76.00000	-71.48909
193	49.50000	-76.00000	-70.03571
194	49.75000	-76.00000	-68.79190
195	50.00000	-76.00000	-67.85001
196	50.12000	-75.86000	-66.20000
197	48.42999	-75.50000	-60.50000
198	48.75000	-75.67000	-66.07550
199	49.00000	-75.67000	-68.86020
200	49.25000	-75.67000	-69.71666
201	49.50000	-75.67000	-69.45953
202	49.75000	-75.67000	-68.64461
203	50.00000	-75.67000	-67.25764
204	50.24001	-75.69000	-65.00000
205	48.66000	-75.44000	-65.60001
206	49.00000	-75.33000	-69.35675
207	49.25000	-75.33000	-69.91988
208	49.50000	-75.33000	-69.88252
209	49.75000	-75.33000	-69.53558
210	50.00000	-75.33000	-69.03131
211	50.21001	-75.22000	-69.10001
212	48.78999	-75.11000	-70.20000
213	49.00000	-75.00000	-71.65132
214	49.25000	-75.00000	-71.17944
215	49.50000	-75.00000	-70.84084
216	49.75000	-75.00000	-70.67863
217	50.00000	-75.00000	-71.07666
218	50.16000	-75.03000	-72.30000
219	48.80000	-74.89999	-74.10001
220	48.86000	-74.58000	-74.10001
221	49.00000	-74.67000	-73.18185
222	49.25000	-74.67000	-72.20673
223	49.50000	-74.67000	-71.49185

224	49.75000	-74.67000	-70.84573
225	50.10001	-74.75000	-70.55830
226	49.00000	-74.33000	-73.37473
227	49.25000	-74.33000	-72.79095
228	49.50000	-74.33000	-72.03752
229	49.75000	-74.33000	-70.91594
230	50.07001	-74.39000	-68.39999
231	48.82001	-74.19000	-73.50000
232	49.17999	-73.88000	-74.30000
233	49.42000	-73.85001	-74.30000
234	49.50000	-74.00000	-73.21823
235	49.75000	-74.00000	-71.83687
236	50.02000	-74.05000	-70.80000
237	49.83000	-73.78000	-71.60001

References

Backus, G. E., and Gilbert, J. F., 1967, Numerical application of a formulism for geophysical inverse problems: Geophys. J. R. astr. Soc., 13, 247-276.

-, 1968, The resolving power of gross earth data: Geophys. J. R. astr. Soc., 16,169-205.

-, 1970, Uniqueness in the inversion of inaccurate gross earth data: Phil. Trans. Roy. Soc. London, ser. A 266, 123-192.

Baranov, V., 1957, A new method for Interpretation of aeromagnetic maps: pseudo-gravitational anomalies: Geophys., 22, 359-385.

-, 1975, Potential fields and thier transformations in applied geophysics: monograph series 1, No.6, Berlin, Gebruder Borntraeger.

Baranov, V., and Haudy, H., 1964, Numerical calculation of the formula of reduction to the magnetic pole: Geophys., 29, 67-79.

Bhattacharyya, B. K., 1965, Two dimensional harmonic analysis as a tool for magnetic interpretation: Geophys., 30, 829-857.

-, 1966, Continuous spectrum of the total-magnetic-field anomaly due to a rectangular prismatic body: Geophys., 31, 97-121.

-, 1978, Computer modeling in gravity and magnetic interpretation: Geophys., 43, 912-929.

Bhattacharyya, B. K., and Chan, K. C., 1977, Reduction of magnetic and gravity data on an arbitrary surface acquired in a region of high topographic relief: Geophys., 42, 1411-1430.

Bhattacharyya, B. K., and Leu, Lei-Kuang, 1975, Spectral analysis of gravity and magnetic anomalies due to two dimensional structure: Geophys., 40, 993-1013.

- and -, 1977, Spectral analysis of gravity and magnetic anomalies due to rectangular prismatic bodies: Geophys., 42, 41-50.

Bhimasankakam, V. L. S.,1977, Interpretation of gravity anomalies due to finite inclined dikes using Fourier transformation: Geophys., 42, 51-59.

Black, D. I., and Scollar, I., 1969, Spatial filtering in the wave vector domain: Geophys., 34, 916-923.

Bosum, W., 1968, An automatic method for interpretation of magnetic anomalies by least squares: Geophys. Pros., 16, 107-126.

Bott, M. H. P., 1963, Two methods applicable to computers for evaluating magnetic anomalies due to finite three-dimensional bodies: Geophys. Pros., 11, 292-.

-, 1967, Solution of the linear inverse problem in magnetic interpretation with application to oceanic magnetic anomalies: Geophys. J. R. astr. Soc., 13, 313-323.

-, 1973, Inverse methods in the interpretation of magnetic and gravity anomalies, In Bruce A. Bolt(ed): Methods In computational Physics, 13, 133-162, Academic Press.

Bott, M. H. P., and Smith, R. A., 1958, The estimation of the limitating depth of gravitating bodies: Geophys. pros., 6, 1-10.

Bozorth, R. M., and Chapin, D. M., 1942, Demagnetizing factors of rods: J. Appl. Phys., 13, 320-.

Bullard, E. C., 1967, The removal of trend from magnetic surveys: Earth and Planetary science letters, 2, 293-300.

Bullard, E. M., Hill, M. N., and Mason, C. S., 1962, Chart of the total force of the earth's magnetic field for the northeastern Atlantic ocean: Geomagnetica, Servico Meteorologico Nacional, Lisbon.

Byerly, P. E., 1965, Convolution filtering of gravity and magnetic maps: Geophys., 30, 281-283.

Cassano, E., and Rocca, f., 1975, Interpretation of magnetic anomalies using spectral estimation techniques: Geophys. Pros., 23, 663-681.

Chalupka, S., 1980, Analytic continuation of a three-dimensional gravity field from a spherical surface: Contr. Geophys. Inst. Slov. Acad. Sci., 10, 105-113.

Cianciara, B., and Marcak, H., 1976, Interpretation of gravity anomalies by means of local power spectra: Geophys. Pros., 24, 273-286.

Clarke, G. K. C., 1969, Optimum second-derivative and downward continuation filter: Geophys., 34, 424-437.

Cochran, J. R., and Talwani, M., 1977, Free-air gravity anomalies in the world's oceans and their relationship to residual elevation: Geophys. J. R. astr. Soc., 50, 495-552.

Coons, R. L., Mack J. W. and Strange, W.,1964, Least-squarers polynomial fitting of gravity data and case histories, Computers in the minirals industries, pt.

2: Stanford Univ. Pub. Geo. Sci., vol. 9, no.2, 498-519.

Cordell, L. and Henderson, R. G., 1968, Iterative three-dimensional solution of gravity anomaly data using a digital computer: Geophys. , 33, 596-601.

Cordell, L. and Grauch, V. J. S., 1982, Reconciliation of the discrete and integral Fourier transforms: Geophys., 47, 237-243.

Courtillot, V., Ducruix, J., and Le Mouel, J. L., 1974, A solution of some problems in geomagnetism and gravimetry: J of geophys. research, 79, 4933-4940.

Cox, A., and Doell, R. R., 1962, Magnetic properties of the basalt in hole EM7, Mohole Project: J. of Geophys. Research, 67, 3997-.

Cuer, M. and Rayer, R., 1980, Fortran routines for linear inverse problems: Geophys., 45, 1706-1713.

Darby, E. K., and Davies, E. B., 1967, The analysis and design of two dimensional filters for two-dimensional data: Geophys. Pros., 15, 383-406.

Danes, Z. F.,1960, On a successive approximation method for interpreting gravity anomalies: Geophys., 25, 1215-1228.

Danes, Z. F., and Oncley, L. A., 1962, An analysis of some second derivative methods: Geophys., 27, 611-615.

Dean, W. C., 1958, Frequency analysis for gravity and magnetic interpretation: Geophys., 23, 97-127.

Duetrix, J., Le Mouel, J. L., and Courtillot, V., 1974, Continuation of three dimensional potential fields measured on an uneven surface: Geophys. J. R. astr. Soc., 38, 299-314.

Duff, G. F. D., and Naylor, D., Differential equations of applied mathematics: John Wiley & Sons, Inc., New York, 1966.

Eby, T. W. F., 1972, The Fourier spectrum of gravity anomalies due to 2-D prisms: Can. SEG J., 8, 14-21.

Filatov, V. A., 1969, Calculation of the magnetic field of a two- dimensional body of arbitrary cross section: Akad. Nauk SSSR Ser. Fizika Zemli, no.2, 82-91.

Fisher, N. J. and Howard, L. E., 1980, Gravity interpretation with the aid of quadratic programming: Geophys., 45, 403-419.

Franklin, J, N., 1970, Well-posed stochastic extension of ill-posed problems: J. Math. Anal. Appl., 31, 682-718.

Fuller, B. D., 1967, Two-dimensional frequency analysis and design of grid operators, in Mining Geophysics, vol. II: SEG, Tulsa, 658-708.

-, 1977, Calculation of the gravity anomaly of Tsumbeb mine: Geophys., 42, 778-787.

Gerard, A. and Debeglia, N., 1975, Automatic three-dimensional modeling for the interpretation of gravity and magnetic anomalies: Geophys., 40, 1014-1034.

Gilbert, F., 1971, Ranking and Winnowing gross Earth data for inversion and

resolution: Geophys. J. R. astr. Soc., 23, 125-128.

Granser, H., 1983, Comments on "Potential field continuation between general surfaces" by F.J.R. Syberg: Geophys. Pros., 31,992-994.

Grant, F. S., 1957, A problem in the analysis of geophysical data: Geophys., 22, 309-344.

-, 1972, Review of data processing and interpretation methods in gravity and magnetics, 1964-1971: Geophys., 37, 647-661.

Grant, F. S., and West, G. F., 1965, Interpretation theory in applied geophysics (Chapter 8-12): New York, Mcgraw-Hill Book Co., Inc.

Green, W. R., 1975, Inversion of gravity profiles by use of a Buckus- Gilbert approach: Geophys., 40, 363-772.

Gunn, P, J., 1975, Linear transformations of gravity and magnetic field : Geophys. Pros., 23, 763-772.

Gupta, V. K., and Ramani, N., 1980, Some aspects of regional-residual separation of gravity anomalies in a precambrian terrain: Geophys., 45, 1412-1426.

Hahn, A., Kind, E. G., and Mishra D. C., 1976, Depth estimation of magnetic sources by means of Fourier amplitude spectra: Geophys. Pros., 24, 287-308.

Henderson, R. H., and Cordell, L., 1971, Reduction of unevenly spaced potential field data to a horizontal plane by means of finite harmonic series: Geophy., 36, 856-866.

Huestis, S. P., and Parker, R. L.,1979, Upward and downward continuation as inverse problems: Geophys. J. R. astr. Soc., 57, 171-188.

Jackson, D. D., 1972, Interpretation of inaccurate, insufficient, and inconsistent data: Geophys. J. R. astr. Soc., 28, 97-109.

-, 1979, The use of a priori data to resolve non-uniqueness in linear inversion: Geophys. J. R. astr. Soc., 57, 137-157.

Johnson, W. W., 1969, A least squares method of interpreting magnetic anomalies caused by two-dimensional structures: Geophys., 34., 65-74.

Jupp, D., and Vozoff, K., 1975, Stable iterative methods for the inversion of geophysical data: Geophys. J. R. astr. Soc., 13, 957-976.

Lange, A. L. and Farguhar, B. P., 1969, New computer graphics can be applied successfully to mineral exploration: Eng. and Mining J., 170, 120-123.

Lanczos, C., 1961, Linear Differential operators: Van Nostrand, London.

Le Mouel, J. L., Courtillot, V., and Galdeano, A., 1974, A simple formalism for the study of transformed aeromagnetic profiles and source location problems: J. of Geophys. research, 79, 324-331.

Lemouel, J. L., Courtillot, V., and Ducruix, J.,1975, A solution of some problems in potential theory: Geophys. J. R. astr. Soc., 42, 251-272.

Loeve, M., 1963, Probability theory: D. Van Nostrand Com. Inc. Pronceton

Lysmer, J., and Drake, L. A., 1972, A finie element method for seismology: in "Methods in Computational Physics", vol. 11, ed. by A. B. Bruce, Academic Press.

Magrath, P. H. and Hood, P. J., 1970, The dipping dike case: A computer curve-matching method of magnetic interpretation: Geophys., 35, 831-848.

- and -, 1973, An automatic least-squares multimodel method for magnetic interpretation: Geophys., 38, 349-358.

Mesko, C. A., 1966, Two-dimensional filtering and the second derivative method: Geophys., 31, 606-617.

Nagata, T., 1961, Rock Magnetism: Maruzen Press, Tokyo.

Nagy, B. S.., Introduction to real functions and orthogonal expansions, Oxford Uni. Press, 1965.

Nash, J. C., Compact numerical methods for computers: linear algebra and function minimization: Adam Hilger Ltd, Bristol, 1979.

Naudu, P. S., 1966, Extraction of a potential field signal from a background of random noise by Strakhov's method: J. Geophy. Res., 71, 5987-5995.

-, 1967, Two-dimensional strakhov's filter for extraction of a potential field signal: Geophys. Pros., 15, 135-150.

Nettleton, L. L., 1954, Regionals, residuals, and structures: Geophys., 19, 10-22.

Newman, M. J., Trowbridge, C. W., and Turner, L. R., 1972, GFUM: An interactive

program as an aid to magnet design: Report RPP/A94, Rutherford High Energy Lab., Chilton, Berks., England.

Nicholls, O. W., 1978, Mineral exploration: Industrial Geology, ed. by J. L. Knill, Oxford Uni. Press, 111-136.

O'Brie, D. P., 1970, Two-dimensional inverse convolution filter for analysis of magnetic field: Presented at 40-th annual international SEG meeting, November, 1970, new Orleans, Louisiana.

Odegard, M. E., and Berg, J. W., 1965, Gravity interpretation using the Fourier integral: Geophys., 30, 424-438.

Oldenburg, D. W., 1974, The inversion and interpretation of gravity anomalies: Geophys. J. R. astr. Soc., 39, 526-536.

-, 1976, Calculation of Fourier transforms by the Backus-Gilbert method: Geophys. J. R. astr. Soc., 44, 413-431.

-, 1981, A comprehensive solution to linear deconvolution problem: Geophys. J., 65, 331-358.

Parasnis, D. S., 1972, Principles of applied geophysics: Chapman and Hill.

Parker, C. L., 1984, A seismic refraction survey in the Abitibi greenstone belt: Unpublished M. Sc. thesis, McGill Univ., Montreal, Quebec.

Parker, R. L., 1973, The rapid calculatin of potential anomalies: Geophys. J. R. astr. Soc., 31, 447-455.

-, 1974, Best bounds on density and depth from gravity data: Geophys. , 39,

644-649.

-, 1975, The theory of ideal bodies for gravity interpretation: Geophys. J. R. astr. Soc., 42, 315-334.

-, 1976, Understanding inverse theory: Ann. Rev. Earth Planet. Sci., 5, 35-64.

Parker, R. L., and Klitgord, K. D., 1972, Magnetic upward continuation from an uneven track: Geophys., 37, 662-668.

Pedersen, L. B., 1977, Interpretation of potential field data - A generalized inverse approach: Geophys. Pros., 25, 199-230.

-, 1978, A statistical analysis of potential fields using a vertical circular cylinder and a dike: Geophys., 43, 943-953.

Phillips, R. J., and Lambeck, K., 1980, Gravity fields of the terrestrial planets, long-wavelength anomalies and tectonics: Review of Geophys. and space physics, 18, 27-76.

Ramo, A. O., and Bradley, J. W., 1982, Bright spots, miligals, and gammas: Gephys., 47, 1693-1705.

Rao, B. S. R. et al., 1975, A succesive approximation method of deriving residual gravity. Geoexplotation, 13, 129-135.

Reford, M. S., 1980, Magnetic method: Geophys., 45, 1640-1658.

Regan, R. d. and Hinze, W. J., 1976, The effect of finite data length in the spectral analysis of ideal gravity anomalies: Geophys., 41, 44-55.

Reitz, J. R., 1967, Foundations of electromagnetic theory, second edition, Addison-Wesley Publishing Co.

Sabatier, P. C., 1977, Positivity constrains in linear problem: Geophys. J. R. astr. Soc., 48, part I, 415-422, part II, 443-469.

Safon C., Vasseur G., and Cuer, M., 1977, Some applications of linear programming to the inverse gravity problem: Geophys, 42, 1215-1229.

Sharma, P. V., 1966, Rapid computation of magnetic anomalies and demagnetization effects caused by bodies of arbitrary shape: Pure and applied geophys., 64, 89-109.

Sharma, B., Geldart, L. P., and Gill, D. E., 1970, Interpretation of gravity anomalies of dike-like bodies by Fourier transformation: Can. J. Earth Sci., 7, 512-516.

Sax, R. L., 1966, Application of filter theory and information theory to the interpretation of gravity measurements: Geophy., 31, 570-575.

Silvester, p. p., and Ferrari, R. L., Finite elements for electrical engineers: Cambrige Uni. Press, 1983.

Silvester, P. P., and Haslam, C. R. S., 1972, Magnetotelluric modelling by the finite element method: Geophy. Pros., 20, 872-891.

Smith, R. A., 1959, Some depth formulae for local magnetic and gravity anomalies: Geophys. Pros., 7, 55-63.

-, 1960, Some formula for interpretation of local gravity anomalies: Geophys.

Pros., 8, 607-613.

Spector, A., and Bhattacharyya, B. K., 1966, Energe density spectrum and autocorrelation function of anomalies due to simple magnetic models: Geophys. Pros., 14, 242-272.

Spector, A. and Grant, F. S., 1970, Statistical models for interpreting aeromagnetic data: geophys., 35, 293-302.

Spector, A. and Parker, W.,1979, Computer compilation and interpretation of geophysical data, in geophysics and geochemistry in the search for metallic ores: P. J. Hood, ed., Geol. Surv. Can. Econ. Geol. rep., 31, 527-544.

Stewart, G. W., Introduction to matrix computations: Academic Press, 1973.

Stoner, E. C., 1945, The damagnetizing factors for ellipsoids: Philosophical Magazine, 36, 803-.

Strakhov, V. N., 1964, The smoothing of observed strength of potential fields: Akad. Nauk. SSSR Izv. Fizika Zemli, Part I, 897-904, Part II, 986-995.

Strangway, D. W., 1967, Magnetic characteristics of rocks: in Mining Geophysics, v.II, 454-473, compiled and edited by SEG.

Swartz, C. A., 1954, Some geometrical properties of residual maps: Geophys., 19, 46-70.

Syberg, F. J. R., 1972, Potential field continuation between general surfaces:

Geophys. Pros., 20, 267-282.

-, 1972, A Fourier method for the regional-residual problem of potential fields: Geophys. Pros., 20, 47-75.

Tanner, J. G., 1967, An automated method of gravity interpretation: Geophys. J. R. astr. Soc., 13, 339-347.

Talwani, M. and Ewing, M., 1960, Rapid computation of gravitational attraction of three dimensional bodies of any shape: Geophys., 25., 203- 225.

Treitel, S., and Lines, L. R., 1982, Linear inverse theory and deconvolution: Geophys., 47, 1153-1159.

Telford, W. M., Geldart, L. P., Sheriff, R. E., and Keys, D. A., Applied geophysics: Cambridge Uni. Press, 1976.

Teskey, D. J.,1978, Design of a semi-automated 3-D interpretation system for potential data: Ph.D. thesis, McGill Univ.

Van Bladel, J., 1964, Electromagnetic field: McGraw-Hill Book Co., Inc.

Van Voorfis, G. D., and Davis, T. M., 1964, Magnetic anomalies North of Puerto Rico: trend removal with orthogonal polynomials: J. Geophys. res., 69, 5363-5371.

Vogel, A., 1963, The application of electronic computers to the calculation of effective magnetization: Geophys. Pros., 11, 51-.

Wiggins, R. A., 1972, The general inverse problem: implication of surface waves and free oscillations for Earth structure: Rev. Geophys. Space phys., 10, 251-285.

Xie, Qin-Fang, 1966, The field theory: Geology Press, Peking.

Yang, Wencai, 1979, Theorem of equivalence between 2-D and 3-D potential fields in the frequency domain: Acta Geophysica Sinica, 22, 89-96.